The penetration resistance

of sands

by

Richard Gisbourne

Volume II

A thesis submitted to the University of Aston
in Birmingham for the degree of Doctor of Philosophy

December 1970

- PREFACE -

This volume of the thesis has been arranged so that it can be read simultaneously with Volume I.

It begins with Appendix I and continues with a complete bibliography of the works referred to in the first volume. Tables, figures and plates follow the references; these are grouped in this order, in chapter sequence.

The figures have been drawn and plotted since the Author left the University of Aston in Birmingham at the end of 1969. As already mentioned these have been completed with the help of Miss P. Sage.

Photographs were taken by the Author either during or at the end of the experimental programme.

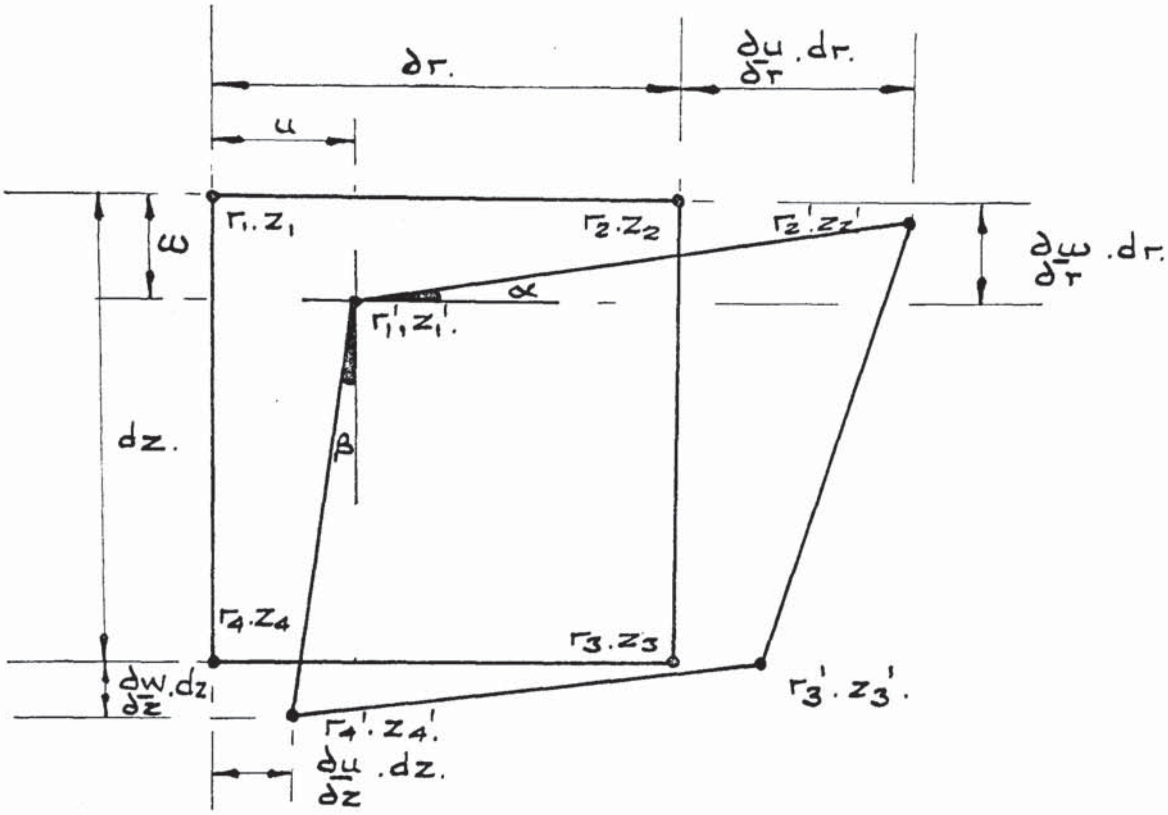

The above figures shows the co-ordinates of an element of soil before and after displacement of the element; the primed co-ordinates are those recorded after displacement.

Strains at a point have been given in terms of displacements, u and w, in the r and z directions respectively and it is possible to express u and w in finite difference form. The following finite difference equations relate the displacement co-ordinates to the strains (or strain-rates) during penetration. These equations are the ones used in computer analysis of displacements to give the complete strain tenser at a point.

$$\epsilon r = -\partial ur/\partial r. = - \frac{(u_2 - u_1) + (u_3 - u_4)}{(r_2 - r_1) + (r_3 - r_4)}$$

$$= \frac{(r_2 - r_1 + r_3 - r_4) - (r_2' - r_1' + r_3' - r_4')}{(r_2 - r_1 + r_3 - r_4)}$$

$$\epsilon z = -\partial w/\partial z = -\frac{(w_4 - w_1) + (w_3 - w_2)}{(z_4 - z_1) + (z_3 - z_2)}$$

$$= \frac{(z_4 - z_1 + z_3 - z_2) - (z_4' - z_1' + z_3' - z_2')}{(z_4 - z_1 + z_3 - z_2)}$$

$$\epsilon rz = -\partial w/\partial r \; -\partial u/\partial z = -\frac{(w_2 - w_1)+(w_3 - w_4)}{(r_2 - r_1) + (r_3 - r_4)} + \frac{(u_4 - u_1)+(u_3 - u_2)}{(z_4 - z_1)+(z_3 - z_2)}$$

$$= \frac{(z_2 - z_1 + z_3 - z_4)-(z_2' - z_1' + z_3' - z_4')}{(r_2 - r_1 + r_3 - r_4)} + \frac{(r_4 - r_1 + r_3 - r_2)-(r_4' - r_1' + r_3' - r_2')}{(z_4 - z_1 + z_3 - z_2)}$$

$$w_\theta = (\partial u/\partial z - \partial w/\partial r)/2.$$

$$= \frac{(z_2 - z_1 + z_3 - z_4)-(z_2' - z_1' + z_3' - z_4')}{(r_2 - r_1 + r_3 - r_4)} - \frac{(r_4 - r_1 + r_3 - r_2)-(r_4' - r_1' + r_3' - r_2')}{(z_4 - z_1 + z_3 - z_2)}$$

$$\epsilon_\theta = u/r. = \frac{(u_2 + u_3) + (u_4 + u_1)}{(r_2 + r_3) + (r_4 + r_1)} = \frac{(u_1 + u_2 + u_3 + u_4)}{(r_1 + r_2) + (r_3 + r_4)}$$

$$= \frac{(r_1' + r_2' + r_3' + r_4') - (r_1 + r_2 + r_3 + r_4)}{(r_1 + r_2 + r_3 + r_4)}$$

- BIBLIOGRAPHY -

AKROYD, T.N.W. (1957) Laboratory testing in soil engineering. Soil Mechanics Ltd., London.

ALLWOOD, R.J. (1956). An experimental investigation of the distribution of pressures in sands. Ph.D.Thesis, University of Birmingham.

ARTHUR, J.R.F. & ROSCOE, K.H. (1965). An examination of the edge effects in plane strain model earth pressure tests. Proc. 6th. Int. Conf. Soil Mech. 2, 363 - 367.

BARENTSEN, P. (1936). Short description of a field testing method with coneshaped sounding apparatus. Proc. 1st. Int. Conf. Soil Mech. 1, 7 - 10.

DE BEER, E.E. (1963). The scale effect in the transposition of the results of deep sounding tests on the ultimate bearing capacity of piles. Geotechnique 13, No. 1, 39 - 75.

DE BEER, E.E. (1965). Influence of the mean normal stress on the shear strength of sand. Proc. 6th. Int. Conf. Soil Mech. 1, 165 - 169.

BEGEMANN, H.K.S. (1953). Improved method of determining resistance to adhesion by sounding through a loose sleeve placed behing the cone. Proc. 3rd. Int. Conf. Soil Mech. 1, 213 - 217.

BEGEMANN, H.K.S. (1965). The friction jacket cone as an aid in determining the soil profile. Proc. 6th. Int. Conf. Soil Mech. 1, 17 - 20.

BENABENQ, J. (1911). Resistance des pieux, theorie et application, étude statique. Annales des pouts et chaussees. 5, 263.

BEREZANTZEV, V. G., KHRISOFOROV, V. & GOLUBKOV, V. (1961). Load bearing capacity and deformation of piled foundations. Proc. 5th. Int. Conf. Soil Mech. 2, 11.

BEREZANTZEV, V.G. (1965). Design of deep foundations. Proc. 6th. Int. Conf. Soil Mech. 2, 234 - 237.

BHATTACHRYA, S.I. (1960). The geometry of slip-line fields in soils. Geotechnique 10, No. 2, 75 - 81.

BOOTH, J.A.H. (1965). Comparison of CBR values for bulk sand and sand contained in standard CBR mould. Unpublished report. University of Aston in Birmingham.

BUCK, G.F. (1961). An interim research report on cell action studies connected with research on pressure measurements in sands. Proc. Mid, Soil Mech. Soc. 4, 96 - 105.

BUISMAN, A.S.K. (1935). De weerstand van pallpunten in zand. De ingenieur. 50, 25 - 28., 31 - 35.

CAQUOT, A. (1934). Equilibre des massifs a frottement interne. Stabilite des terres pulverulents en coheriantes. Gauthier-Villars, Paris.

CAQUOT, A. & KERISEL, J. (1948). Theories generale de la force portante des pieux. Traveaux. 32, 313 - 314.

CAQUOT, A. & KERISEL, J. (1956). Traite de mechanique des soils. Gauthier-Villars, Paris.

CHAPLIN, T. K. (1961). Compressibility of sands and settlements of model footings and piles in sand. Proc. 5th. Int. Conf. Soil Mech. 2, 33 - 40.

CHAPLIN, T. K. (1965). A fundamental stress-strain pattern in granular materials sheared with small or no volume change. Proc. 6th. Int. Conf. Soil Mech. 1, 193 - 197.

COX, A.D., EASON, G. & HOPKINS, H.G. (1961). Axially-symmetric plastic deformation in soils. Phil. Trans. Roy. Soc. A 254,1.

COX, A.D. (1962). Axially-symmetric plastic deformation in soils - II. Indentation of ponderable soils. Int. J. Mech. Sci. 4, 371 - 380.

COULOMB, C.A. (1776). Essai sur une application des regles de maximis et minimis à quelques problème de statique relatifs à l'architecture. Mém. Acad. R. prés. p. div. sav. T.7, Paris.

DELFT SOIL MECHANICS LABORATORY. (1936). The predetermination of the required length and the prediction of the toe resistance of piles. Proc. lst. Int. Conf. Soil Mech. 1, 181 - 184.

DOERR, H. (1922). Die tragfaehigkeit der pfaelhe. Ernst, Berlin.

DRUCKER, D.C., GREENBERG, H.J. & PRAGER, W. (1952). Extended limit design theorems for continuous media. Q. Appl. Math. 9, 381 - 389.

DYSON, S.M. (1970). The strength and deformational behaviour of a cohesionless soil under generalised stress conditions. Ph.D. thesis, University of Aston in Birmingham.

EBRAHIMI, S. (1969). Behaviour of a combined pile/pile cap foundation. M.Sc. thesis, University of Aston.

FLEMING, W.G.K. (1957). Bearing capacity of pile groups. Ph.D. thesis, Queen's University of Belfast.

FLORENTIN, J., L'HERITEAU, G. & FAHRI, M. (1948). Essais sur modeles reduits de pieux. Traveaux. 32, 340 - 344.

GIBBS, H.J. & HOLTZ, W.G. (1957). Research on determining the density of sands by spoon penetration testing. Proc. 4th. Int. Conf. Soil Mech. 1, 35 - 39.

GOLUSHKEVICH, S.S. (1957). Statics of the limiting condition in a soil mass. Gost ek hizdat, Moscow.

GORBUNOV-PASSADOV, M.I. (1965). Calculations for the stability of a sand bed by a solution combining the theories of elasticity and plasticity. Proc. 6th. Int. Conf. Soil Mech. 2, 51 - 55.

GRAHAM, J. (1966). Plastic failure in granular material : plane strain problems in soil mechanics. Ph.D. thesis, Queen's University of Belfast.

GRAHAM, J. (1968). Plane plastic failure in cohesionless soils. Geotechnique 18, No. 4, 301 - 316.

HAAR, A. & KÁRMÁN, Th.V. (1909). Zur theorie der spannungszustaende in plastichen und sandartigen medien. Nachr. Ges. Wiss. Gottingen, Math-phys. Klasse, 204.

HANNA, T.H. (1963). Model studies of foundation groups in sand. Ph.D. thesis. Queen's University of Belfast.

HARR, M.E. (1966). Foundations of theoretical soil mechanics. McGraw-Hill, New York.

HUIZINGA, T.K. (1951). Application of results of deep penetration test to foundation piles. Bldg. Res. Cong. 1, 173 - 179.

JAKY, J. (1948). On the bearing capacity of piles. Proc. 2nd. Int. Conf. Soil Mech. 1, 100 - 103.

JOSSELIN DE JONG, G. DE. (1959). Statics and kinematics in the failable zone of a granular material. Uitgeverij-Waltman, Delft.

KALLSTENIUS, J. & BERGAU, W. (1956). Investigations of soil pressure measuring by means of cells. Roy. Swedish Inst. Geot. Proc. 12.

KERISEL, J.L. (1939). La force portante des pieux. Anneles des ponts et chaussees. 109, 579.

KERISEL, J. L. (1961). Fondations profondes en milieux sableux : variation de la force portante limite en fonction de la densité, de la profondeur, du diamètre et de la vitesse d'enfoncement. Prof. 4th. Int. Conf. Soil Mech. 2, 73 - 83.

KERISEL, J.L., L'HERMINIER, R.L. & TCHENG, Y. (1965). Resistance du pointe en mileux pulvérulents de serrages divers. Proc. 6th. Int. Conf. Soil Mech. 2, 265 - 269.

KIRKPATRICK, W.M. (1957). The condition of failure for sands. Proc. 4th. Int. Conf. Soil Mech. 1, 172 - 175.

KOLBUSZEWSKI, J. (1948, a). An experimental study of the maximum and minimum porosities of sand. Proc. 2nd. Int. Conf. Soil Mech. 2, 16 - 20.

KOLBUSZEWSKI, J. (1948, b). General investigation of the fundamental factors controlling loose packaging of sands. Proc. 2nd. Int. Conf. Soil Mech. 7, 47 - 49.

KOLBUSZEWSKI, J. & JONES, R.H. (1961). The preparation of sand samples for laboratory testing. Proc. Mid. Soil Mech. Soc. 4, 108 - 123.

KREY, H. (1936). Erddruck, erdwiderstand und tragfaehigkeit des baugrundes. Ernst, Berlin.

KRUMBEIN, W.C. (1941). Measurement of geological significance of shape and roundness of particles. J. Sed. Pet. 11, No. 2, 64 - 72.

LADANYI, B. (1963). Discussion on Roscoe. et. al. (1963). A.S.T.M. Spec. Tech. Publ. No. 361, 129.

LEE, I.K. & BROWN, E.B. (1957). The design and construction of a laboratory earth pressure cell. Aust. J. Appl. Sc. 8, No. 2, 71.

MACKEY, R.D. (1966). A three dimensional pressure cell. Civ. Eng. Pub. Wks. Rev. 61, No. 725.

MARTINS, J.B. & FURTADO, R. (1963). Standard penetration test and deep sounding test foundations engineering. 3rd. Reg. Conf. Africa Soil Mech. 2, 157.

MAYERHOF, G.G. (1948). An investigation of the bearing capacity of shallow footings on dry sand. Proc. 2nd. Int. Conf. Soil Mech. 1, 237 - 243.

MEYERHOF, G.G. (1950). The bearing capacity of piles. Ph.D. thesis. University of London.

MEYERHOF, G.G. (1951). The ultimate bearing capacity of foundations. Geotechnique 2, No. 4, 301 - 332.

MEYERHOF, G.G. (1956). Penetration tests and bearing capacity of cohesionless soils. Proc. Am. Soc. Civ. Engrs. 866, SM 1, 1 - 19.

MOHAN, D., JAIN, G.S. & KUMAR, V. (1963). Load-bearing capacity of piles. Geotechnique 13, No. 1, 76 - 86.

MOHR, O. (1900). Abhandlungden aus dem gebiete der technischen mechanik. Ernst & Son, Berlin.

MONFORE, G.E. (1950). An analysis of stress distribution in and near strain gauges embedded in elastic solids. U.S. Bureau of Reclamation, Report SP 26, June.

MULLER, T. (1939). Modellversuche ueber das zusamm enwirken von mantelreiburg, spitsenwiderstand und tragfarelingkeit von pfaehlen. Ver. Inst. Degelbo. No. 7, 10.

NEWLAND, P.L. & ALLELY, B.H. (1957). Volume changes in drained triaxial tests on granular materials. Geotechnique 7, No. 1, 17 - 34.

PALMER, D.Y. & STUART, J.G. (1957). Some observations on the standard penetration test and a correlation of the test with a new penetrometer. Proc. 4th. Int. Conf. Soil Mech. 1, 231 - 236.

PEATTIE, K.R. & SPARROW, R.W. (1954). The fundamental action of earth pressure cells. J. Mech. Phys. Solids. 2, 141 - 155.

PECK, R.B., HANSON, W.E. & THORNBURN, T.H. (1953). Foundation engineering. J. Wiley & Sons, New York.

PELLEGRINO, A. (1965). Geotechnical properties of coarse grained soils. Proc. 6th. Int. Conf. Soil Mech. 1, 87 - 91.

PLANTEMA, I.G. (1948). Construction and method of operating a new deep sounding apparatus. Proc. 2nd. Int. Conf. Soil Mech. 1, 277.

PLANTEMA, I.G. (1957). Influence of density on sounding results in dry, moist and saturated soils. Proc. 4th. Int. Conf. Soil Mech. 1, 216.

PRANDTL, L. (1920). Uber die haerte plasticher koerper. Nachr. d. Gess. d. Wiss. Math-phys. Klasse, Gottingen, 74.

REDSHAW, S.C. (1954). A sensitive miniature pressure cell. J. Sci. Inst. 31 : 12, 467 - 469.

REISSNER, H. (1924). Zum erddruckproblem. Proc. 1st. Int. Congr. App. Mechs., Delft.

RITTENHOUSE, G. (1943). A visual method of estimating two-dimensional sphericity. J. Sed. Pet. 13, 79 - 81.

ROBINSKY, E.I. & MORRISON, C.F. (1964). Sand displacement and compaction around model friction piles in sand. Can. Geotechnical J. 1, No. 2, 81.

ROBINSKY, E.I. & MORRISON, C.F. (1969). Private communication.

RODIN, S. (1961). Experiences with penetrometers, with particular reference to the standard penetration test. Proc. 5th. Int. Conf. Soil Mech. 1, 517 - 521.

ROSCOE, K.H. (1953). An apparatus for the application of simple shear to soil samples. Proc. 3rd. Int. Conf. Soil Mech. 1, 186 - 191.

ROSCOE, K.H., ARTHUR, J.R.F. & JAMES, R.G. (1963). The determination of strains in soils by an X-ray method. Civ. Eng. Publ. Wks. Rev. 58, 873 - 876 and 1009 - 1012.

ROSCOE, K.H., SCHOFIELD, A.N. & THURAIRAJAH, A. (1963). An evaluation of test data for selecting a yield criteria for soils. A.S.T.M. Special Technical Public. 36, 111 - 128.

ROSCOE, K.H., SCHOFIELD, A.N. & WROTH, C.P. (1958). On the yielding of soils. Geotechnique 8, No. 1, 22 - 53.

ROWE, P.W. (1954). A soil pressure gauge for laboratory model research. Proc. Am. Soc. Civ. Engrs. 80, SM3, 569.

ROWE, P.W. (1962). The stress-dilatancy relation for static equilibrium of an assembly of particles in contact. Proc. R. Soc. A 269, 500 - 527.

ROWE, P.W. & BARDEN, L. (1964). Importance of free ends in triaxial testing. Proc. Am. Soc. Civ. Engrs. 90, SM 1.

ROWE, P.W., BARDEN, L. & LEE, I.K. (1964). Energy components during the triaxial cell and direct shear tests. Geotechnique 14, No. 3, 247 - 261.

RUMYATSEV, V. (1965). Industrial radiology. Foreign Langs. Publ. House, Moscow.

SCHULTZE, E. & KNAUSENBERGER, H. (1957). Experience with penetrometers. Proc. 4th. Int. Conf. Soil Mech. 1, 249.

SCHULTZE, E. & MENZENBACK, E. (1961). Standard penetration tests and compressibility of sand. Proc. 5th. Int. Conf. Soil Mech. 1. 527.

SCHULTZE, E. & MOUSSA, A. (1961). Factors affecting the compressibility of sand. Proc. 5th. Int. Conf. Soil Mech. 1, 335.

SIRWAN, K.Z. (1965). Deformations of soil specimens. Ph.D. thesis, University of Cambridge.

SOKOLOVSKI, V.V. (1965). Statics of soil media (transl. D.H. Jones & A.N. Schofield). Butterworths, London.

TAYLOR, D.W. (1947). Review of pressure distribution theories, earth pressure cell investigations and pressure distribution data. Soil. mech. fact finding survey progress report. U.S. Waterways Experimental Station.

TAYLOR, D.W. (1948). Fundamentals of soil mechanics. J. Wiley & Sons, New York.

TERZAGHI, K. (1943). Theoretical soil mechanics. J. Wiley & Sons, New York.

TERZAGHI, K. & PECK, R.B. (1948). Soil mechanics in engineering practice. J. Wiley & Sons, New York.

THOMAS, D. (1968). Deep sounding test results and the settlement of spread footings on normally consolidated sands. Geotechnique 18, No. 4, 472 - 487.

THOMAS, H.S.H. (1966). The measurement of strain in tunnel linings using the vibrating-wire technique. Strain 2, July, 16 - 21.

THOMAS, H.S.H. & WARD, W.H. (1969). Vibrating-wire earth pressure cell. Geotechnique 19, No. 1, 39 - 51.

THORBURN, T.H. (1963). Tentative correction chart for the standard penetration test in non-cohesive soils. Civ. Eng. Pub. Wks. Rev. 58, No. 683, 752.

TORY, A.C. (1966). Behaviour of a soil mass under dynamic loading. Proc. Am. Soc. Civ. Engrs. 92, SM 3, 59.

TROLLOPE, D.H. & CURRIE, D.T. (1960). Small embedded earth pressure cells - their design and calibration. Proc. 3rd. Aust - N.Z. Conf. Soil Mech., 145.

TROLLOPE, D.H. & LEE, I.K. (1957). The performance of a laboratory earth pressure cell. Aust. J. App. Sci. 8, 84 - 87.

TROW, N.A. (1952). Deep sounding methods for evaluating the bearing capacity of foundations on soils. 5th. Canad. Soil Mech. Conf. Tech. memo 23, 19 - 33.

TRUESDALE, W.B. & RUSIN, R.W. (1963). Discussion after Roscoe et. al. (1963). A.S.T.M. Spec. Tech. Pub. 36, 129 - 133.

TSCHEBOTARIOFF, G.P. & PALMER, D.V. (1948). Some experiences with tests on model piles. Proc. 2nd. Int. Conf. Soil Mech. 2, 195 - 199.

U.S. WATERWAYS EXPERIMENTAL STATION. (1944). Soil pressure cell investigation. Interim Report. Tech. memo. 210, 1.

VAN DER VEEN, C. (1953). The bearing capacity of a pile. Proc. 3rd. Int. Conf. Soil Mech. 2, 84.

VAN DER VEEN, C. (1957). The bearing capacity of a pile pre-determined by a cone penetration test. Proc. 4th. Int. Conf. Soil Mech. 2, 72 - 75.

VAN WEELE, A.F. (1957). A method of separating the bearing capacity of a test pile into skin friction and point resistance. Proc. 4th. Int. Conf. Soil Mech. 2, 76 - 79.

VAN WEELE, A.F. (1961). Deep sounding tests in relation to the driving resistance of piles. Proc. 5th. Int. Conf. Soil Mech. 2, 165 - 169.

VER MEIDEN, J. (1948). Improved sounding apparatus, as developed in Holland since 1936. Proc. 2nd. Int. Conf. Soil Mech. 1, 280 - 287.

WALKER, B.P. & WHITAKER, T. (1967). An apparatus for forming uniform beds of sand for model foundation tests. Geotechnique 17, No. 2, 161 - 167.

WHIFFIN, A.C. & SMITH, R.T. (1951). A gauge for measuring sustained stresses in soil. Engineer 192, 5 - 6.

YASSIN, A.A. (1950). Model studies of piles. Ph.D. thesis, University of London.

FIGURE 1.1. INITIAL PROGRAM FOR THE DESIGN, MANUFACTURE AND USE OF RESEARCH APPARATUS.

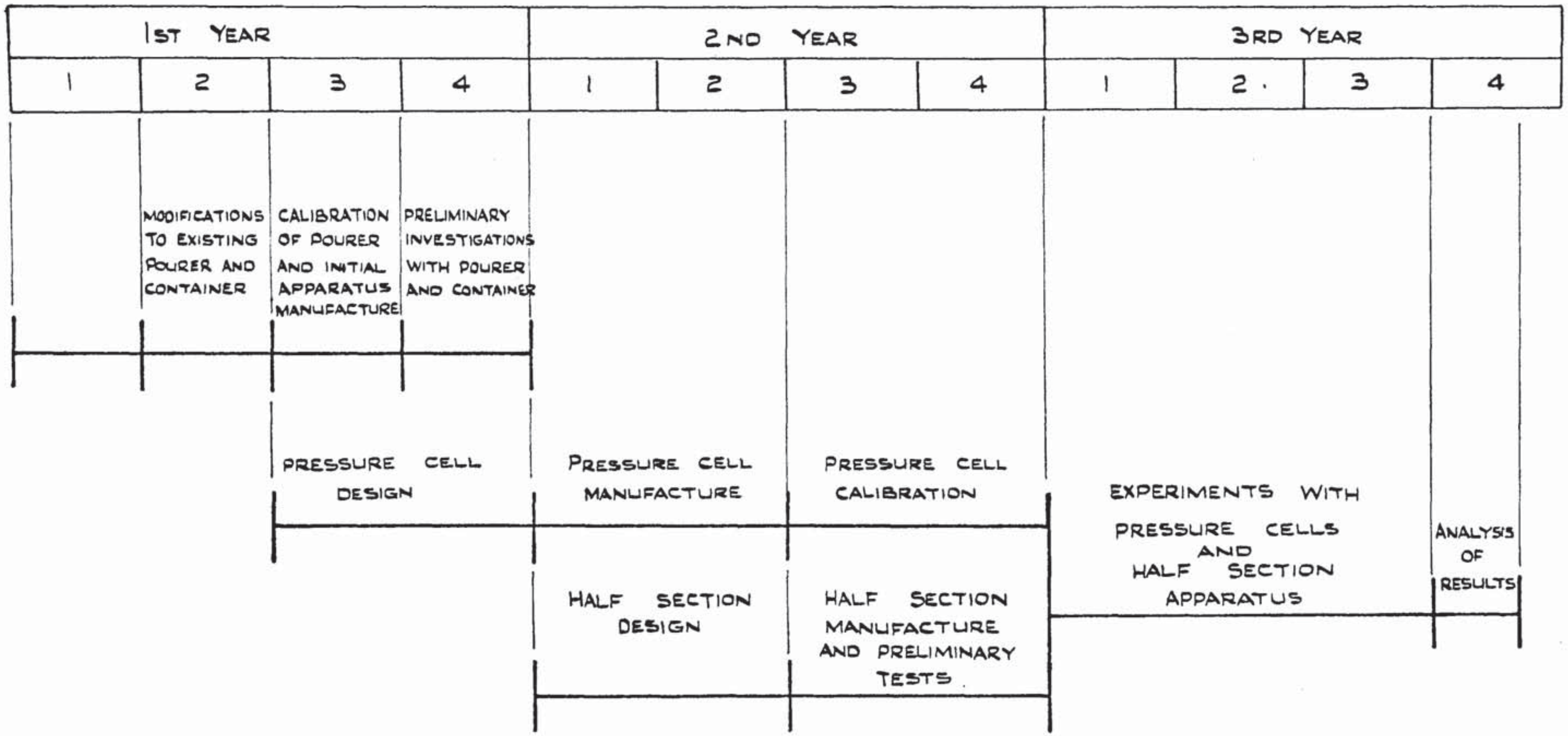

TABLE 2.1

TYPE OF TEST	TEST 1	TEST 2	TEST 3	TEST 4	MEAN POROSITY
MINIMUM POROSITY					
AKROYD	32·69	33·09	32·89	32·66	32·83
AUTHOR	35·64	35·34	35·57	35·69	35·56
MAXIMUM POROSITY					
AKROYD	45·95	45·90	46·01	45·94	45·95
AUTHOR	47·04	47·11	47·04	47·05	47·06

FIGURE 2.1.

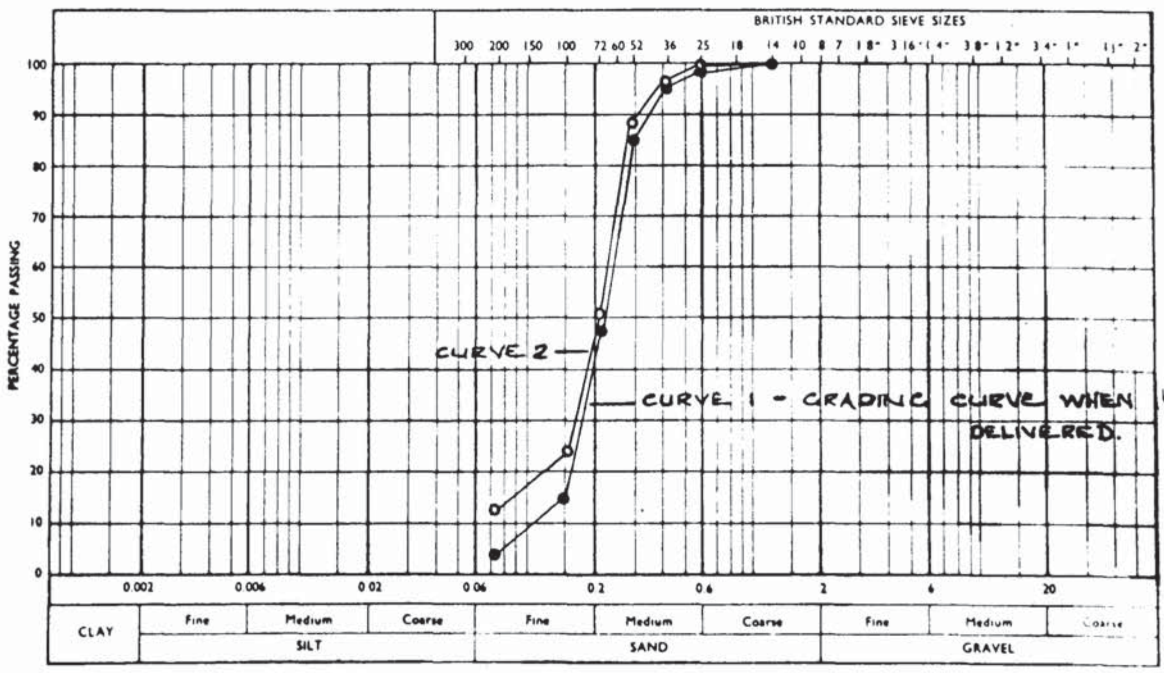

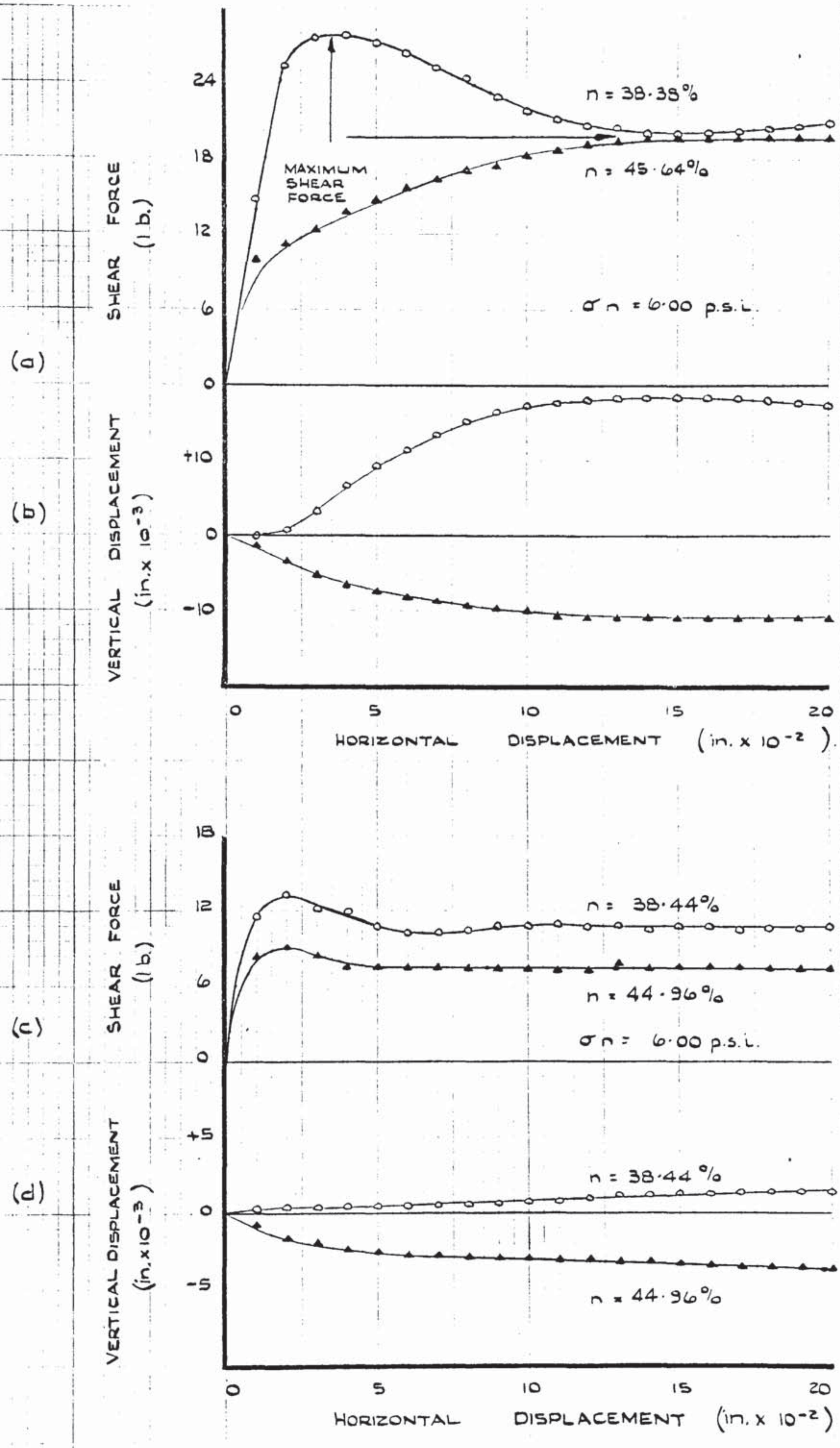

FIGURE 2.2. TYPICAL LOAD - DISPLACEMENT CURVES FOR LOOSE AND DENSE SAND IN DIRECT SHEAR BOX -
(a) AND (b) CONVENTIONAL
(c) AND (d) SAND AGAINST BRASS

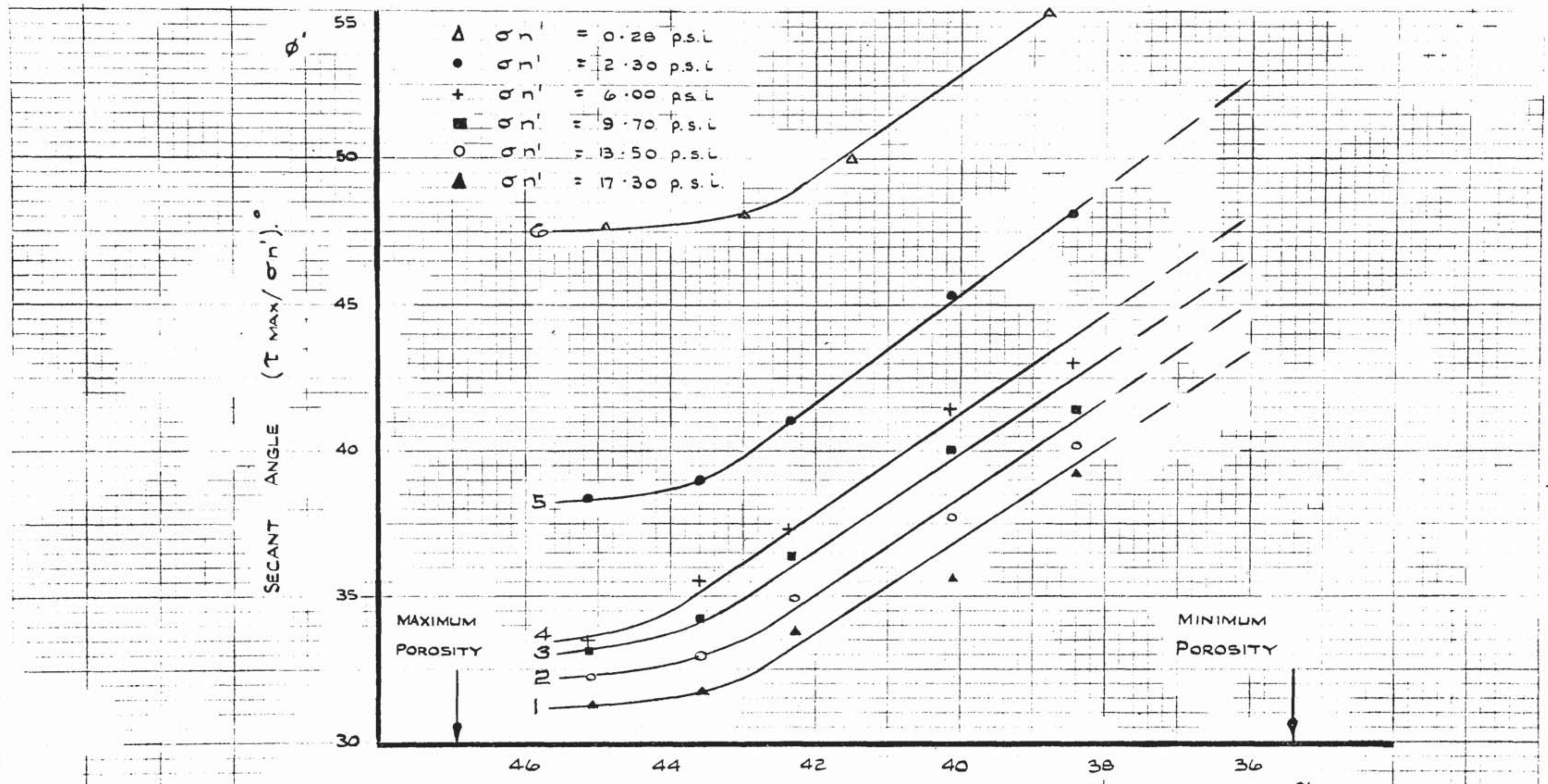

FIGURE 2.3. φ' VERSUS POROSITY FOR FINE WHITE SAND – OBTAINED FROM DIRECT SHEAR TESTS.

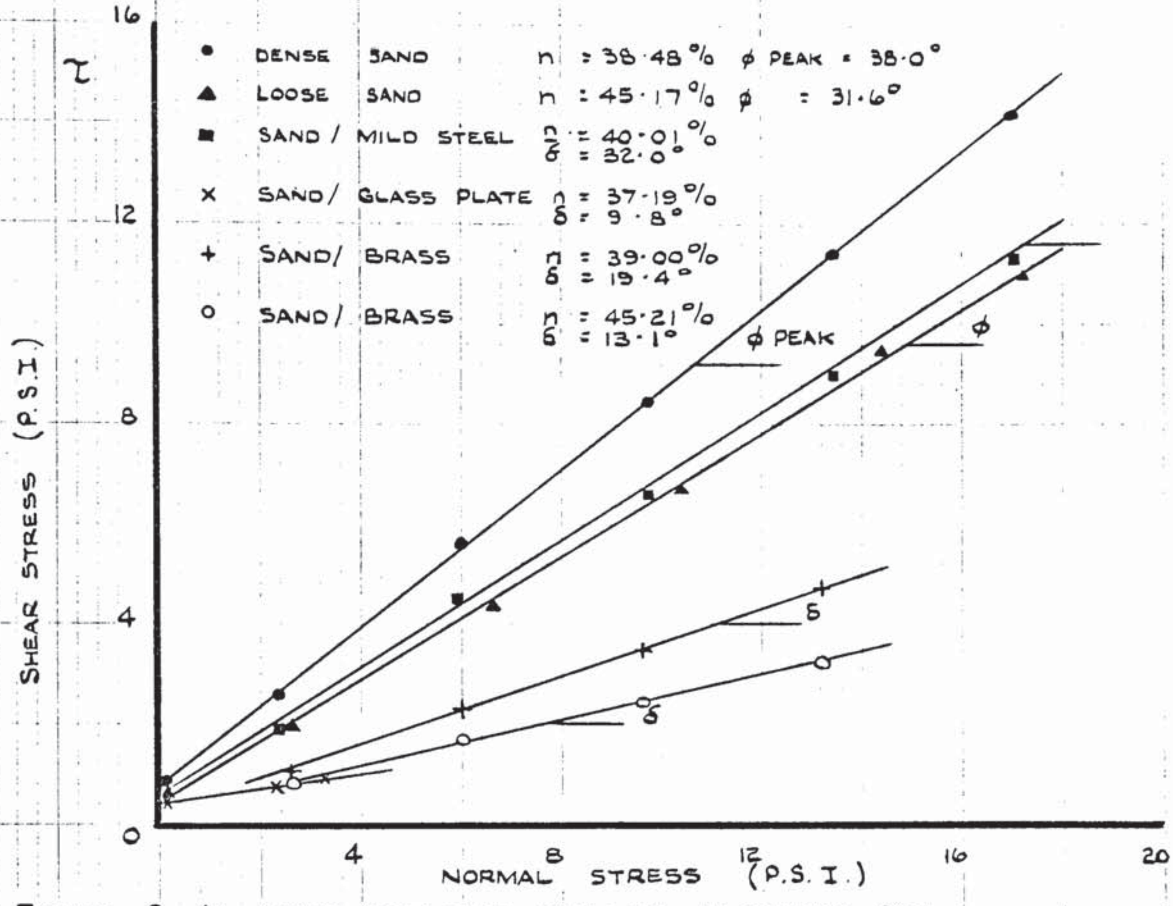

FIGURE 2.4: MOHR COULOMB FAILURE SURFACES. FOR FINE WHITE SAND - SAND, SAND ON BRASS, MILD STEEL AND GLASS.

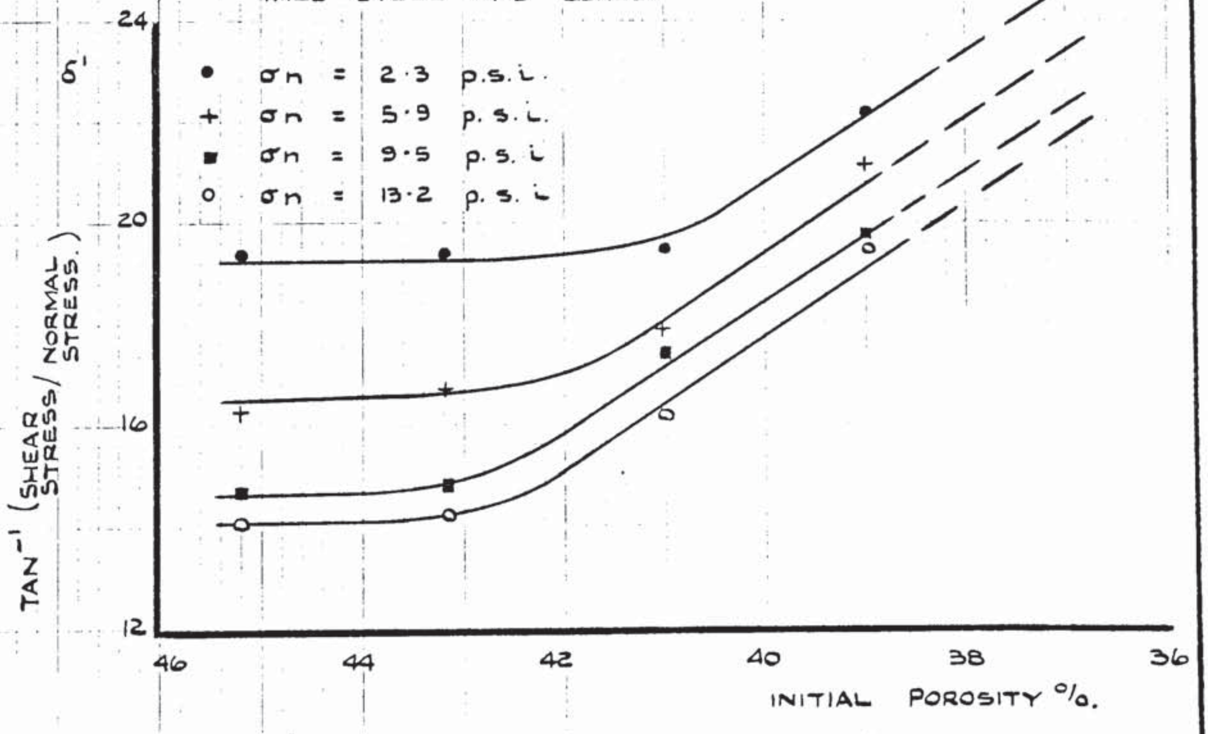

FIGURE 2.5: δ' VERSUS POROSITY FOR FINE WHITE SAND - DIRECT SHEAR TESTS FOR SAND ON BRASS.

FIGURE 2.7 ANGLE OF FRICTION BETWEEN BRASS AND FINE WHITE SAND - COMPARISON OF VALUES FOR COMPACTED AND POURED SAND SPECIMENS.

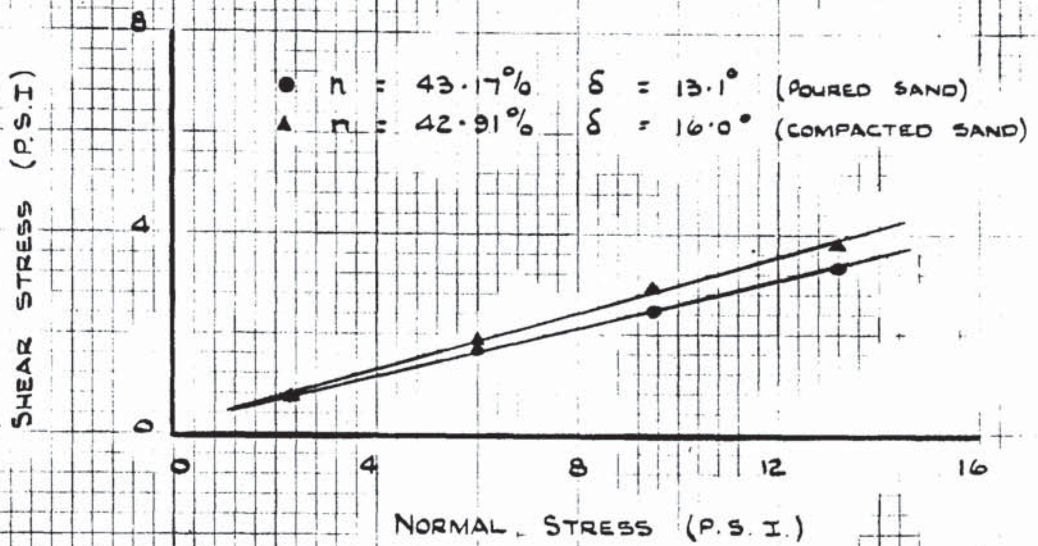

FIGURE 2.6 CORRECTED AND TOTAL ANGLES OF SHEARING RESISTANCE FOR FINE WHITE SAND.

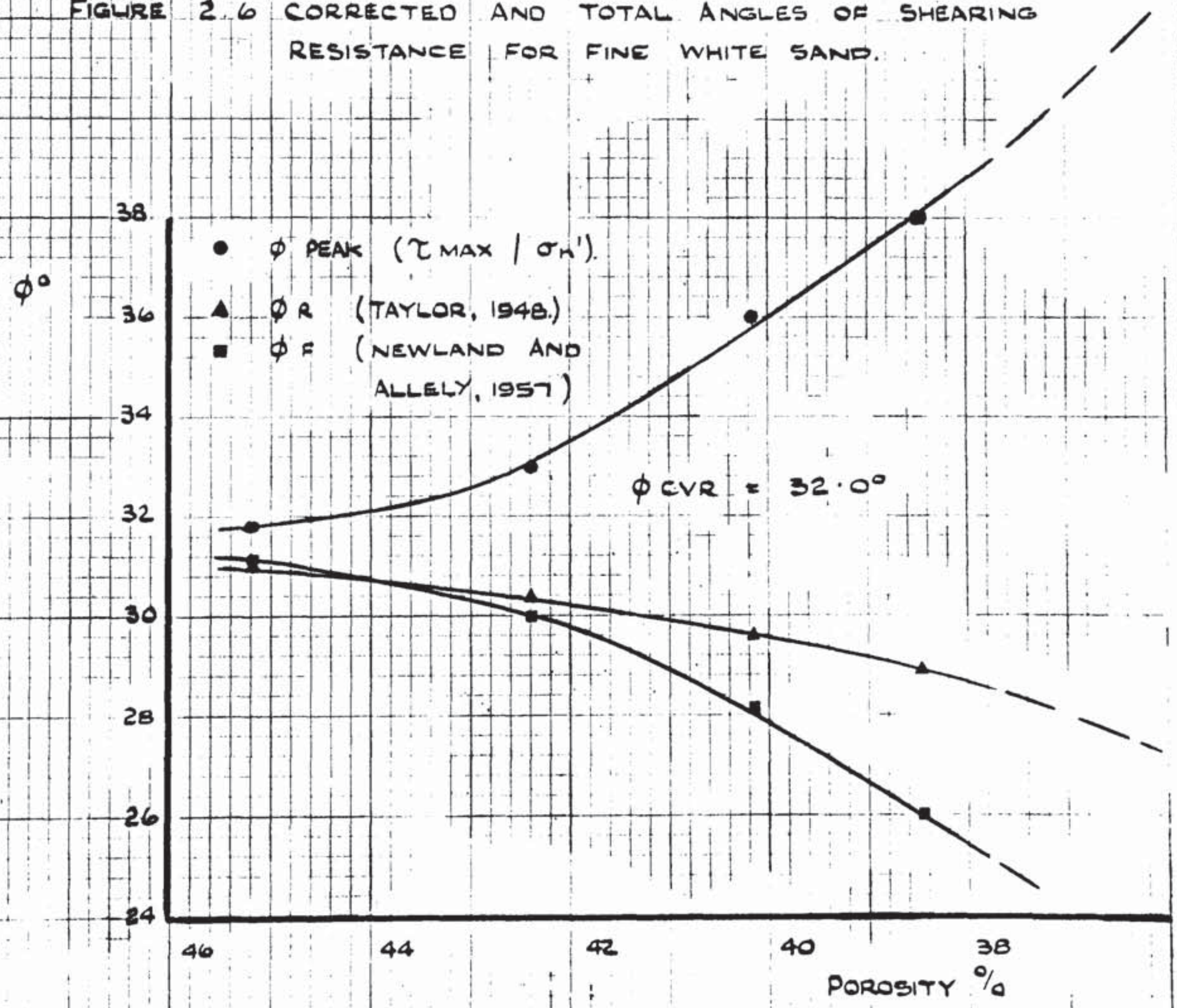

FIGURE 2.8 TOTAL PENETRATION RESISTANCE VERSUS PENETRATION FOR MILD STEEL PENETROMETERS IN DENSE SAND.

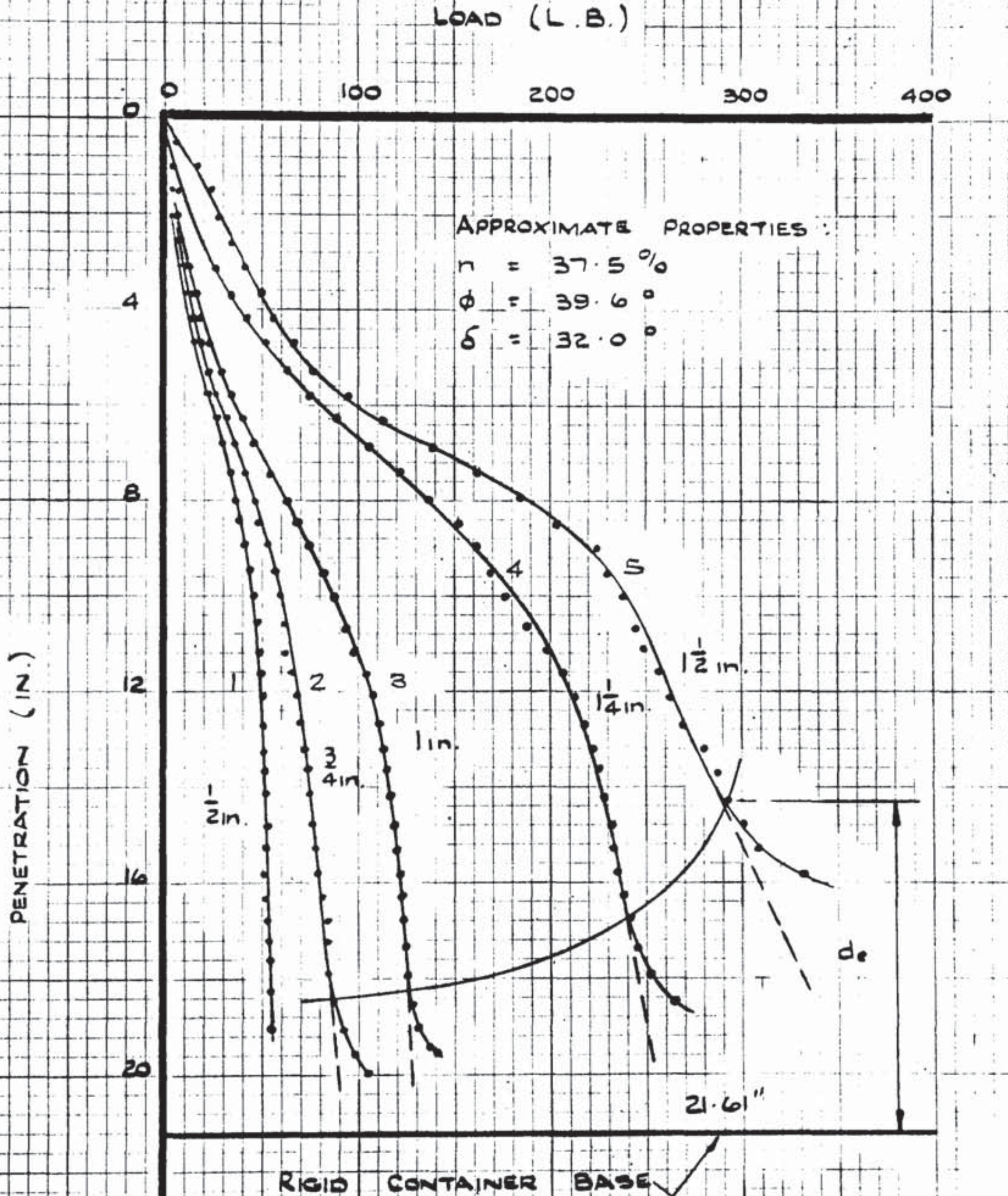

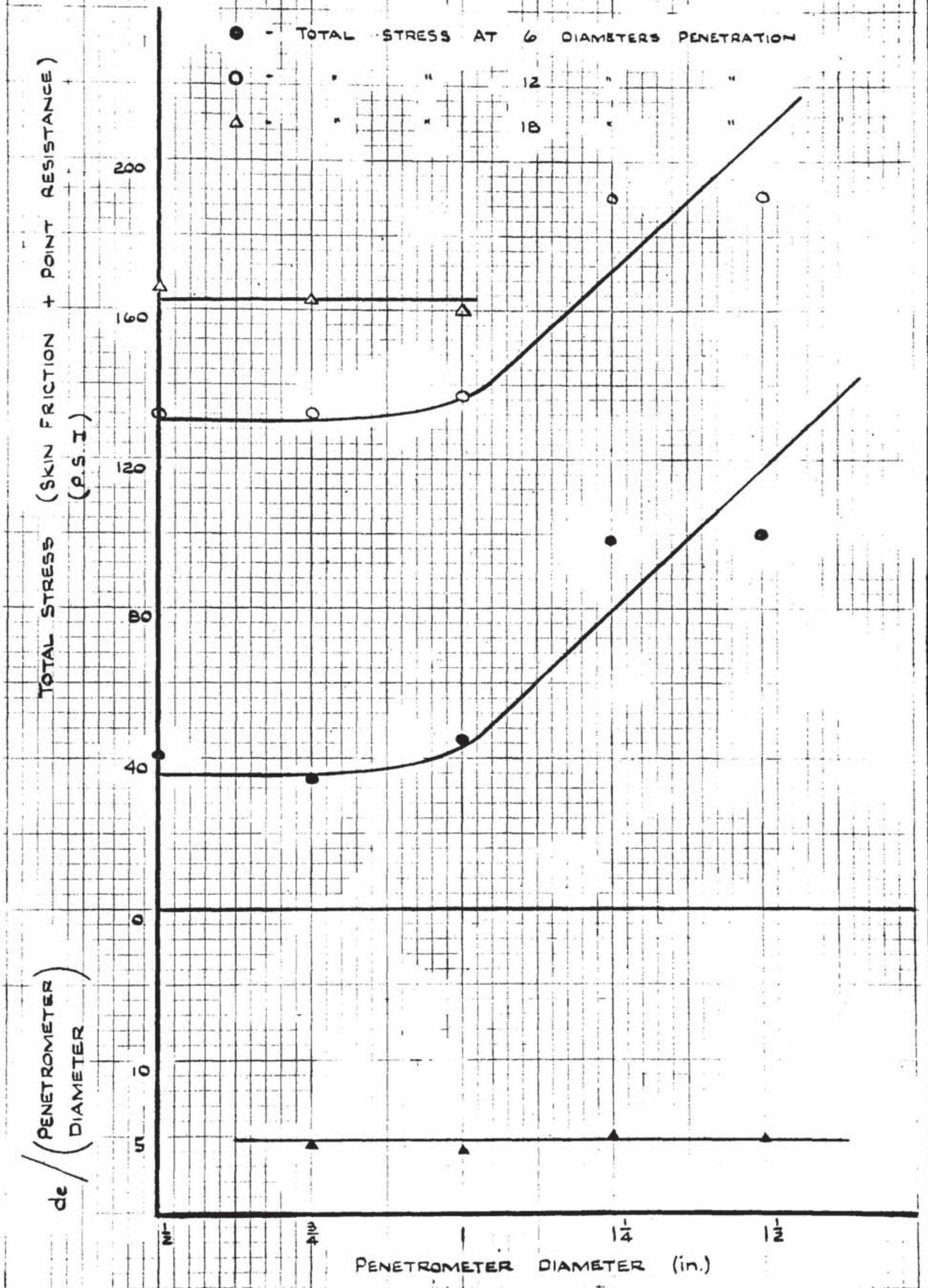

FIGURE 2.9, TOTAL STRESS AND DEPTH EFFECT VERSUS PENETROMETER DIAMETER.

FIGURE 2.10 (a) THEORETICAL FAILURE MECHANISM (FROM JAKY, 1948).

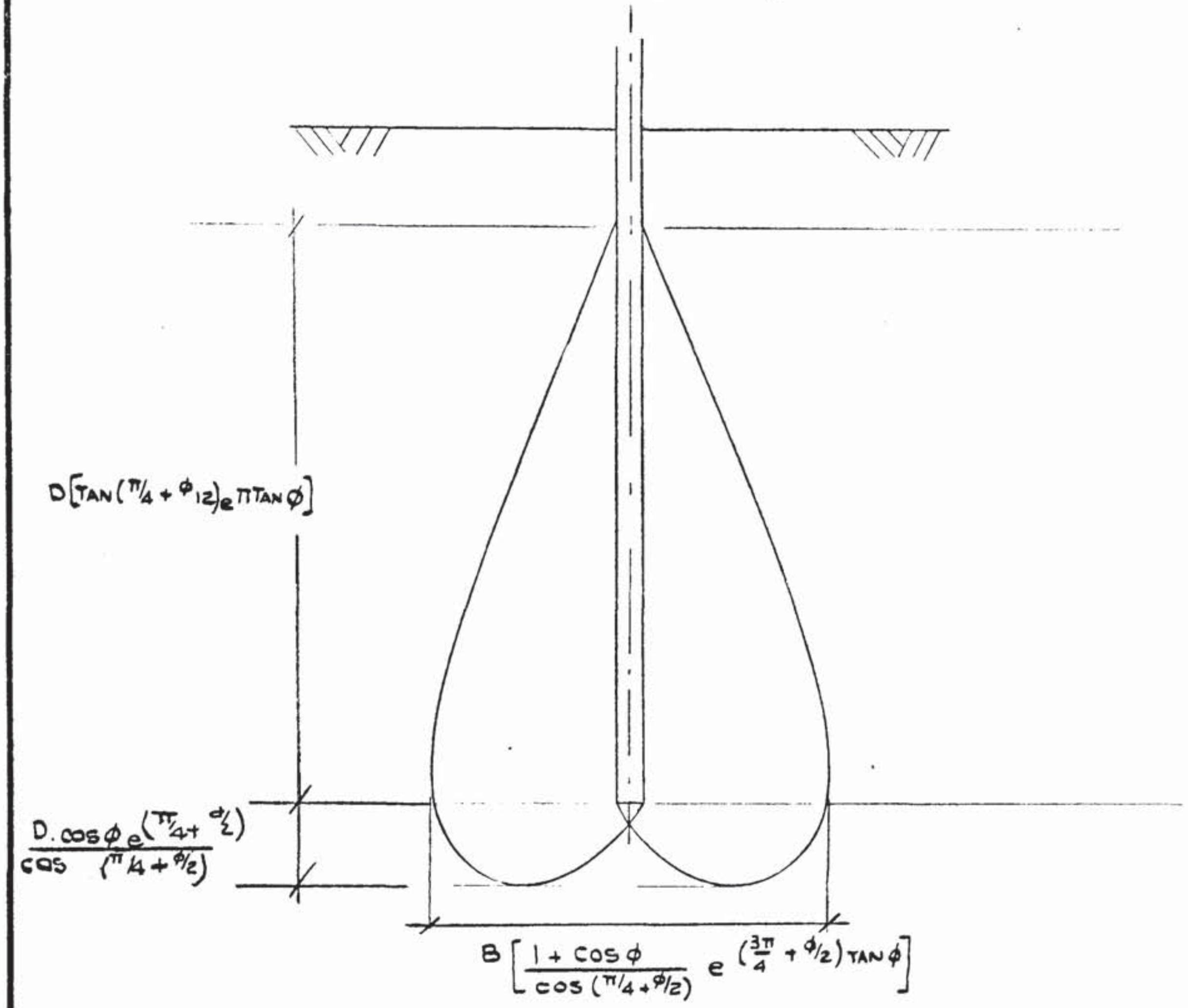

FIGURE 2.10 (b). APPROXIMATE SHAPE OF FAILURE SURFACES AS DEDUCED FROM EXPERIMENT.

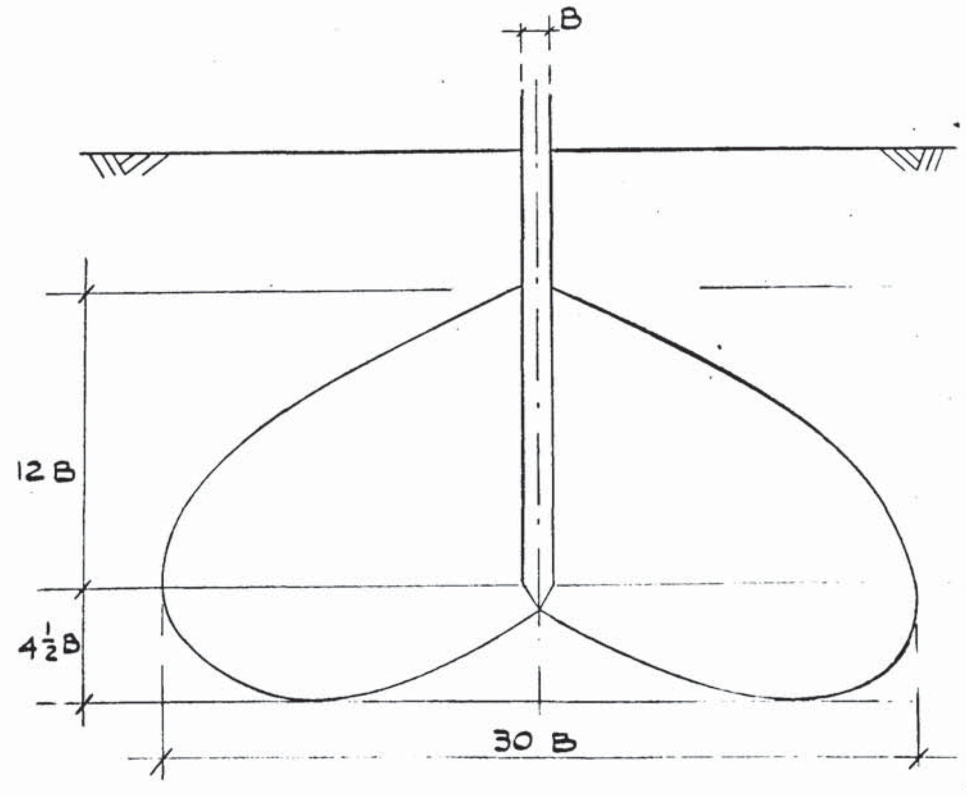

FIGURE 2.11 (a) COMPARISON OF CONTAINER SIZES

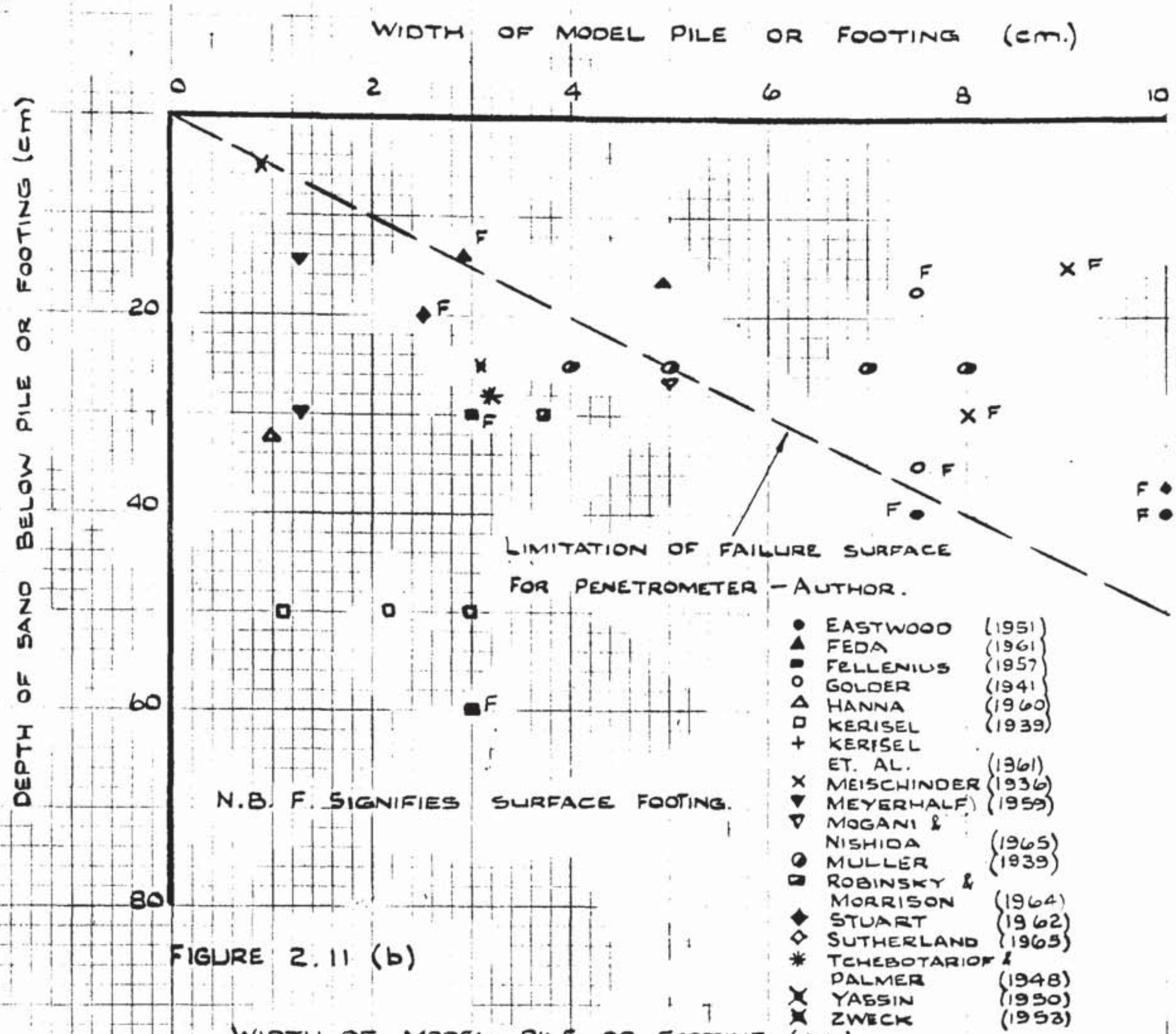

FIGURE 2.11 (b)

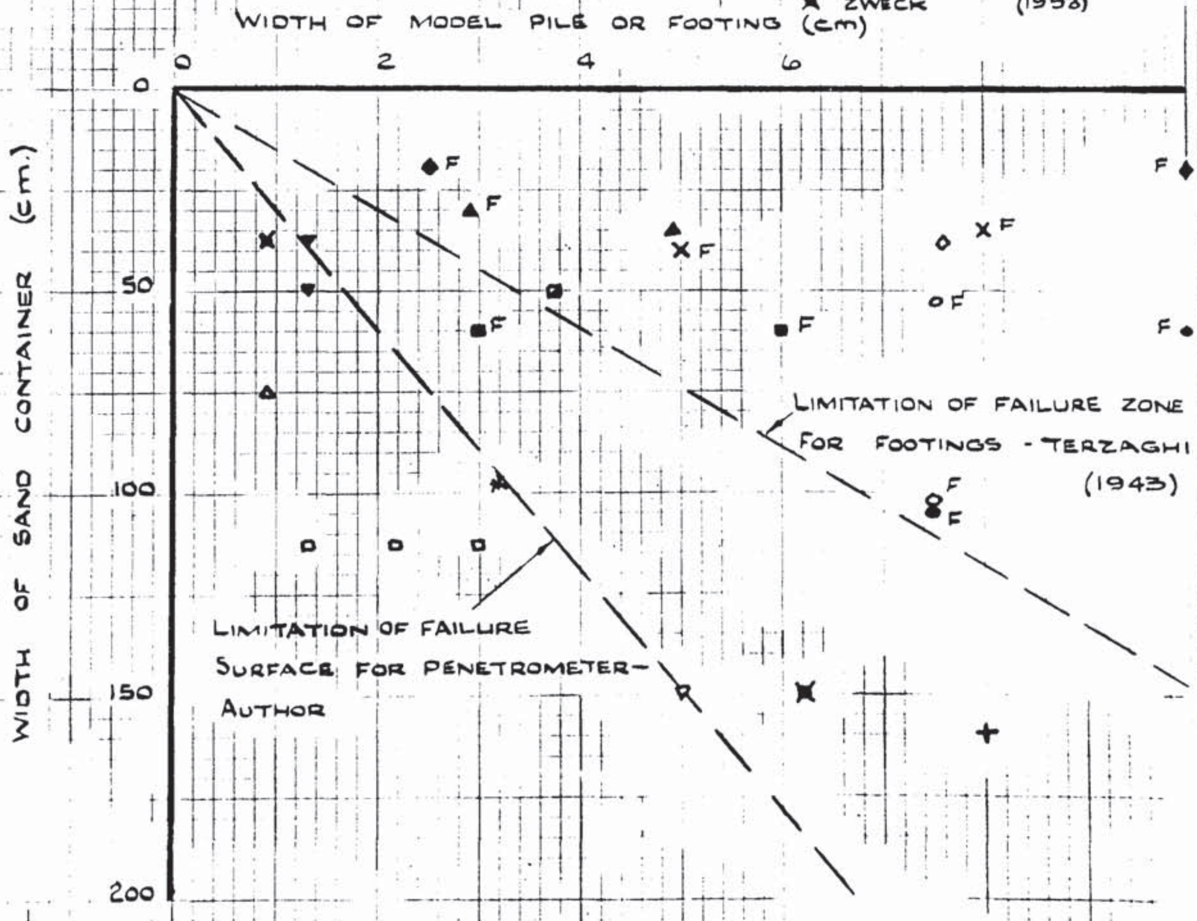

FIGURE 2.12. TOTAL AND POINT LOAD VERSUS PENETRATION FOR A 1 IN. BRASS PENETROMETER.

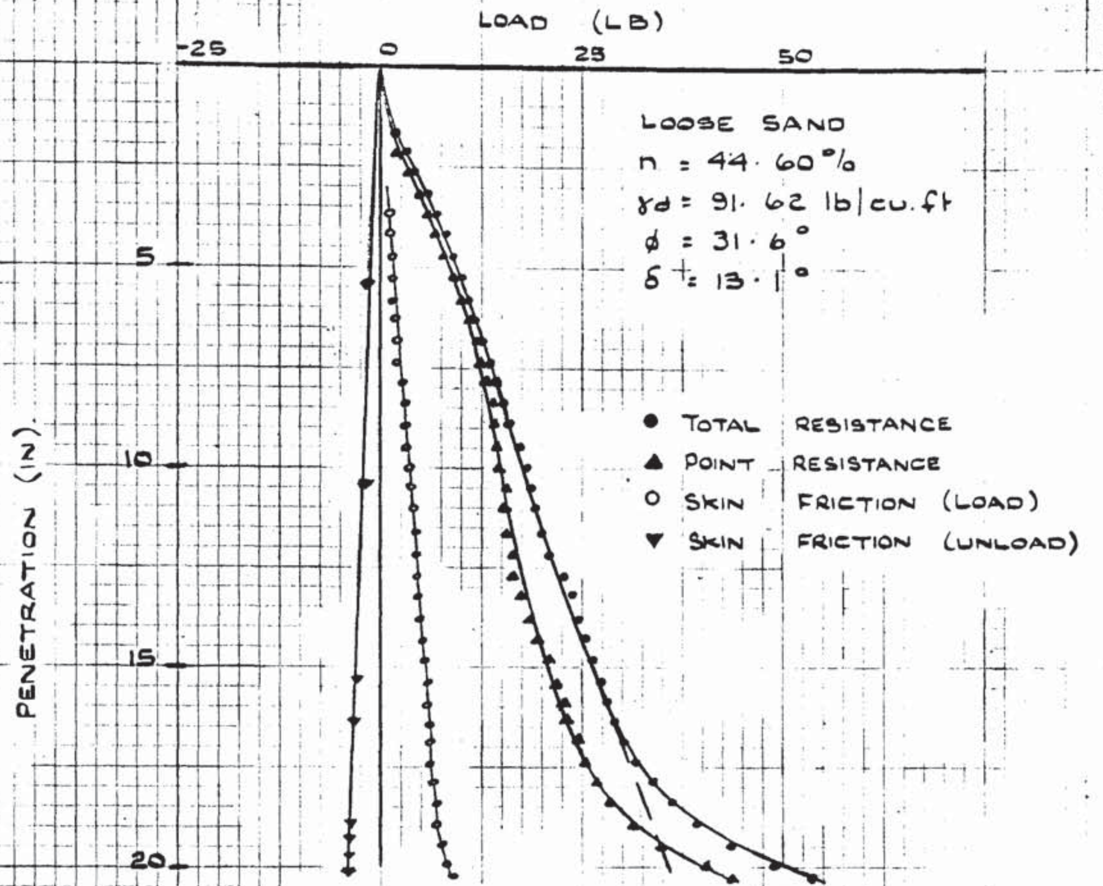

FIGURE 2.13 TOTAL AND POINT LOAD VERSUS PENETRATION FOR 1 IN. DIAMETER BRASS PENETROMETER

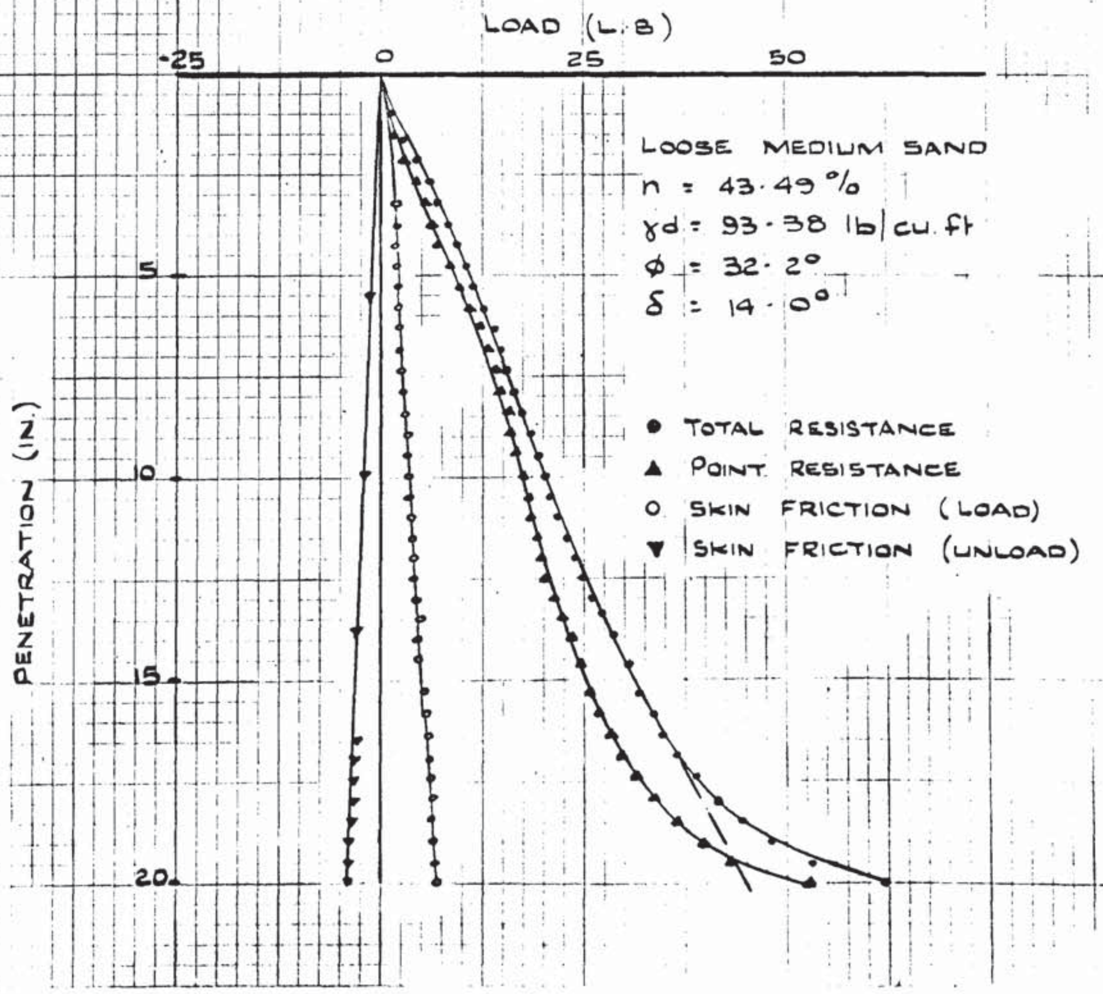

FIGURE 2.14. TOTAL AND POINT LOAD VERSUS PENETRATION FOR 1 IN. DIAMETER BRASS PENETROMETER

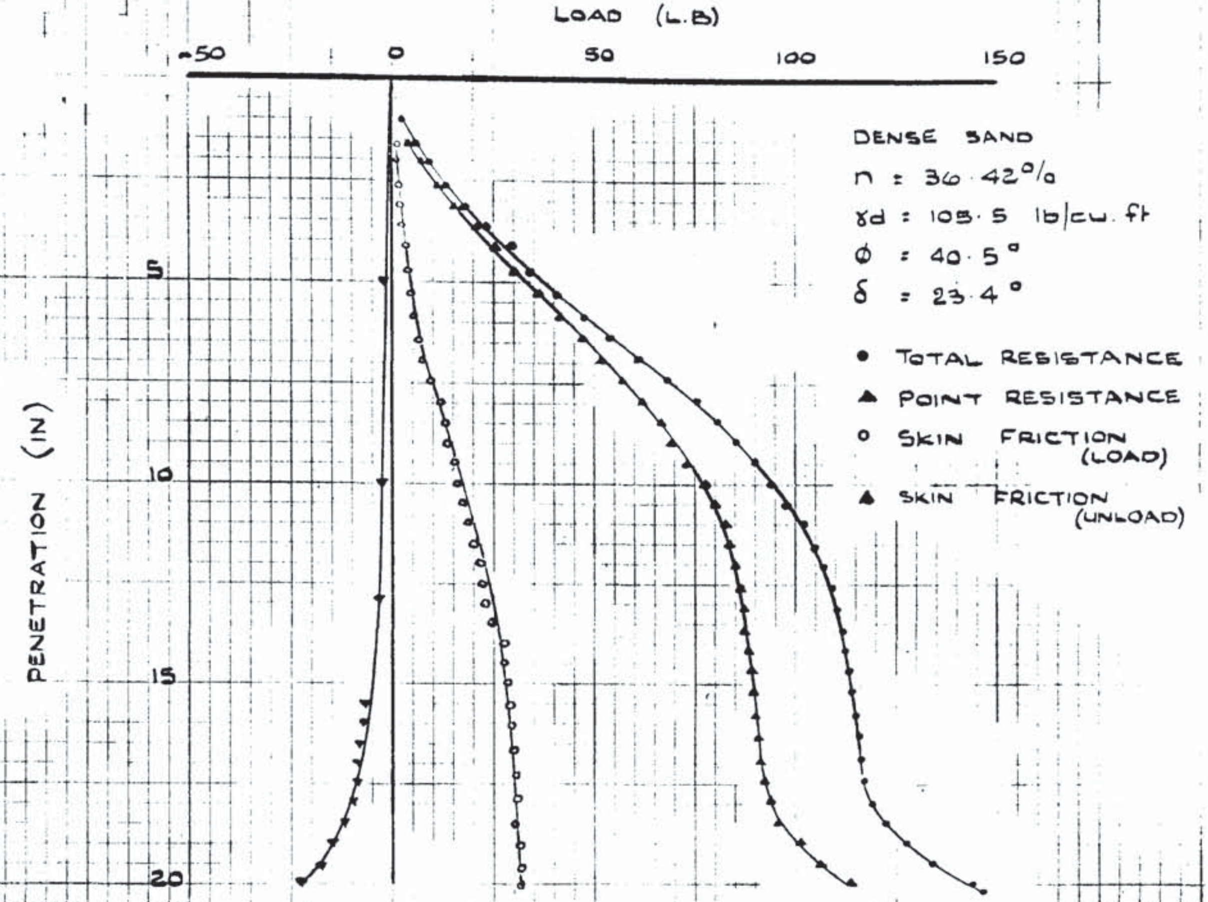

FIGURE 2.16. POINT RESISTANCE OF 1 IN. DIAMETER BRASS PENETROMETER - THEORETICAL AND EXPERIMENTAL

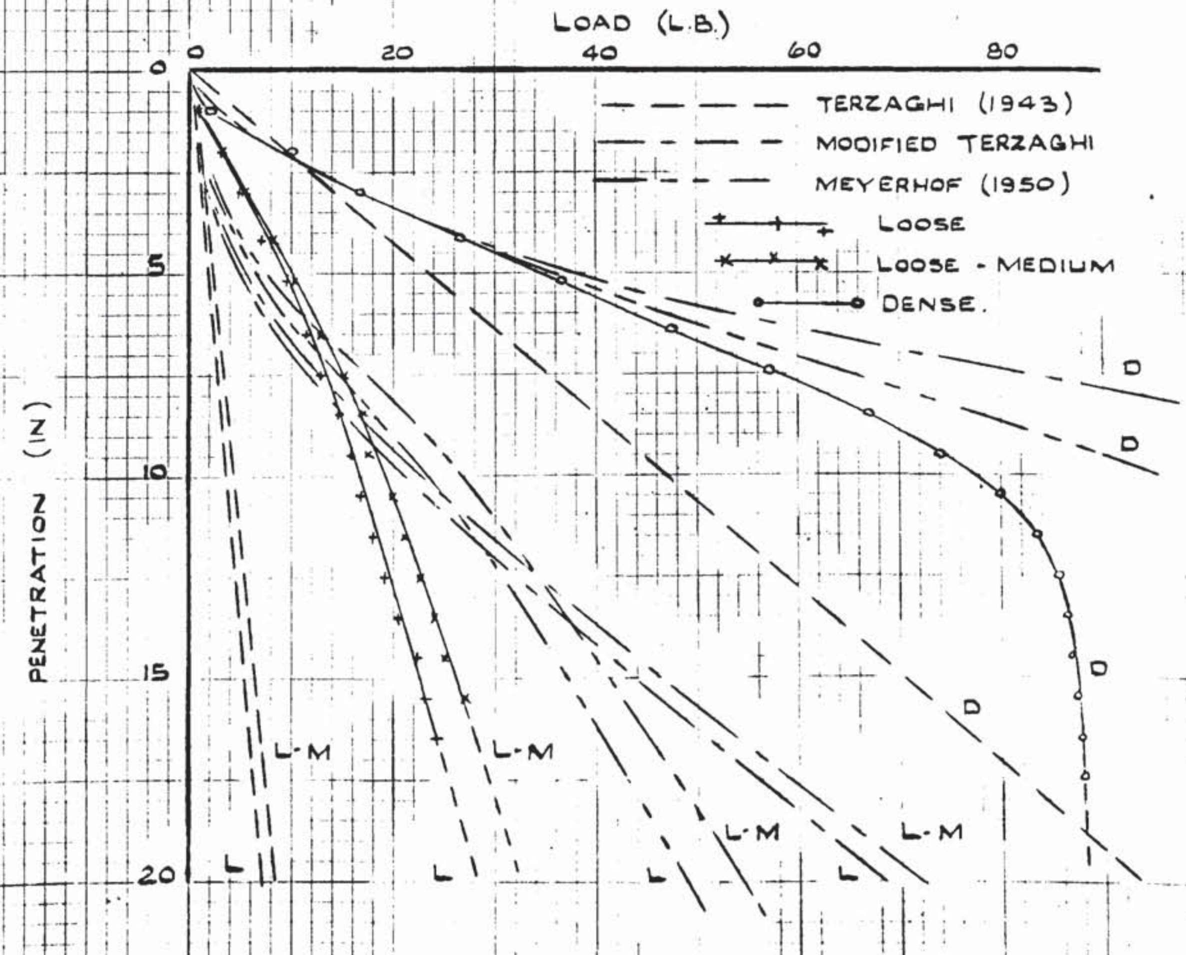

FIGURE 2.15 (a)
Kf TAN δ VERSUS PENETRATION FOR LOOSE, LOOSE - MEDIUM AND DENSE SANDS.

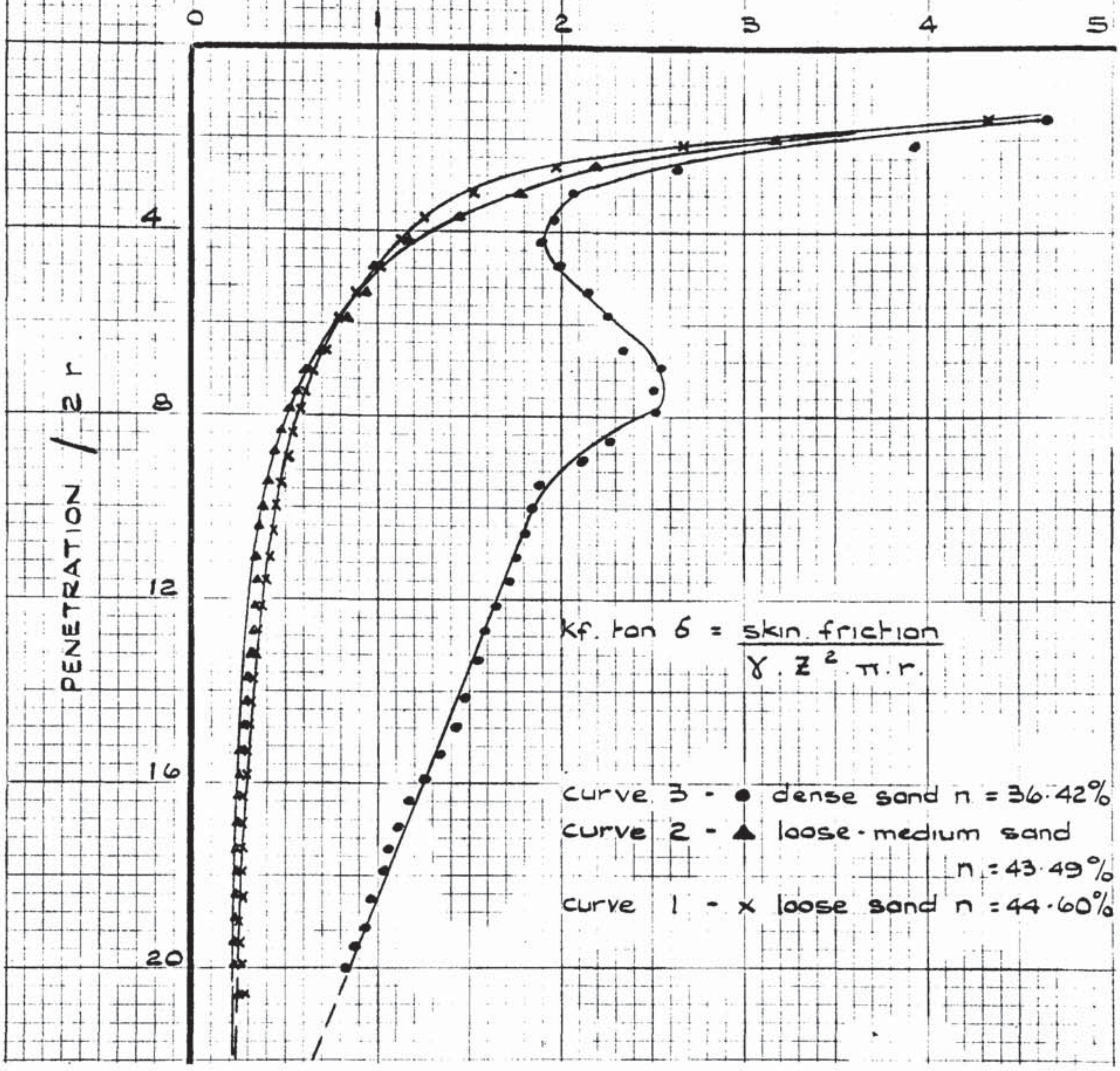

FIGURE 2.15 (b).
POSSIBLE REGIONS OF PLASTIC DEFORMATION FOR PENETROMETER.

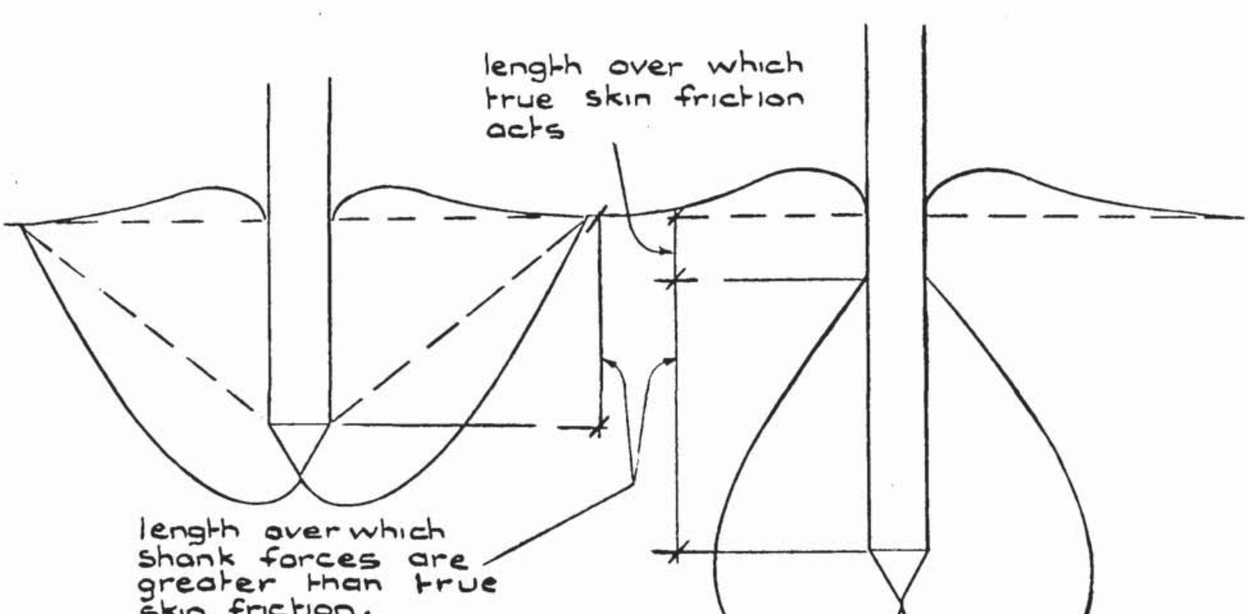

FIGURE 2.17 POINT RESISTANCE OF A 1 IN. DIAMETER BRASS PENETROMETER – THEORETICAL AND EXPERIMENTAL

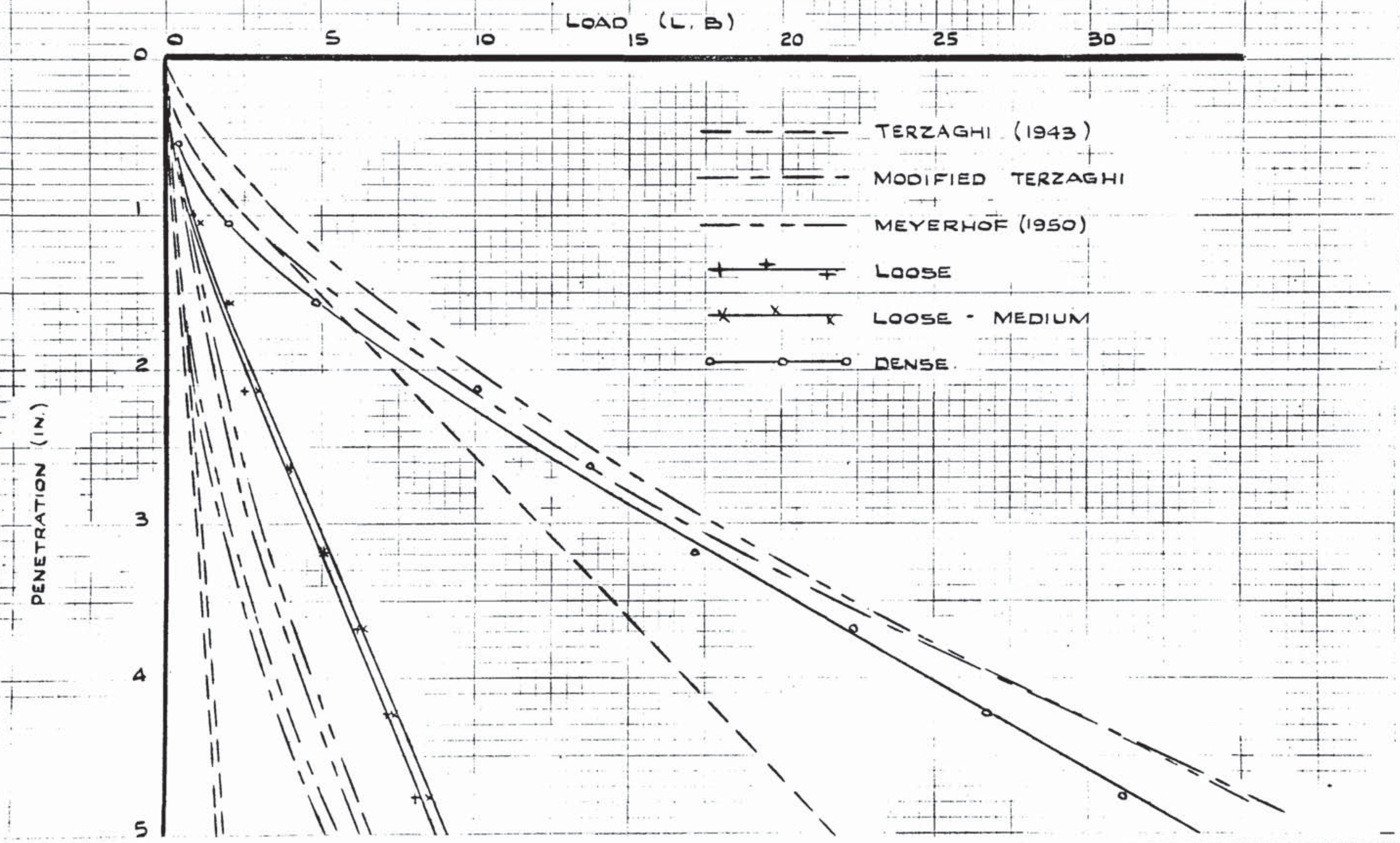

FIGURE 2.18 (a)

(i) TERZAGHI (1943) FAILURE MECHANISM FOR SHALLOW FOUNDATIONS.

(ii) MODIFIED TERZAGHI MECHANISM FOR DEEP FOUNDATIONS.

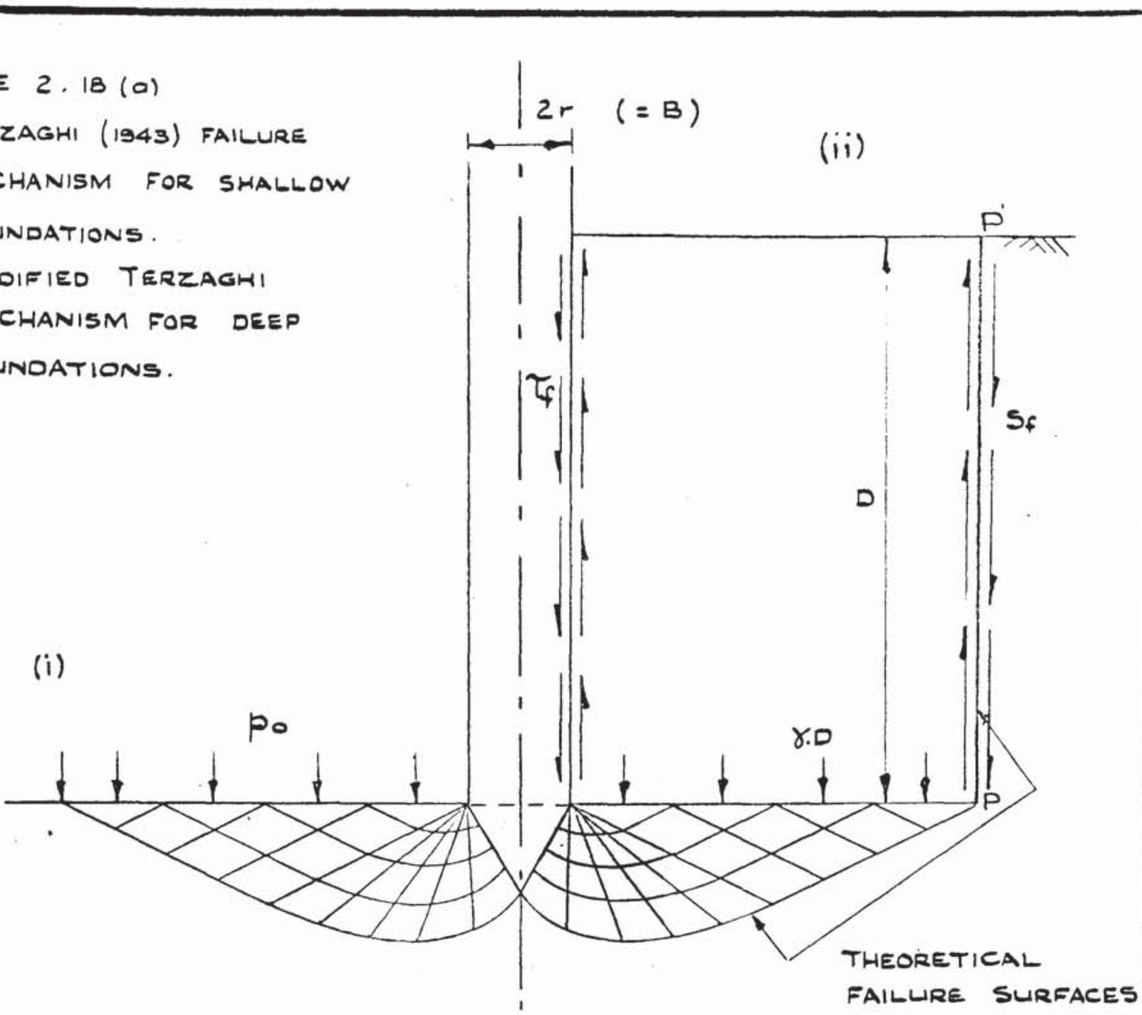

FIGURE 2.18. (b)

(i) MEYERHOF (1950) FAILURE MECHANISM FOR SHALLOW FOUNDATIONS

(ii) MEYERHOF FAILURE MECHANISM FOR DEEP FOUNDATIONS

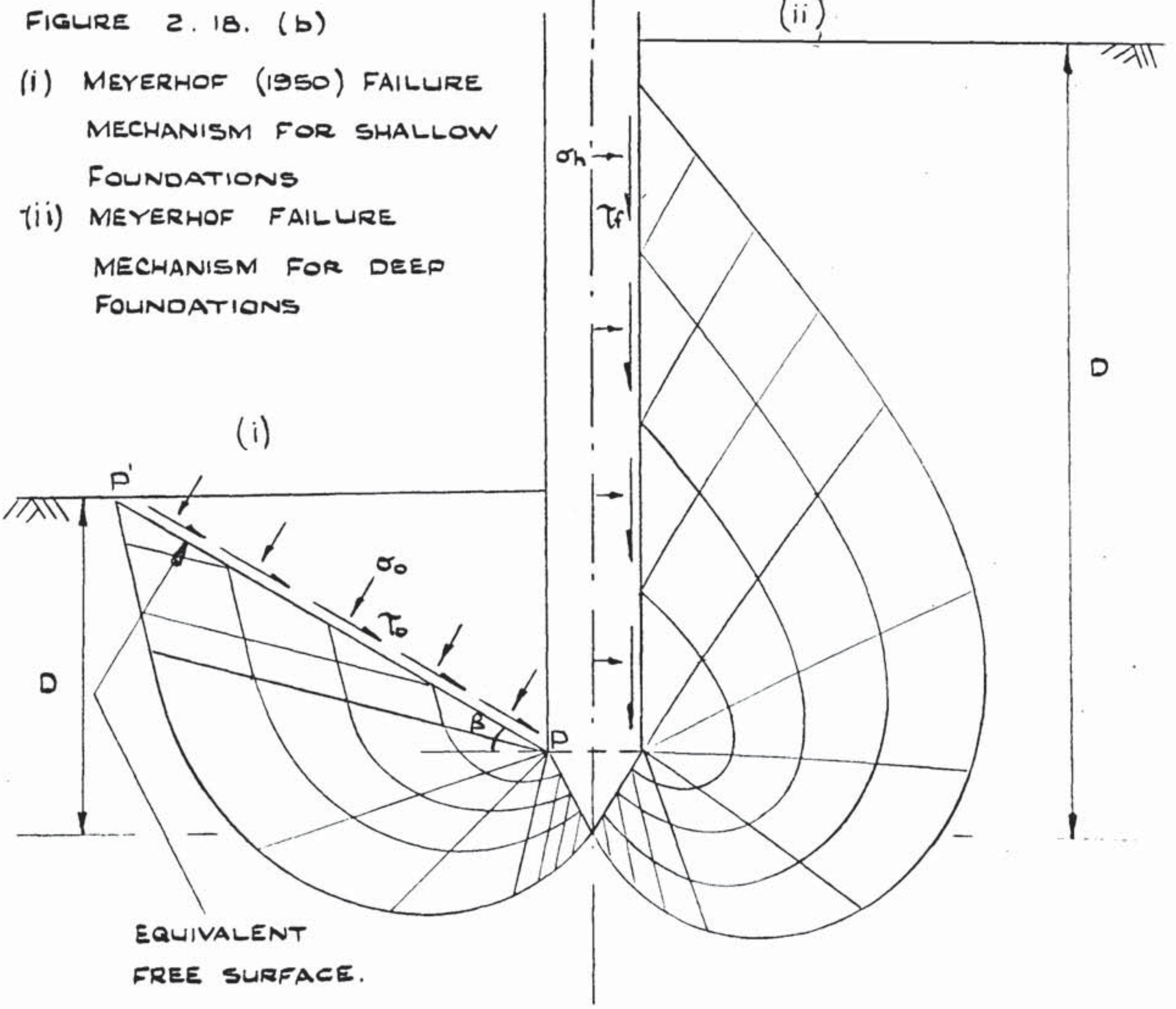

PLATE 2.1. FINE WHITE SAND USED FOR PENETRATION EXPERIMENTS

PLATE 2.2. FULL SECTION CONTAINER WITH LOAD CELL IN OPERATION

PLATE 2.1. FINE WHITE SAND USED FOR PENETRATION EXPERIMENTS

PLATE 2.2. FULL SECTION CONTAINER WITH LOAD CELL IN OPERATION

TABLE 3.1

δwo = 0·0264"
δmo = 0·0587"
δm_i = 0·0736"
} Mean of 6 measurements.

	SERIES I MEAN POROSITY %	SERIES II MEAN POROSITY %	SERIES III MEAN POROSITY %	SERIES I CORRECTION FACTOR	SERIES II CORRECTION FACTOR
LOOSE SAND	47·46 ± 0·25	46·90 ± 0·59	47·21 ± 0·24	1/1·005647 = 0·9943847	1/0·993747 = 1·0062923
DENSE SAND	36·97 ± 0·40	35·92 ± 0·39	36·54 ± 0·32		

TABLE 3.2.

TYPE OF TEST	1 BULK DENSITY lb/cu ft	2 POROSITY %	3 APERTURE COEFF. y	4** TIME OF POUR (secs)	5++ INTENSITY OF RAIN (gm/sec)	6* RATE OF FLOW PER APERTURE (gm/sec) ACTUAL	7+ THEORY	8 % DIFF OF COLS 6 & 5
LOOSEST	91·91	44·42	1·00	2·20	16273	37·4	41·9	16·7
LOOSE - MEDIUM	92·09	44·31	0·778	2·75	13018	29·8	28·6	-4·3
C. V. R.	93·80	43·28	0·617	3·64	9835	22·5	20·7	-9·2
MEDIUM	95·59	42·19	0·507	4·81	7443	17·1	13·2	-28
MEDIUM - DENSE	103·23	37·57	0·247	16·9	2118	4·9	3·6	-33
DENSE	104·34	36·90	0·064	171·3	208·8	0·48	0·32	-50
DENSEST POSSIBLE	104·90	35·59	0·059	222·5	160·9	0·37	0·23	-60

** For 3" pour time was mean of 6 tests

++ Calculated from known vol. of hopper and density of sand - giving weight of sand per pour (g)

* Obtained by dividing col. 5 by no. of apertures (15 x 29)

\+ i.e. $q = Qm . yD^{1.8}$ where Qm is col. 6 for y = 1·0

TABLE 3.3.

	LOOSEST SAND	LOOSE-MEDIUM SAND	SAND AT C.V.R.	MEDIUM SAND	MEDIUM DENSE SAND	DENSE SAND	DENSEST POSSIBE SAND
APERTURE COEFF. y.	1·000	0·778	0·617	0·507	0·247	0·064	0·055
INITIAL POROSITY OF 18" SAND %	44·42	44·31	43·28	42·19	37·57	36·90	36·56
INTENSITY PER APERTURE gm	37·41	29·83	22·54	17·06	4·85	0·48	0·37
INITIAL HEADS FOR PERM.'Y TESTS.	29·30 / 22·20	29·40 / 22·10	29·75 / 21·75	30·05 / 21·45	31·60 / 19·90	31·90 / 19·60	31·80 / 19·70
HEAD DIFF Δh_1	7·10	7·30	8·00	8·60	11·70	12·30	12·10
DIFF. IN HEADS DURING km TEST	33·20 / 20·30	32·90 / 18·60	32·70 / 18·80	32·50 / 19·00	32·60 / 18·90	32·00 / 19·50	31·90 / 19·60
HEAD DIFF Δh_2	7·90	7·10	6·00	4·90	1·90	0·20	0·20
DIFF. IN HEADS FOR 5 am TEST	33·66 / 17·90	33·05 / 18·45	32·75 / 18·75	32·55 / 18·95	32·85 / 18·65	32·15 / 19·35	32·00 / 19·50
HEAD DIFF Δh_3	8·60	7·10	6·00	5·00	2·50	0·50	0·40
k_{a1} +	11·01	10·78	9·81	9·15	6·72	6·39	6·58
k_{a2} *	12·29	11·24	9·91	9·07	6·70	6·14	5·81
k_{a3} **	11·49	11·15	9·80	8·99	5·12	3·15	2·43

+ $k_{a1} = 78.6725 / \Delta h_1$

* $k_{a2} = 2.6287 \cdot qm / \Delta h_2$

** $k_{a3} = 2.6287 \cdot qm / \Delta h_3$

TABLE 3.4.

TEST No.	OVERALL (BULK) POROSITY %	MEAN OF INDIVIDUAL (CONTAINER) POROSITIES %	ST. DEV. OF INDIVIDUAL POROSITIES	% DIFF. BETWEEN OVERALL AND INDIV. POROSITIES
DENSE 1	37·43	37·09	± 0·22	0·90
" 2	37·42	36·65	± 0·16	2·06
" 3	37·57	36·70	± 0·15	2·31
" 4	37·74	36·96	± 0·52	2·07
" 5	37·38	36·77	± 0·31	1·63
" 6	37·52	36·68	± 0·19	2·24
MEAN	37·51 ± 0·23	36·80 ± 0·19		1·89
DENSE S1	36·82	36·13	± 0·12	1·87
" S2	36·69	35·96	± 0·10	1·99
MEAN	36·76 ± 0·07	36·04 ± 0·09		1·95
LOOSE 1	44·57	44·24	± 0·27	0·74
" 2	44·70	44·57	± 0·20	0·42
" 3	44·56	44·38	± 0·31	0·40
MEAN	44·61 ± 0·10	44·38 ± 0·14		0·51
LOOSE S1	44·83	44·53	± 0·09	0·67
" S2	44·62	44·34	± 0·04	0·63
" S3	44·72	44·44	± 0·16	0·62
MEAN	44·72 ± 0·11	44·43 ± 0·1		0·64
MEDIUM 1	43·75	43·49	± 0·16	0·59
" 2	43·64	43·38	± 0·17	0·60
MEAN	43·70 ± 0·05	43·43 ± 0·06		0·62
MEDIUM S1	42·62	42·26	± 0·09	0·84
" S2	42·74	42·48	± 0·10	0·61
" S3	42·71	42·42	± 0·09	0·68
MEAN	42·69 ± 0·07	42·39 ± 0·13		0·70
MEDIUM 3	39·96	39·60	± 0·24	0·90

* DENOTES SUCTION

TABLE 3.5.

TEST No.	MEASURED DRY DENSITY (lb/cu.ft)	MEAN POROSITY LAYER 1 %	MEAN POROSITY LAYER 2 %	MEAN POROSITY LAYER 3 %	MEAN INDIVIDUAL POROSITY % (COLUMN 3 TABLE 3.4)	POROSITY LIMIT %
DENSE 1	103·47	37·31	37·07	36·89	37·09	± 0·22
" 2	103·48	36·49	36·65	36·82	36·65	± 0·16
" 3	103·23	36·85	36·69	36·56	36·70	± 0·15
" 4	102·94	36·44	37·28	37·16	36·96	± 0·52
" 5	103·55	36·46	36·98	36·87	36·77	± 0·31
" 6	103·32	36·87	36·64	36·53	36·68	± 0·19
DENSE S1	104·47	36·01	36·19	36·19	36·13	± 0·12
" S2	104·69	35·86	36·02	36·00	35·96	± 0·10
LOOSE 1	91·65	44·51	44·05	44·16	44·24	± 0·27
" 2	91·44	44·71	44·47	44·35	44·51	± 0·20
" 3	91·68	44·69	44·08	44·37	44·38	± 0·31
LOOSE S1	91·23	44·57	44·40	44·62	44·53	± 0·13
" S2	91·58	44·32	44·32	44·38	44·34	± 0·04
" S3	91·40	44·58	44·46	44·28	44·44	± 0·16
MEDIUM 1	93·1	43·58	43·53	43·36	43·49	± 0·16
" 2	93·19	43·38	43·54	43·21	43·38	± 0·17
MEDIUM S1	94·87	42·20	42·23	42·35	42·26	± 0·09
" S2	94·69	42·58	42·43	42·43	42·48	± 0·10
" S3	94·73	42·40	42·51	42·35	42·42	± 0·09
MEDIUM 3	99·28	39·84	39·45	39·59	39·60	± 0·24

* S DENOTES SUCTION.

FIGURE 3.1. DEVELOPMENT OF POURING METHODS FOR VARIABLE SUCTION APPARATUS

3.1(i) POURER OVERLAPPING CONTAINER

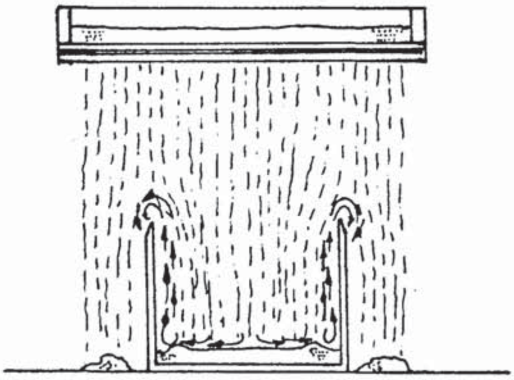

3.1.(ii) POURER AND CONTAINER SAME SIZE

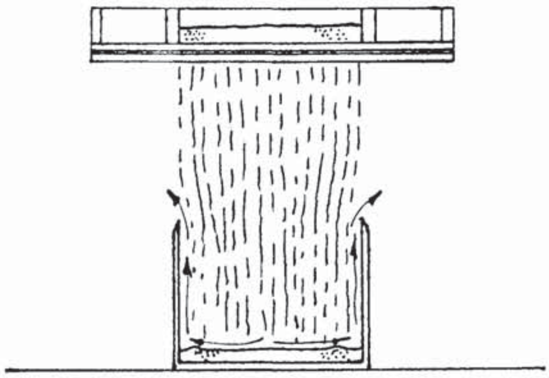

3.1(iii) AS (ii) WITH PERMEABLE CONTAINER BASE

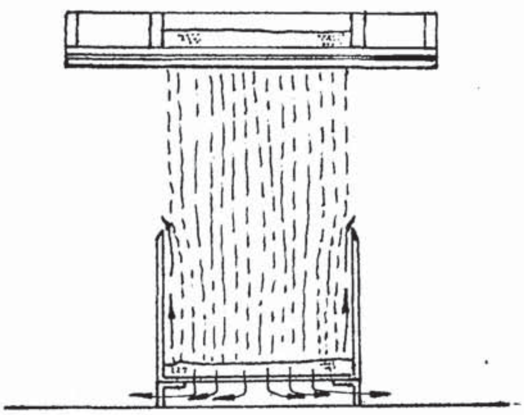

3.1.(iv) IDEAL CONDITION - AIR ENTERING EQUALS AIR FORCED OUT

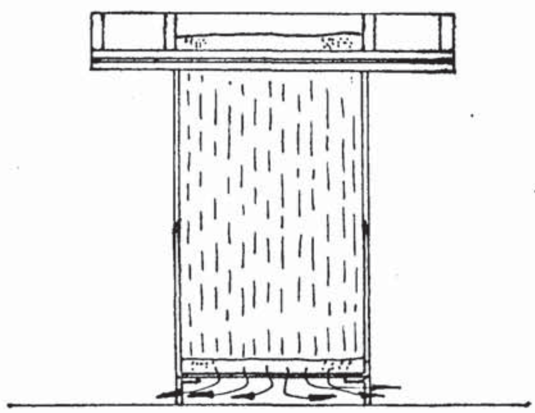

3.1.(v) ACTUAL CONDITION WITH FLUME.

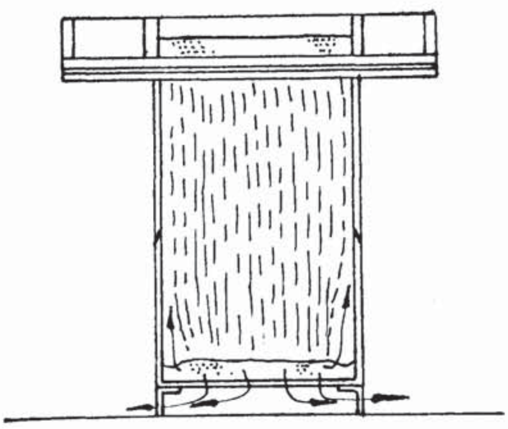

3.1(vi) POURER WITH FLUME AND SUCTION BASE TO CONTAINER.

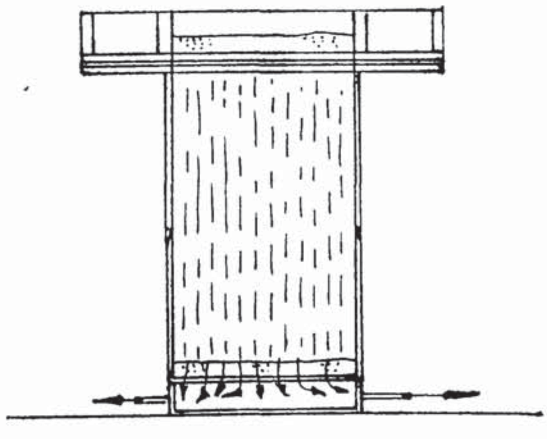

FIGURE 3. 2. PATTERN OF $\frac{1}{2}$ IN. DIAM. HOLES WITH LATERAL AND LONGITUDINAL SPACINGS

SCALE : FULL SIZE

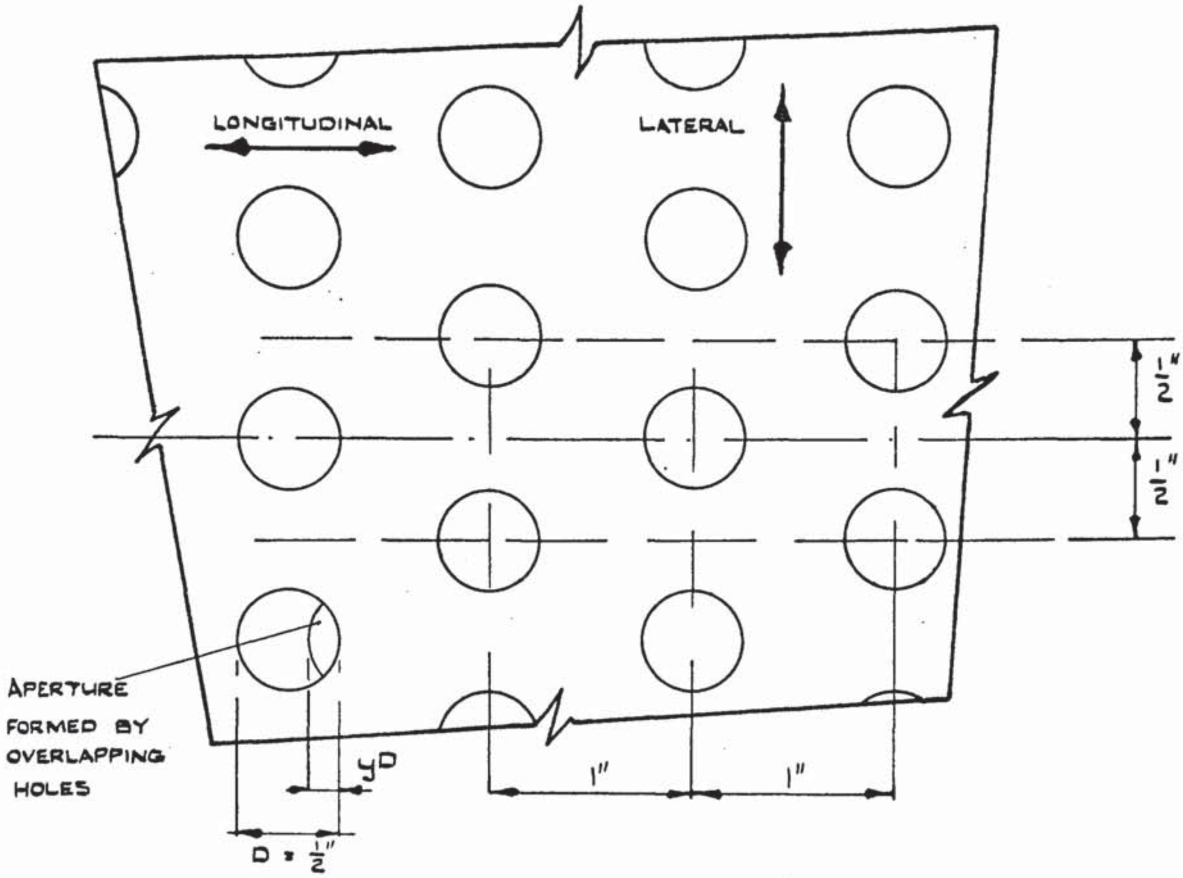

FIGURE 3. 3. ELEVATION OF VARIABLE APERTURE SECTION OF DEPOSITION APPARATUS

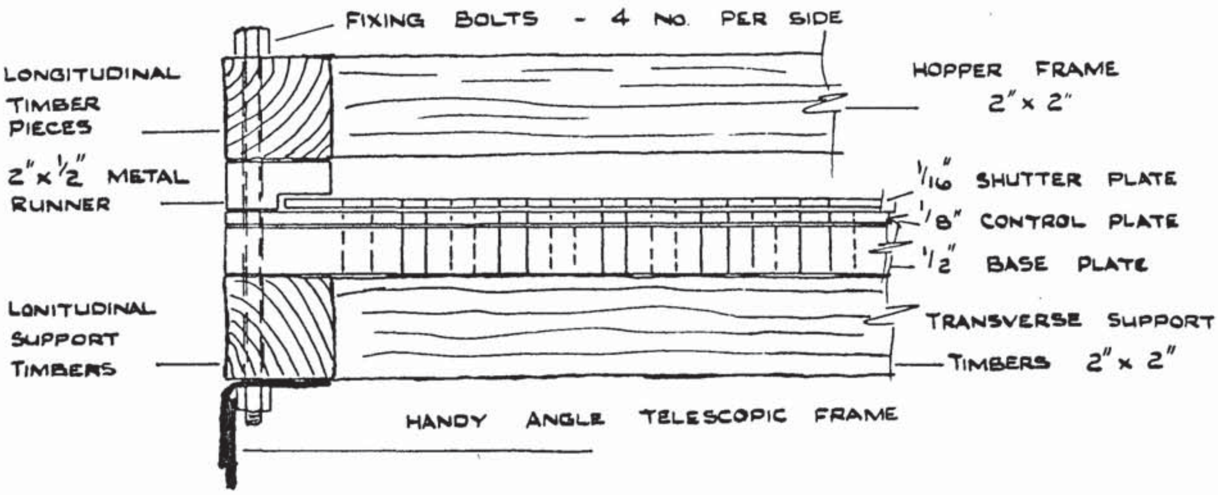

FIGURE 3. 5 SAMPLING CONTAINERS SHOWING FLEXIBLE BASE DEFLECTIONS

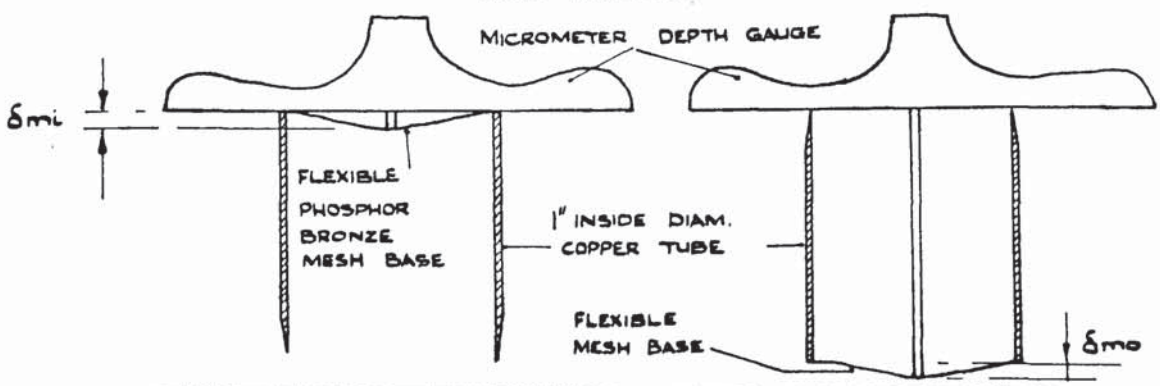

FIGURE 3.4. DIAGRAMMATIC DRAWING OF MANOMETER USED IN DEPOSITION EXPERIMENTS.

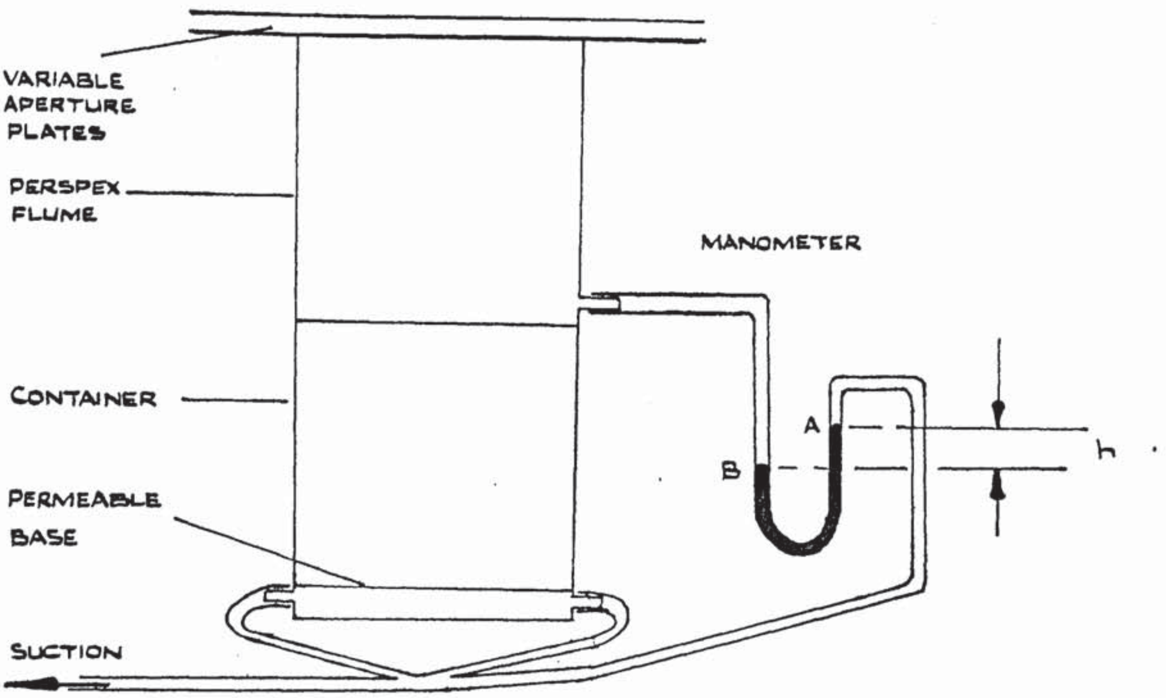

FIGURE 3.6. THEORETICAL AND EXPERIMENTAL RATES OF DEPOSITION FOR VARIABLE APERTURE HOPPER

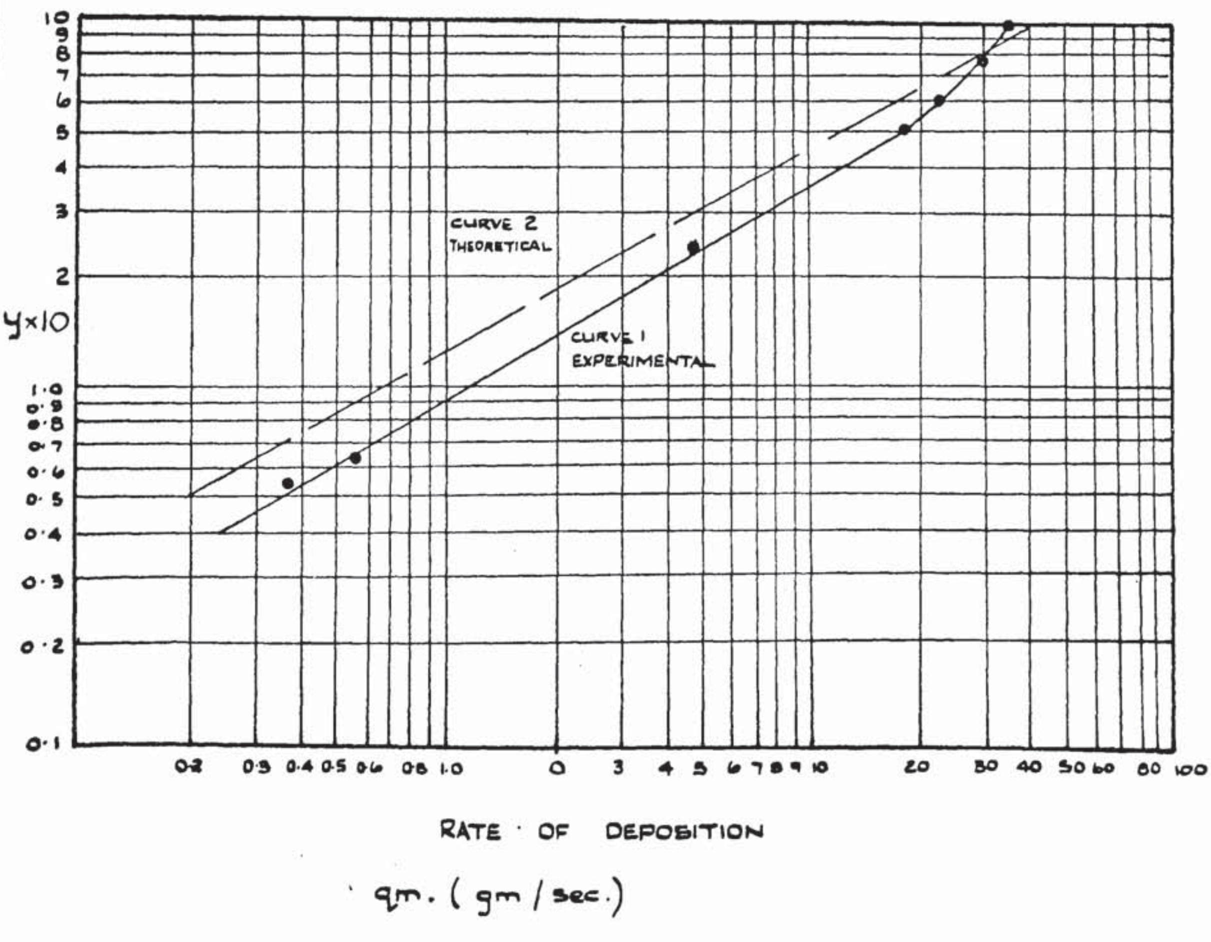

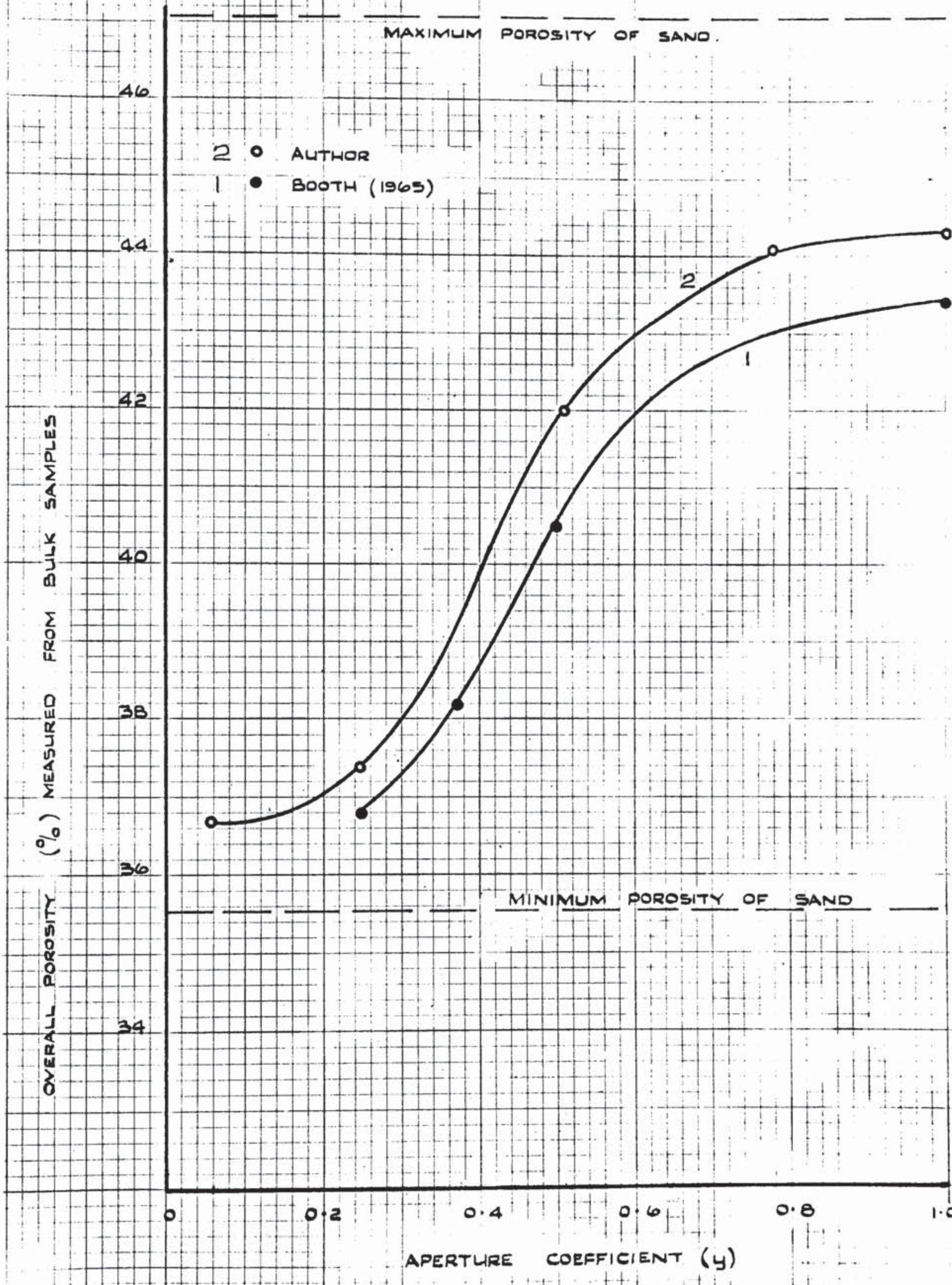

FIGURE 3.7. COMPARISON OF RESULTS OF EXISTING AND MODIFIED SAND POURER.

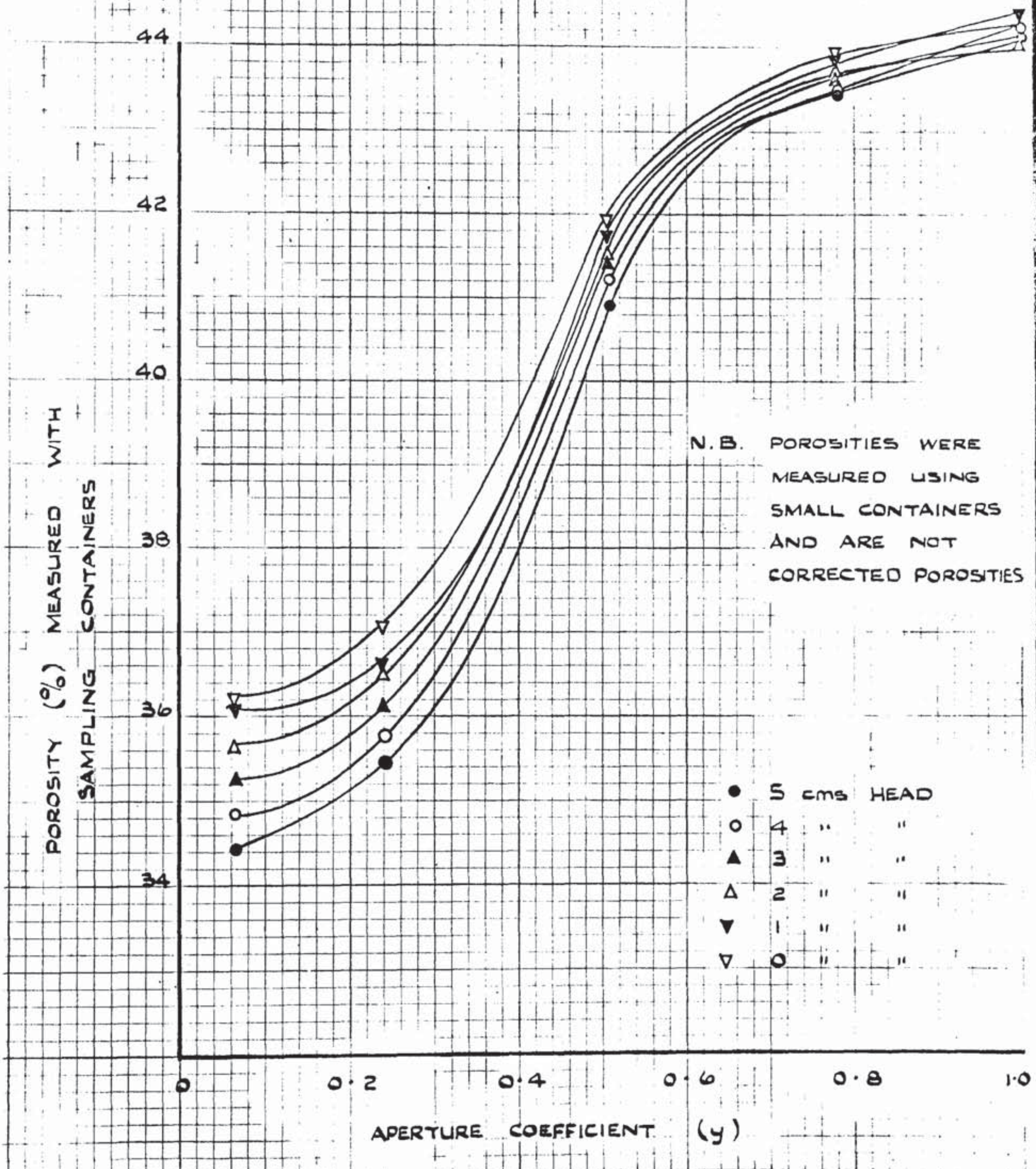

FIGURE 3.8 EFFECTS OF NEGATIVE PRESSURE ON THE FINAL POROSITY.

FIGURE 3.9. COMPARISON OF COEFFICIENTS OF PERMEABILITY WITH AND WITHOUT SUCTION

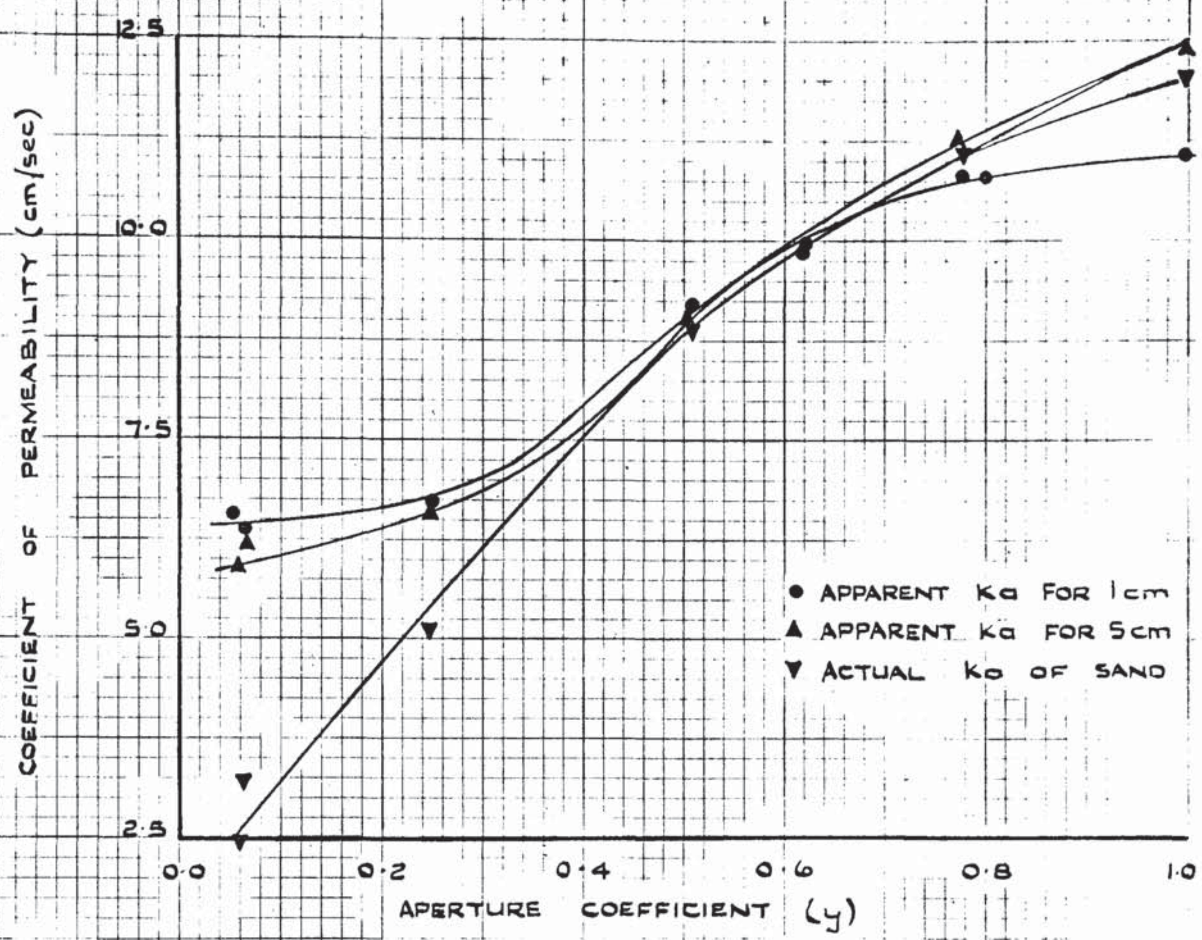

FIGURE 3.10 RELATIONSHIP BETWEEN OVERALL AND MEAN INDIVIDUAL POROSITIES

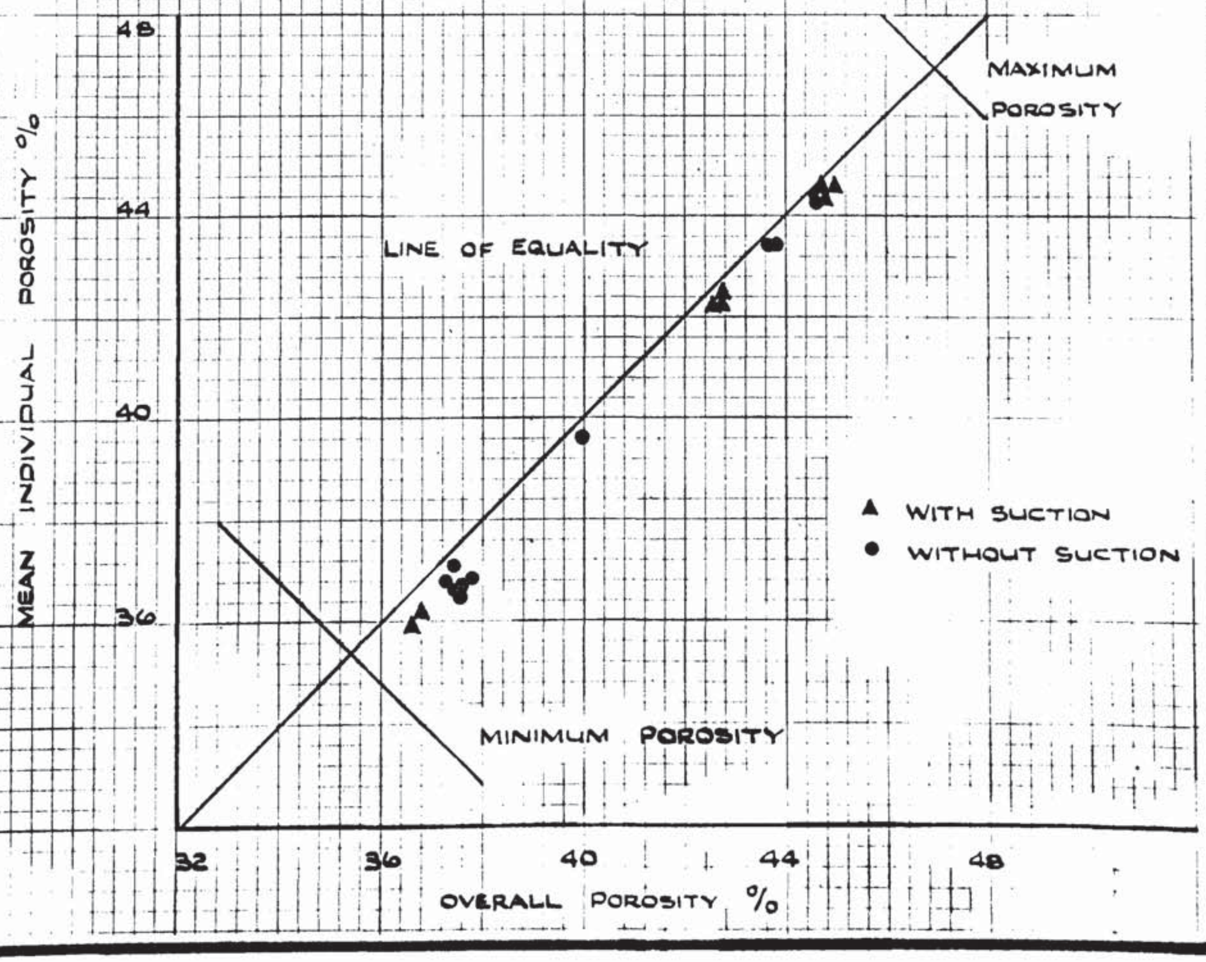

PLATE 3.1. SAND DEPOSITION APPARATUS

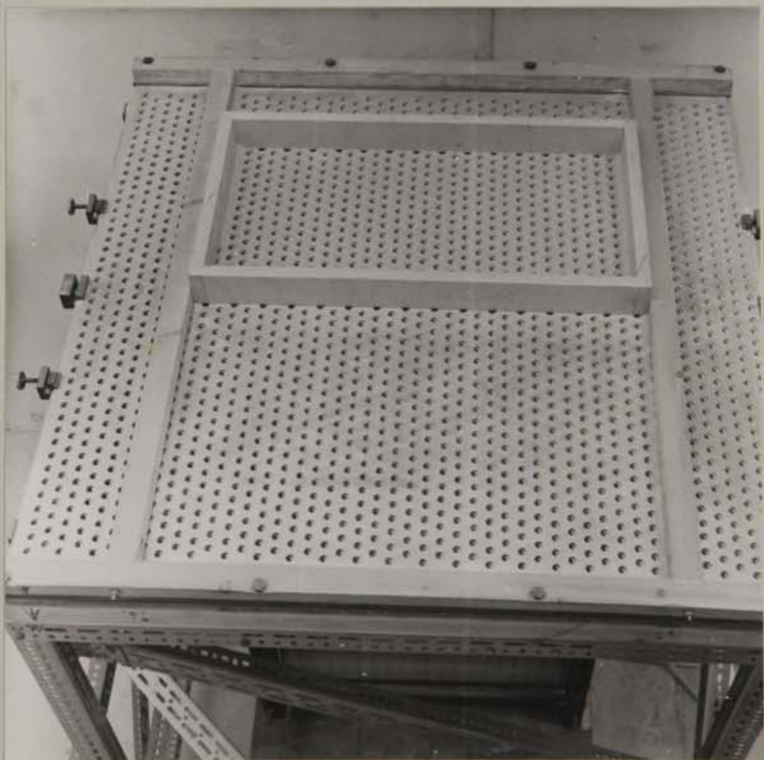

PLATE 3.2. VARIABLE APERTURE HOPPER

TABLE 4.1

PRESSURE CELL CORRECTION MATRICES

PRESSURE CELL 1

7.06134	0.31777	0.16737
0.17639	7.07121	0.23187
0.192440	0.22236	7.08163

PRESSURE CELL 2

7.08136	0.21330	0.61217
0.18316	7.09132	0.41365
0.19210	0.31116	7.00236

PRESSURE CELL 3

7.09241	0.21364	0.19538
0.21076	7.09423	0.30140
0.19538	0.30276	7.09622

PRESSURE CELL 5

7.07331	0.20811	0.31700
0.16635	7.09162	0.18236
0.19976	0.30116	7.07276

PRESSURE CELL 6

7.10023	0.18866	0.19011
0.3161 0	7.08416	0.26131
0.21932	0.24467	7.09521

PRESSURE CELL 7

7.08779	0.21364	0.21713
0.18731	7.09124	0.31762
0.19376	0.31084	7.09571

PRESSURE CELL 8

7.08433	0.32172	0.31281
0.19799	7.09211	0.31876
0.23615	0.18334	7.08369

PRESSURE CELL 9

7.09441	0.18317	0.19933
0.24310	7.08632	0.18720
0.20634	0.18212	7.09317

PRESSURE CELL 0

7.08412	0.18611	0.18228
0.29340	7.06331	0.16313
0.19869	0.30421	7.10311

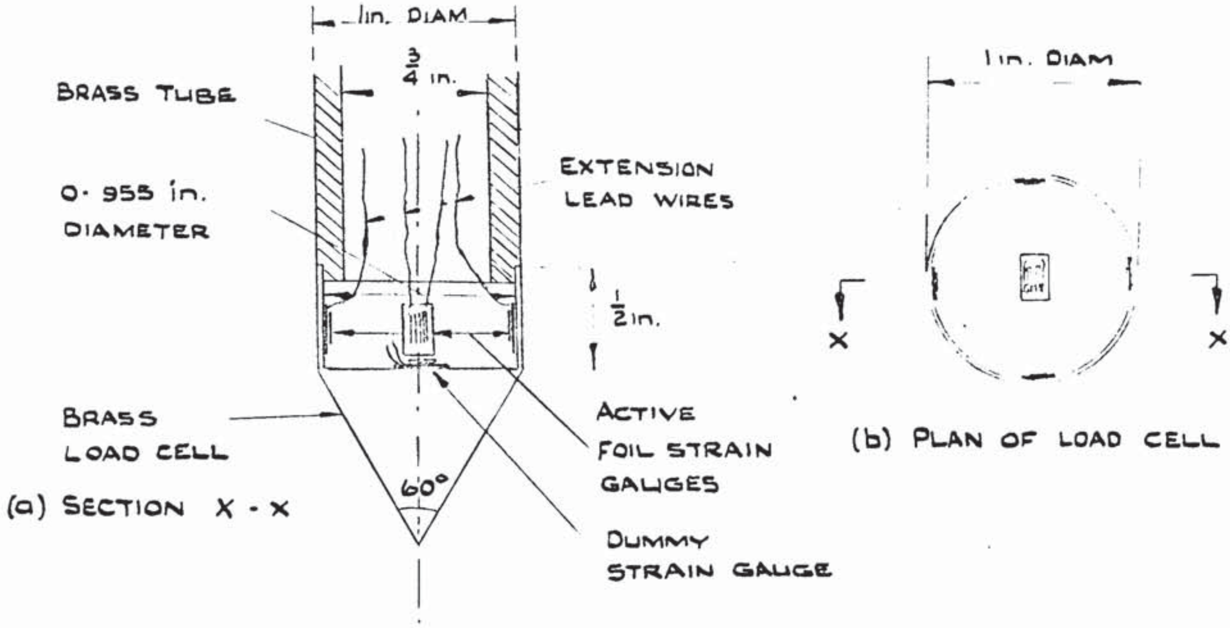

FIGURE 4.1. PENETROMETER LOAD CELL

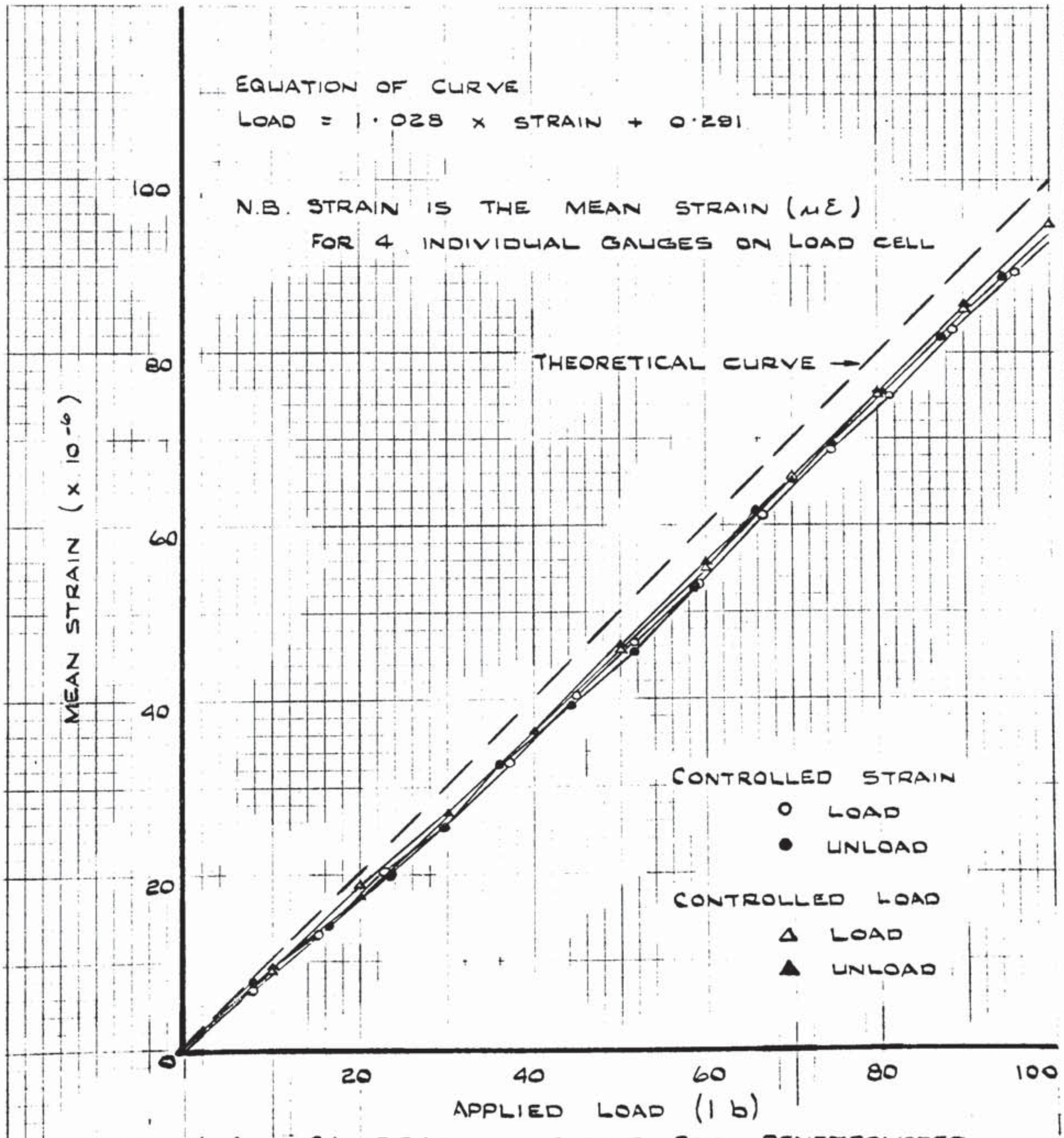

FIGURE 4.2. CALIBRATION CURVE FOR PENETROMETER LOAD CELL - LOAD VERSUS STRAIN

FIGURE 4.3. DISTRIBUTION OF RADIAL STRAIN ON A UNIFORMLY LOADED CIRCULAR DIAPHRAGM WITH CLAMPED EDGES (TIMOSHENKO - THEORY OF PLATES AND SHELLS).

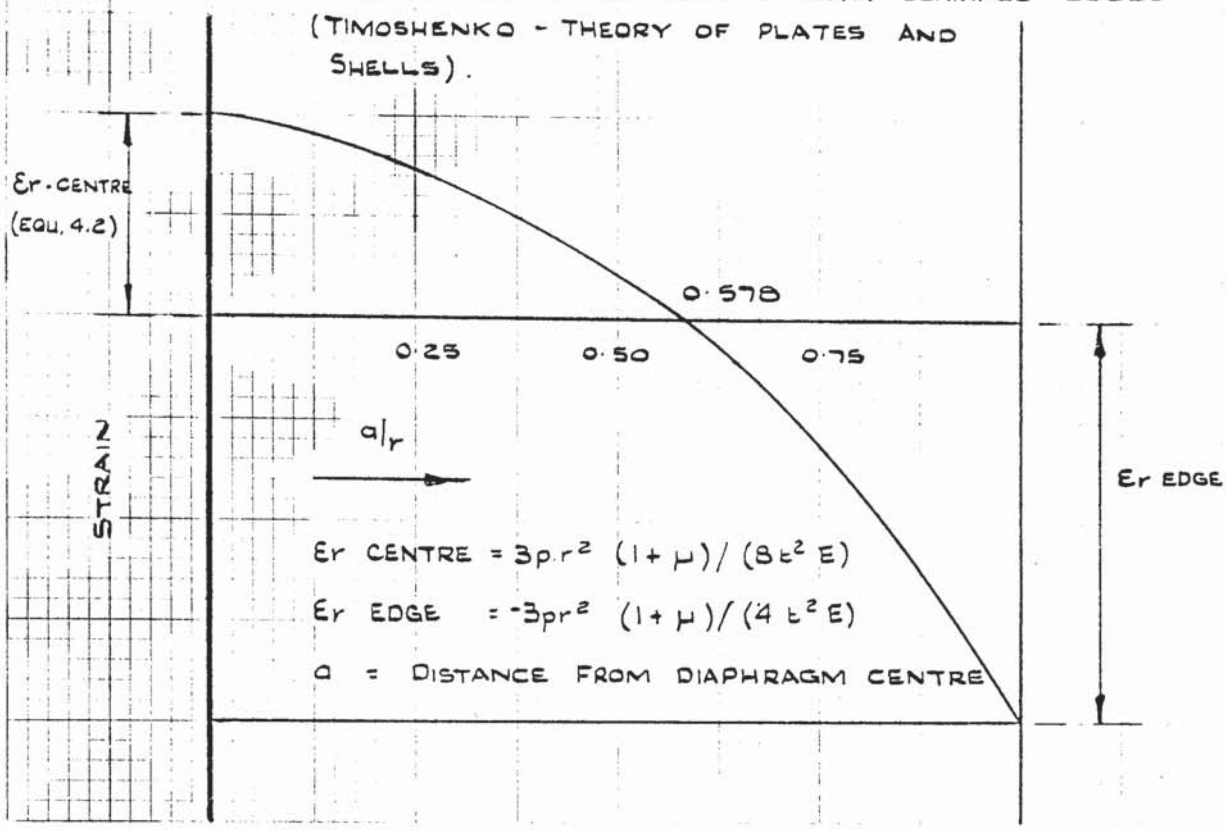

FIGURE 4.4 MILD STEEL PRESSURE CELL FRAME

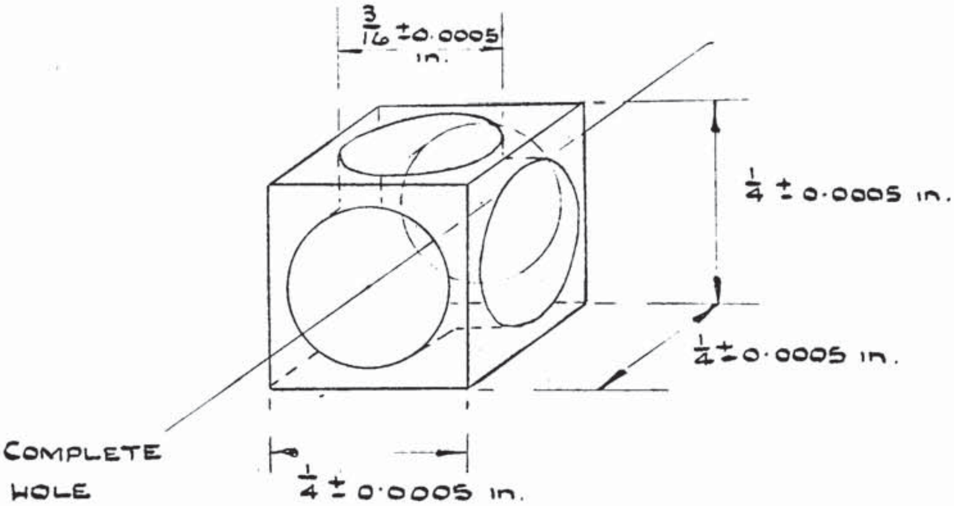

FIGURE 4.5 (a) SIDE AND (b) END DIAPHRAGMS - SPRING STEEL

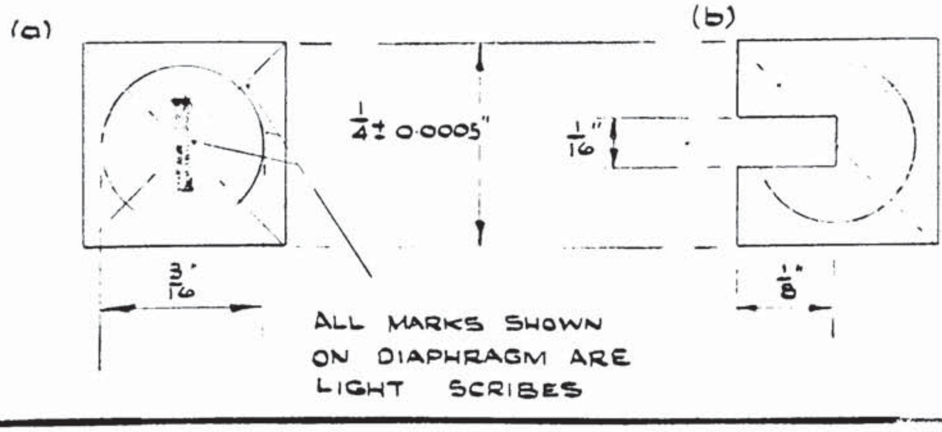

FIGURE 4.6 WHEATSTONE BRIDGE CIRCUIT AS USED IN CONJUNCTION WITH RECORDING OSCILLOGRAPH

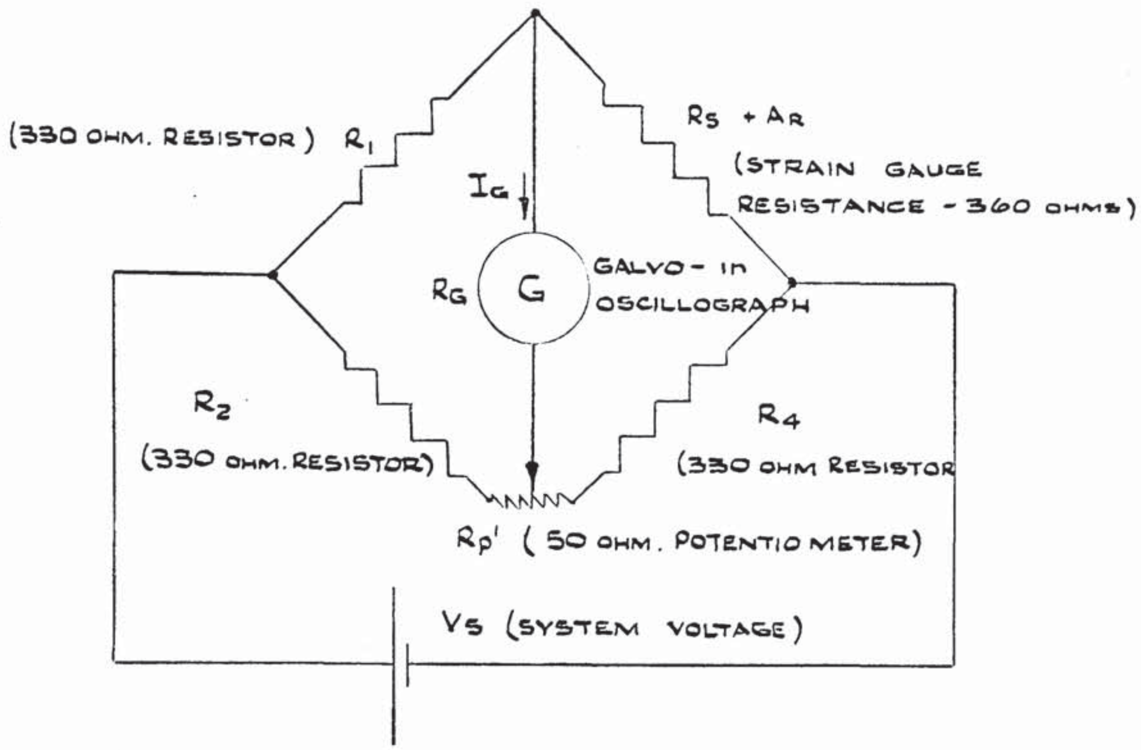

FIGURE 4.7. THEORETICAL PRESSURE DISTRIBUTION ACROSS A CELL FACE AFTER ALLWOOD (1956).

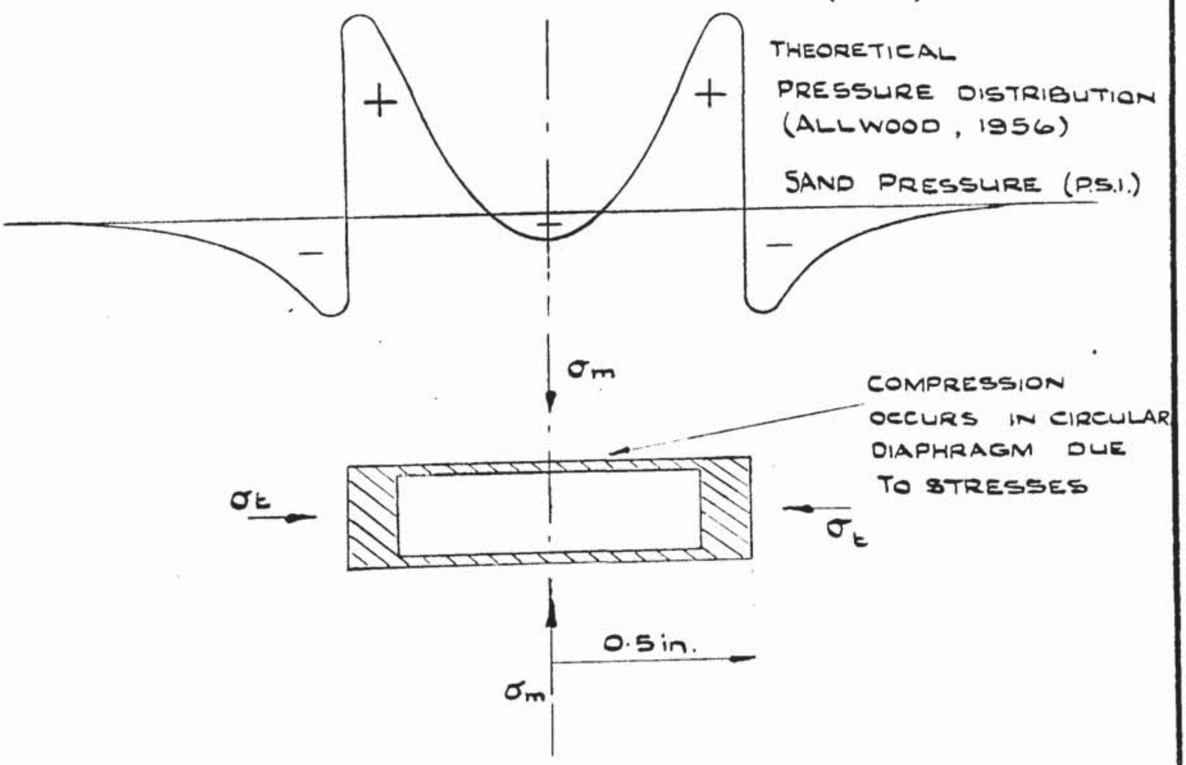

FIGURE 4.8. STRESSES IN A SAND MASS ADJACENT TO A ONE DIMENSIONAL PRESSURE CELL.

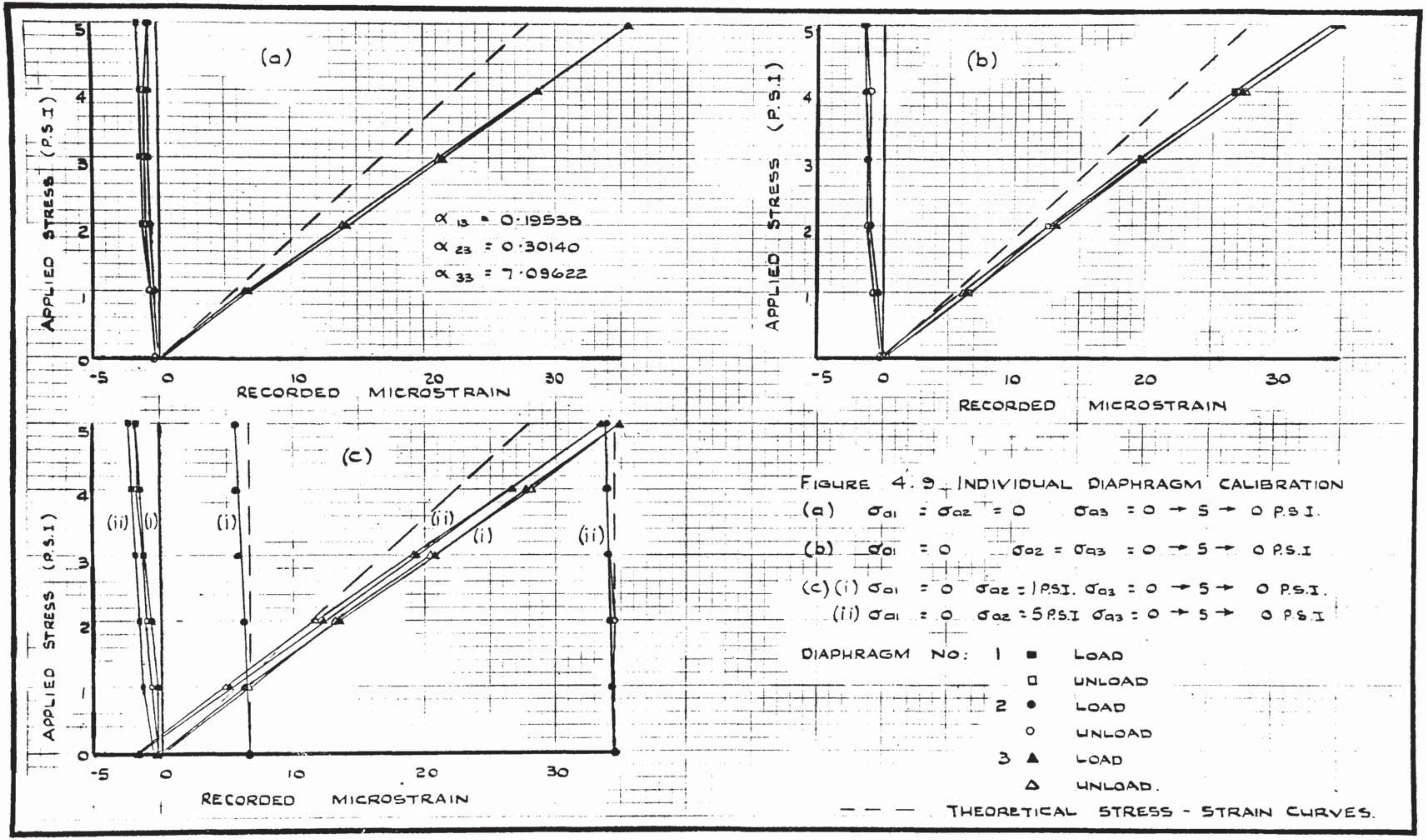

FIGURE 4.9 INDIVIDUAL DIAPHRAGM CALIBRATION

(a) $\sigma_{a1} = \sigma_{a2} = 0 \quad \sigma_{a3} = 0 \rightarrow 5 \rightarrow 0$ P.S.I.

(b) $\sigma_{a1} = 0 \quad \sigma_{a2} = \sigma_{a3} = 0 \rightarrow 5 \rightarrow 0$ P.S.I

(c) (i) $\sigma_{a1} = 0 \quad \sigma_{a2} = 1$ P.S.I. $\sigma_{a3} = 0 \rightarrow 5 \rightarrow 0$ P.S.I.

(ii) $\sigma_{a1} = 0 \quad \sigma_{a2} = 5$ P.S.I $\sigma_{a3} = 0 \rightarrow 5 \rightarrow 0$ P.S.I

DIAPHRAGM NO: 1 ■ LOAD
□ UNLOAD
2 ● LOAD
○ UNLOAD
3 ▲ LOAD
△ UNLOAD.

— — — THEORETICAL STRESS - STRAIN CURVES.

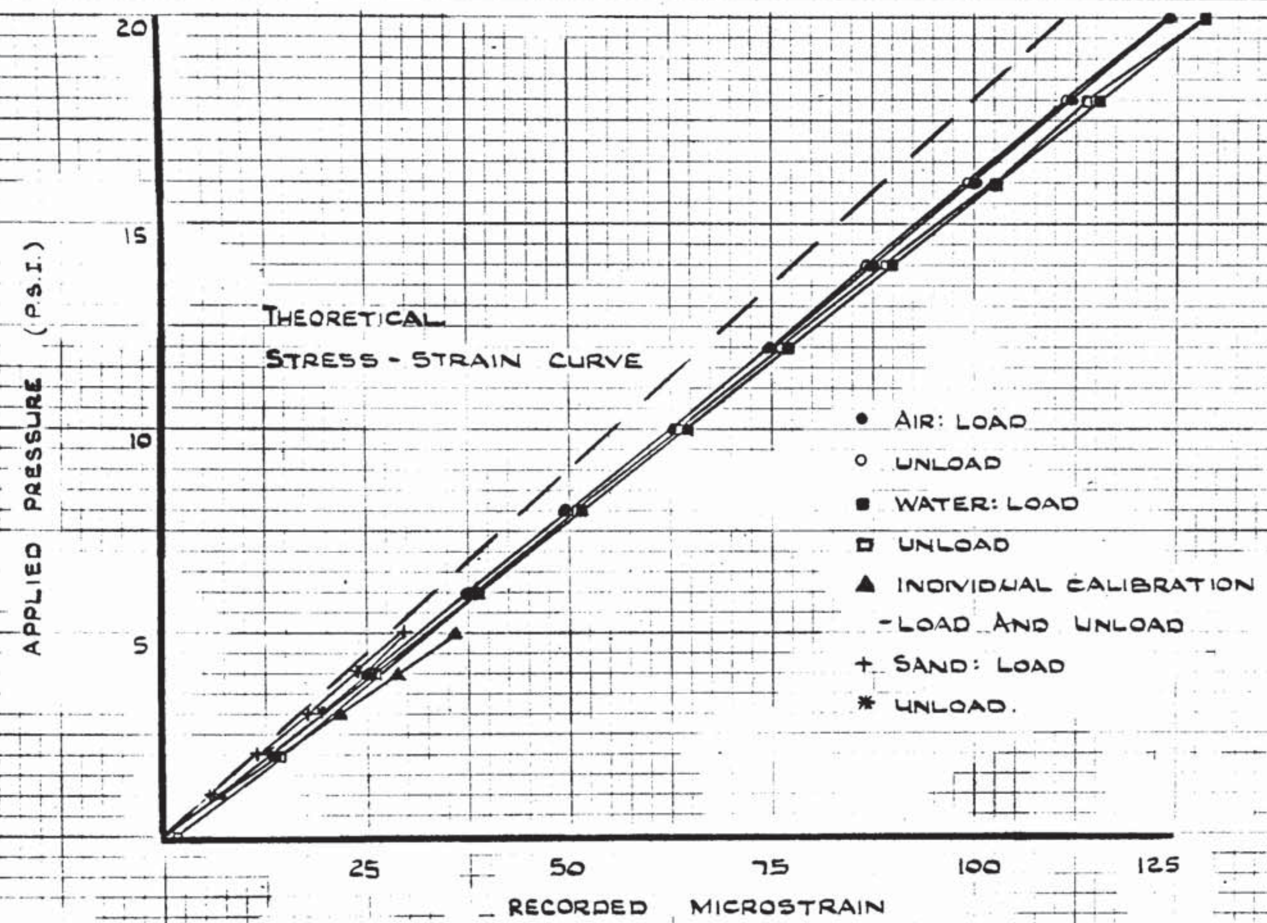

FIGURE 4. 10. INDIVIDUAL, EQUAL ALL-ROUND AIR, WATER AND SAND PRESSURE ON DIAPHRAGM N° 1. PRESSURE CELL N°3.

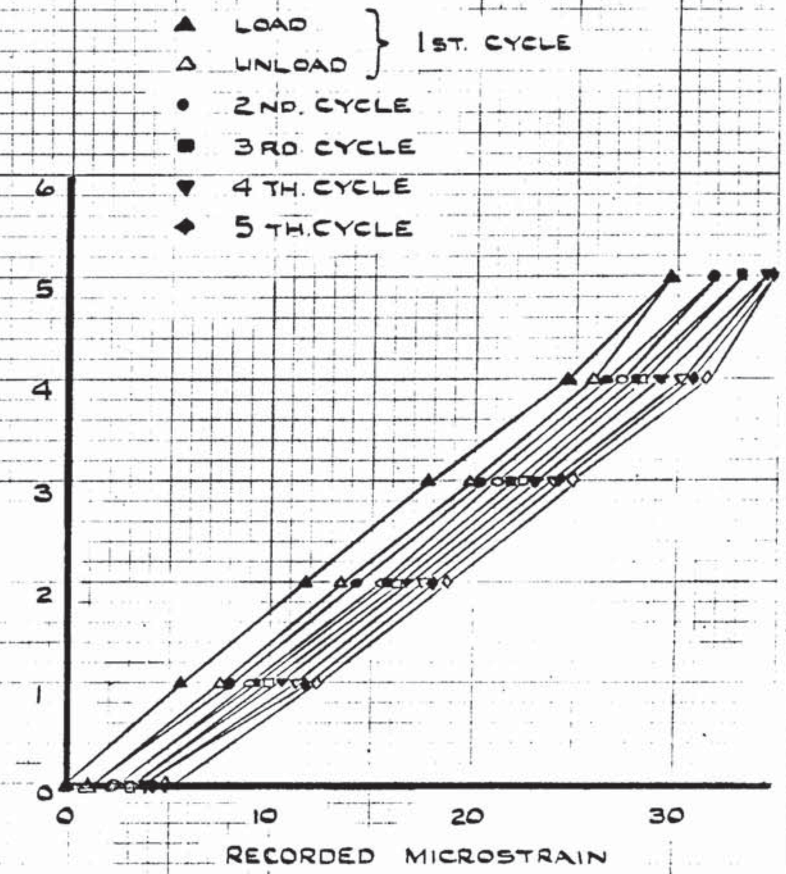

FIGURE 4. 11. PRESSURE CELL NO. 3
DIAPHRAGM N° 1
LOAD - UNLOAD CYCLES UP TO 5 P.S.I FOR EQUAL ALL ROUND SAND PRESSURE

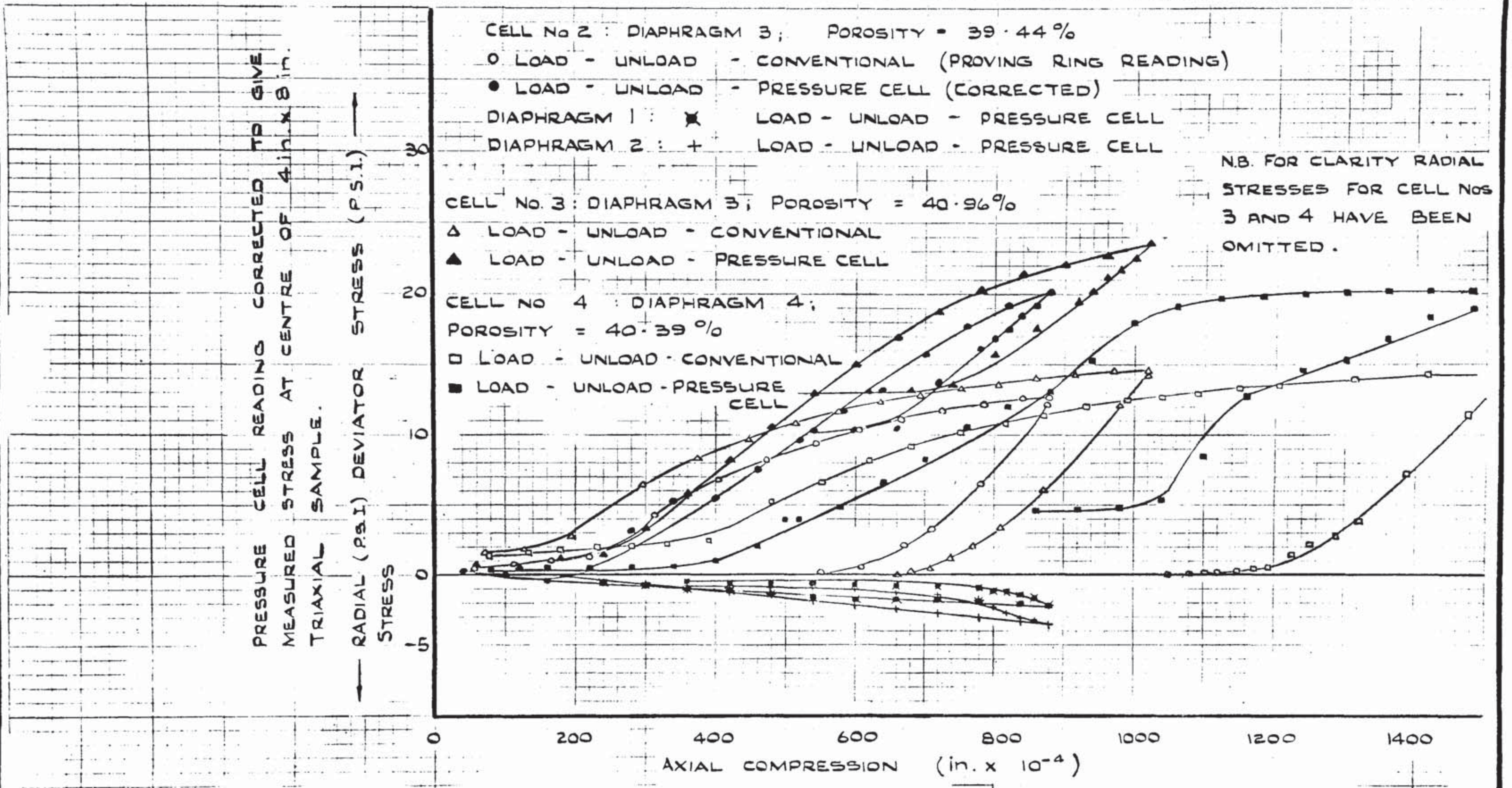

FIGURE 4.12 TRIAXIAL TESTS ON 4 in DIAMETER x 8 in. HIGH SAND SAMPLES AT CELL PRESSURE OF 5 P.S.I.

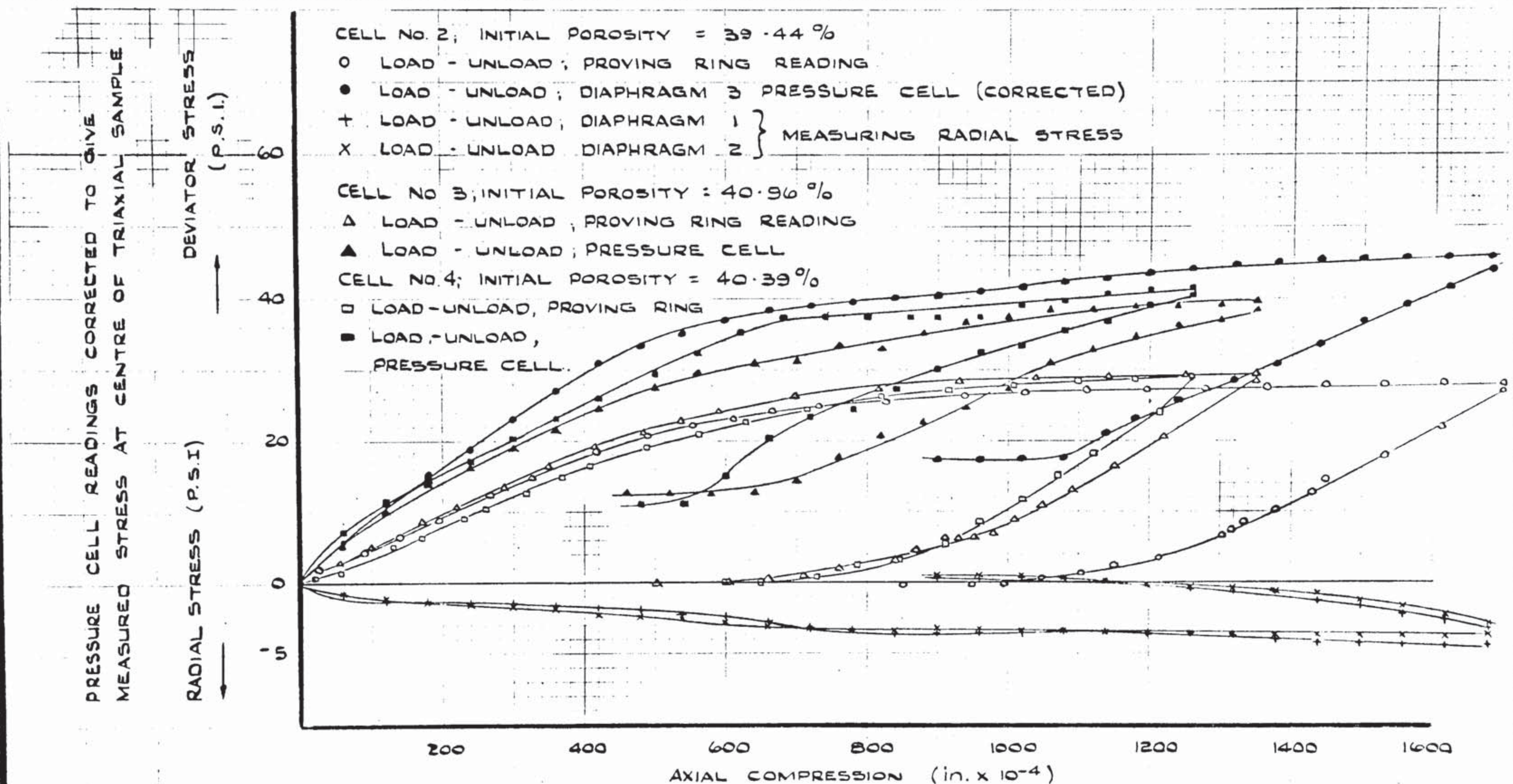

FIGURE 4.13. TRIAXIAL TESTS ON 4 in. DIAMETER x 8 in. HIGH SAND SAMPLES AT CELL PRESSURE OF 10 P.S.I. (ie. σ_3)

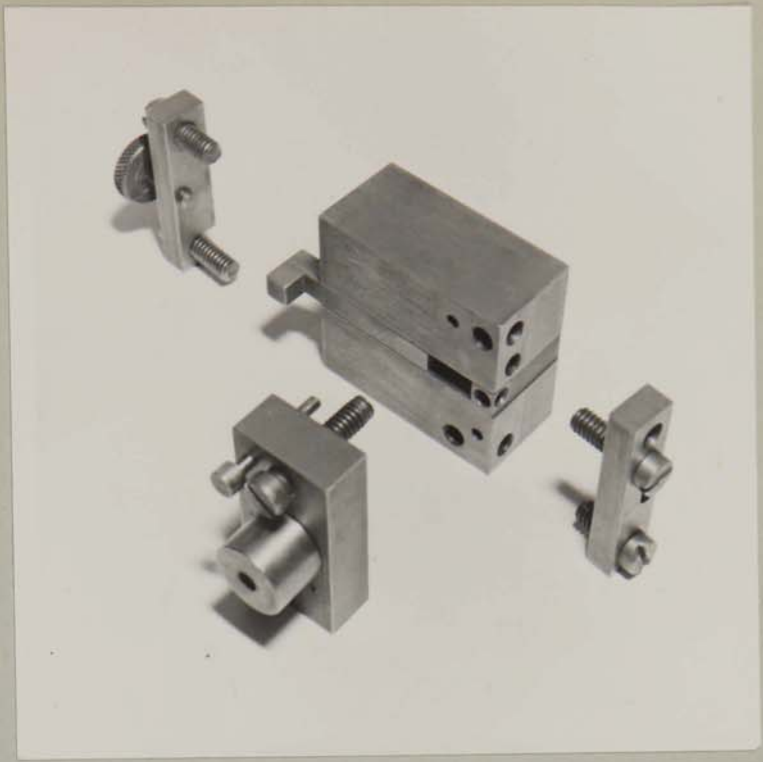

PLATE 4.1. PRESSURE CELL DRILLING JIG.

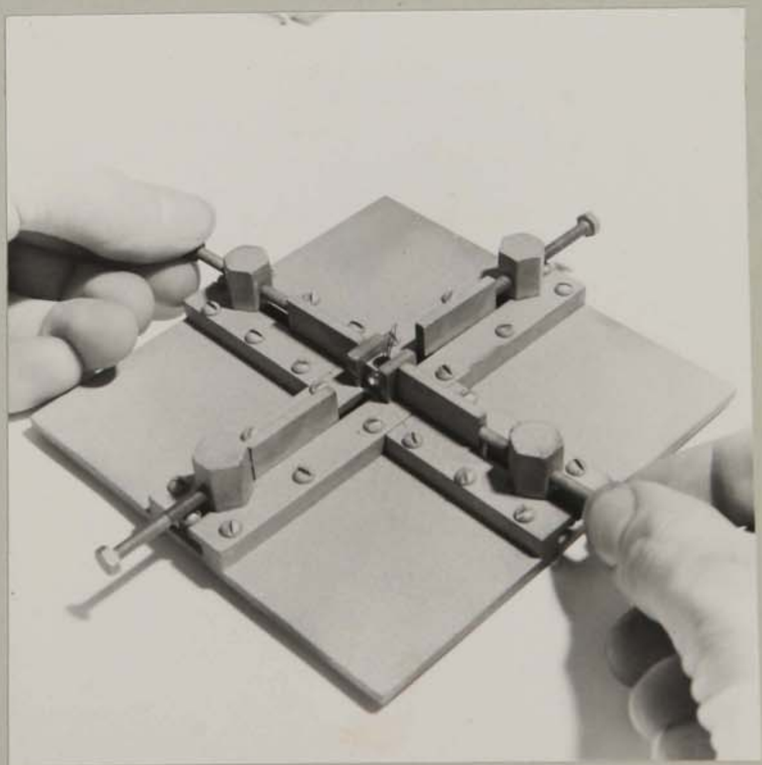

PLATE 4.2 PRESSURE CELL ASSEMBLY RIG

PLATE 4. 3. COMPLETED PRESSURE CELL AND FRAME.

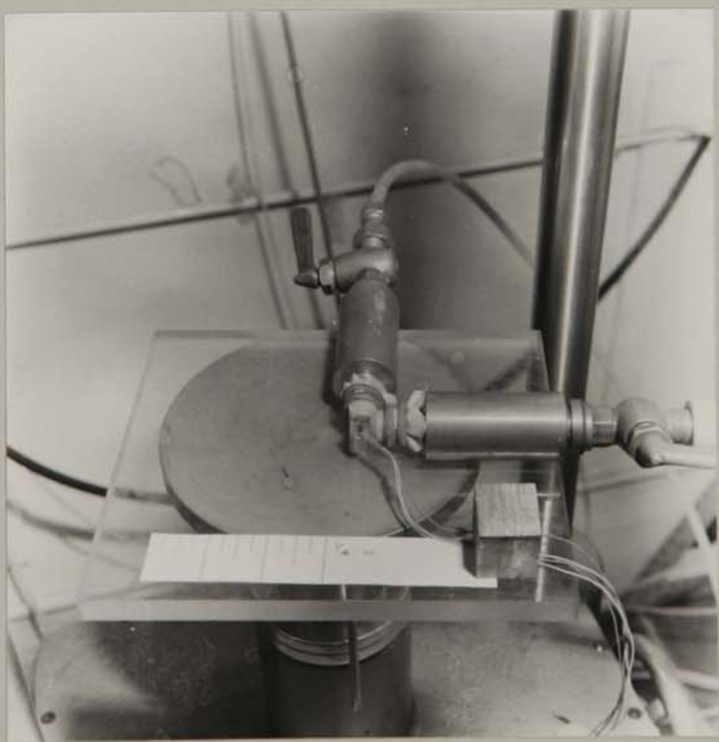

PLATE 4.4 INDIVIDUAL DIAPHRAGM PRESSURE CELL CALIBRATION APPARATUS.

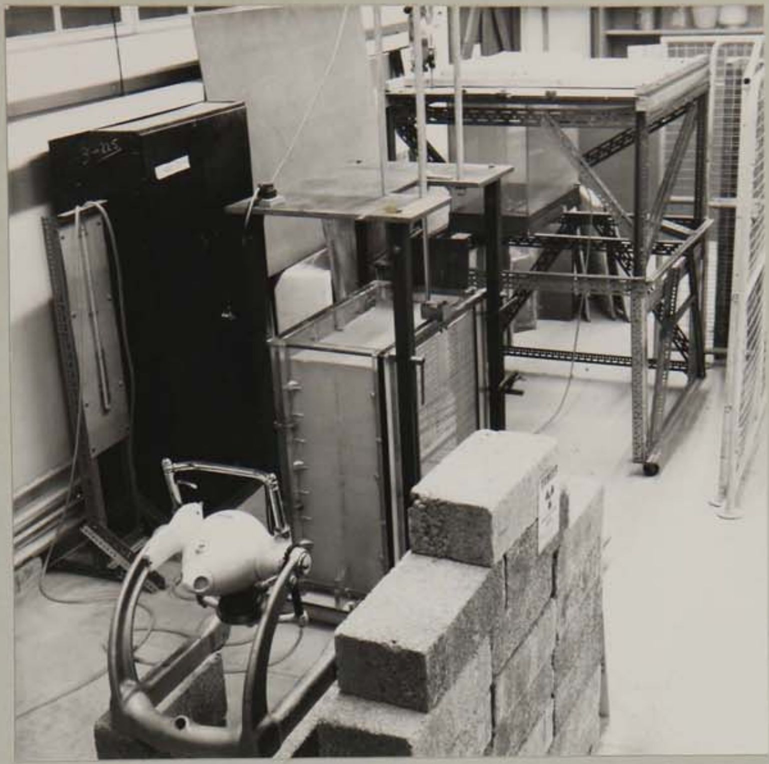

PLATE 4.5 HALF - SECTION APPARATUS WITH COBALT -60 γ - RAY SET UP.

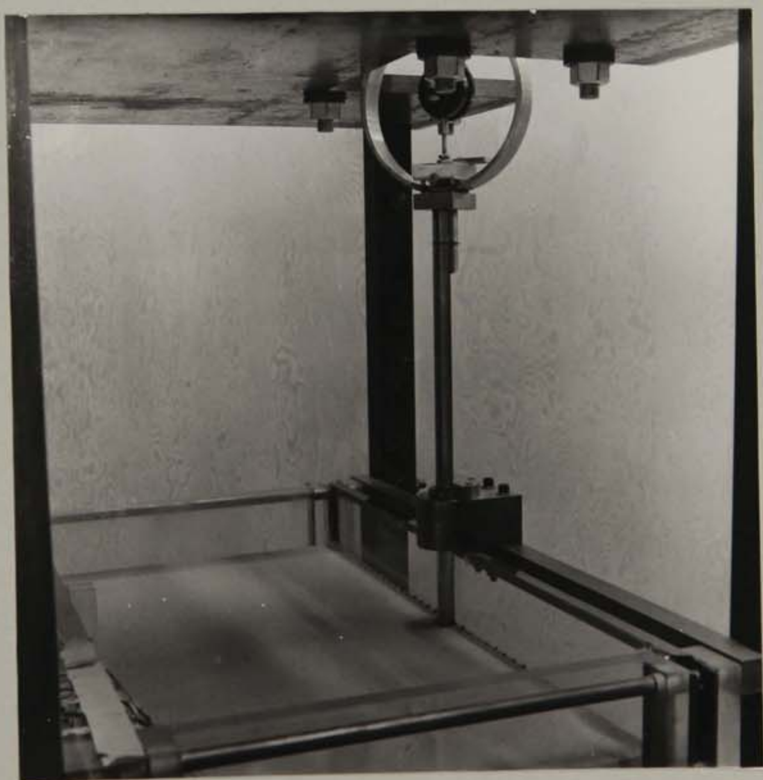

PLATE 4.6 HALF - SECTION PENETROMETER AGAINST GLASS PLATE.

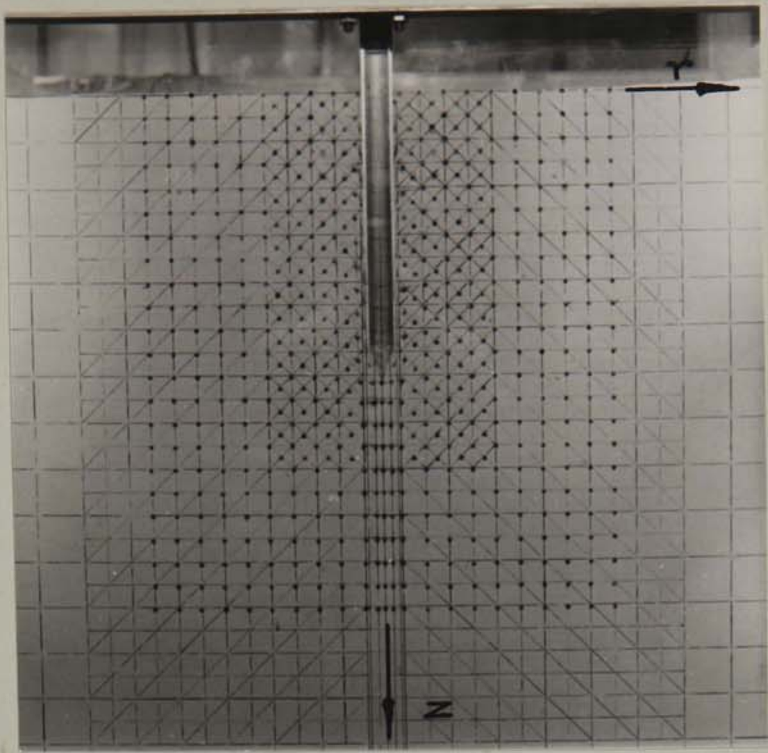

PLATE 4.7. PENETROMETER AGAINST GLASS FACE DURING TEST IN LOOSE SAND

PLATE 4.8 ASSEMBLED HALF - SECTION CONTAINER AT START OF TEST

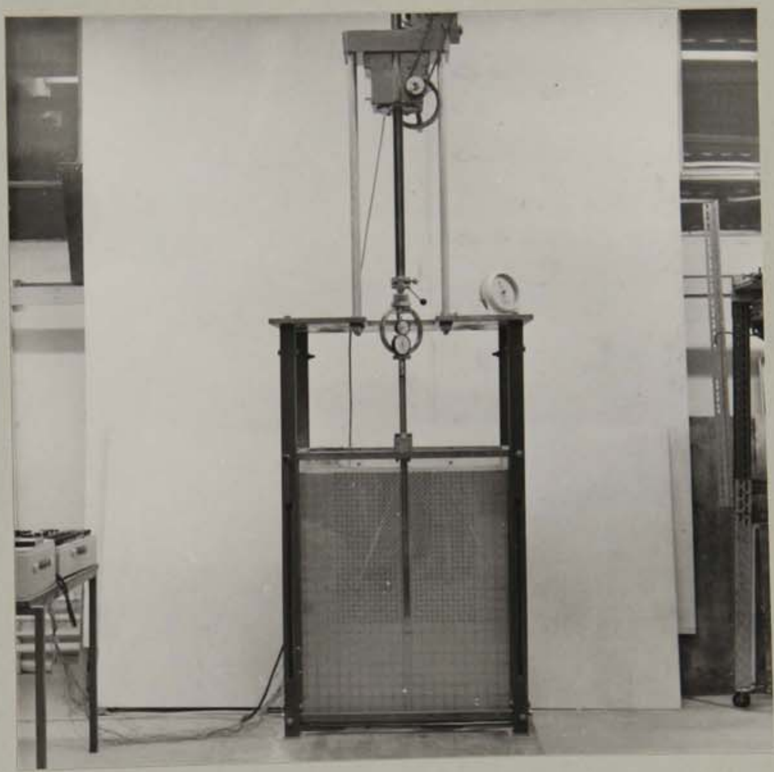

PLATE 4.9. FRONT ELEVATION OF HALF - SECTION CONTAINER AT END OF TEST.

FIGURE 5.1 (a). CYLINDRICAL POLAR CO-ORDINATES

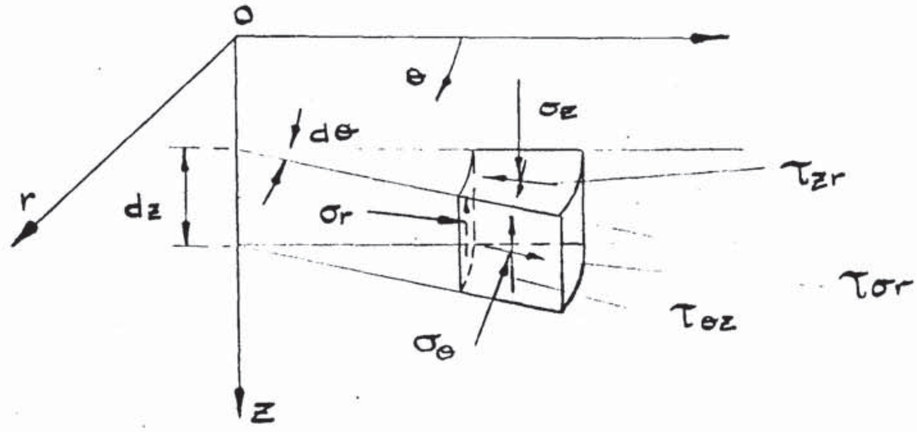

FIGURE 5.1 (b). SOIL ELEMENT IN Z - CONSTANT PLANE

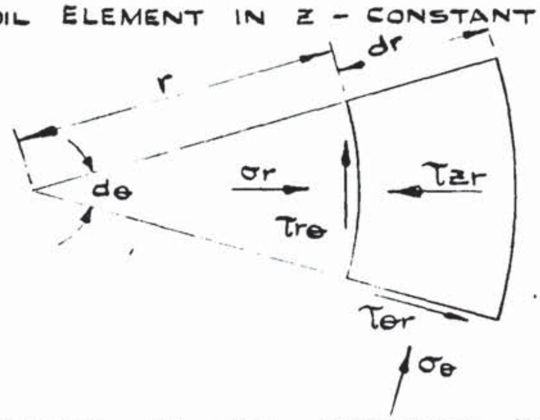

FIGURE 5.1.(c). STRESSES ON SOIL ELEMENT IN Z-CONSTANT PLANE

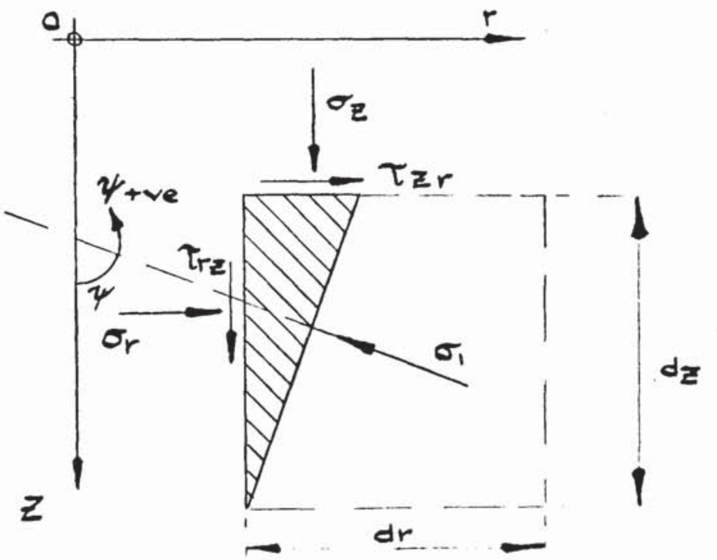

FIGURE 5.1. (d). MOHR STRESS DIAGRAM FOR FIGURE 5.1. (c)

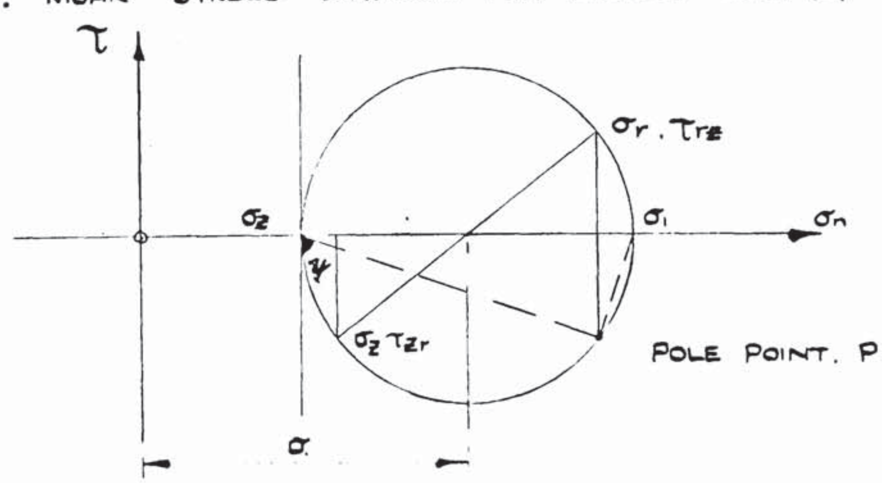

FIGURE 5.2. (a). STRAINED ELEMENT IN Z - CONSTANT PLANE

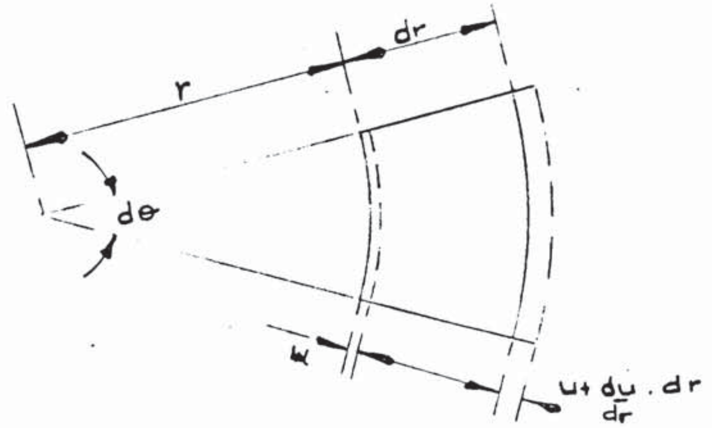

FIGURE 5.2. (b). STRAINED ELEMENT IN θ - CONSTANT PLANE

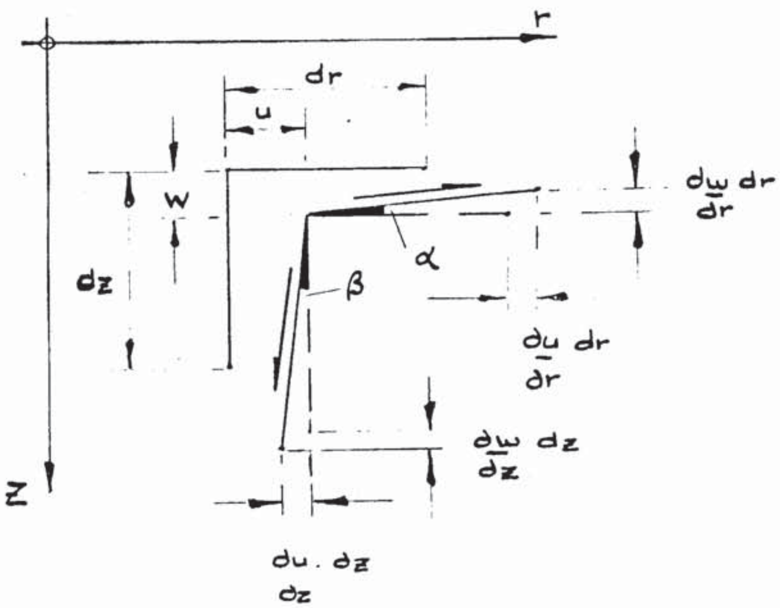

FIGURE 5.2. (c). MOHR STRAIN DIAGRAM FOR FIGURE 5.2 (b)

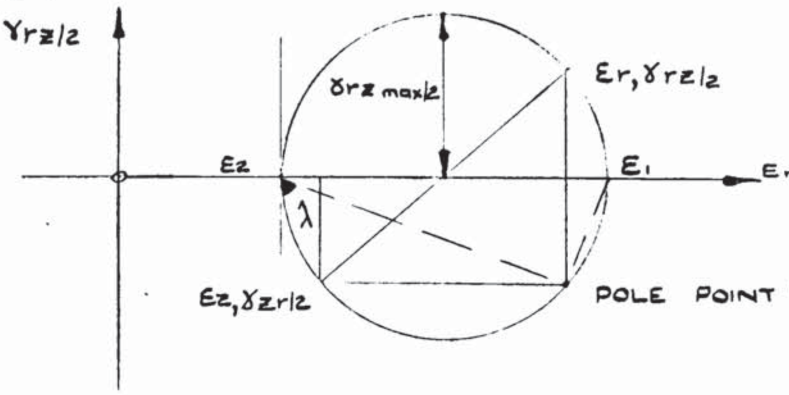

FIGURE 5.2 (d). STRAIN COMPONENTS AND PRINCIPAL STRAIN DIRECTIONS IN θ - CONSTANT PLANE

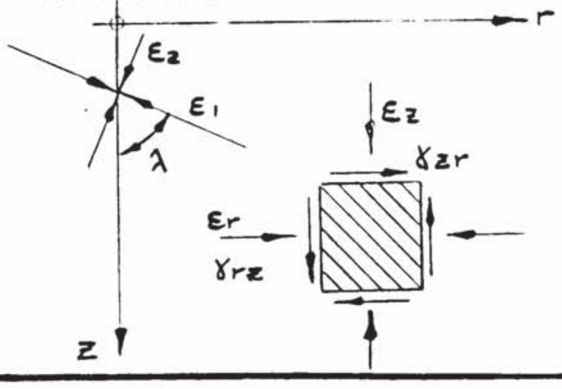

FIGURE 5.3 (a). MOHR - COULOMB YIELD CRITERION

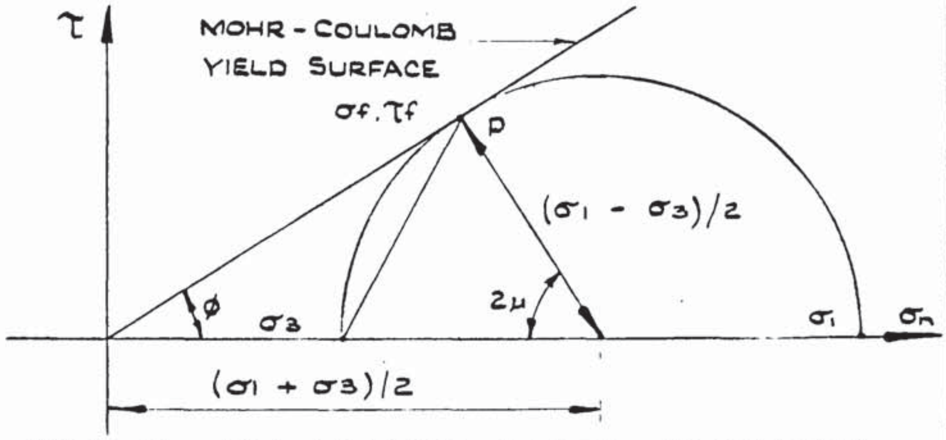

FIGURE 5.3 (b). PRINCIPAL AND LIMITING STRESS COMPONENTS AT A POINT P

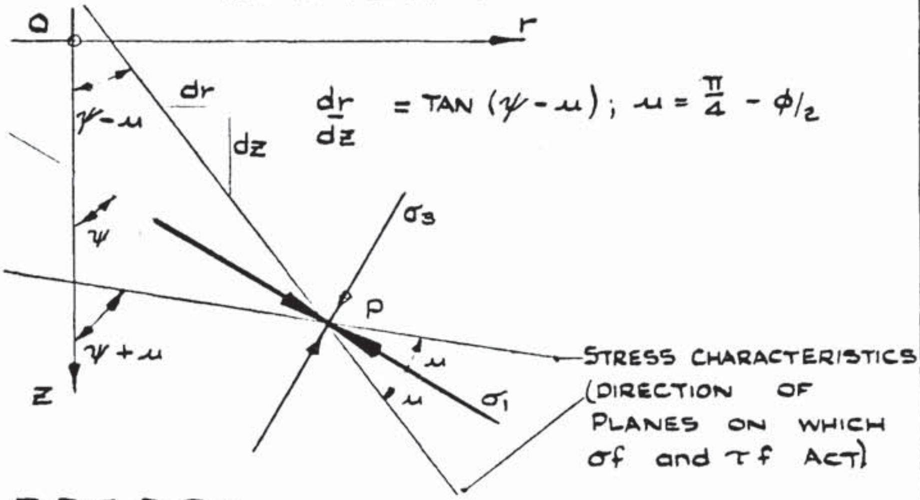

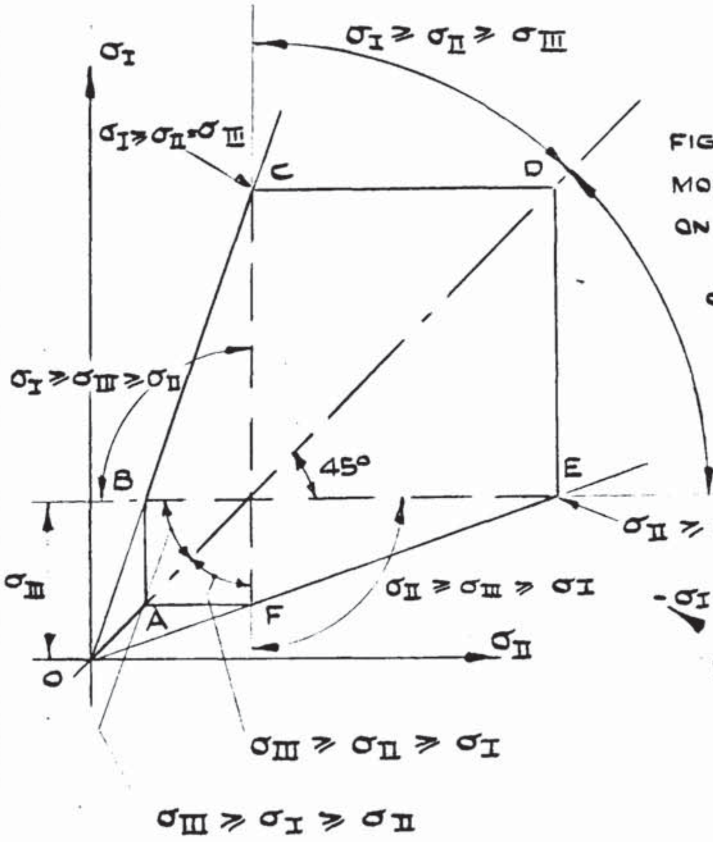

FIGURE 5.4. SECTION OF MOHR-COULOMB YIELD SURFACE ON A σIII = CONSTANT PLANE

σII ≥ σI ≥ σIII

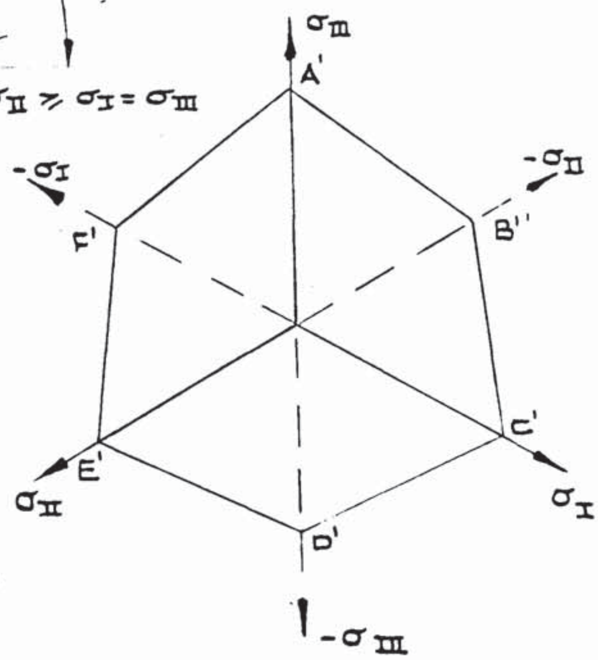

FIGURE 5.5. MOHR - COULOMB YIELD LOCUS ON A DEVIATORIC PLANE.

FIGURE 5.6. STRESS COMPONENTS FOR GENERAL CO-ORDINATES ON A θ-CONSTANT PLANE

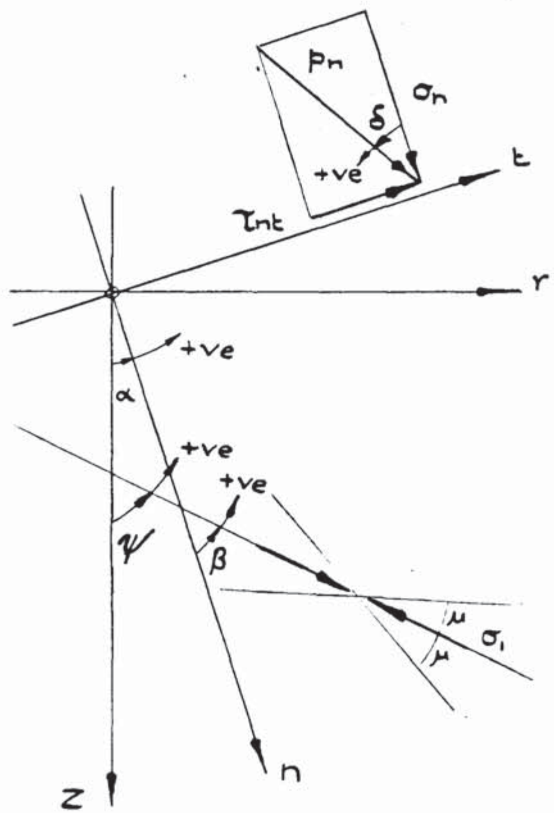

FIGURE 5.7. STRESS CHARACTERISTICS IN THE PHYSICAL PLANE (r - z)

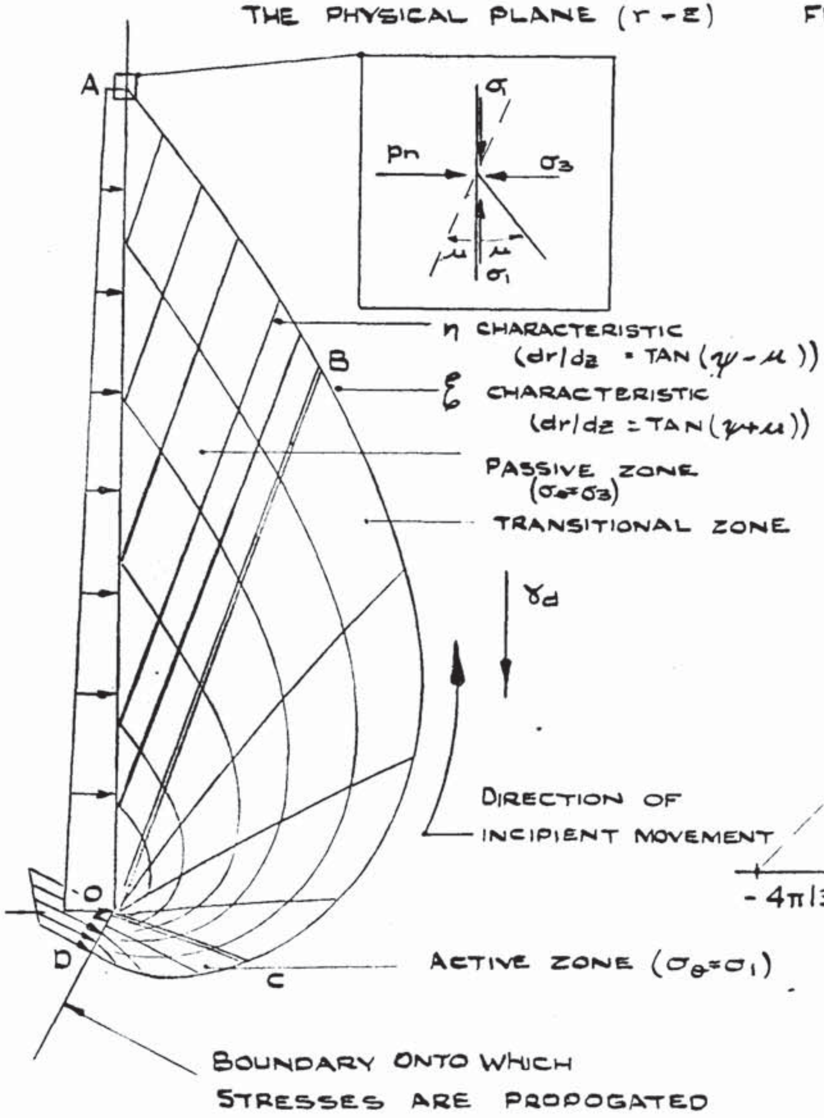

FIGURE 5.8. CHARACTERISTICS MAPPED FROM FIG. 5.7 ONTO ξ-η PLANE.

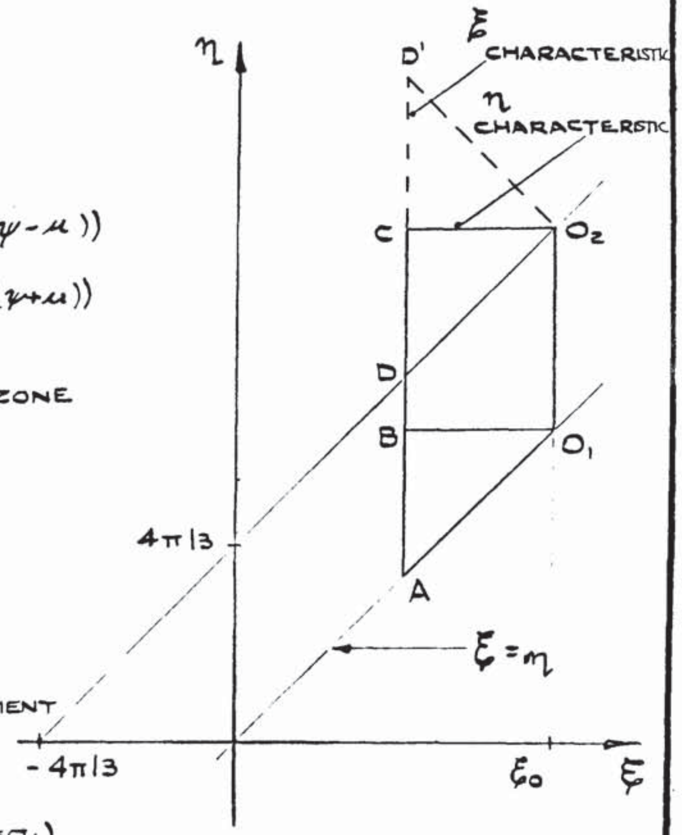

FIGURE 5.9.(a). SMALL SECTION OF ξ-η PLANE REPRODUCED FROM FIGURE 5.8.

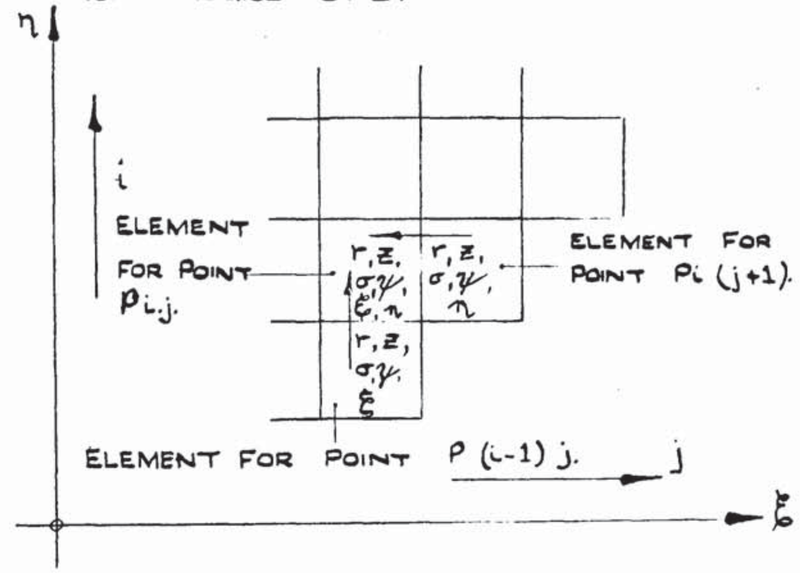

FIGURE 5.9.(b). SMALL SECTION OF r-z PLANE REPRODUCED FROM FIGURE 5.7.

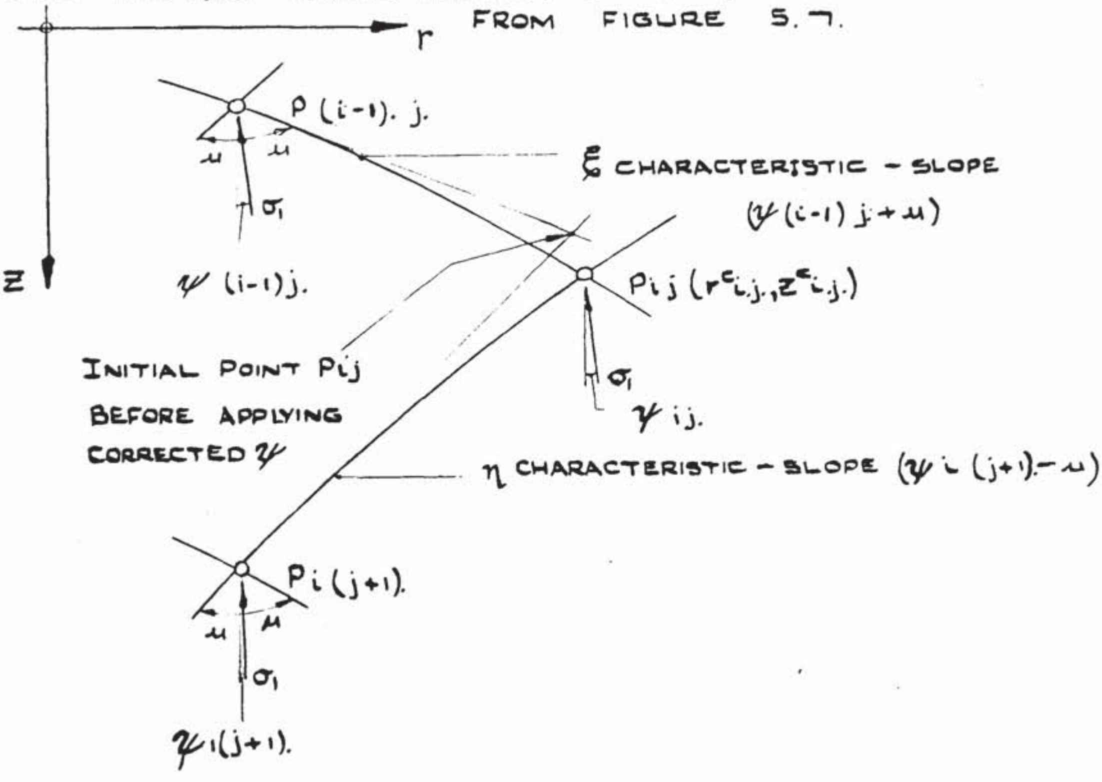

FIGURE 5.11.

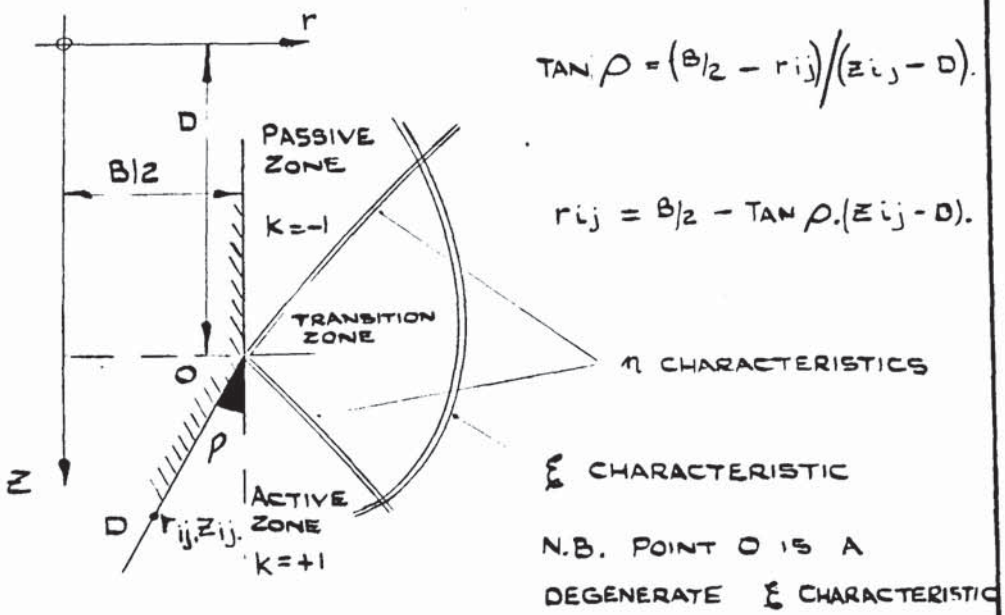

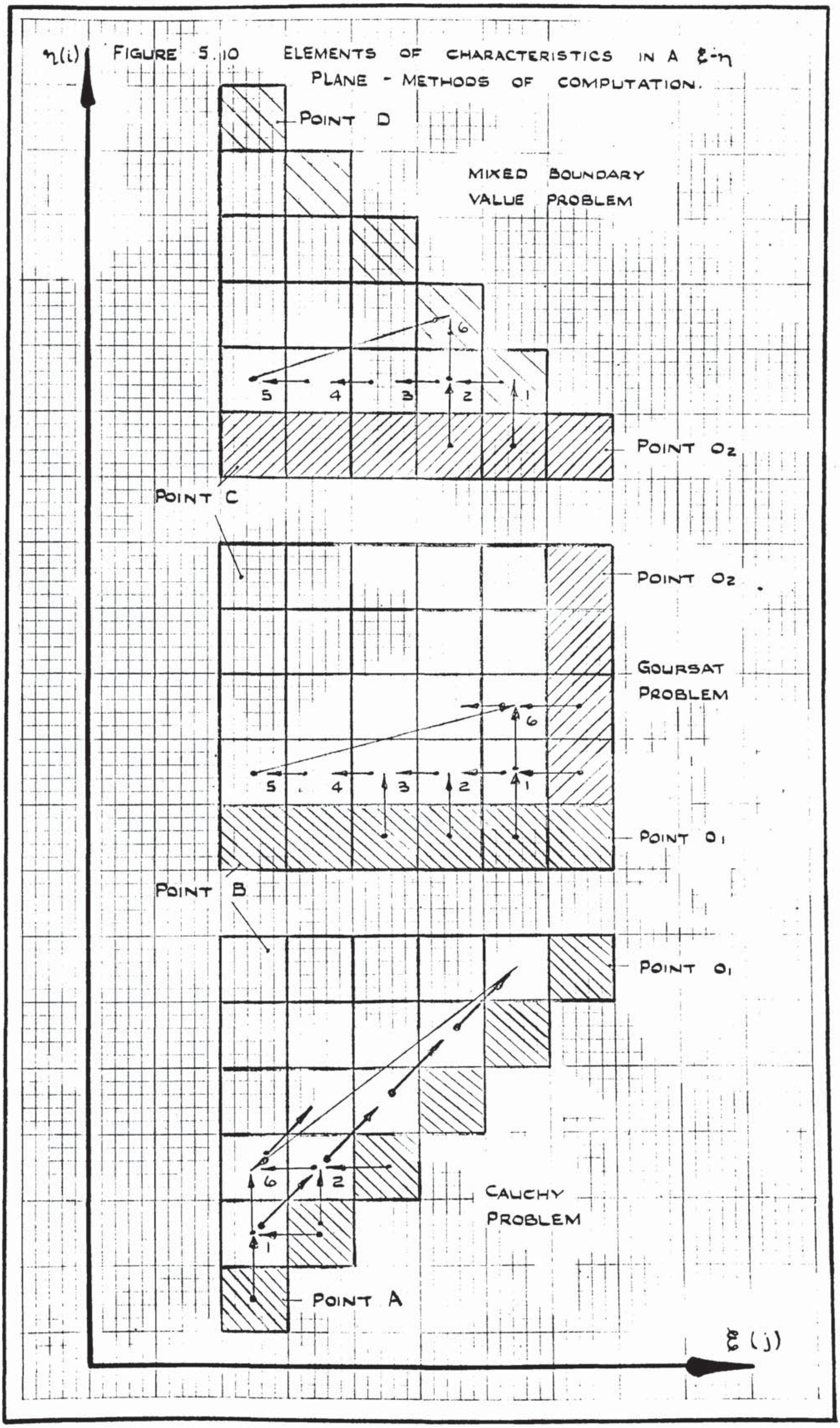
η(i)
FIGURE 5.10 ELEMENTS OF CHARACTERISTICS IN A ξ-η PLANE - METHODS OF COMPUTATION.
POINT D
MIXED BOUNDARY VALUE PROBLEM
6
5
4
3
2
1
POINT O2
POINT C
POINT O2
GOURSAT PROBLEM
6
5
4
3
2
1
POINT O1
POINT B
POINT O1
6
2
1
CAUCHY PROBLEM
POINT A
ξ (j)

FIGURE 5.12 ASSUMED BOUNDARY CONDITIONS ALONG VERTICAL AND INCLINED PENETROMETER FACES

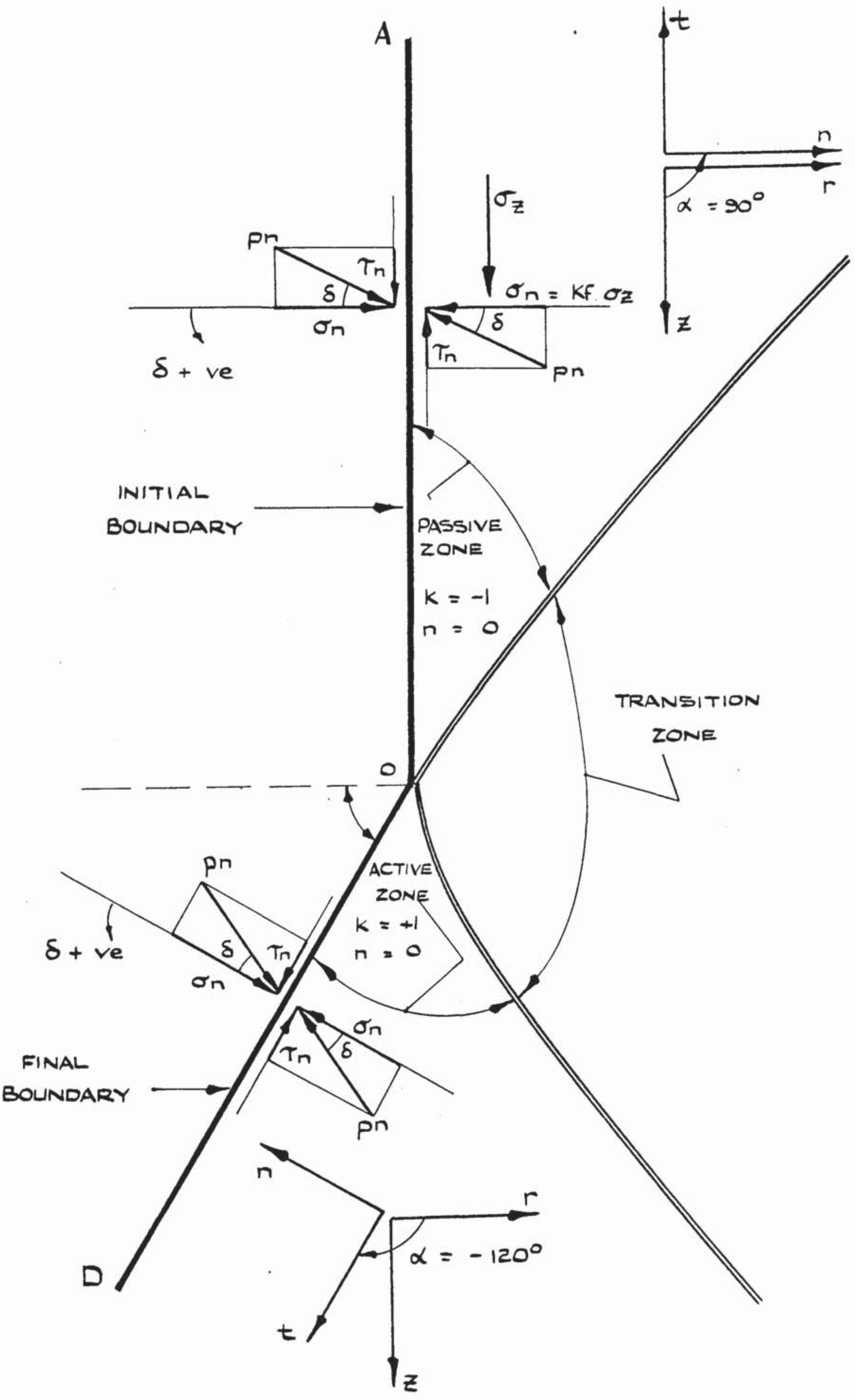

FIGURE 5.13. STRESS CHARACTERISTICS FOR AXIALLY-SYMMETRIC PENETRATION

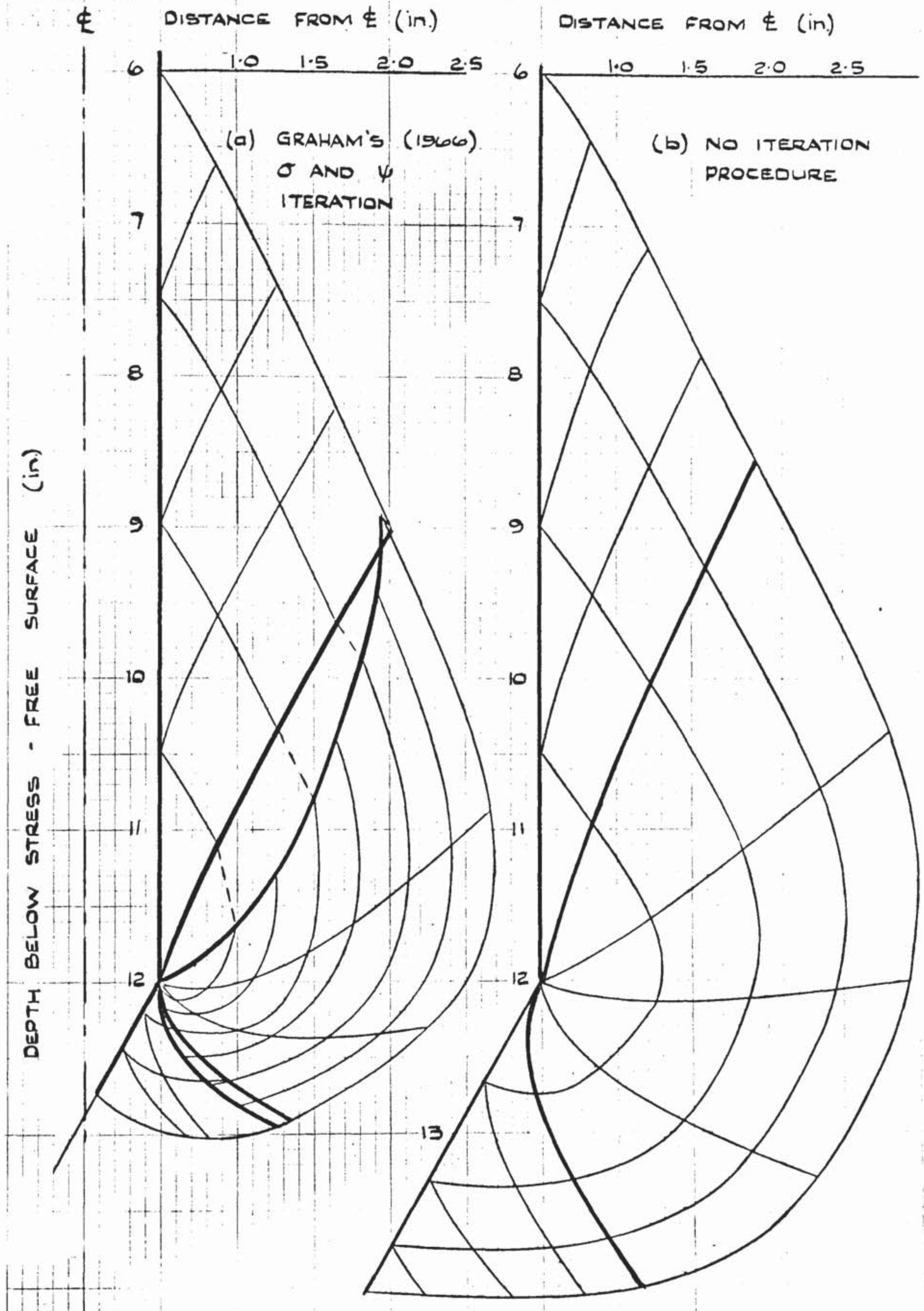

SAND PROPERTIES USED IN COMPUTATIONS:

γ_d = 94 lb/cu ft. ϕ = 35° δ = −23°.

BOUNDARY CONDITIONS:

Kf VARIES FROM 1·0 AT 6 in. to 0·6 AT 12 in. in increments of 0·1.

FIGURE 5.14. STRESS CHARACTERISTICS FOR AXIALLY-SYMMETRIC AND PLANE STRAIN PENETRATION

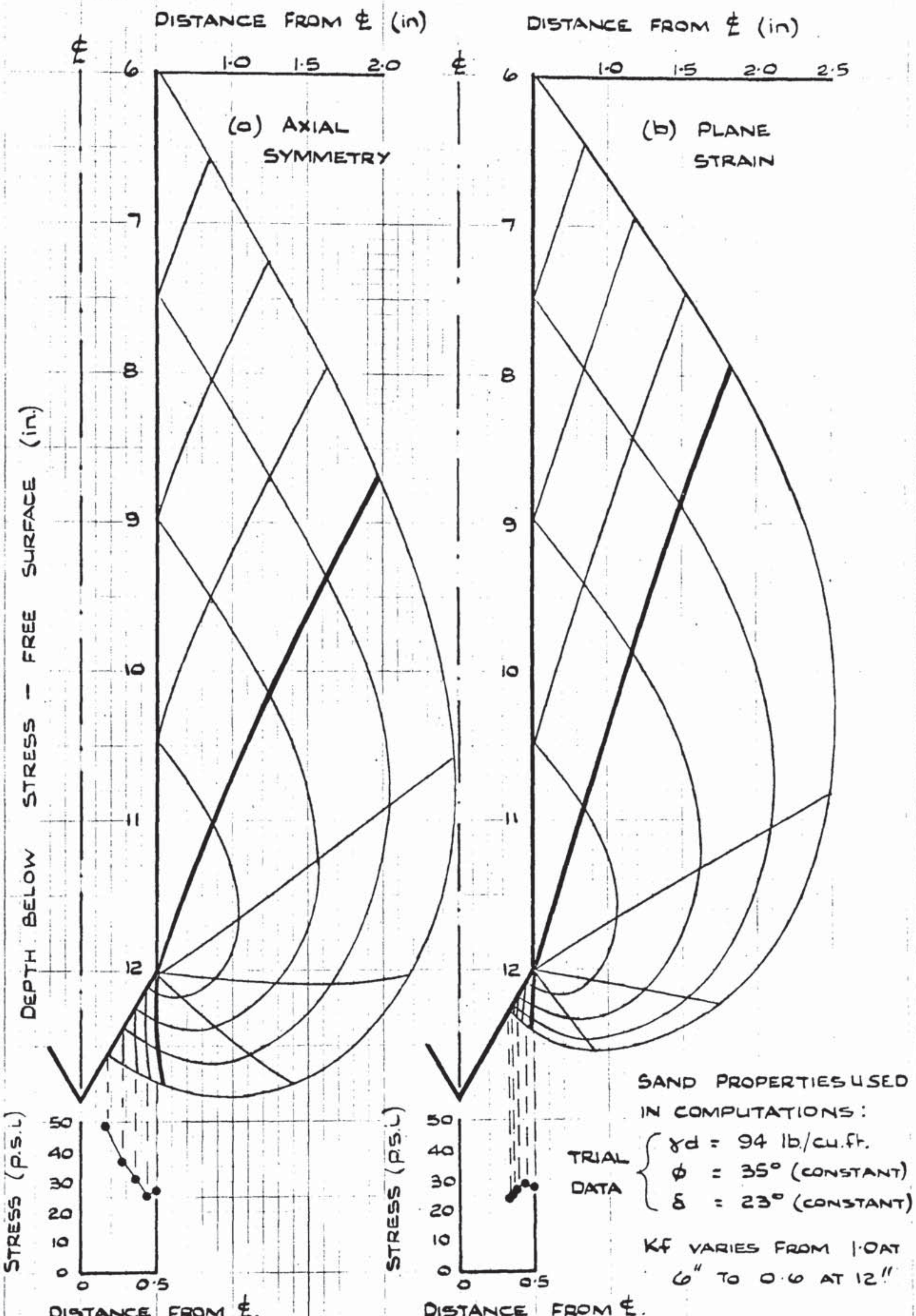

DISTRIBUTION OF VERTICAL STRESS ALONG THE INCLINED BASE OF A PENETROMETER FOR EQUAL DISTRIBUTION OF σ ALONG INITIAL BOUNDARY

FIGURE 5.15. DISTRIBUTION OF VERTICAL STRESS ALONG THE INCLINED BASE OF A PENETROMETER IN LOOSE SAND – 18.866 in. PENETRATION

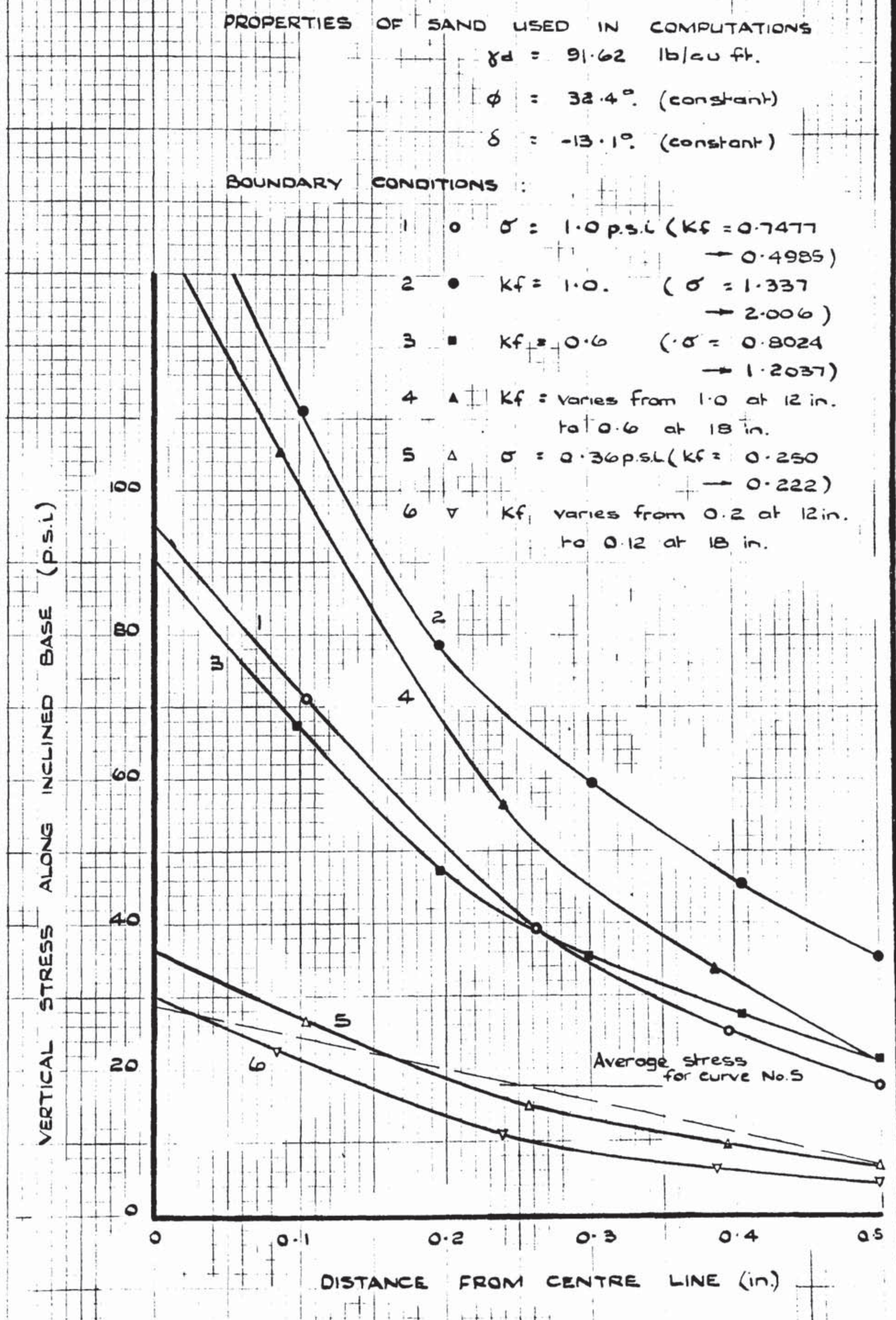

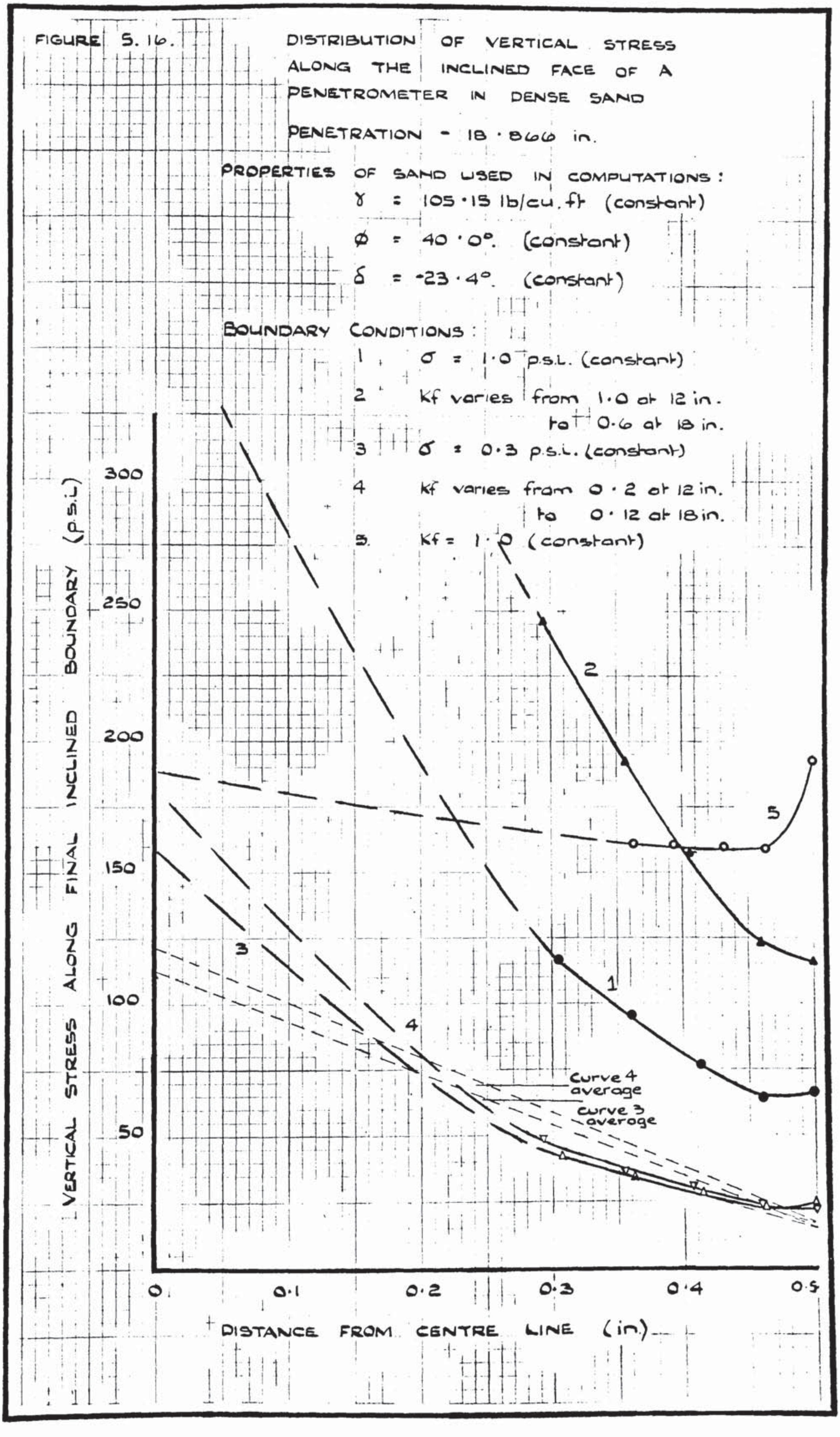

FIGURE 5.16. DISTRIBUTION OF VERTICAL STRESS ALONG THE INCLINED FACE OF A PENETROMETER IN DENSE SAND

FIGURE 5.17. STRESS CHARACTERISTICS FOR AXIALLY-SYMMETRIC PENETRATION INTO LOOSE SAND

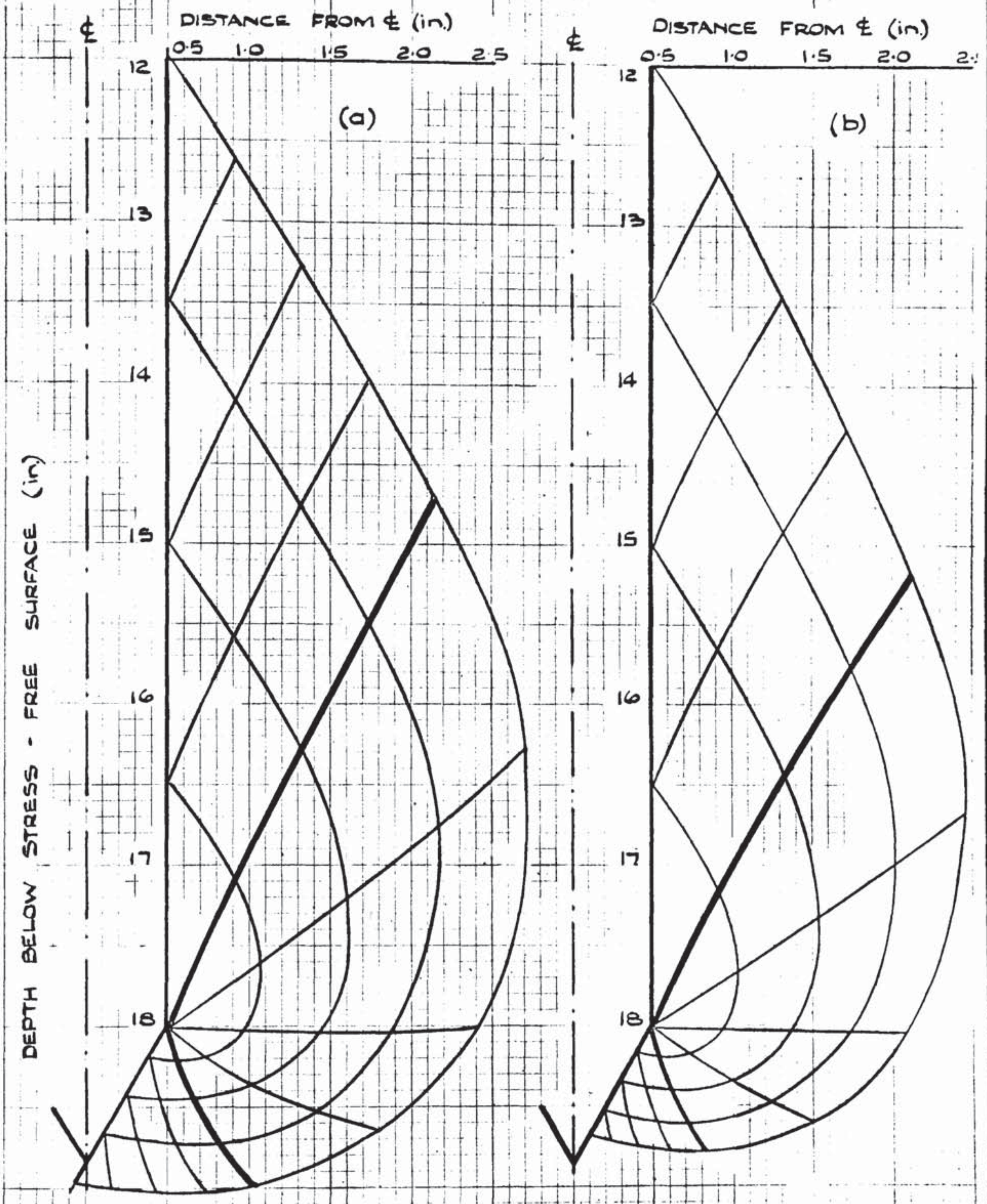

INITIAL BOUNDARY CONDITIONS:

(a) σ = 0·357 p.s.i. (constant) (b) kf = 1·0 (constant)

SAND PROPERTIES USED IN COMPUTATIONS:

γ_d = 91·62 lb/cu ft. (constant)

ϕ = 32·4° (constant)

δ = 13·1° (constant)

FIGURE 5.18. STRESS CHARACTERISTICS FOR AXIALLY-SYMMETRIC PENETRATION INTO DENSE SAND

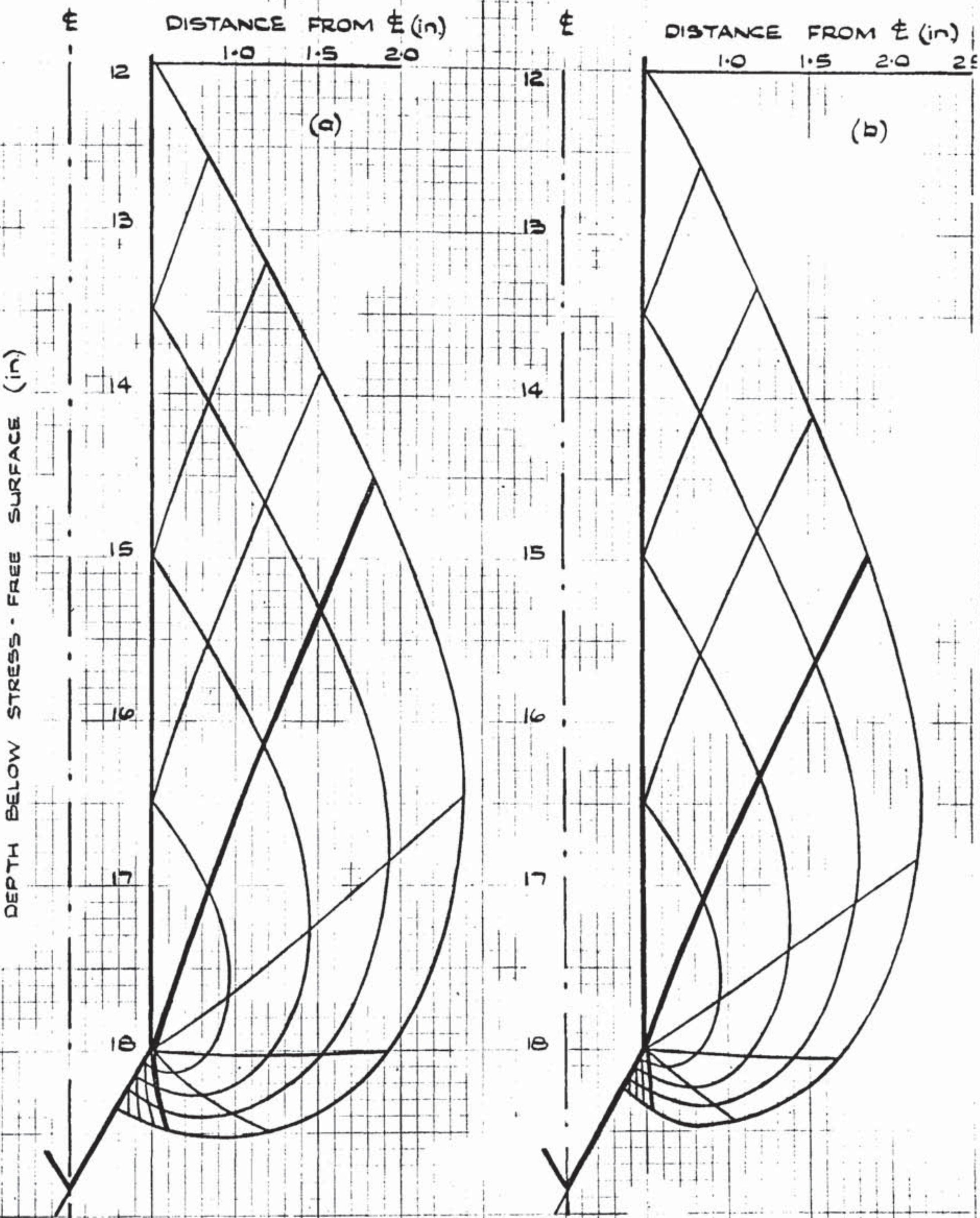

INITIAL BOUNDARY CONDITIONS:

(a) Kf varies from 2·0 at 12 in. to 0·12 at 18 in.

(b) Kf = 1·0 (constant)

SAND PROPERTIES USED IN COMPUTATION:

γ_d = 105·15 lb/cu ft. (constant)

ϕ = 40·0° (constant)

δ = -23·4° (constant)

FIGURE 5.19. DISTRIBUTION OF VERTICAL STRESS ALONG THE INCLINED BASE OF A PENETROMETER IN LOOSE SAND

CONSTANT σ ALONG PENETROMETER SHANK

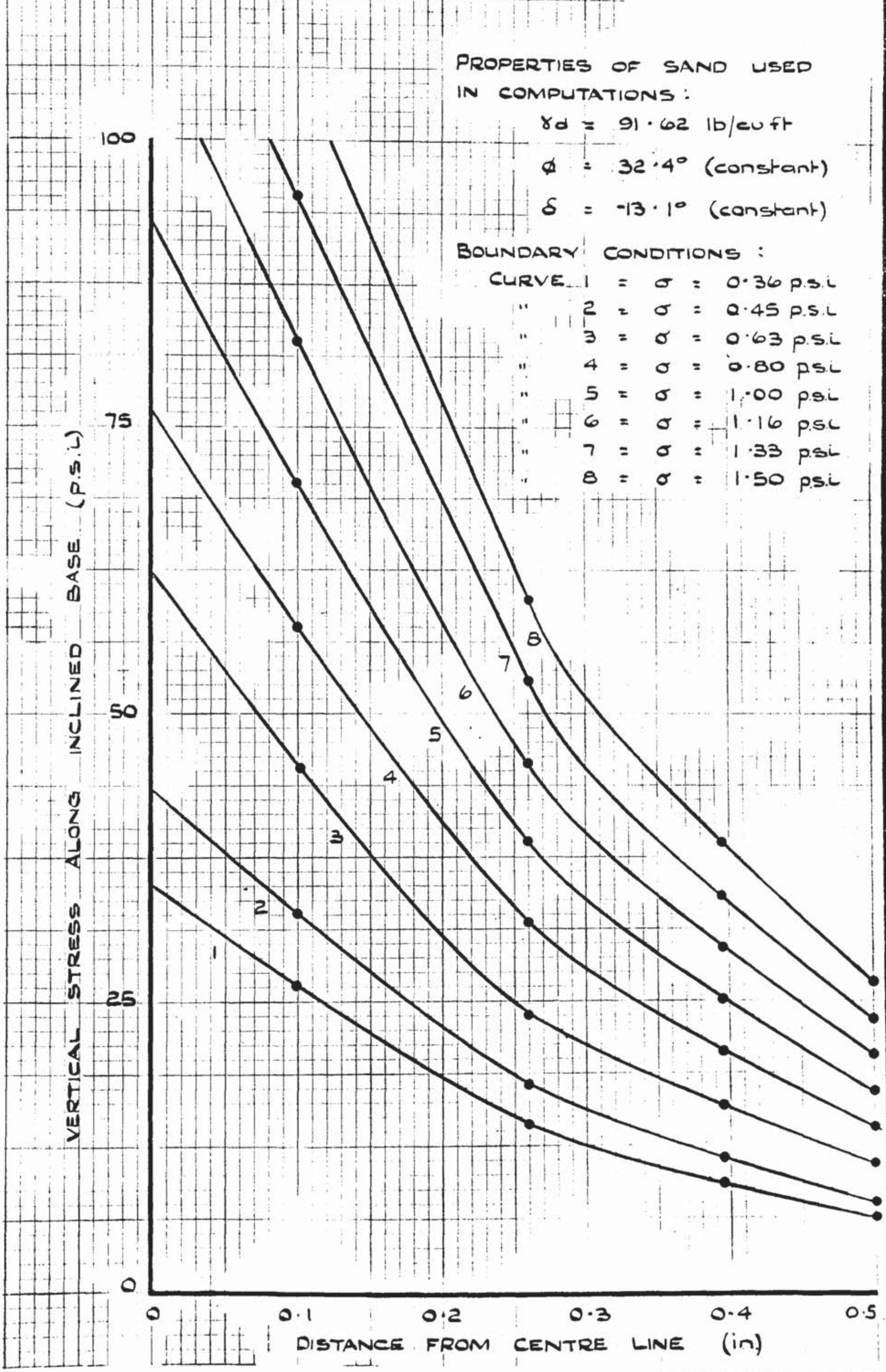

FIGURE 5.20. (a). STRESS CHARACTERISTICS FOR AXIALLY-SYMMETRIC PENETRATION INTO DENSE SAND

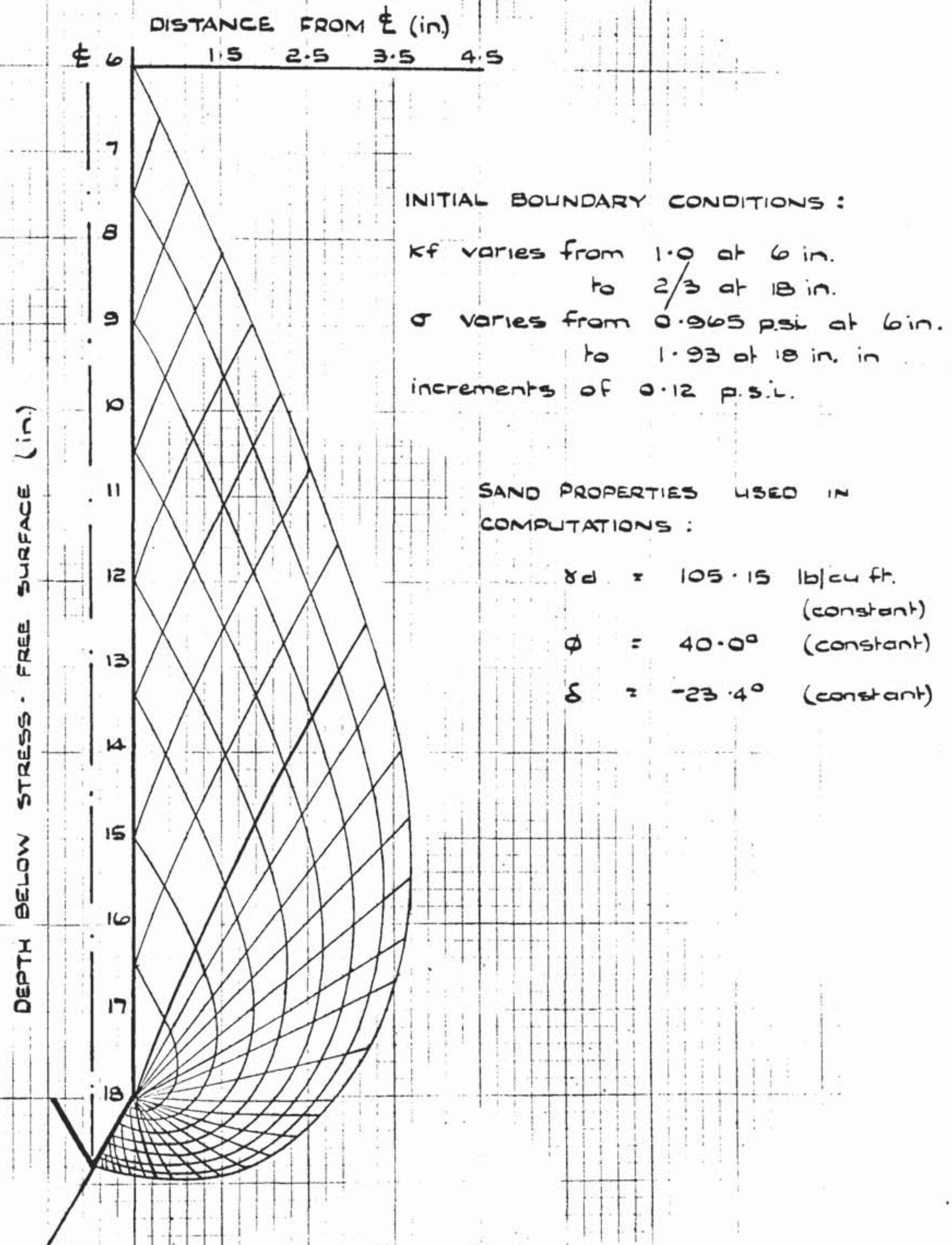

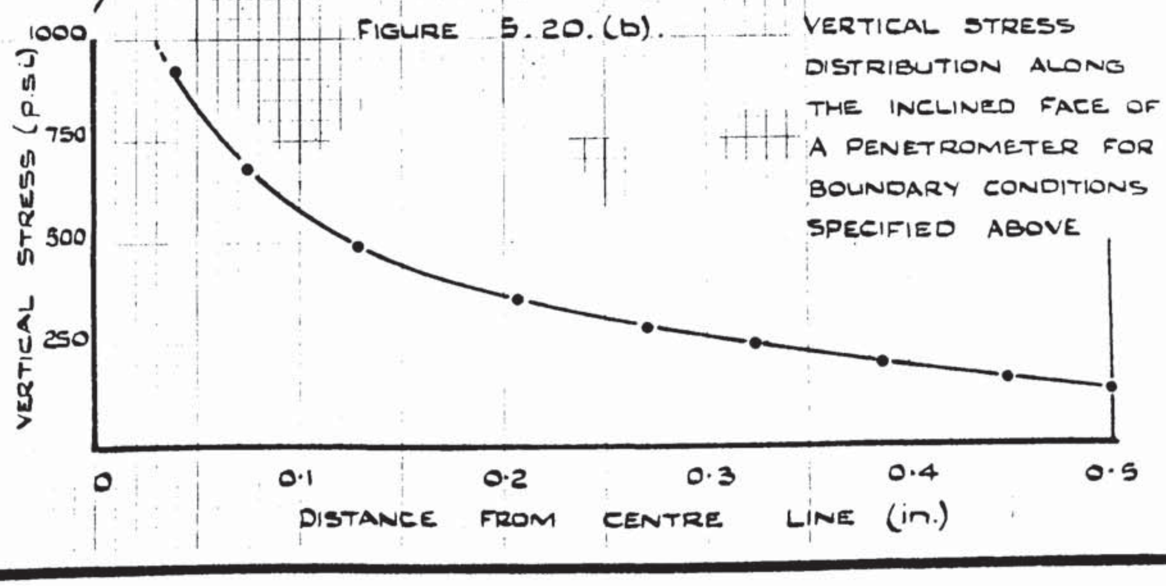

FIGURE 5.20. (b). VERTICAL STRESS DISTRIBUTION ALONG THE INCLINED FACE OF A PENETROMETER FOR BOUNDARY CONDITIONS SPECIFIED ABOVE

TABLE 6.1.

	LOOSE SAND	DENSE SAND
δ° SAND / BRASS SHEAR / TEST	-13.1	-23.4
ϕ° DIRECT SHEAR TESTS	31.6	40.5
ψ° INITIAL *	5.97	7.38
ψ° FINAL *	-139.06	-150.78
ANGLE OF ROTATION OF σ_1° (ie. $\psi F - \psi I$)	145.03	158.16
ψ° INITIAL +	70.93	59.22
ψ° FINAL +	-49.07	-60.78
λ° INITIAL **	80.0	75.0
λ° FINAL **	0.0	15.0

* These values were used in limiting stress field computations.

\+ Theoretically correct values.

** Obtained from experimental strain-rate fields.

FIGURE 6.1.(a) & (b) MEASURED STRESS VERSUS PENETRATION FOR CELLS IN LOOSE SAND.

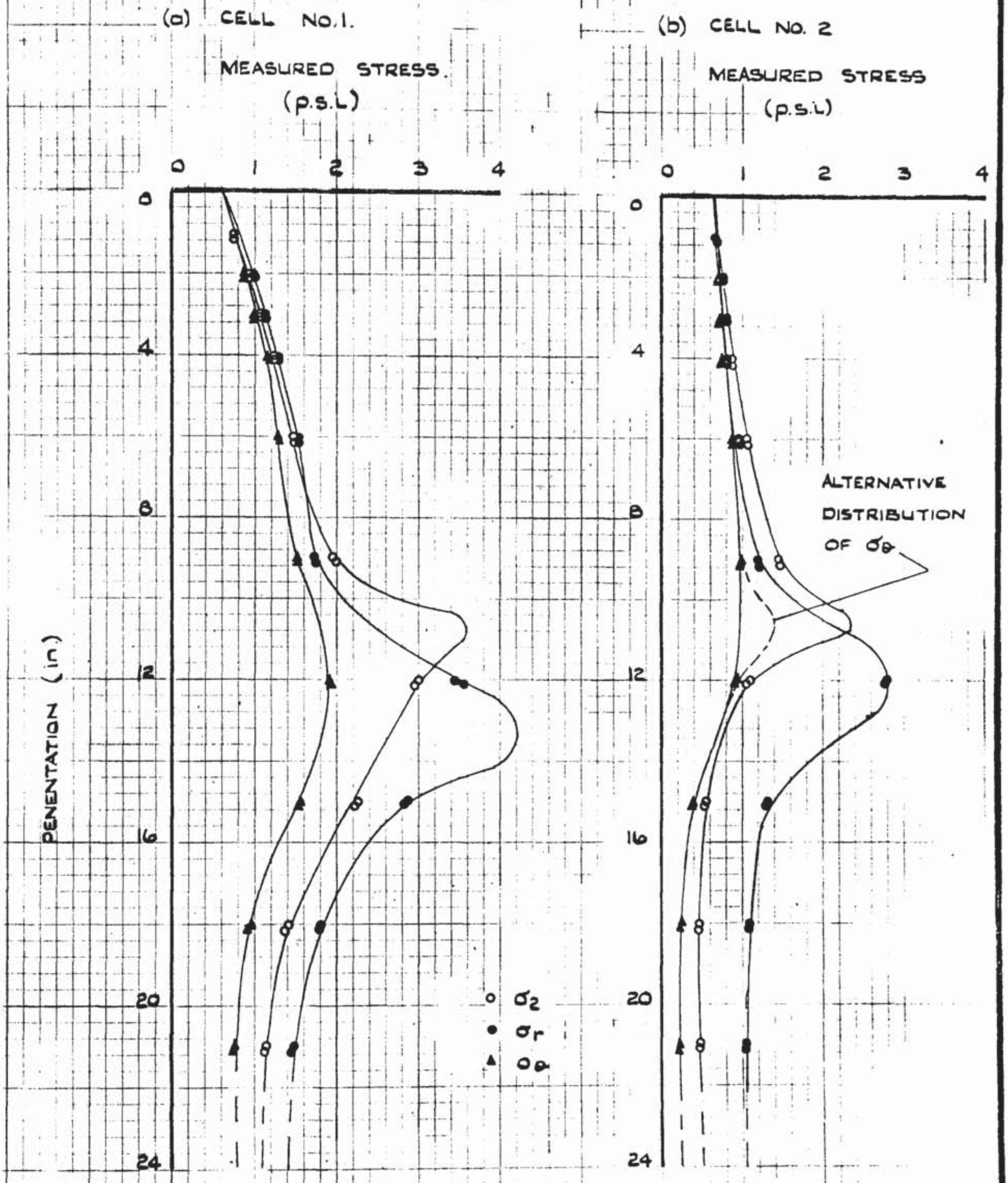

CO-ORDINATES OF CELL FACES:

$r = 1.08$ in.

$z = 13.02$ in.

CO-ORDINATES OF CELL FACES:

$r = 0.82$ in.

$z = 12.74$ in.

INITIAL PROPERTIES OF SAND:

$\gamma_d = 91.58$ lb/cu ft

$\eta = 44.62$ %

COULOMB $\phi = 31.8°$ (DIRECT SHEAR TESTS)

FIGURE 6.1. (c) & (d) MEASURED STRESS VERSUS PENETRATION FOR CELLS IN LOOSE SAND

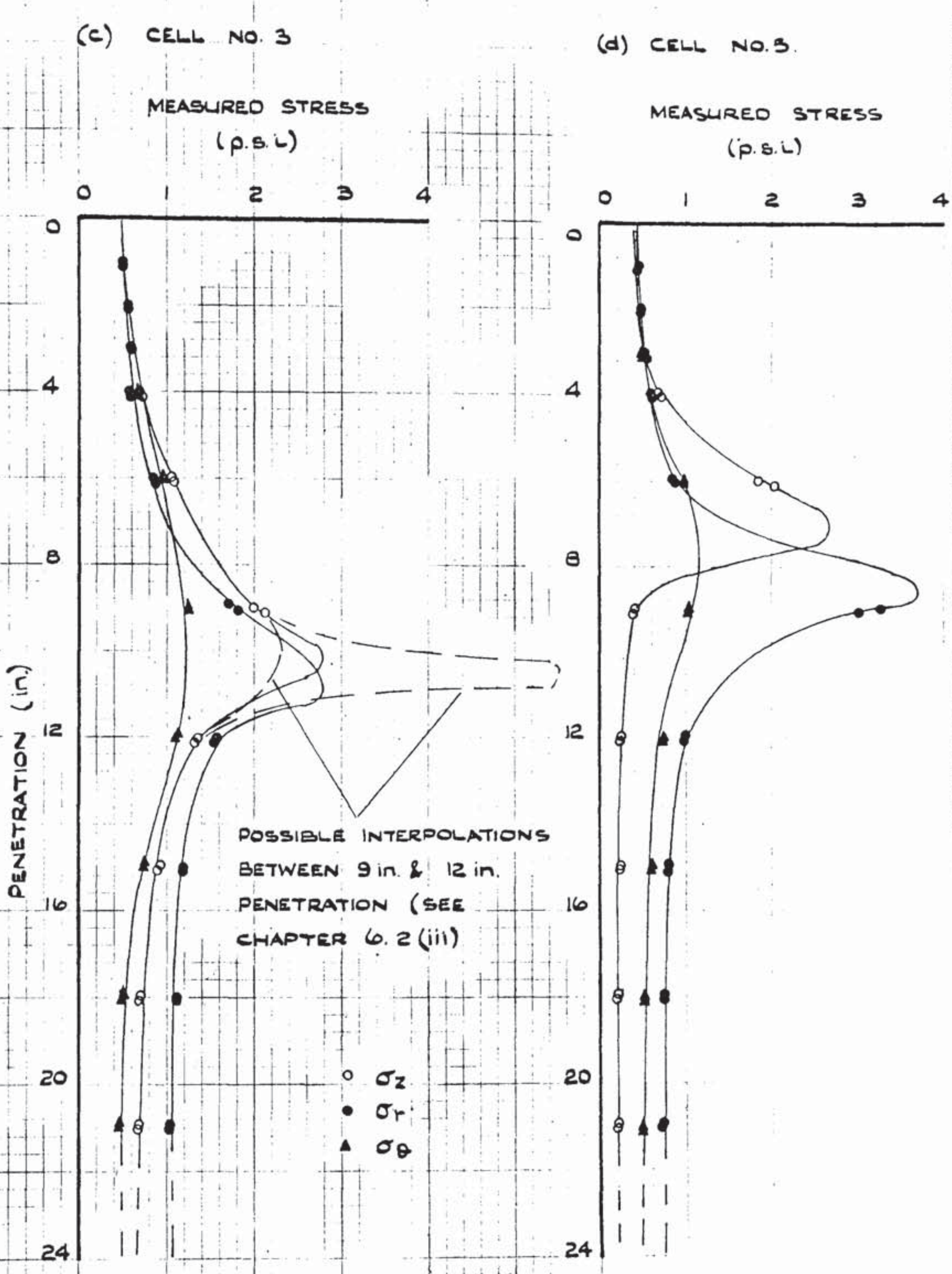

CO-ORDINATES OF CELL FACES

r = 0.54 in.

z = 9.83 in.

CO-ORDINATES OF CELL FACES

r = 1.24 in.

z = 8.08 in.

INITIAL PROPERTIES OF SAND:

γ_d = 91.58 lb/cu.ft.

η : 44.62 %

COULOMB ϕ = 31.8° (DIRECT SHEAR TESTS)

FIGURE 6.1.(e) & (f) MEASURED STRESS VERSUS PENETRATION FOR CELLS IN LOOSE SAND.

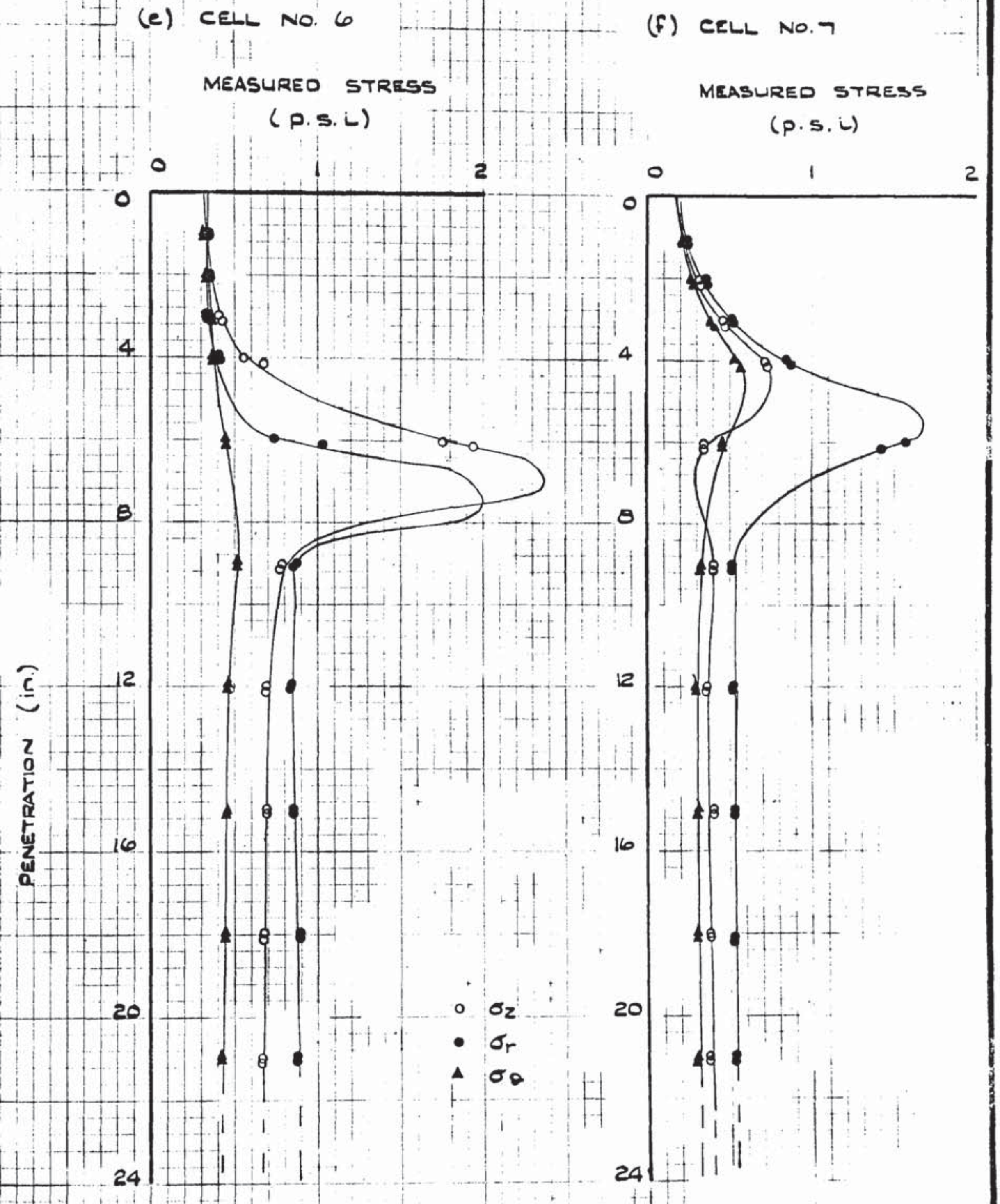

CO-ORDINATES OF CELL FACES:

r = 0.78 in.

z = 6.69 in.

CO-ORDINATES OF CELL FACES

r = 1.42 in.

z = 4.91 in.

INITIAL PROPERTIES OF SAND

γ_d = 91.58 lb/cu ft.

η = 44.62 %

COULOMB ϕ = 31.8° (DIRECT SHEAR TESTS)

FIGURE 6.1 (g), (h) & (j) MEASURED STRESS VERSUS PENETRATION FOR CELLS IN LOOSE SAND.

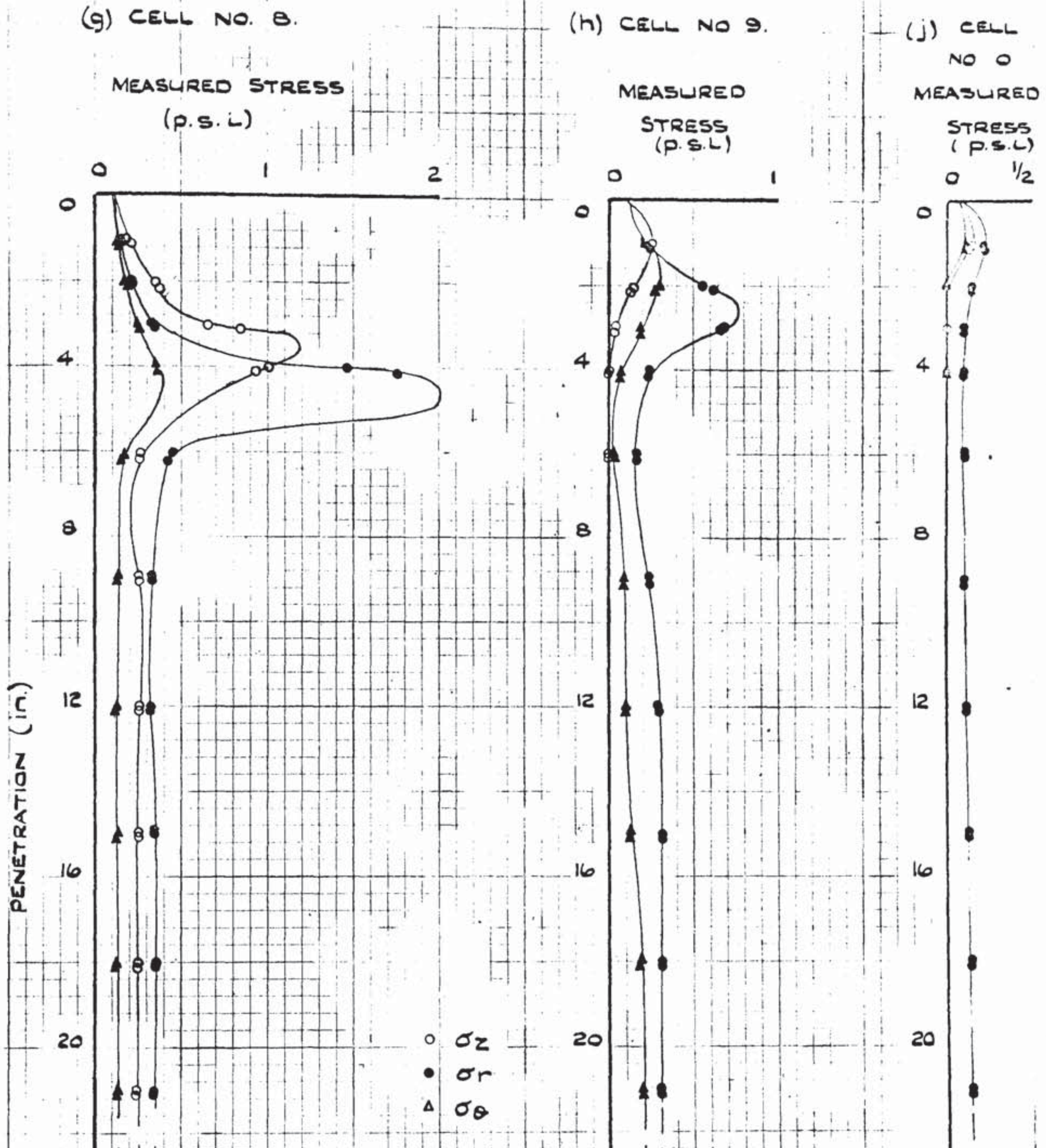

CO-ORDINATES OF CELL FACES: r = 1·06 in. z = 3·54 in.

CO-ORDINATES OF CELL FACES: r = 1·17 in. z = 2·20 in.

CO-ORDINATES OF CELL FACES: r = 1·03 in. z = 0·48 in.

INITIAL PROPERTIES OF SAND:

γ_d = 91·58 lb/cu.ft.

η = 44·62 %

COULOMB ϕ = 31·8° (DIRECT SHEAR TESTS)

FIGURE 6.2.(a) & (b) MEASURED STRESS VERSUS PENETRATION FOR CELLS IN LOOSE-MEDIUM SAND

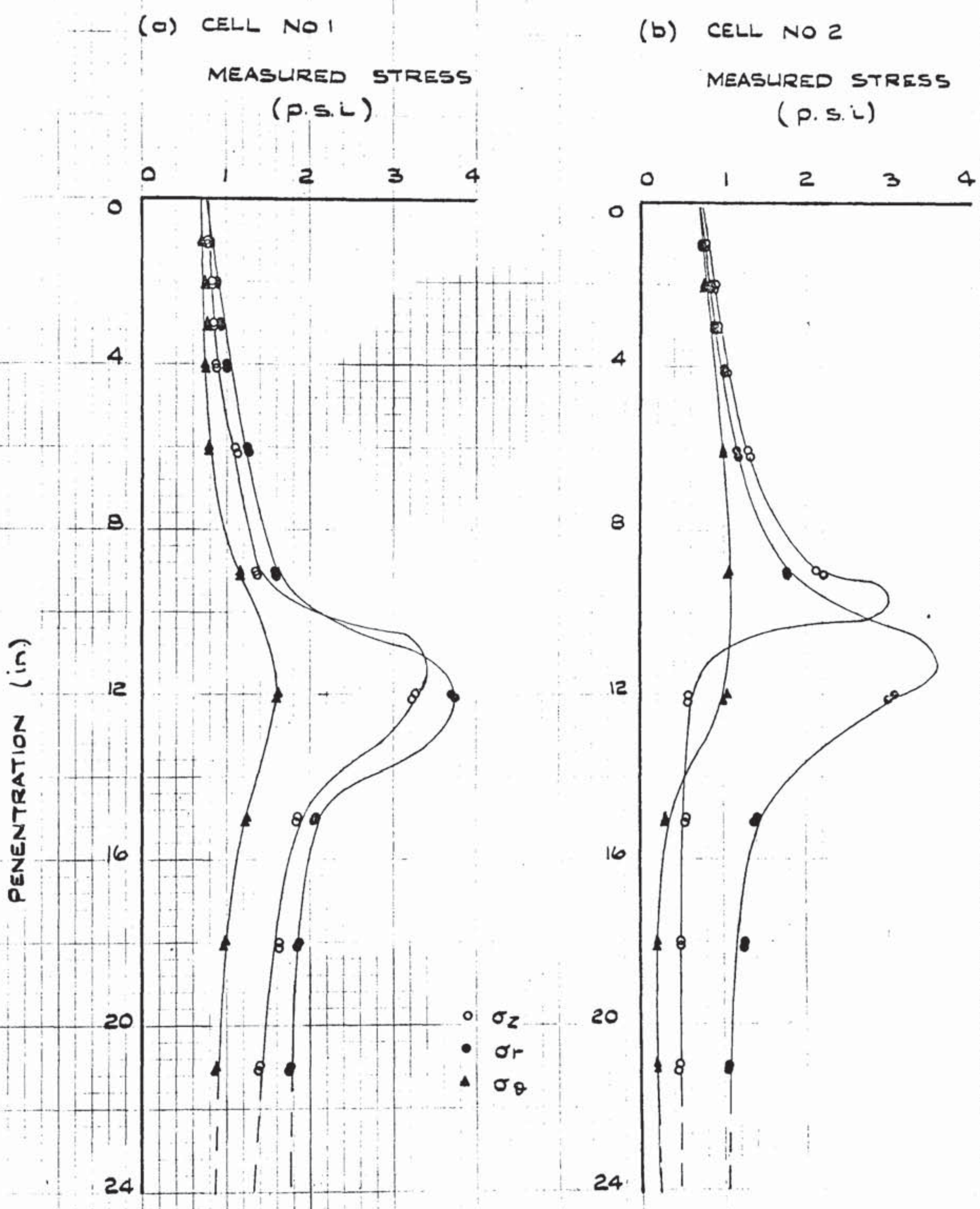

CO-ORDINATES OF CELL FACES:
$r = 0.82$ in.
$z = 12.74$ in.

CO-ORDINATES OF CELL FACES
$r = 1.55$ in.
$z = 10.71$ in.

INITIAL PROPERTIES OF SAND:

γ_d : 94.69 lb/cu.ft

η = 42.74%

COULOMB ϕ = 32.2° (DIRECT SHEAR TESTS)

FIGURE 6. 2. (c) MEASURED STRESS VERSUS PENETRATION FOR CELL IN LOOSE - MEDIUM SAND

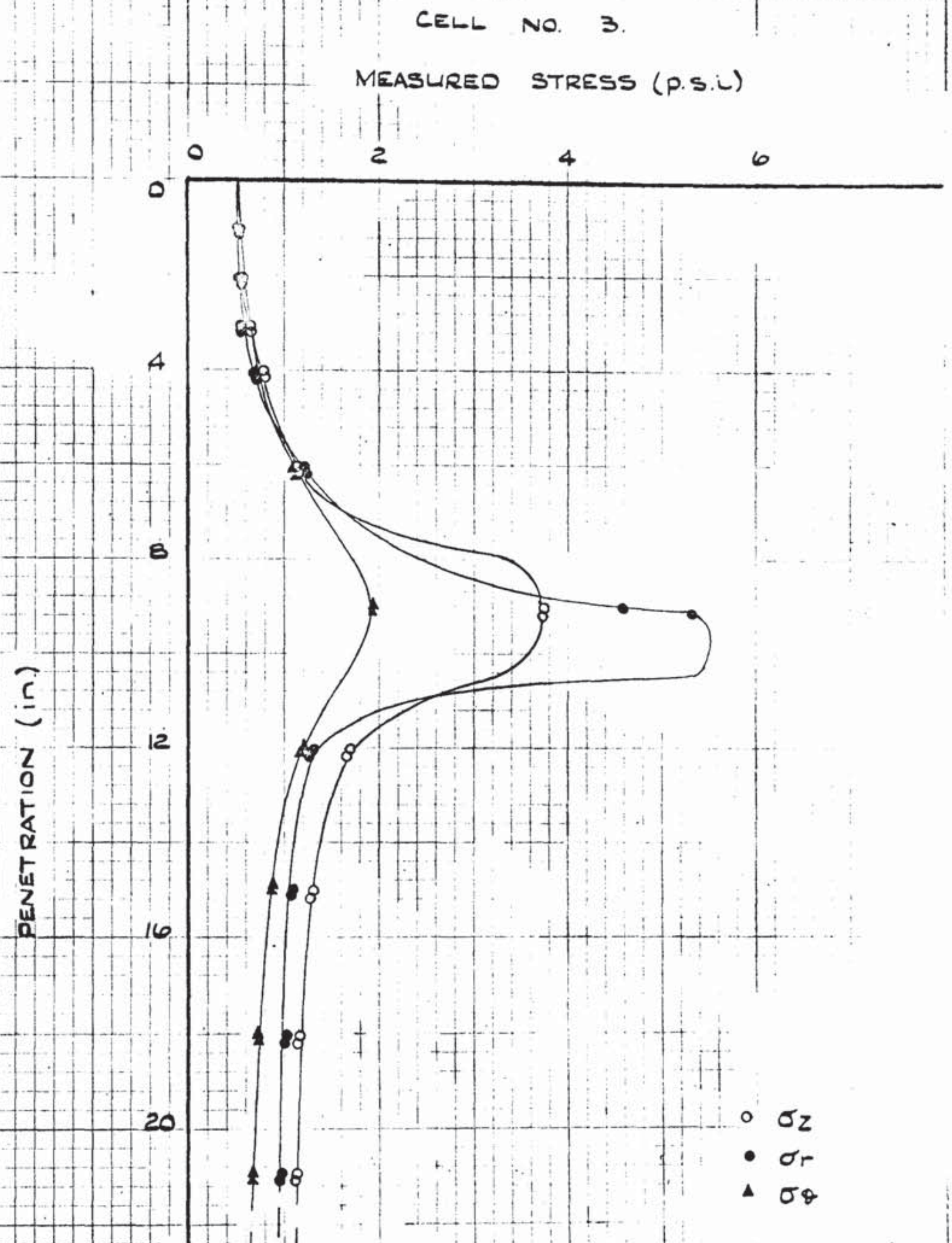

CO-ORDINATES OF CELL FACES:

$r = 0 \cdot 73$ in.

$z = 9 \cdot 30$ in.

INITIAL PROPERTIES OF SAND:

$\gamma_d = 94 \cdot 69$ lb/cu.ft.

$\eta = 42 \cdot 74$ %

COULOMB $\phi = 32 \cdot 2^{\circ}$ (DIRECT SHEAR TESTS)

FIGURE 6.2.(d) & (e) MEASURED STRESS VERSUS PENETRATION FOR CELLS IN LOOSE - MEDIUM SAND.

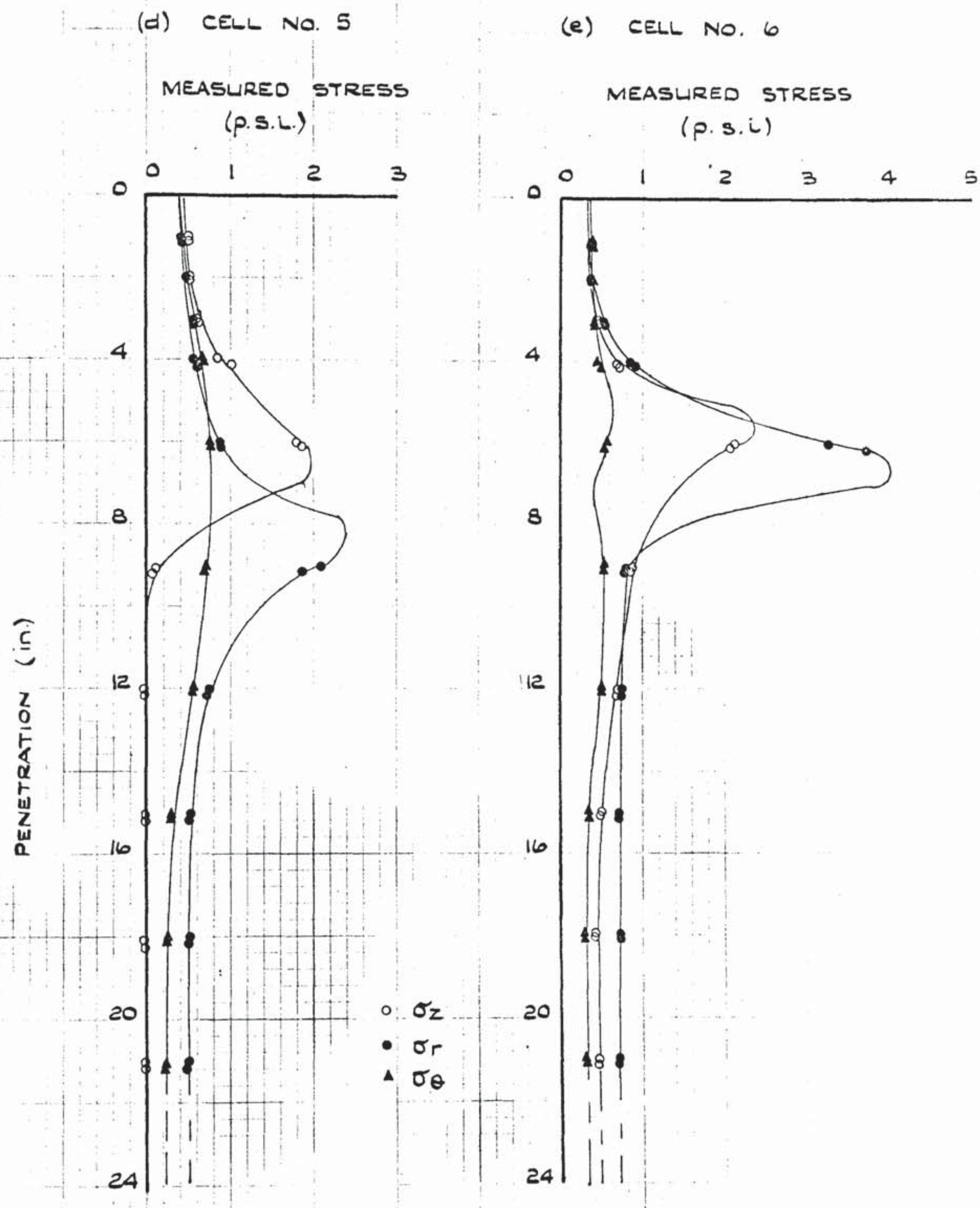

CO-ORDINATES OF CELL FACES
$r = 1.40$ in.
$z = 7.70$ in.

CO-ORDINATES OF CELL FACES:
$r = 0.92$ in.
$z = 6.13$ in.

INITIAL PROPERTIES OF SAND:

$\gamma_d = 94.69$ lb/cu ft

$\eta = 42.74\ \%$

COULOMB $\phi = 32.2°$ (DIRECT SHEAR TESTS)

FIGURE 6.2. (f) & (g) MEASURED STRESS VERSUS PENETRATION FOR CELLS IN LOOSE - MEDIUM SAND.

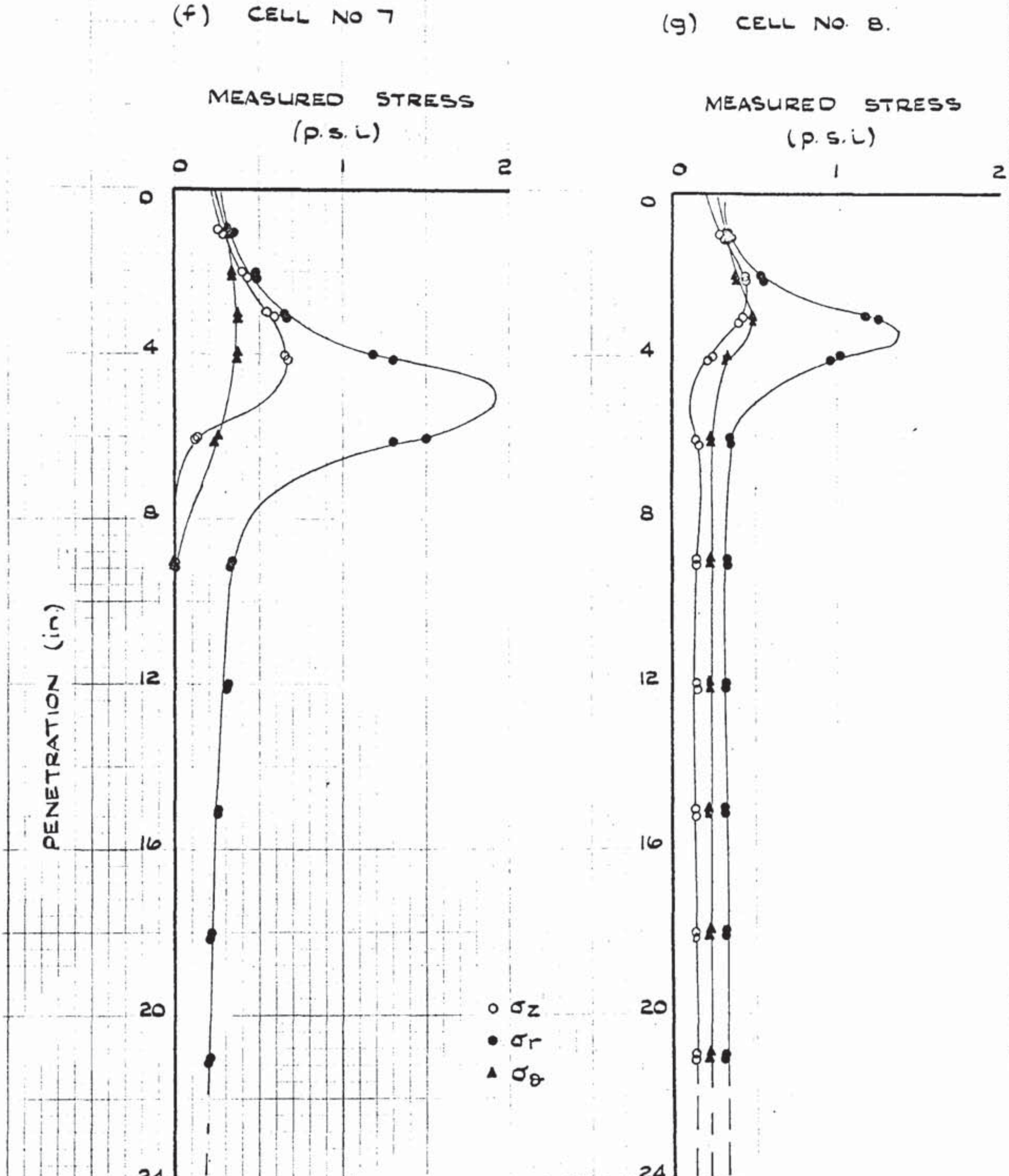

CO-ORDINATES OF CELL FACES.
r = 1·65 in.
z = 4·70 in.

CO-ORDINATES OF CELL FACES.
r = 1·34 in.
z = 2·89 in.

INITIAL PROPERTIES OF SAND :

γ_d = 94·69 lb/cu.ft.

η = 42·74 %

COULOMB ϕ = 32·2° (DIRECT SHEAR TESTS)

FIGURE 6.2.(h) & (j) MEASURED STRESS VERSUS PENETRATION FOR CELLS IN LOOSE - MEDIUM SAND

(h) CELL NO. 9. (j) CELL NO. 0

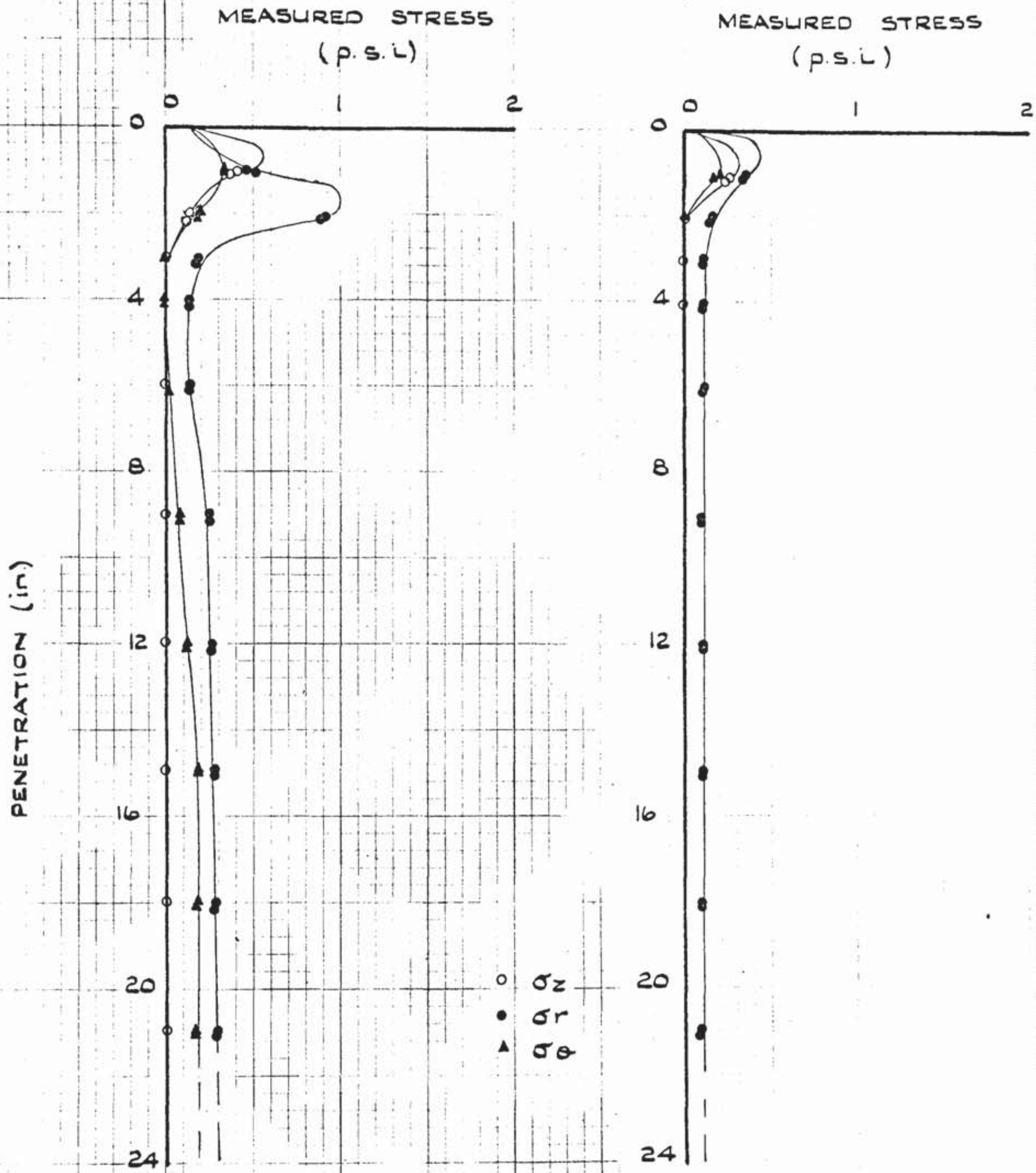

CO-ORDINATES OF CELL FACES

r = 0·90 in.

z = 1·54 in.

CO-ORDS OF CELL FACES

r = 1·56 in.

z = 0·52 in.

INITIAL PROPERTIES OF SAND :

γd = 94·69 lb/cu.ft.

η = 42·74°

COULOMB ϕ = 32·2° (DIRECT SHEAR TEST)

FIGURE 6.3 (a) MEASURED STRESS VERSUS PENETRATION FOR CELL IN DENSE SAND

CELL No 1.

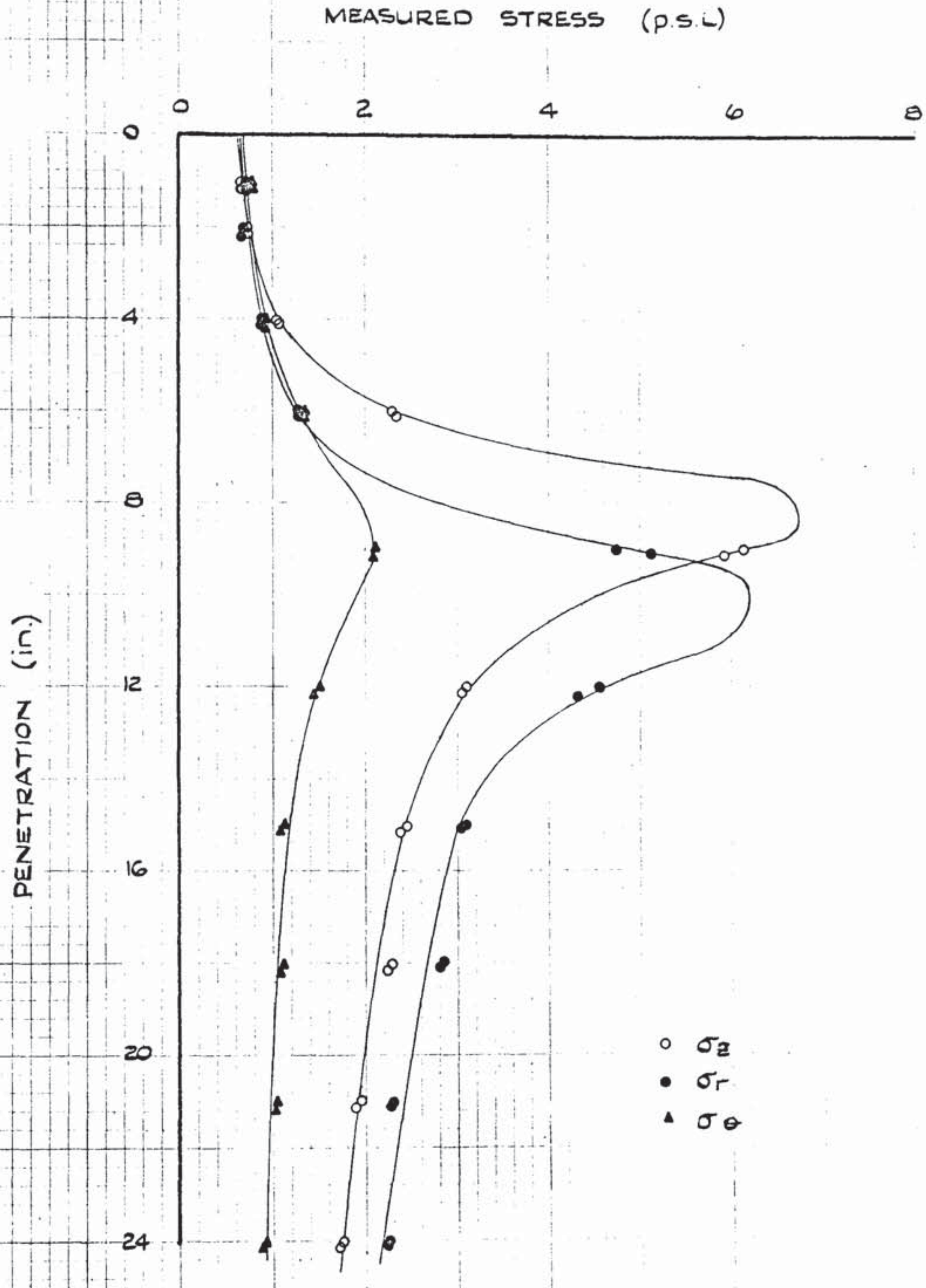

CO-ORDS OF CELL FACES :

r = 1·37 in.

z = 10·1 in.

INITIAL PROPERTIES OF SAND :

γ_d = 104·74 lb/cu.ft.

η = 36·82 %

COULOMB ϕ = 40·8° (DIRECT SHEAR TESTS)

FIGURE 6.3 (b) & (c) MEASURED STRESS VERSUS PENETRATION FOR CELLS IN DENSE SAND

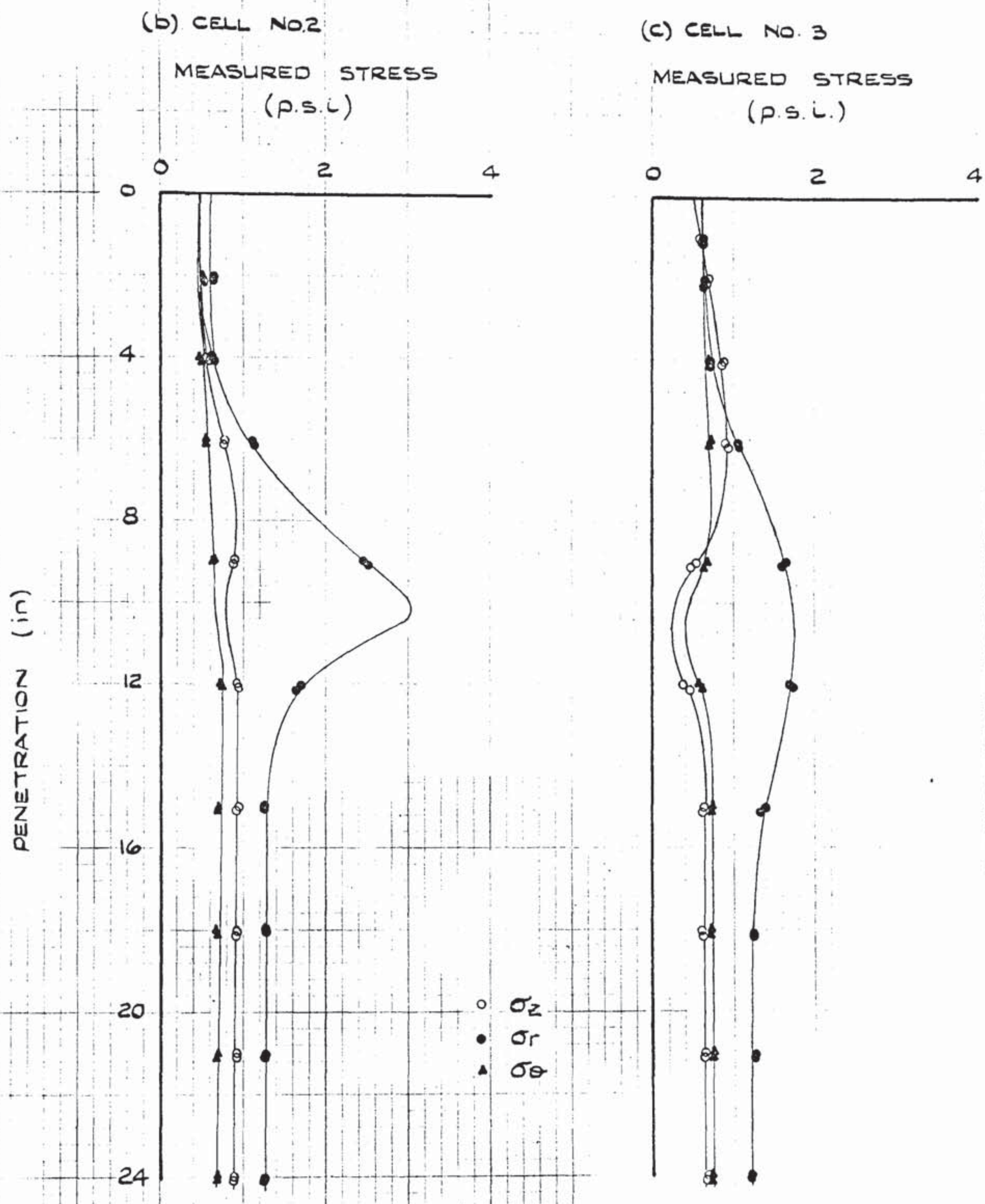

CO-ORDS OF CELL FACES:
$r = 4\cdot79$ in.
$z = 9\cdot75$ in.

CO-ORDS OF CELL FACES:
$r = 8\cdot28$ in.
$z = 9\cdot75$ in.

INITIAL PROPERTIES OF SAND:
$\gamma_d = 104\cdot74$ lb/cu. ft.
$\eta = 36\cdot82$ %
COULOMB $\phi = 40\cdot8°$ (DIRECT SHEAR TESTS)

FIGURE 6.3(d) MEASURED STRESS VERSUS PENETRATION FOR CELL IN DENSE SAND

CELL No. 5.

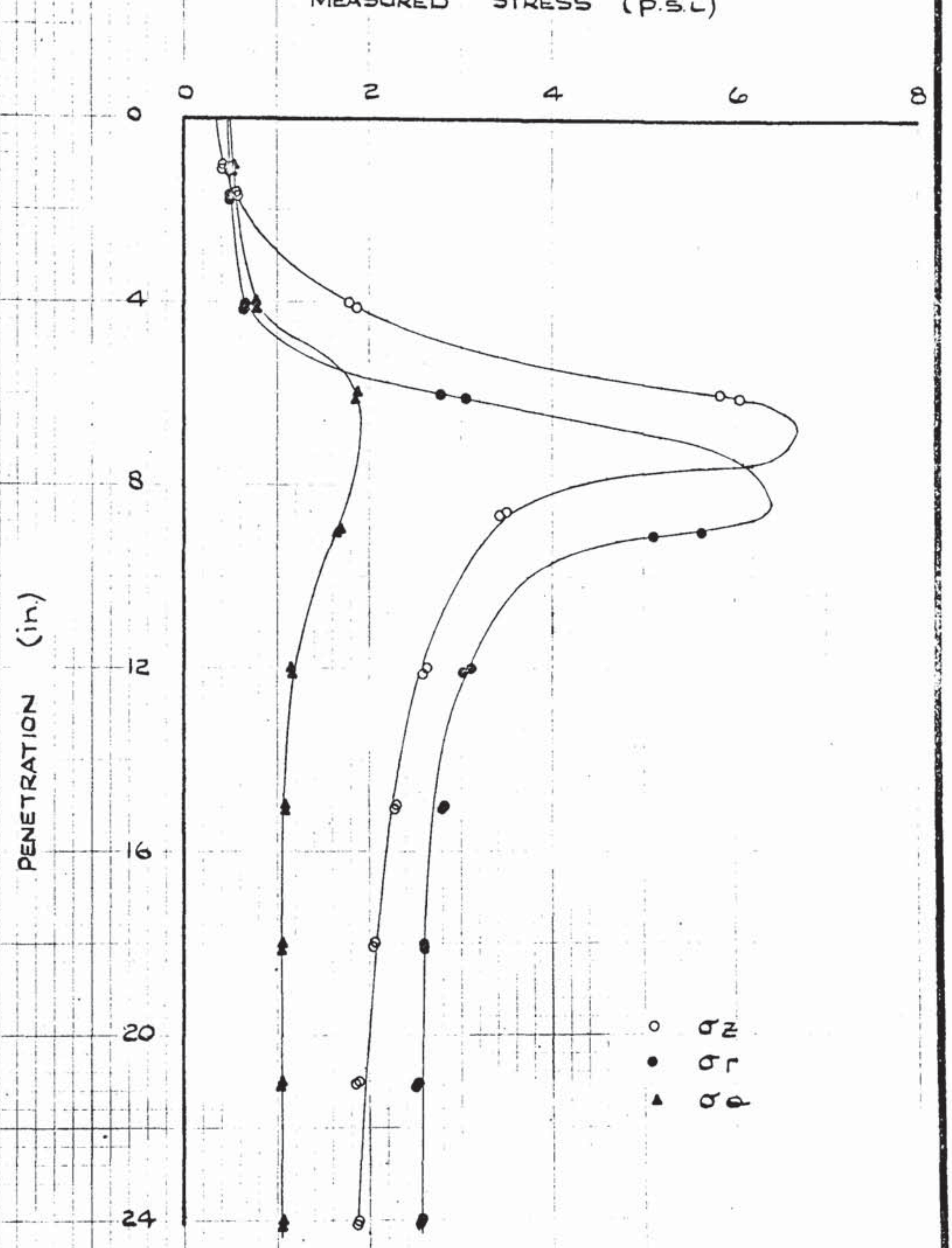

CO-ORDS OF CELL FACES :

$r = 1 \cdot 3$ in.

$z = 7 \cdot 25$ in.

INITIAL PROPERTIES OF SAND :

$\gamma_d = 104 \cdot 74$ lb/cu. ft.

$\eta = 36 \cdot 82$ %

COULOMB. $\phi = 40 \cdot 8°$ (DIRECT SHEAR TESTS)

FIGURES 6.3 (e) & (g) MEASURED STRESS VERSUS PENETRATION FOR CELLS IN DENSE SAND

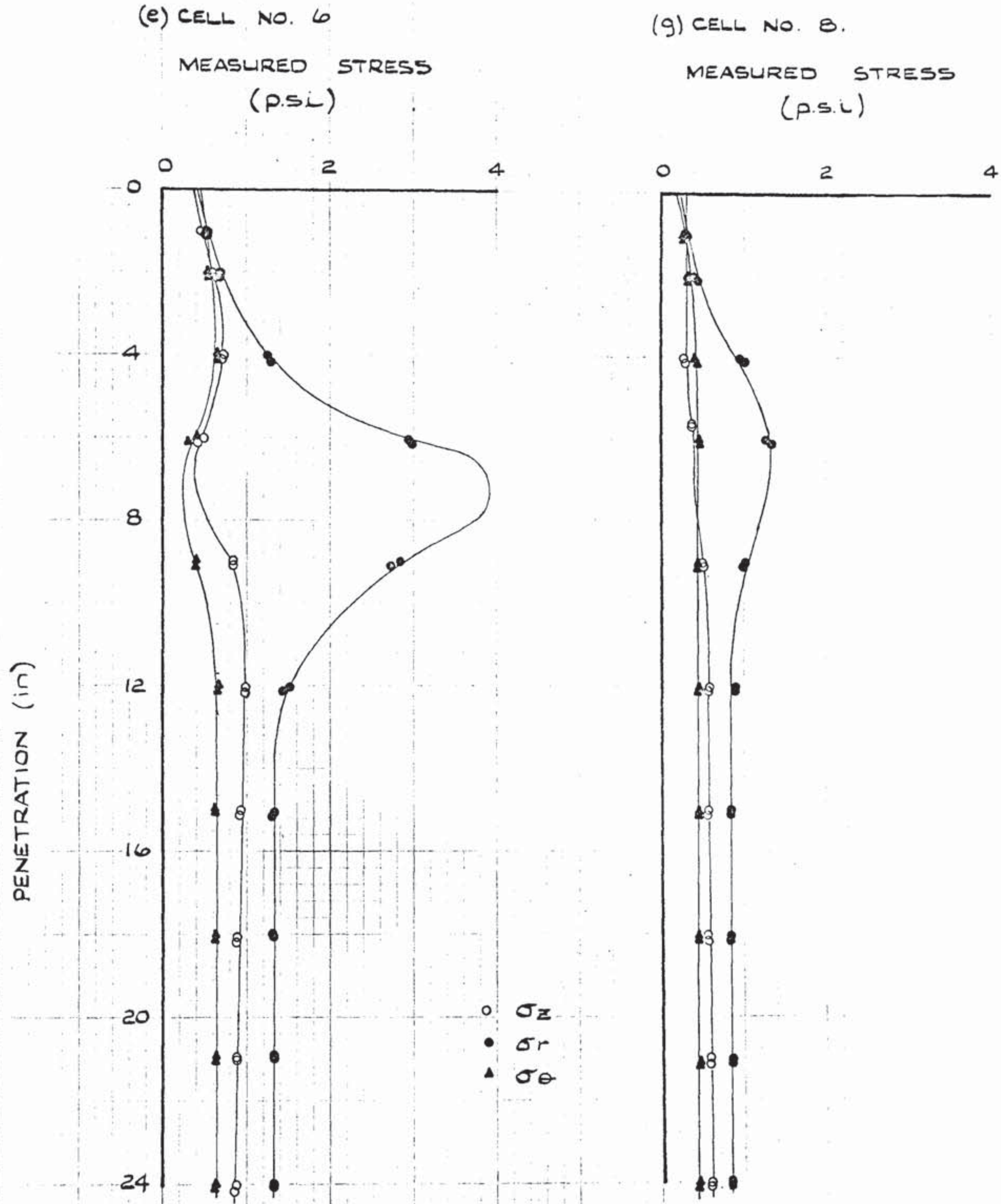

CO-ORDS OF CELL FACES :
$r = 3 \cdot 9$ in.
$z = 7 \cdot 0$ in.

CO-ORDS OF CELL FACES :
$r = 5 \cdot 10$ in.
$z = 4 \cdot 10$ in.

INITIAL PROPERTIES OF SAND :

$\gamma_d = 104 \cdot 74$ lb/cu.ft.

$\eta = 36 \cdot 82$ %

COULOMB $\phi = 40 \cdot 8°$ (DIRECT SHEAR TESTS)

FIGURE 6.3(f) MEASURED STRESS VERSUS PENETRATION FOR CELL IN DENSE SAND.

CELL NO. 7

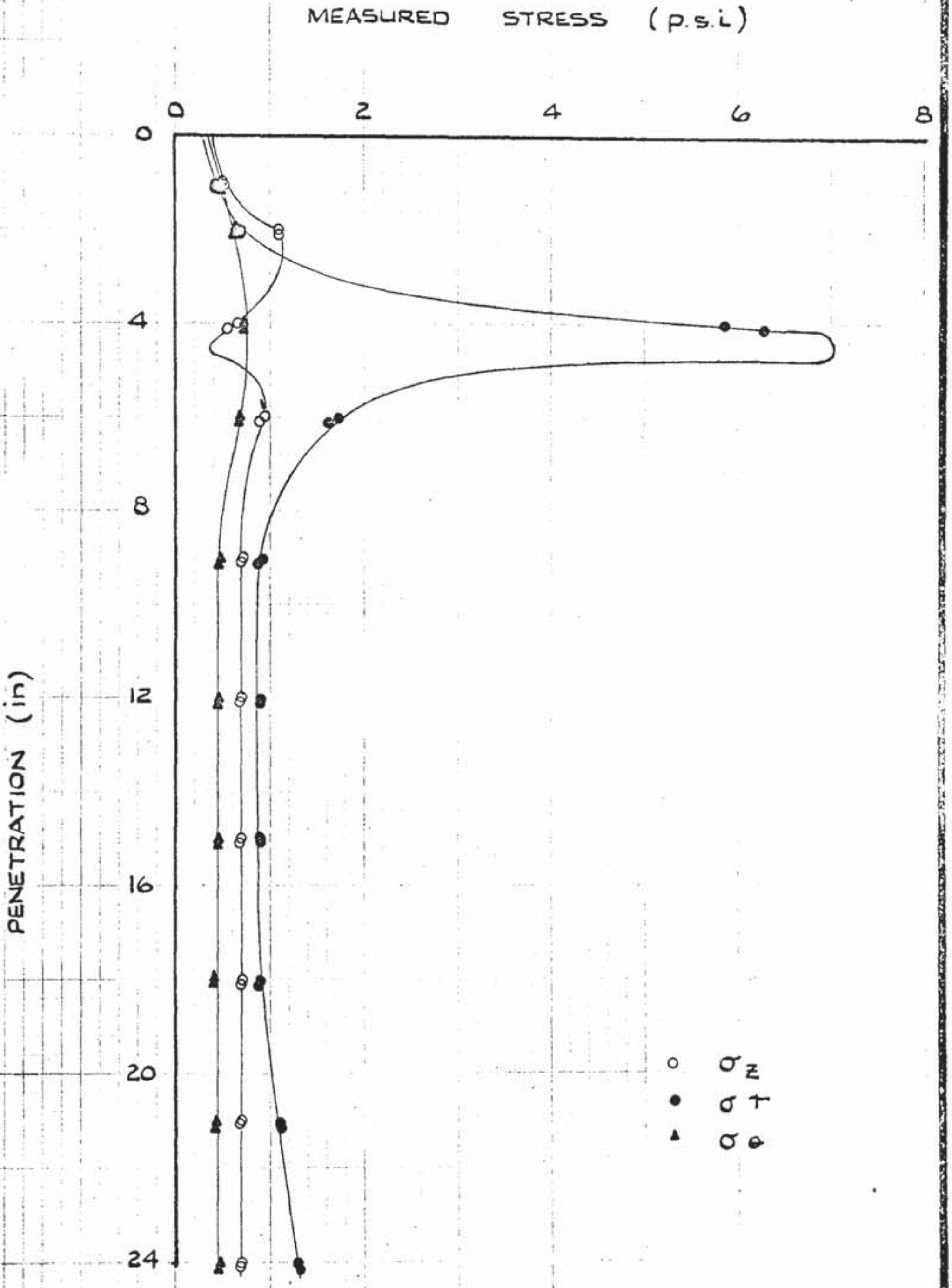

CO-ORDS OF CELL FACES :

r = 1·31 in.

z = 4·10 in.

INITIAL PROPERTIES OF SAND :

γ_d = 104·74 lb/cu.ft.

η = 36·82 %

COULOMB ϕ = 40·8° (DIRECT SHEAR TESTS)

FIGURE 6.3 (h) & (j) MEASURED STRESS VERSUS PENETRATION FOR CELLS IN DENCE SAND

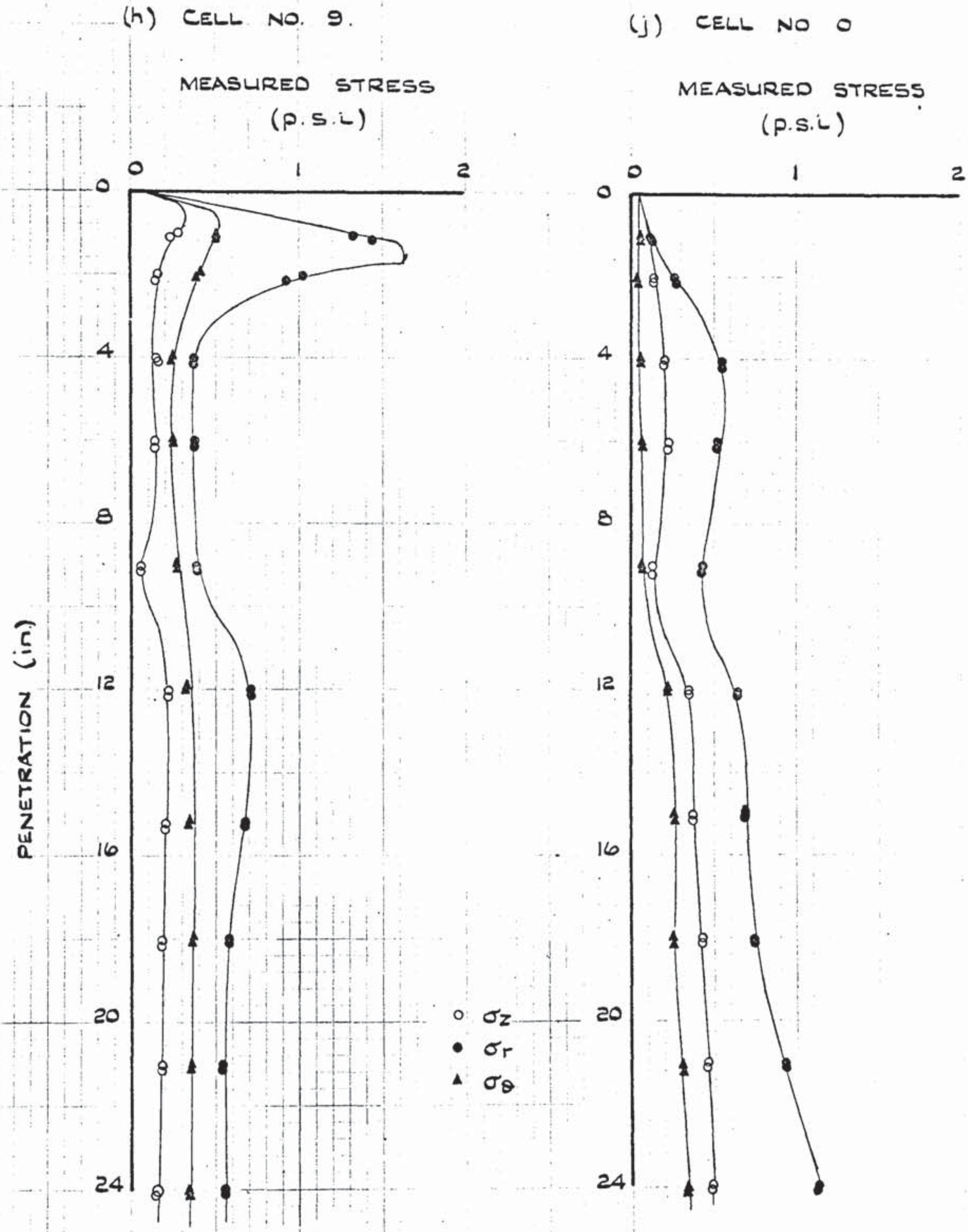

CO-ORDINATES OF CELL FACES
$r = 1 \cdot 17$ in.
$z = 1 \cdot 14$ in.

CO-ORDINATES OF CELL FACES
$r = 3 \cdot 47$ in.
$z = 1 \cdot 23$ in.

INITIAL PROPERTIES OF SAND

$\gamma_d = 104 \cdot 74$ lb/cu.ft.

$\eta = 36 \cdot 82$ %

COULOMB $\phi = 40 \cdot 8°$ (DIRECT SHEAR TESTS)

FIGURE 6.4 (a) & (b) POSITIONS OF MINUATURE PRESSURE CELL IN A θ - CONSTANT PLANE (A - A)

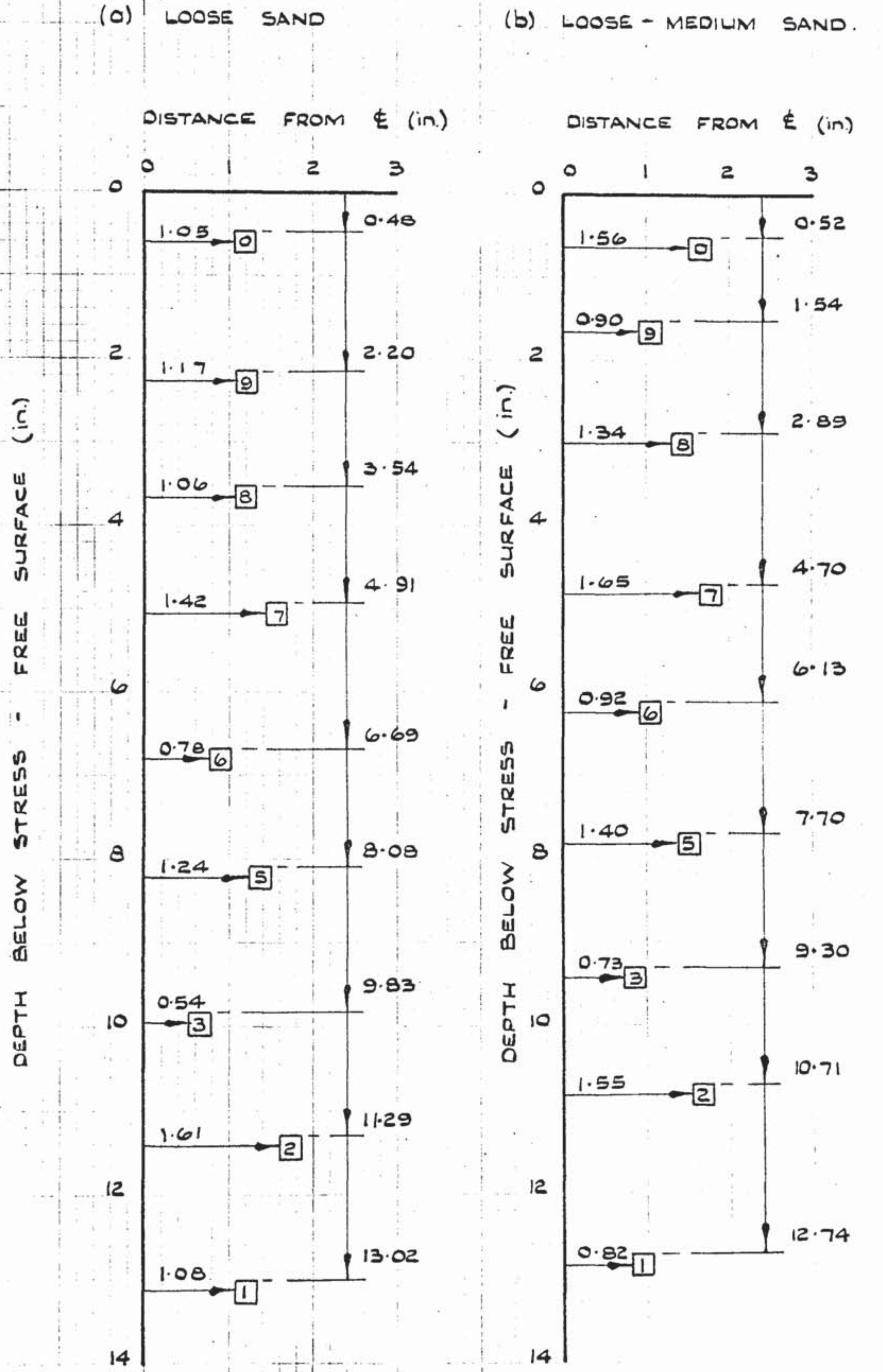

FIGURE 6.4. (c) POSITIONS OF MINUATURE PRESSURE CELLS IN A θ - CONSTANT PLANE (A-A) IN DENSE SAND.

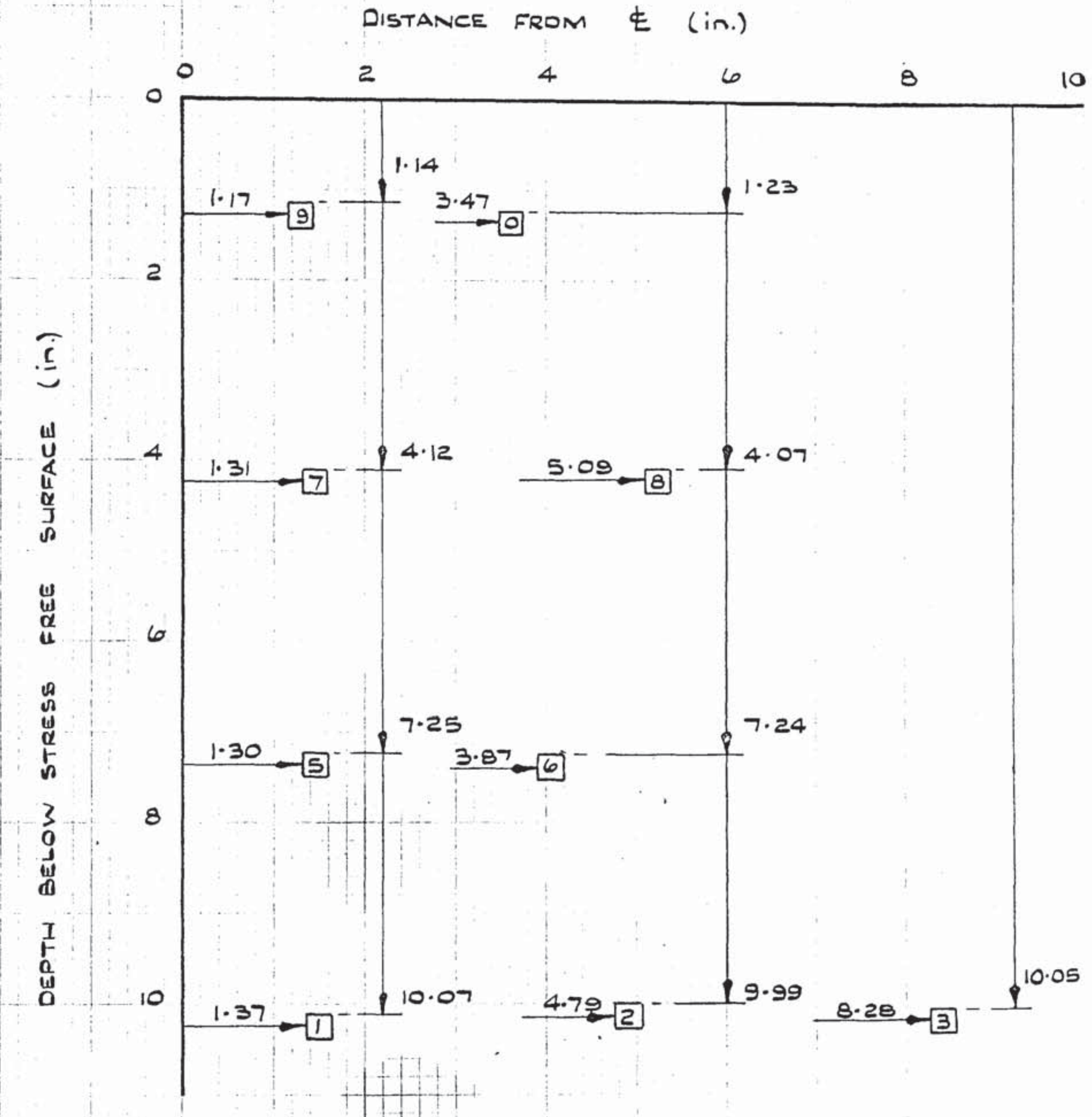

FIGURE 6.4 (d) θ - CONSTANT PLANE (A-A)

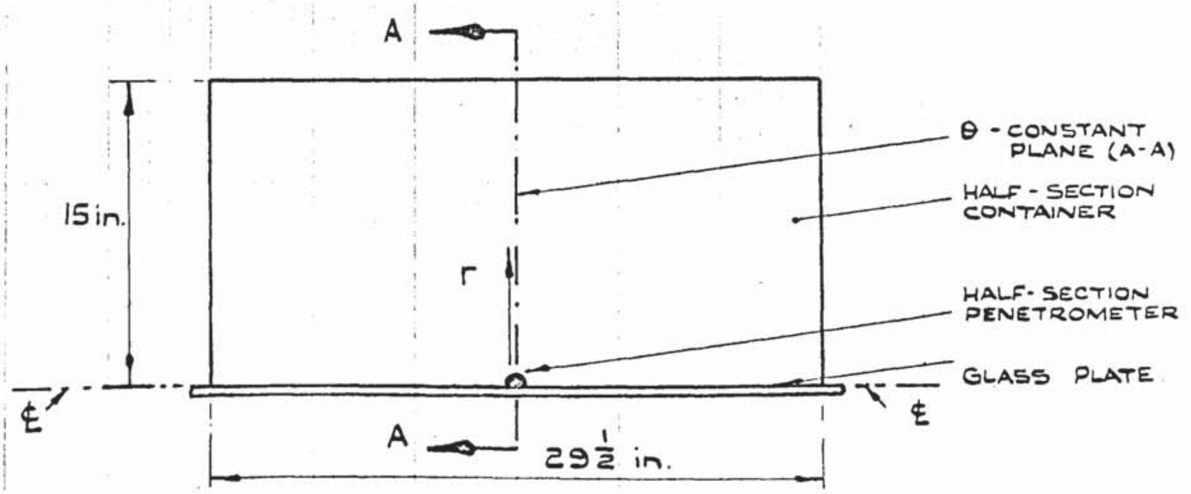

FIGURE 6.5. PENETRATION RESISTANCE FOR 'HALF SECTION' PENETROMETER IN LOOSE SAND.

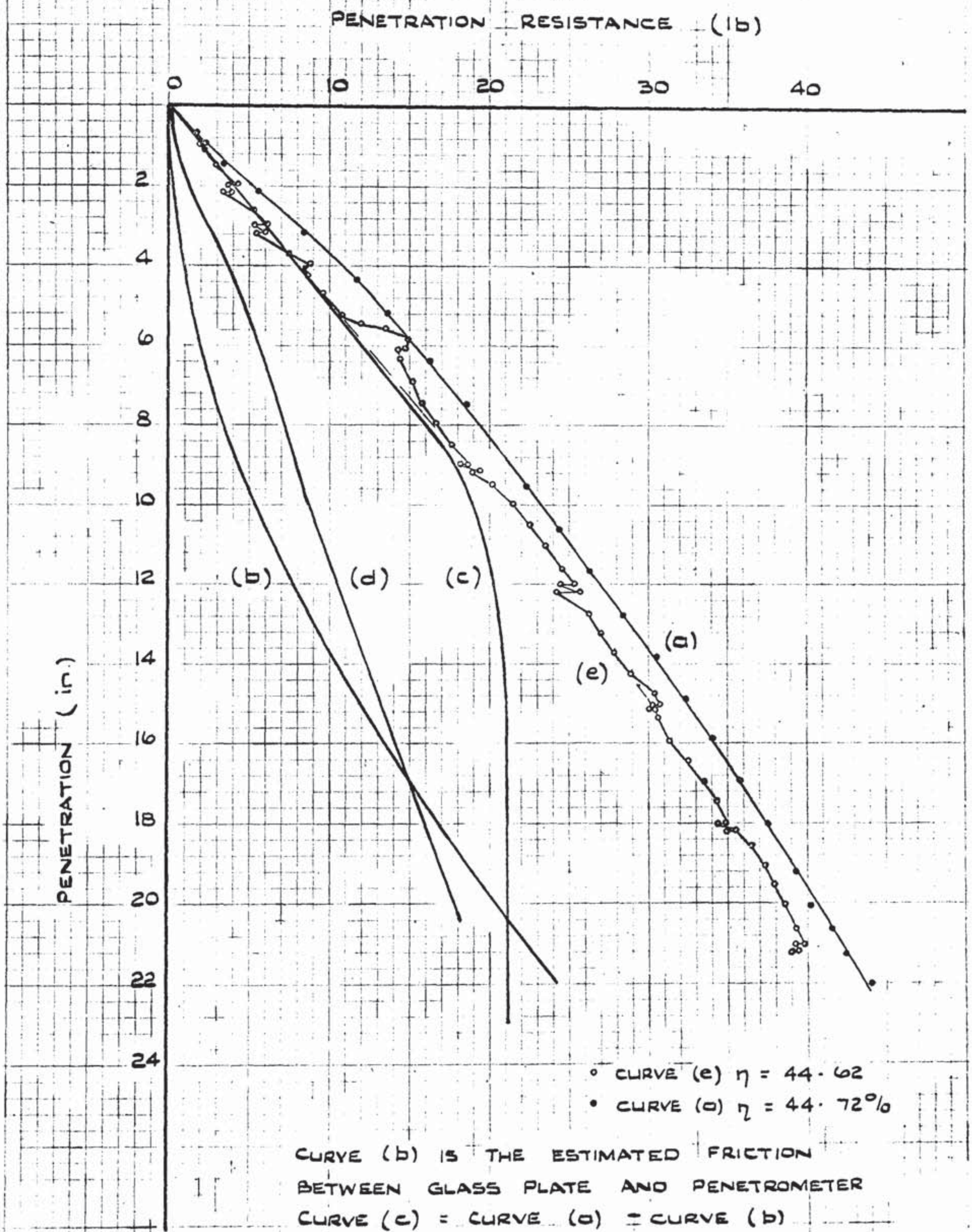

CURVE (b) IS THE ESTIMATED FRICTION BETWEEN GLASS PLATE AND PENETROMETER

CURVE (c) = CURVE (a) − CURVE (b)

CURVES (a) (d) AND (e) ARE EXPERIMENTAL RESULTS.

FIGURE 6.6.

PENETRATION RESISTANCE FOR 'HALF - SECTION' PENETROMETER IN LOOSE - MEDIUM SAND.

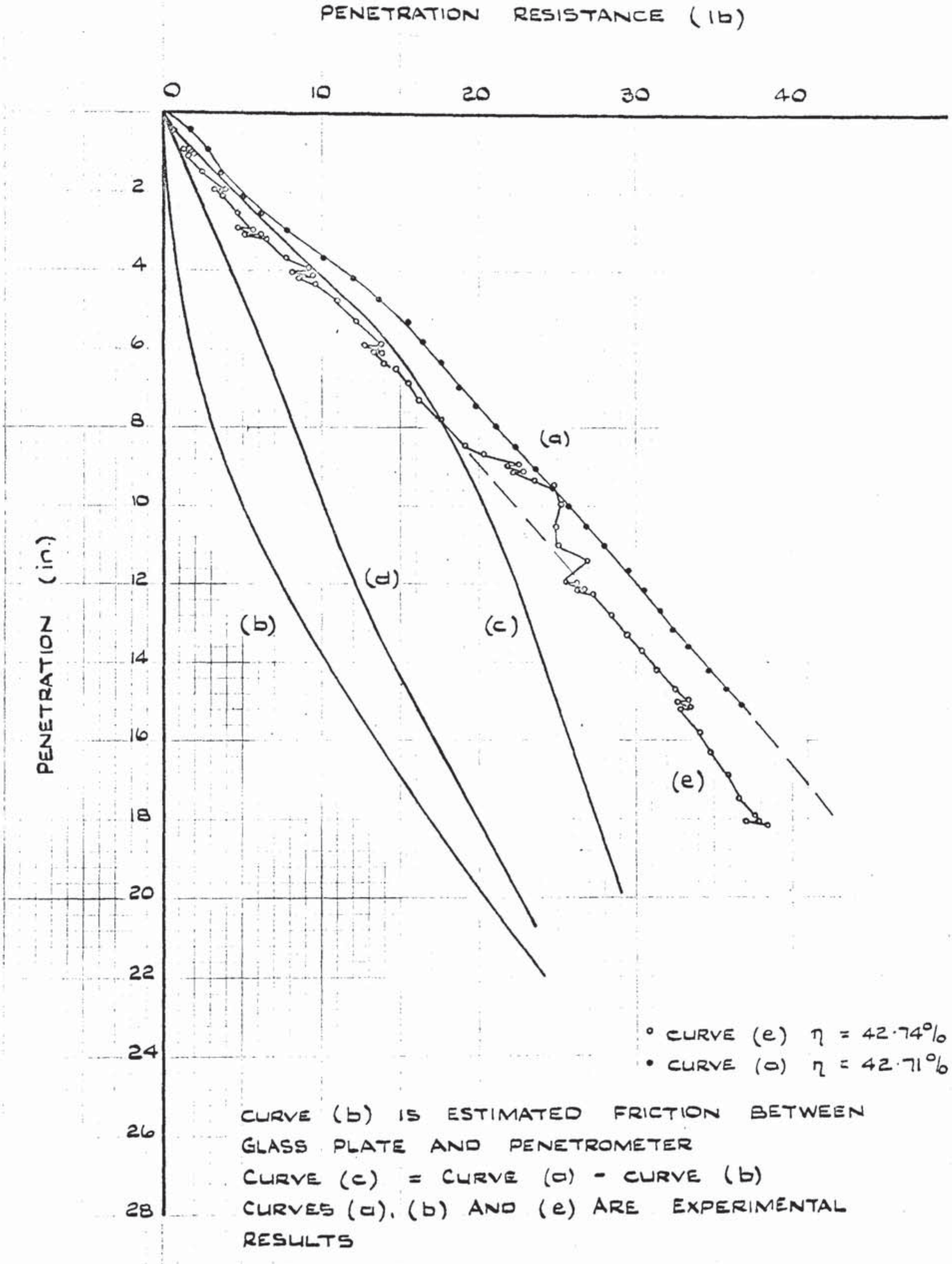

FIGURE 6.7. PENETRATION RESISTANCE FOR 'HALF - SECTION' PENETROMETER IN DENSE SAND.

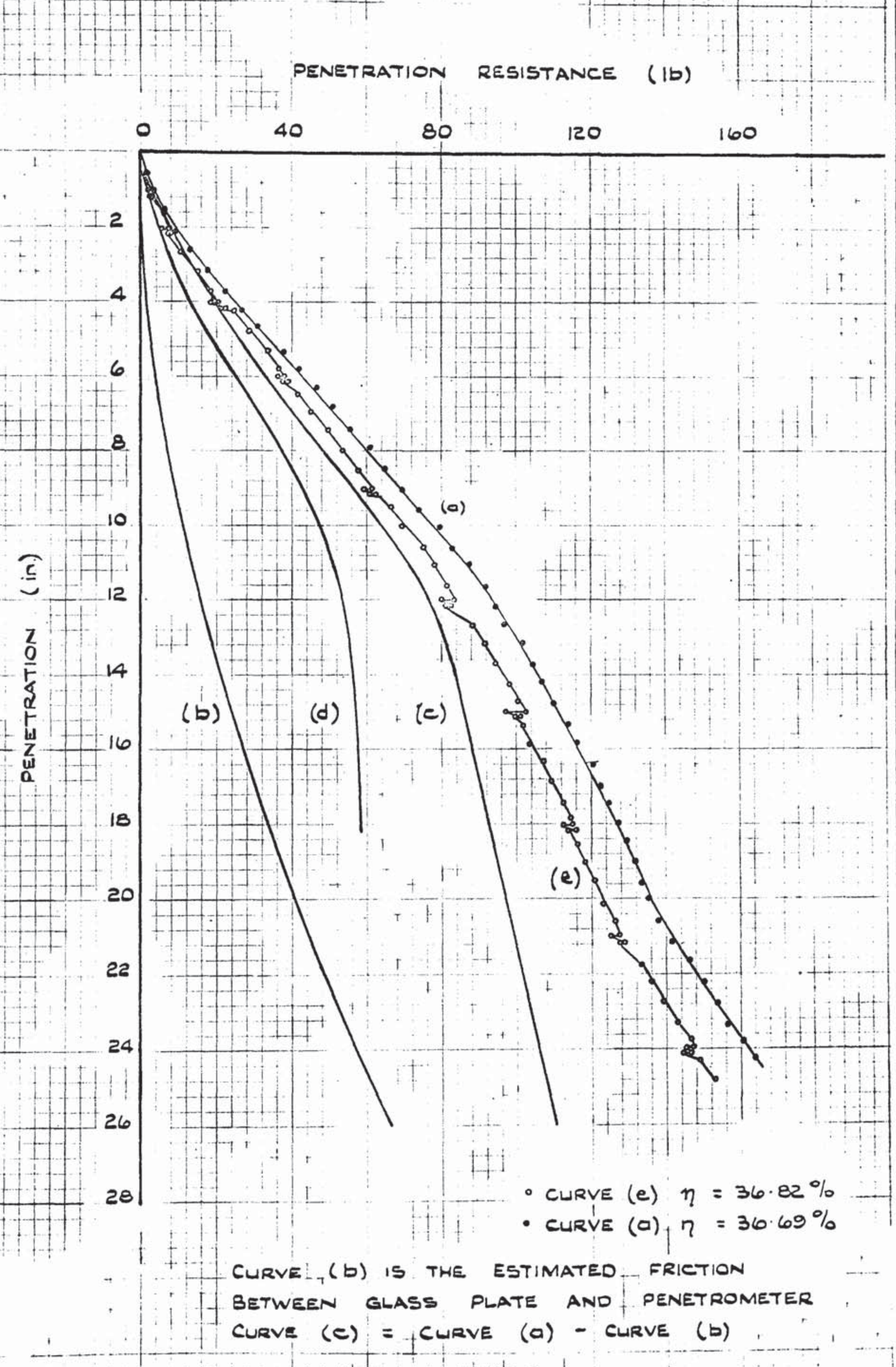

FIGURE 6.8. SURFACE HEAVE DURING PENETRATION INTO DENSE SAND - MEASURED THROUGH HALF SECTION CONTAINER FRONT FACE

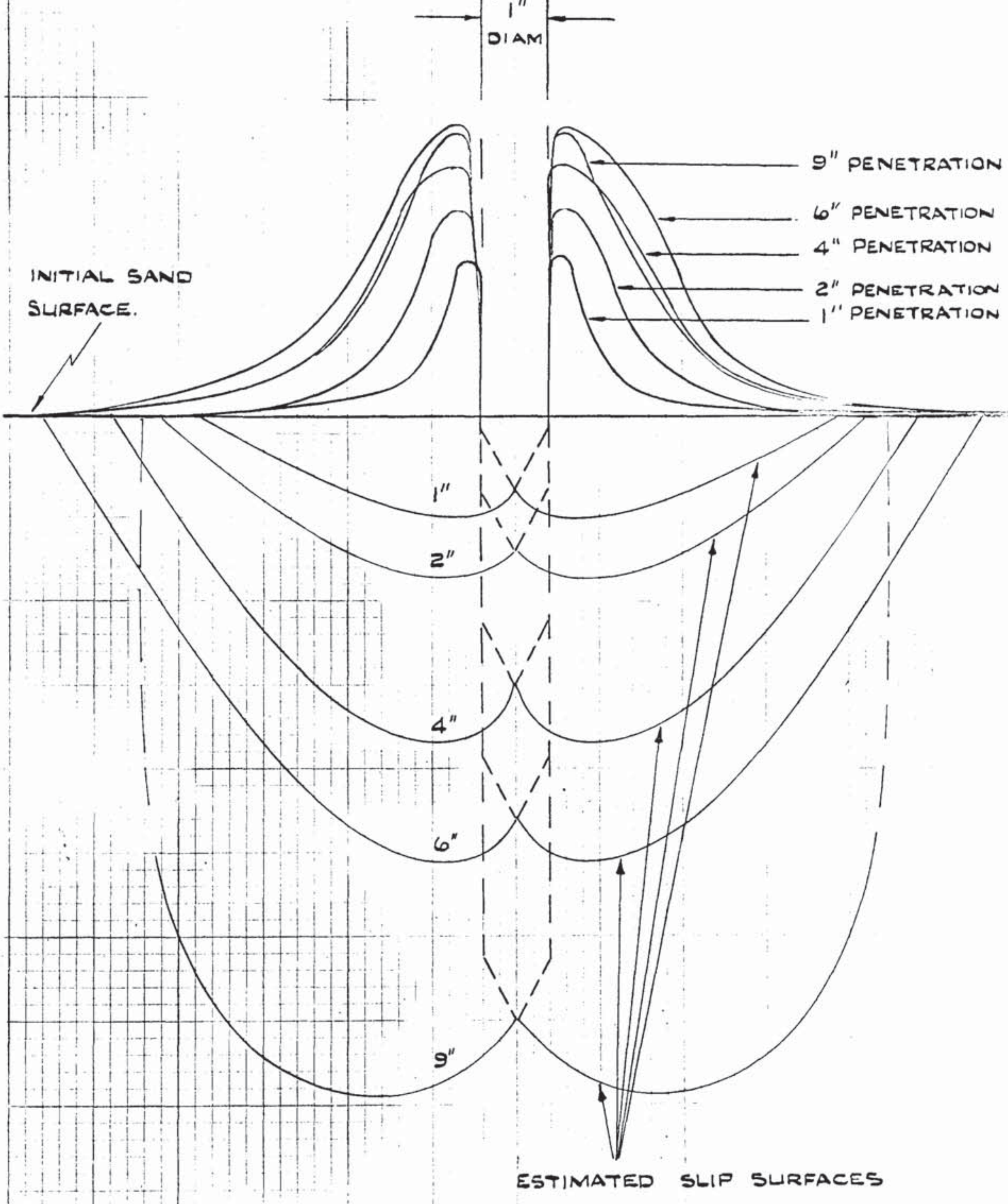

ABOVE THE INITIAL SAND SURFACE THE VERTICAL SCALE IS 20 x THE HOZIZONTAL SCALE.

BELOW THE INITIAL SAND SURFACE THE VERTICAL AND HORIZONTAL SCALES ARE EQUAL.

FIGURE 6.9. (a) & (b) MOHR STRESS CIRCLES FROM PRESSURE CELL MEASUREMENTS IN LOOSE SAND - ASSUMING $\sigma_3 = \sigma_\theta$ AND $\sigma = (\sigma_z + \sigma_r) . \frac{1}{2}$

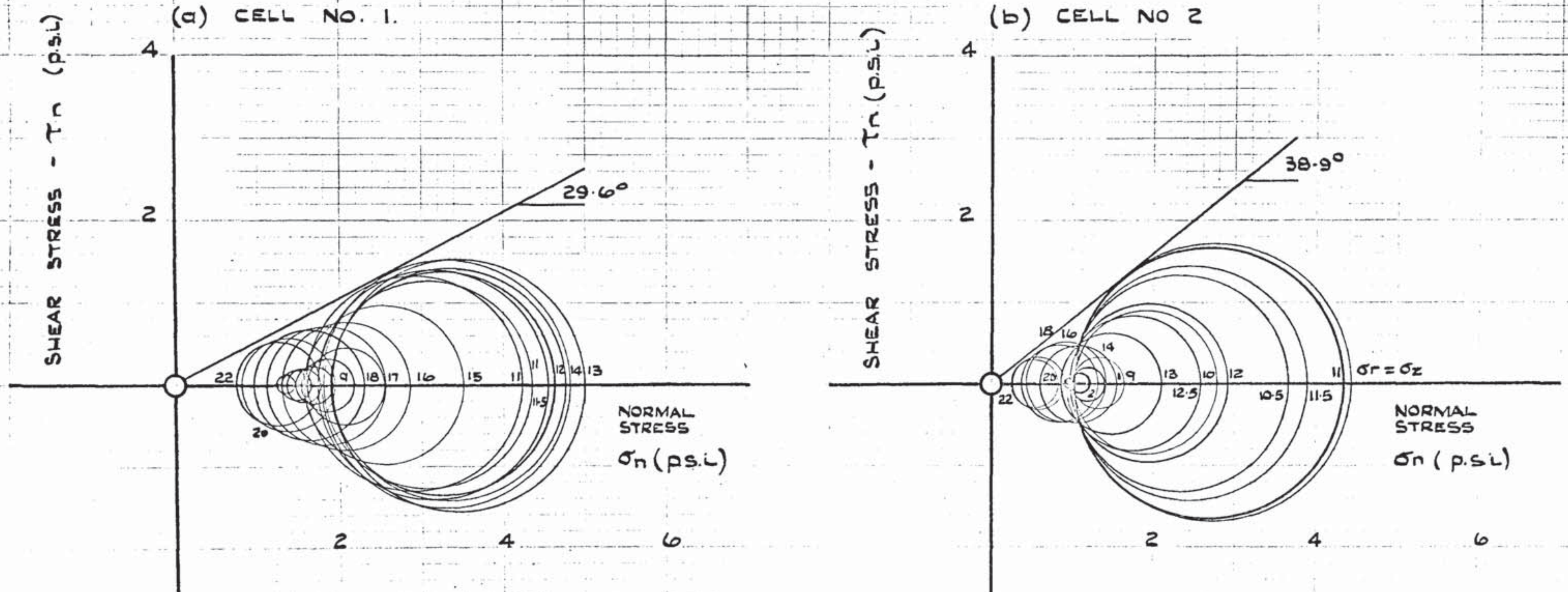

N.B. FIGURE BY EACH CIRCLE INDICATES PENETRATION (in.)

CO-ORDINATES OF CELL FACES :

r = 1·08 in.

z = 13·02 in.

CO-ORDINATES OF FACES :

r = 1·61 in.

z = 11·29 in.

DRY DENSITY OF SAND = 91·68 lb/cu. ft.

COULOMB ϕ FROM DIRECT SHEAR TESTS = 31·8°

FIGURE 6.9. (c) & (d). MOHR CIRCLES OF STRESS OBTAINED FROM PRESSURE CELL MEASUREMENTS IN LOOSE SAND - ASSUMING $\sigma_3 = \sigma_\theta$ AND $\sigma = (\sigma_r + \sigma_z) . \frac{1}{2}$

(c) CELL NO 3

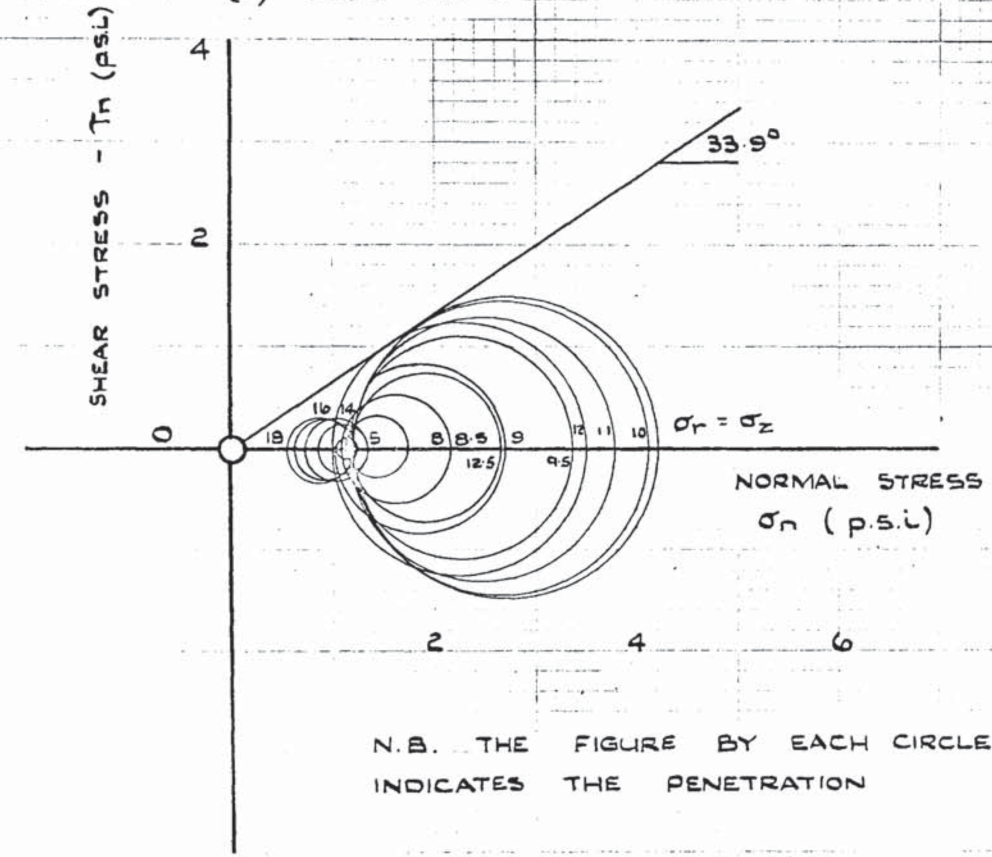

N.B. THE FIGURE BY EACH CIRCLE INDICATES THE PENETRATION

CO-ORDINATES OF CELL FACES:

r = 0·54 in.

z = 9·83 in.

(d) CELL NO. 5

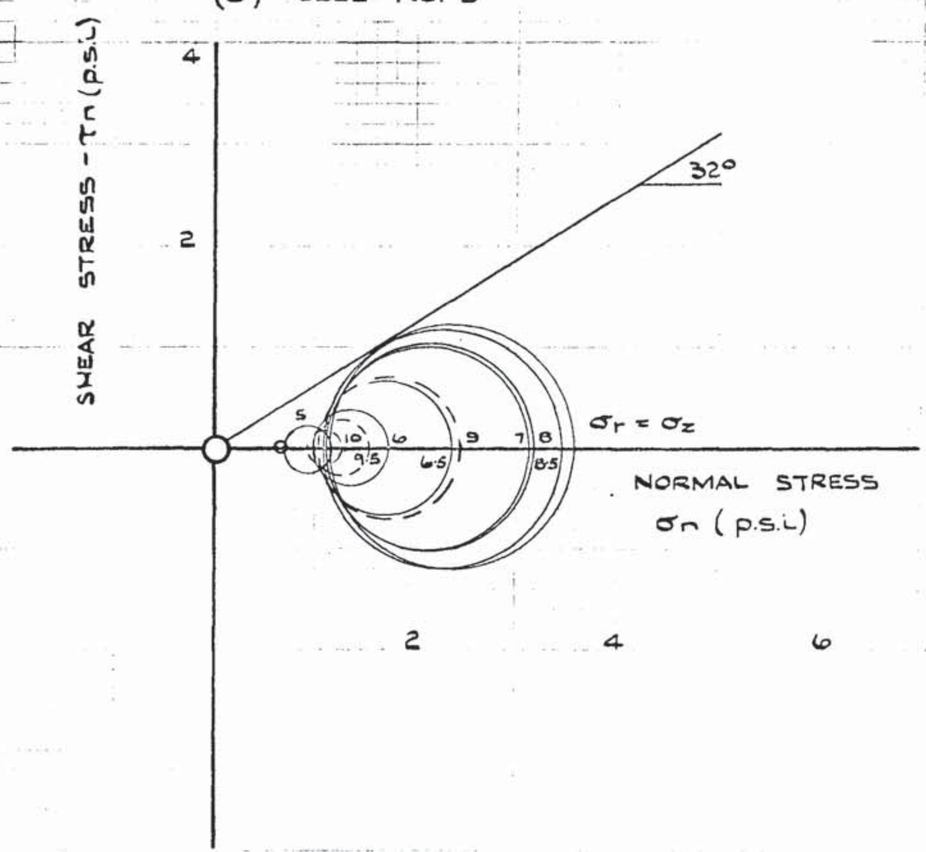

CO-ORDINATES OF CELL FACES:

r = 1·24 in.

z = 8·08 in.

DRY DENSITY OF SAND = 91·58 lb/cu.ft

COULOMB Ø OBTAINED FROM DIRECT SHEAR TESTS = 31·8°

FIGURE 6.9. (e) & (f) MOHR CIRCLES OF STRESS OBTAINED FROM PRESSURE CELL MEASUREMENTS IN LOOSE SAND ASSUMING $\sigma_3 = \sigma_\theta$ AND $\sigma = (\sigma_r + \sigma_z) \cdot \frac{1}{2}$

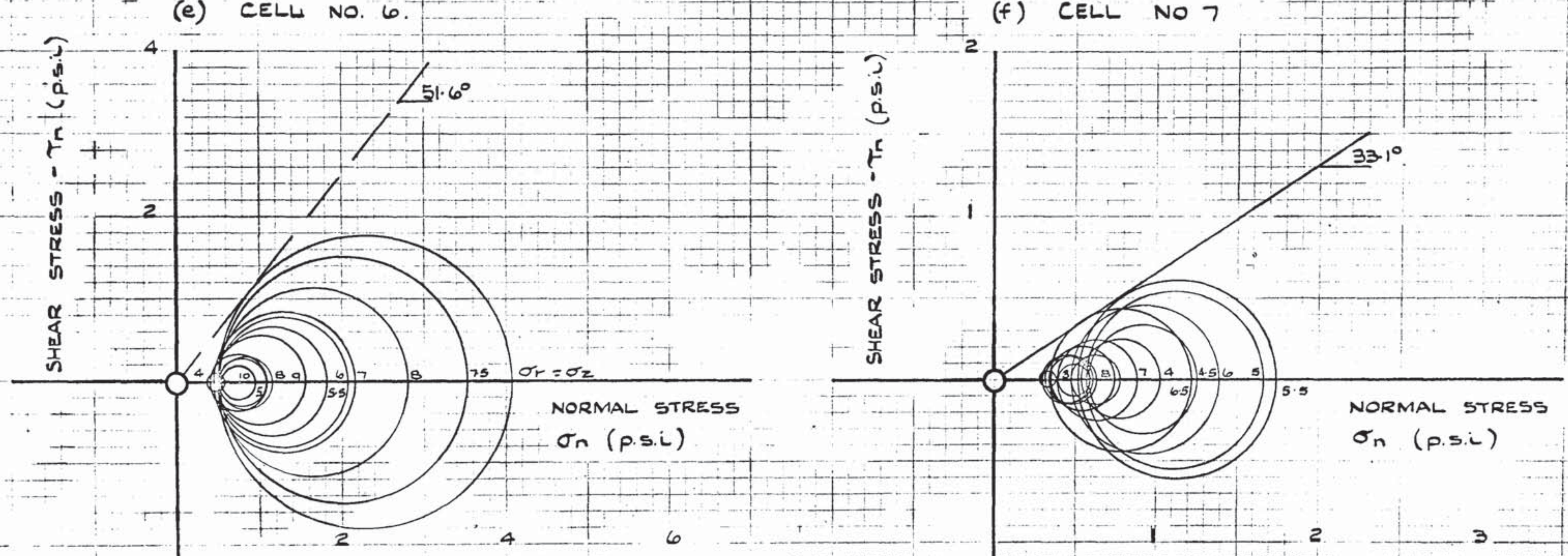

N.B. THE FIGURE BY EACH CIRCLE INDICATES THE PENETRATION (in.)

CO-ORDINATES OF CELL FACES (CELL NO. 6)

r = 0·78 in.

z = 6·69 in.

CO-ORDINATES OF CELL FACES (CELL NO 7):

r = 1·42 in.

z = 4·91 in.

DRY DENSITY OF SAND = 91·68 lb/cu.ft.

COULOMB ϕ FROM DIRECT SHEAR TESTS = 31·8°

FIGURE 6.9. (g).(h) & (j) MOHR STRESS CIRCLES OBTAINED FROM PRESSURE CELL MEASUREMENTS IN LOOSE SAND - ASSUMING $\sigma_3 = \sigma_\theta$ AND $\sigma = (\sigma_r + \sigma_z) . \frac{1}{2}$

(g) CELL No 8. (h) CELL No. 9 (j) CELL No. 0

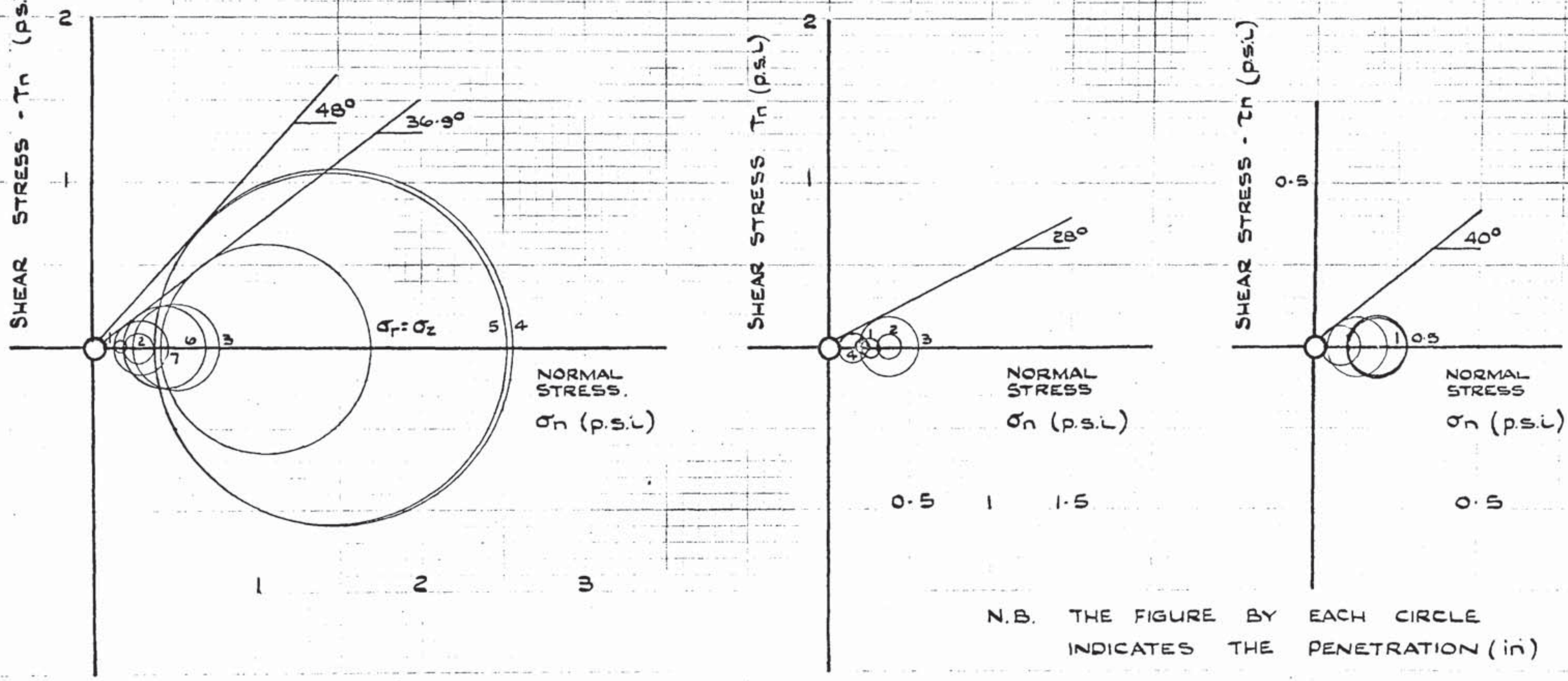

N.B. THE FIGURE BY EACH CIRCLE INDICATES THE PENETRATION (in)

CO-ORDINATES OF CELL PACES :
r = 1.06 in.
z : 3.54 in.

CO-ORDINATES OF CELL FACES :
r = 1.17 in.
z = 2.20 in.

CO-ORDINATES OF CELL FACES :
r = 1.05 in.
z = 0.48 in.

DRY DENSITY OF SAND = 91.68 lb/cu.ft.
COULOMB ϕ FROM DIRCT SHEAR TESTS = 31.8°

FIGURE 6.10 (a) & (b) MOHR CIRCLES OF STRESS OBTAINED FROM PRESSURE CELL MEASUREMENTS IN LOOSE - MEDIUM SAND - ASSUMING $\sigma_3 = \sigma_\theta$ AND $\sigma = (\sigma_r + \sigma_z) \cdot \frac{1}{2}$

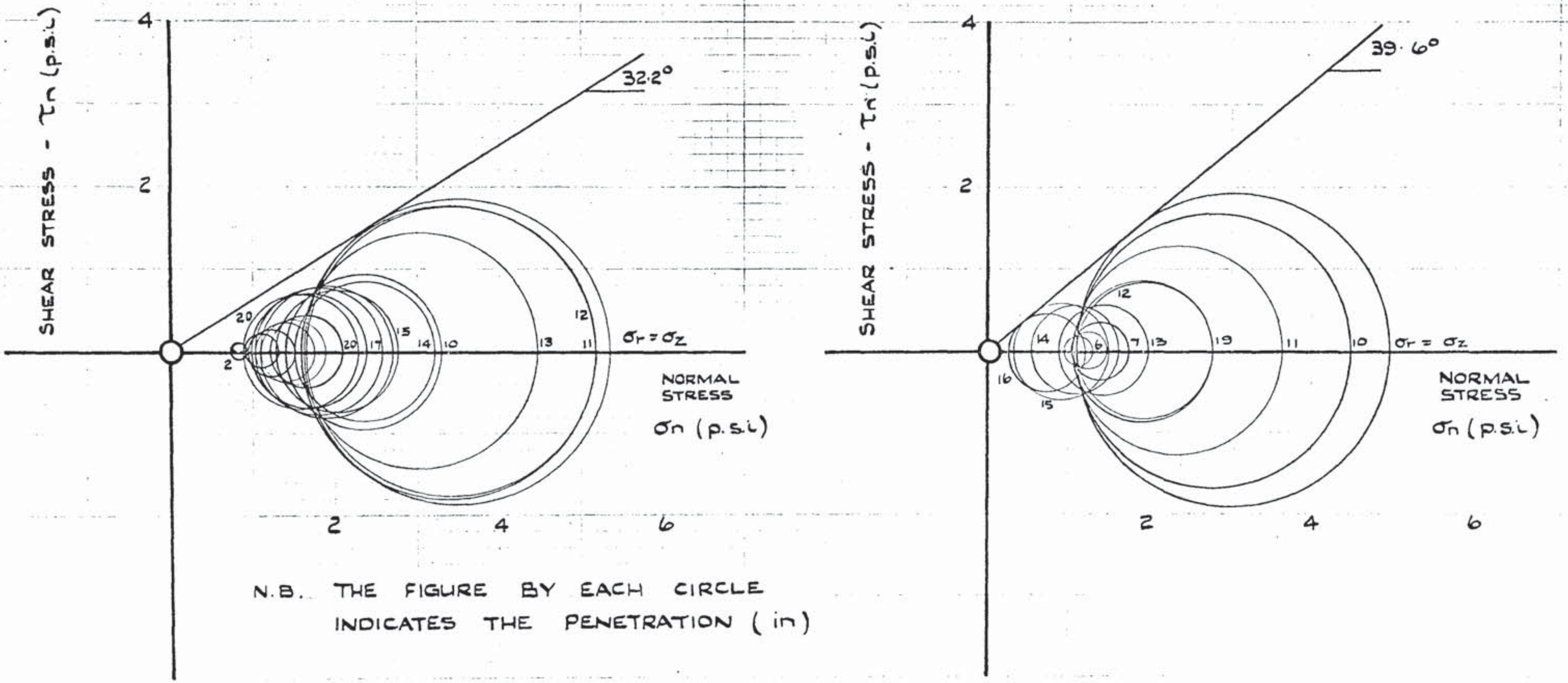

CO-ORDINATES OF CELL FACES :
r = 0·82 in.
z = 12·74 in.

CO-ORDINATES OF CELL FACES :
r = 1·55 in.
z = 10·71 in.

DRY DENSITY OF SAND = 94·69 lb/cu.ft.

COULOMB ϕ FROM DIRECT SHEAR TESTS = 32·2°

FIGURE 6.10. (c) & (d) MOHR CIRCLES OF STRESS FROM PRESSURE CELL MEASUREMENTS IN LOOSE - MEDIUM SAND - ASSUMING $\sigma_3 = \sigma_\theta$ AND $\sigma = (\sigma_z + \sigma_r) \cdot \frac{1}{2}$.

(c) CELL NO. 3.

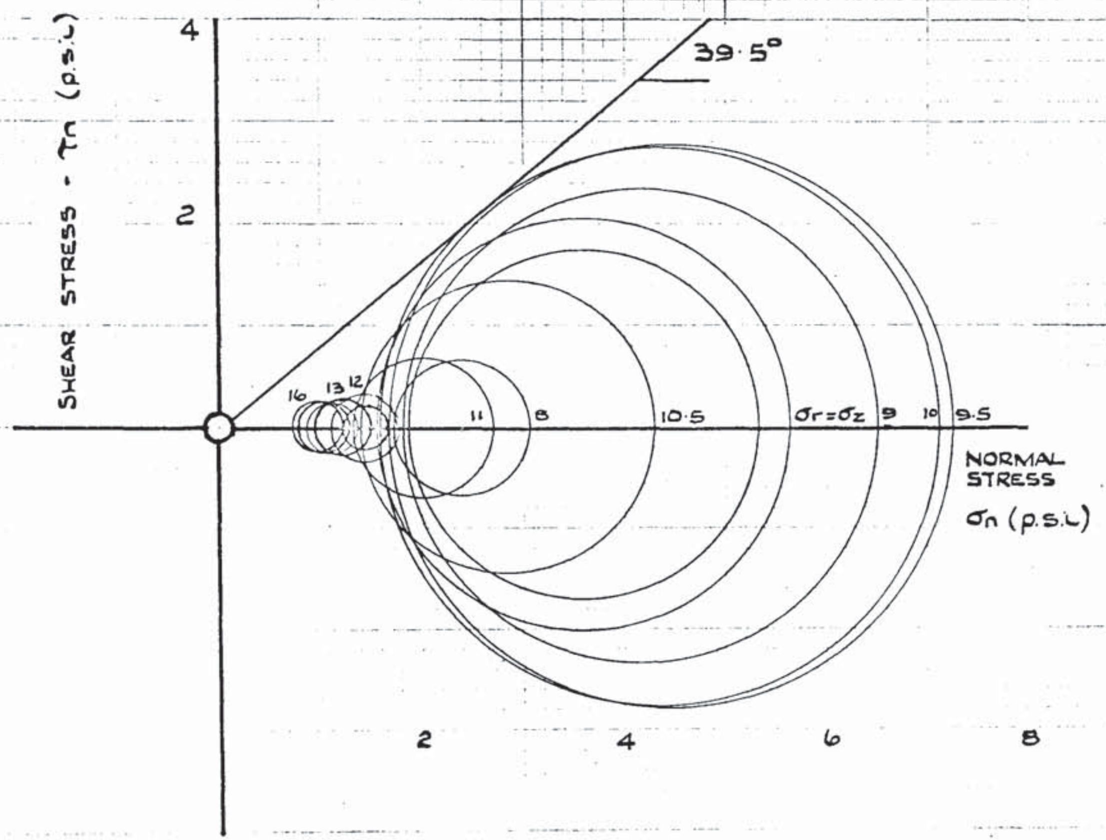

CO-ORDINATES OF CELL FACES :

r = 0·73 in.

z = 9·30 in.

(d) CELL NO 5

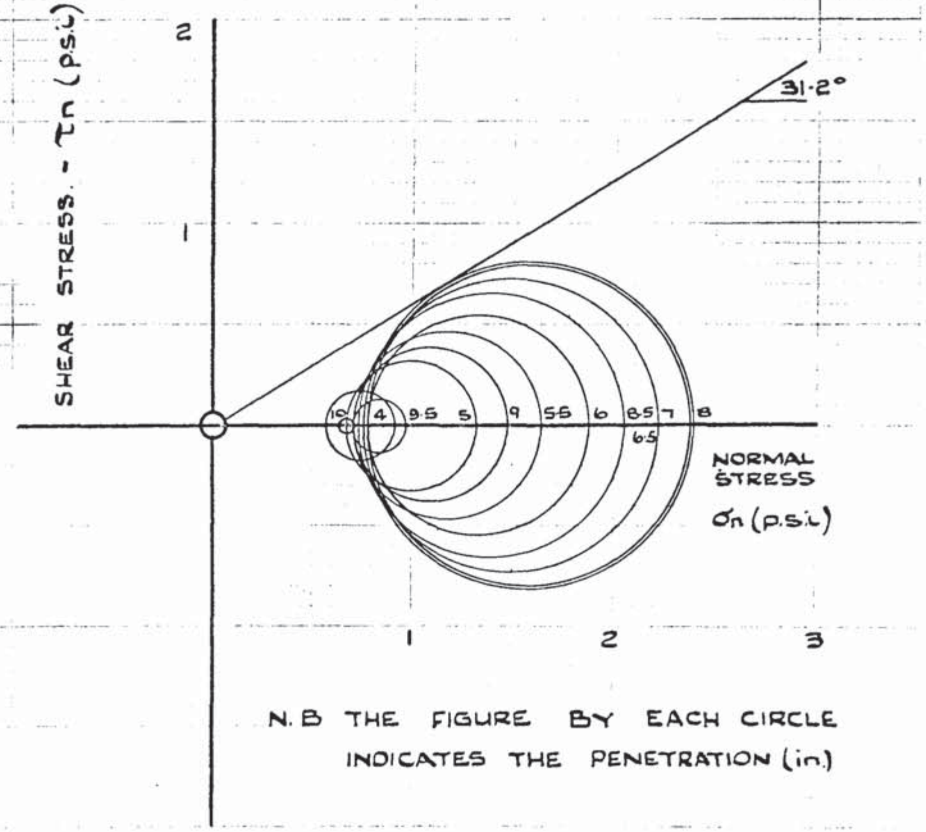

N.B THE FIGURE BY EACH CIRCLE INDICATES THE PENETRATION (in.)

CO-ORDINATES OF CELL FACES :

r = 1·40 in.

z = 7·70 in.

DRY DENSITY OF SAND = 94·69 lb/cu.ft.

COULOMB ϕ FROM DIRECT SHEAR TESTS = 32·2°

FIGURE 6.10 (e) & (f) MOHR CIRCLES OF STRESS OBTAINED FROM PRESSURE CELL MEASUREMENTS IN LOOSE - MEDIUM SAND - ASSUMING $\sigma_3 = \sigma_\theta$ AND $\sigma = (\sigma_z + \sigma_r) \cdot 1/2$.

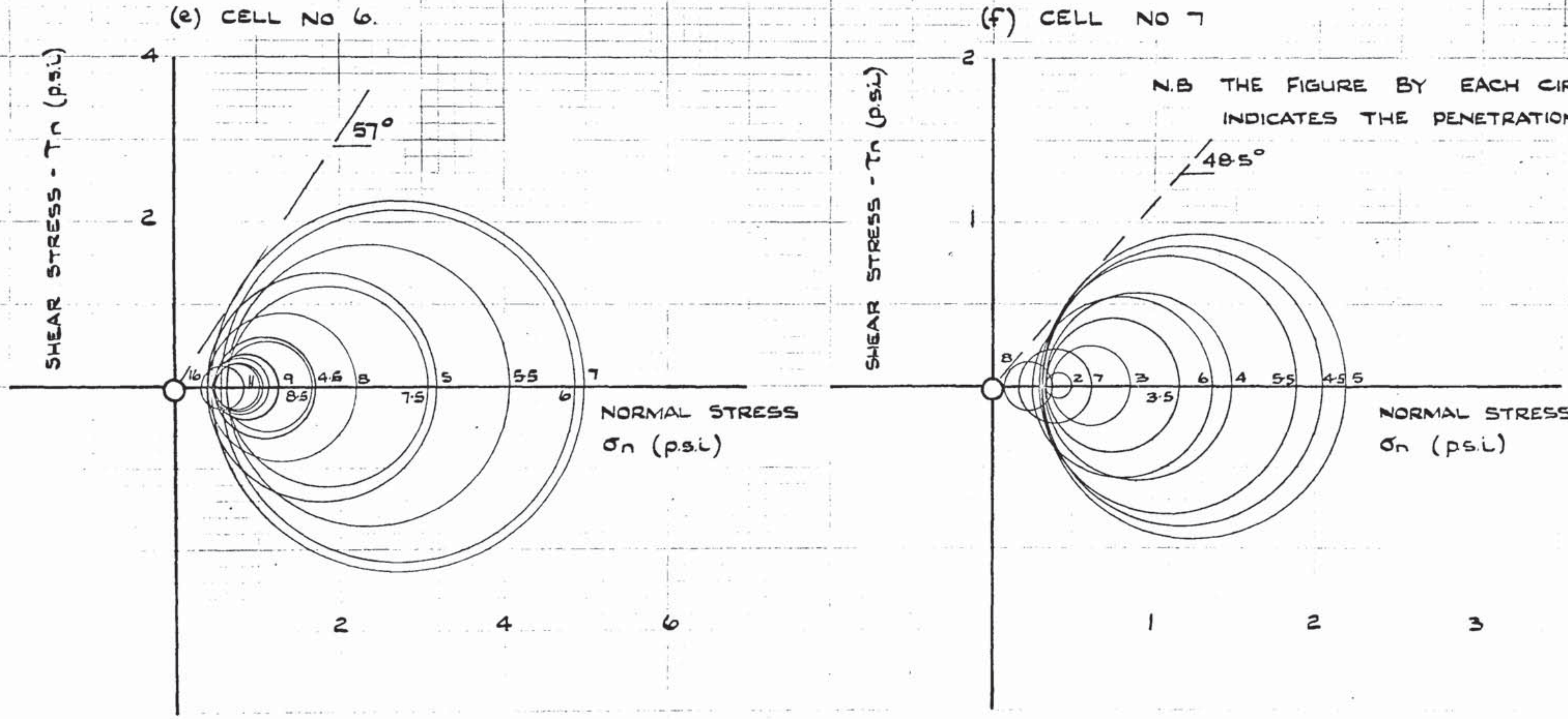

CO-ORDINATES OF CELL FACES

r = 0·92 in.

z = 6·13 in

CO-ORDINATES OF CELL FACES :

r = 1·65 in.

z = 4·70 in.

DRY DENSITY OF SAND = 94·69 lb/cu.ft.

COULOMB ϕ FROM DIRECT SHEAR TESTS = 32·2°

FIGURE 6.10.(g),(h) & (j) MOHR STRESS CIRCLES FROM PRESSURE CELL MEASUREMENTS IN LOOSE - MEDIUM SAND - ASSUMING $\sigma_3 = \sigma_\theta$ AND $\sigma = (\sigma_r + \sigma_z).\frac{1}{2}$.

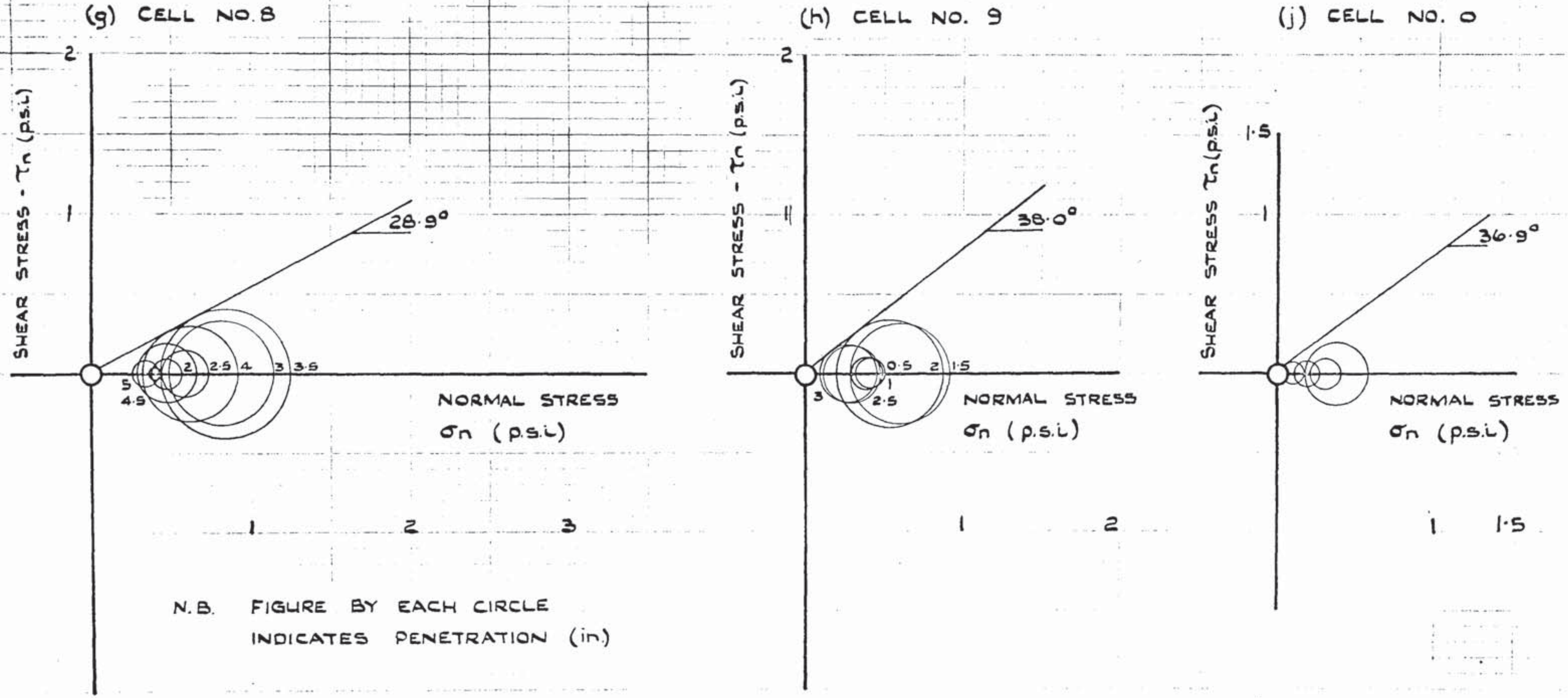

CO-ORDINATES OF CELL FACES:
r = 1·34 in.
z = 2·89 in.

CO-ORDINATES OF CELL FACES:
r = 0·90 in.
z = 1·54 in

CO-ORDINATES OF CELL FACES:
r = 1·56 in.
z = 0·52 in.

DRY DENSITY OF SAND 94·69 lb/cu.ft.

COULOMB ϕ FROM DIRECT SHEAR TESTS = 32·2°

FIGURE 6.11 (a) MOHR CIRCLES OF STRESS OBTAINED FROM PRESSURE CELL MEASUREMENTS IN DENSE SAND - ASSUMING $\sigma_3 = \sigma_\theta$ AND $\sigma = (\sigma_r + \sigma_z).\frac{1}{2}$

CELL No. 1.

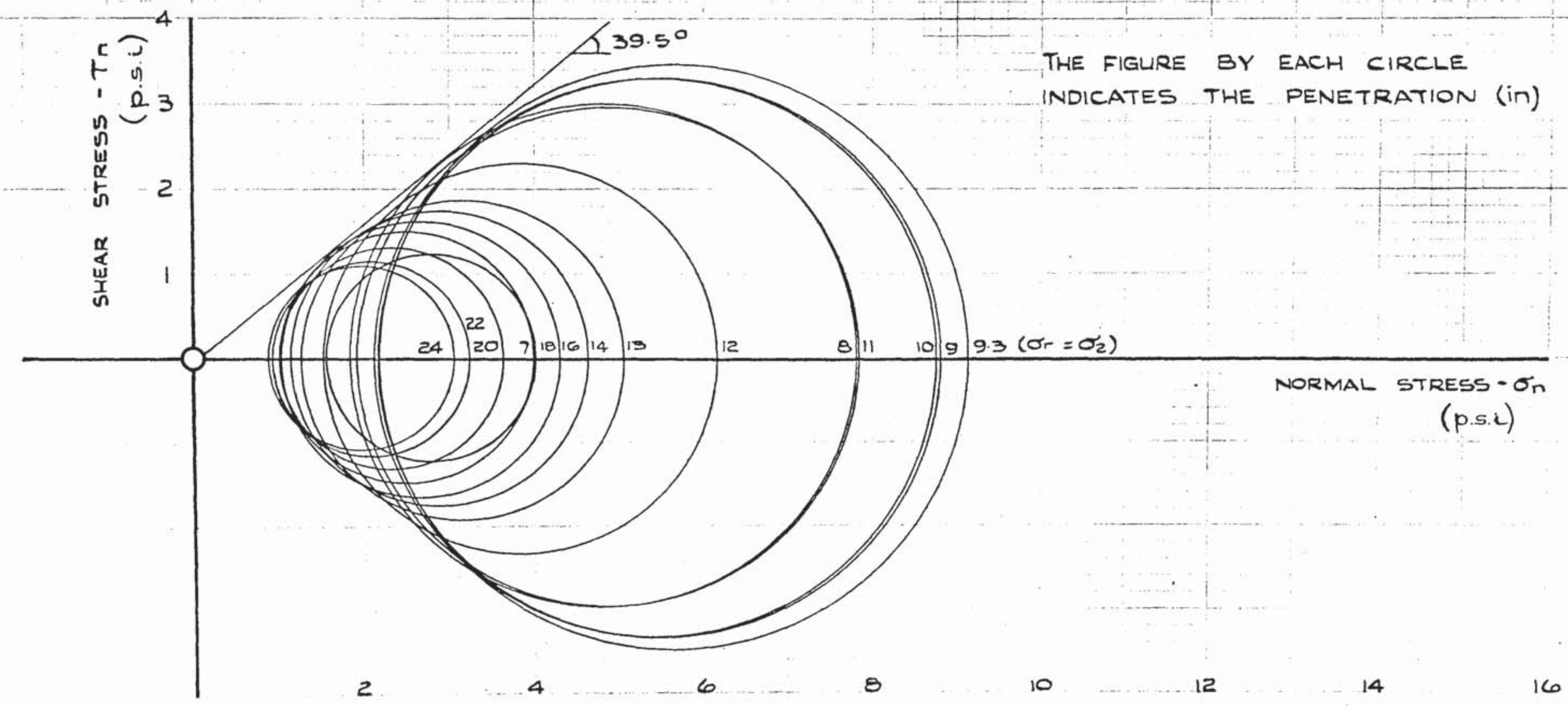

CO-ORDS OF CELL FACES :
r = 1.36 in
z = 10.10 in

DRY DENSITY OF SAND = 104.47 lb/cu.ft.
COULOMB ϕ FROM DIRECT SHEAR TESTS = 40.8°

FIGURE 6. 11. (b) & (c). MOHR CIRCLES OF STRESS OBTAINED FROM PRESSURE CELL MEASUREMENTS IN DENSE SAND - ASSUMING $\sigma_3 = \sigma_\theta$ AND $\sigma = (\sigma_r + \sigma_z) . \frac{1}{2}$.

(b) CELL NO. 2. (c) CELL NO 3.

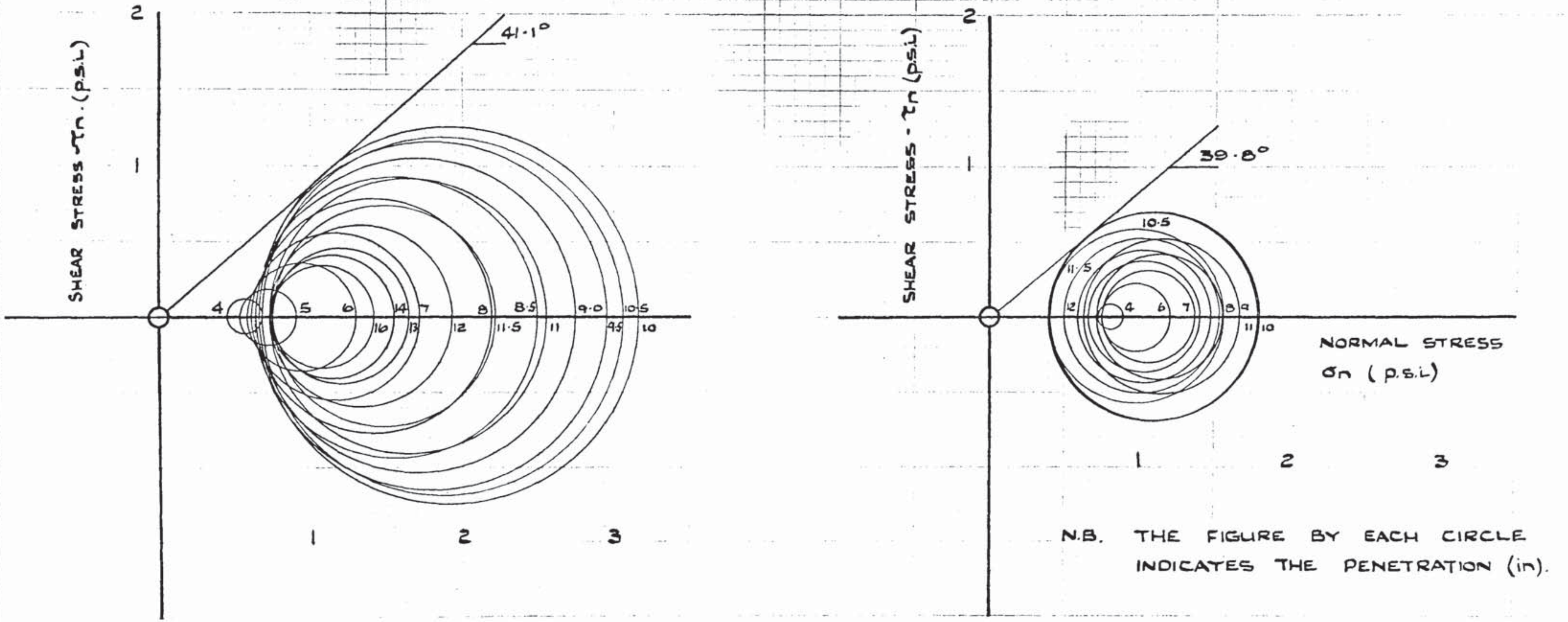

N.B. THE FIGURE BY EACH CIRCLE INDICATES THE PENETRATION (in).

CO-ORDINATES OF CELL FACES :
r = 4·79 in.
z = 9·99 in.

CO-ORDINATES OF CELL FACES :
r = 8·28 in.
z = 10·05 in.

DRY DENSITY OF SAND = 104·47 lb/cu.ft.
COULOMB ϕ FROM DIRECT SHEAR TESTS. 40·8°

FIGURE 6.11. (d). MOHR CIRCLES OF STRESS OBTAINED FROM PRESSURE CELL MEASUREMENTS IN DENSE SAND - ASSUMING $\sigma_3 = \sigma_\theta$ AND $\sigma = (\sigma_r + \sigma_z).\frac{1}{2}$.

CELL No. 5.

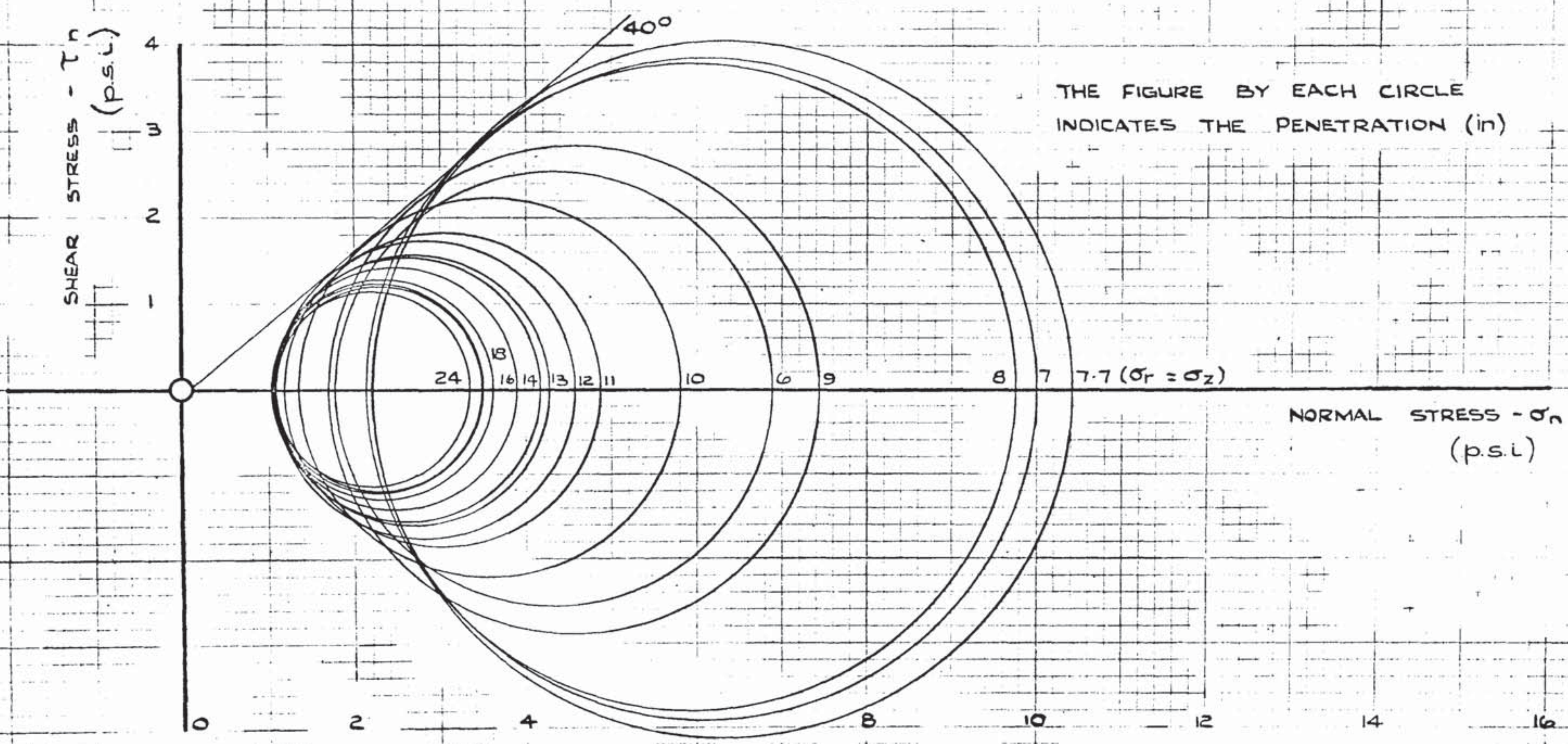

CO-ORDS OF CELL FACES:

r = 1·3 in.

z = 7·25 in.

DRY DENSITY OF SAND = 104·47 lb/cu. ft.

COULOMB ϕ FROM DIRECT SHEAR TESTS = 40·8°

FIGURE 6.11 (e). & (g). MOHR STRESS CIRCLES OBTAINED FROM PRESSURE CELL MEASUREMENTS IN DENSE SAND - ASSUMING $\sigma_3 = \sigma_\theta$ AND $\sigma = (\sigma_r + \sigma_z).^{1/2}$

(e) CELL NO. 6.

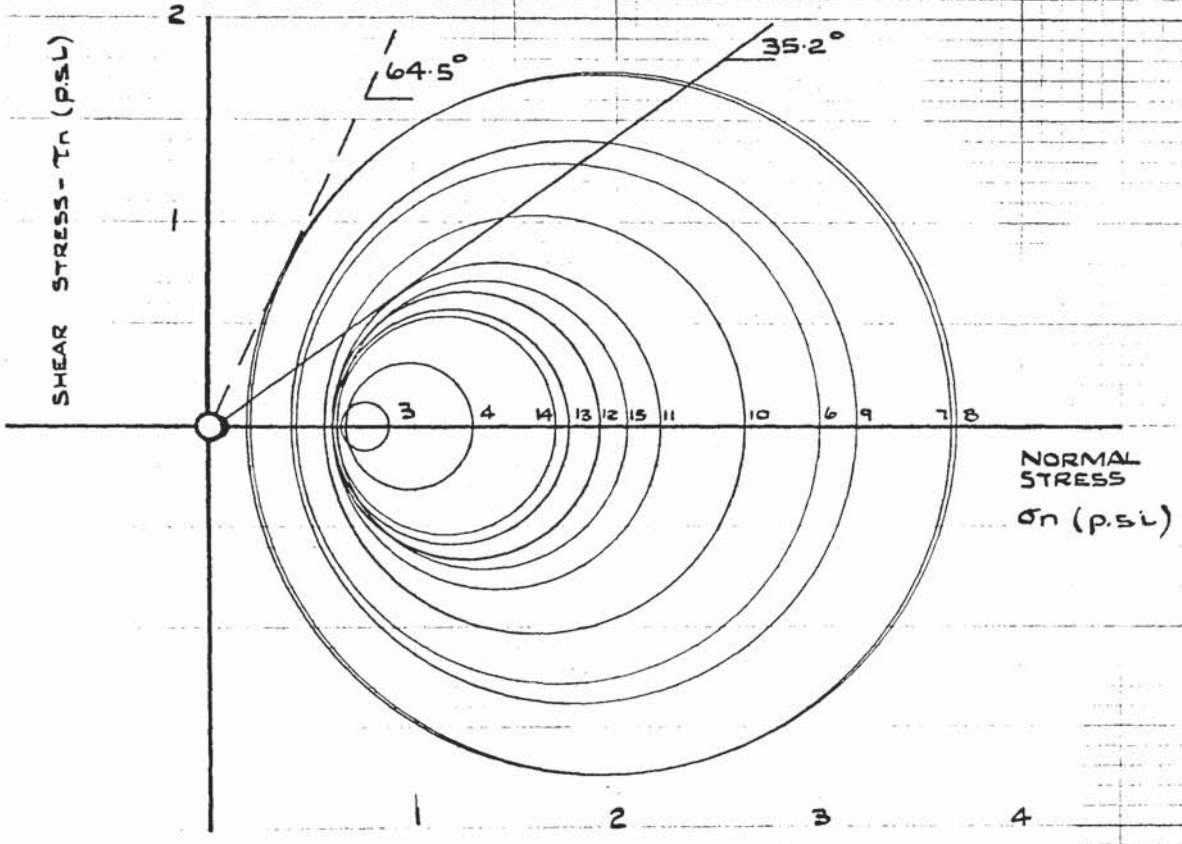

CO-ORDINATES OF CELL FACES :

r = 3.87 in.

z : 7.24 in.

(e) CELL NO. 8.

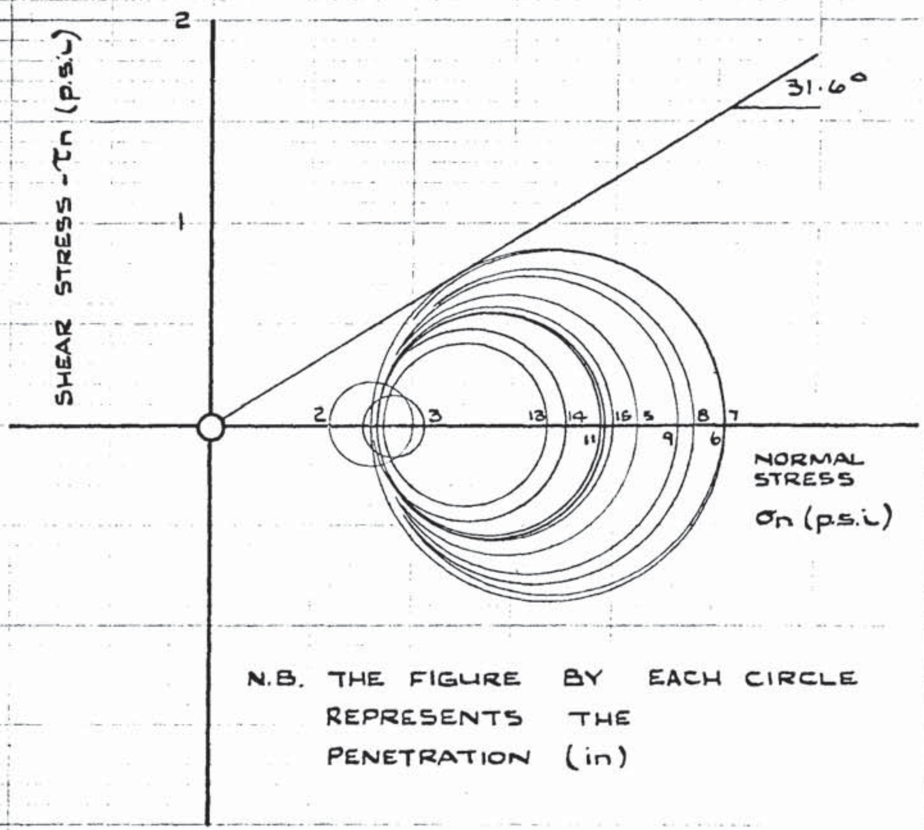

CO-ORDINATES OF CELL FACES :

r = 5.09 in.

z = 4.07 in.

DRY DENSITY OF SAND = 104.47 lb/cu.ft.

COULOMB ϕ FROM DIRECT SHEAR TESTS = 40.8°

FIGURE 6.11 (f) MOHR STRESS CIRCLES OBTAINED FROM PRESSURE CELL MEASUREMENTS IN DENSE SAND - ASSUMING $\sigma_3 = \sigma_\theta$ AND $\sigma = (\sigma_r + \sigma_z) \cdot \frac{1}{2}$.

CELL NO 7.

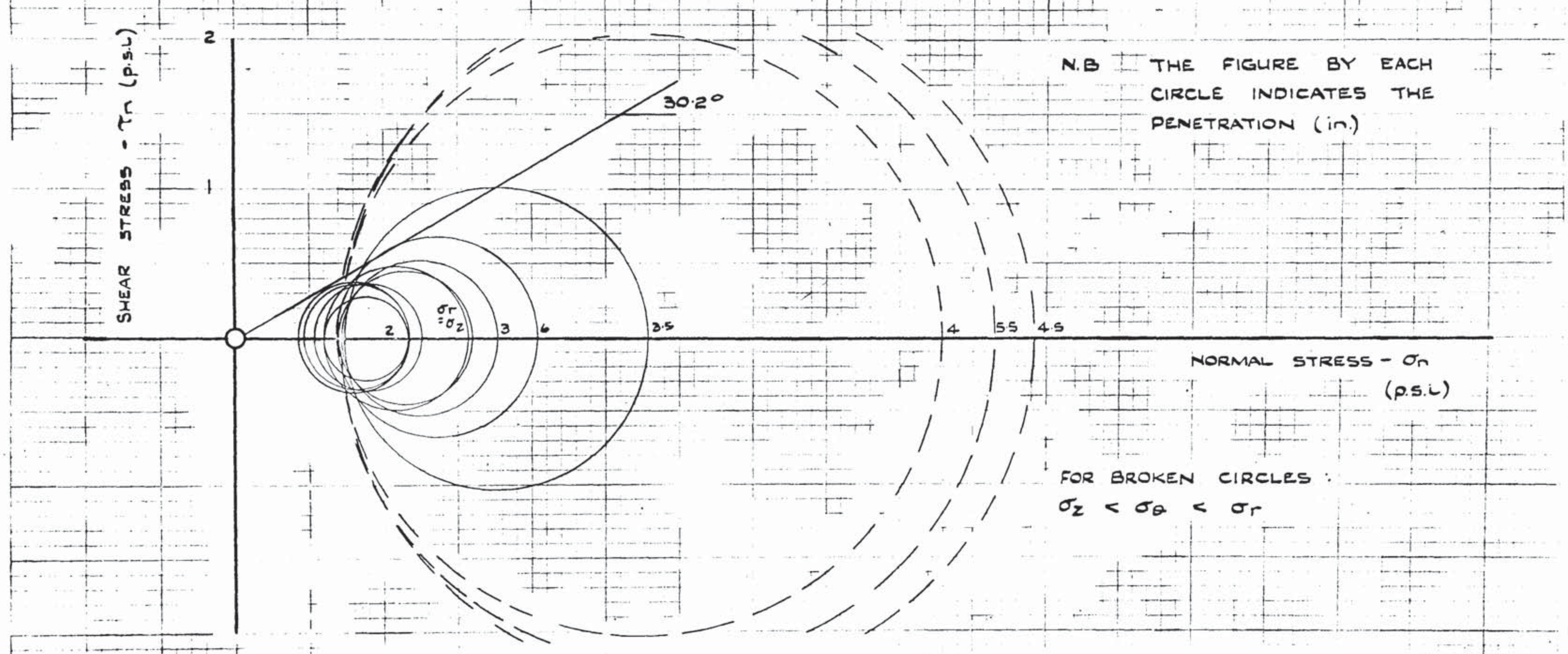

CO-ORDINATES OF CELL FACES

r = 1·31 in.

z = 4·12 in.

DRY DENSITY OF SAND = 104·47 lb/cu.ft

COULOMB ϕ FROM DIRECT SHEAR TESTS = 40·8°

FIGURE 6.11 (h) & (j). MOHR STRESS CIRCLES OBTAINED FROM PRESSURE CELL MEASUREMENTS IN DENSE SAND - ASSUMING $\sigma_3 = \sigma_\theta$ AND $\sigma = (\theta_z + \sigma_r) \cdot 1/2$

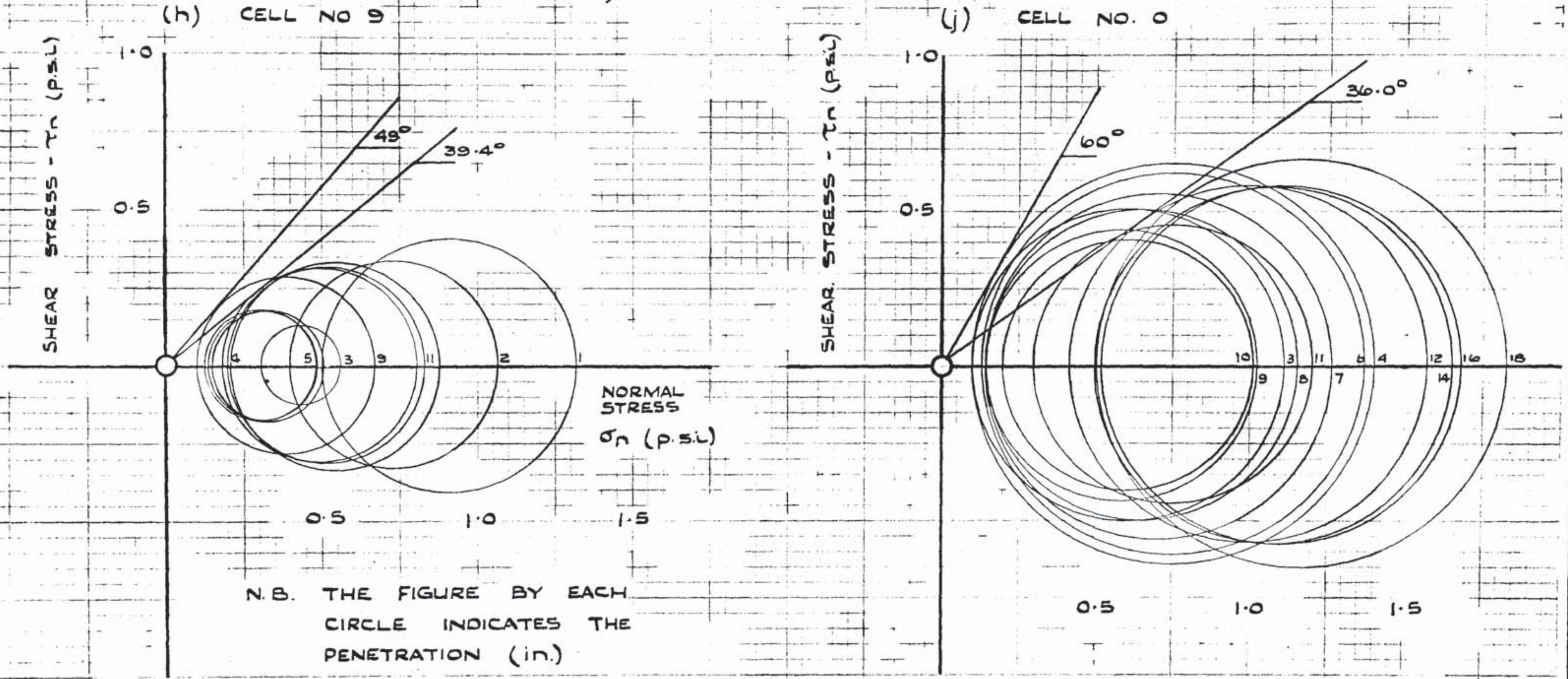

N.B. THE FIGURE BY EACH CIRCLE INDICATES THE PENETRATION (in.)

CO-ORDINATES OF CELL FACES

r = 1·17 in.

z = 1·14 in.

CO-ORDINATES OF CELL FACES :

r = 3·47 in.

z = 1·23 in.

DRY DENSITY OF SAND = 104·47 lb/cu.ft.

COULOMB Ø FROM DIRECT SHEAR TESTS = 40.8°

FIGURE 6.12 (a) & (b) PRINCIPAL STRAIN RATE DIRECTIONS DURING AXIALLY - SYMMETRIC PENETRATION INTO LOOSE SAND.

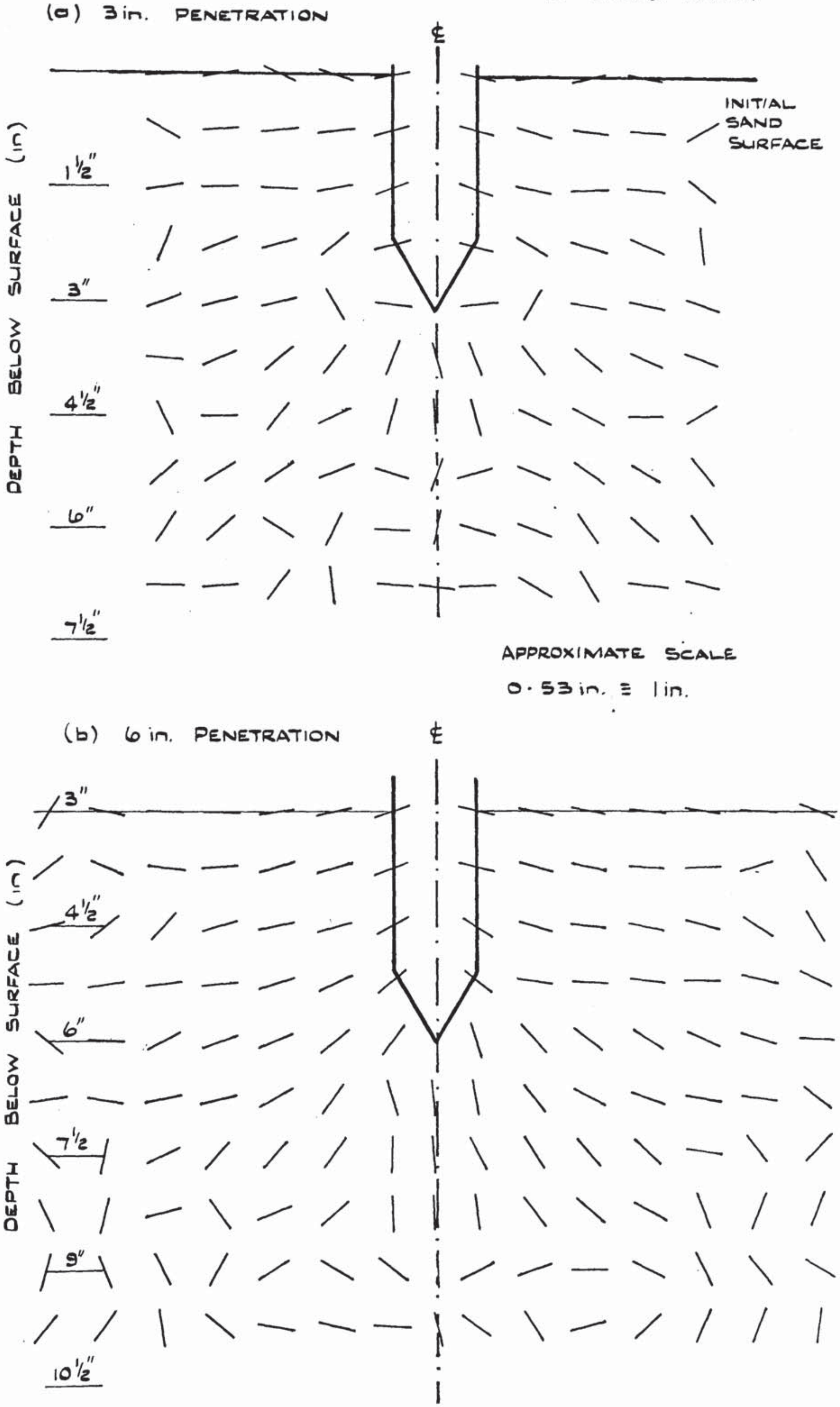

FIGURE 6.12 (c) & (d) PRINCIPAL STRAIN RATE DIRECTIONS DURING AXIALLY - SYMMETRIC PENETRATION INTO LOOSE SAND

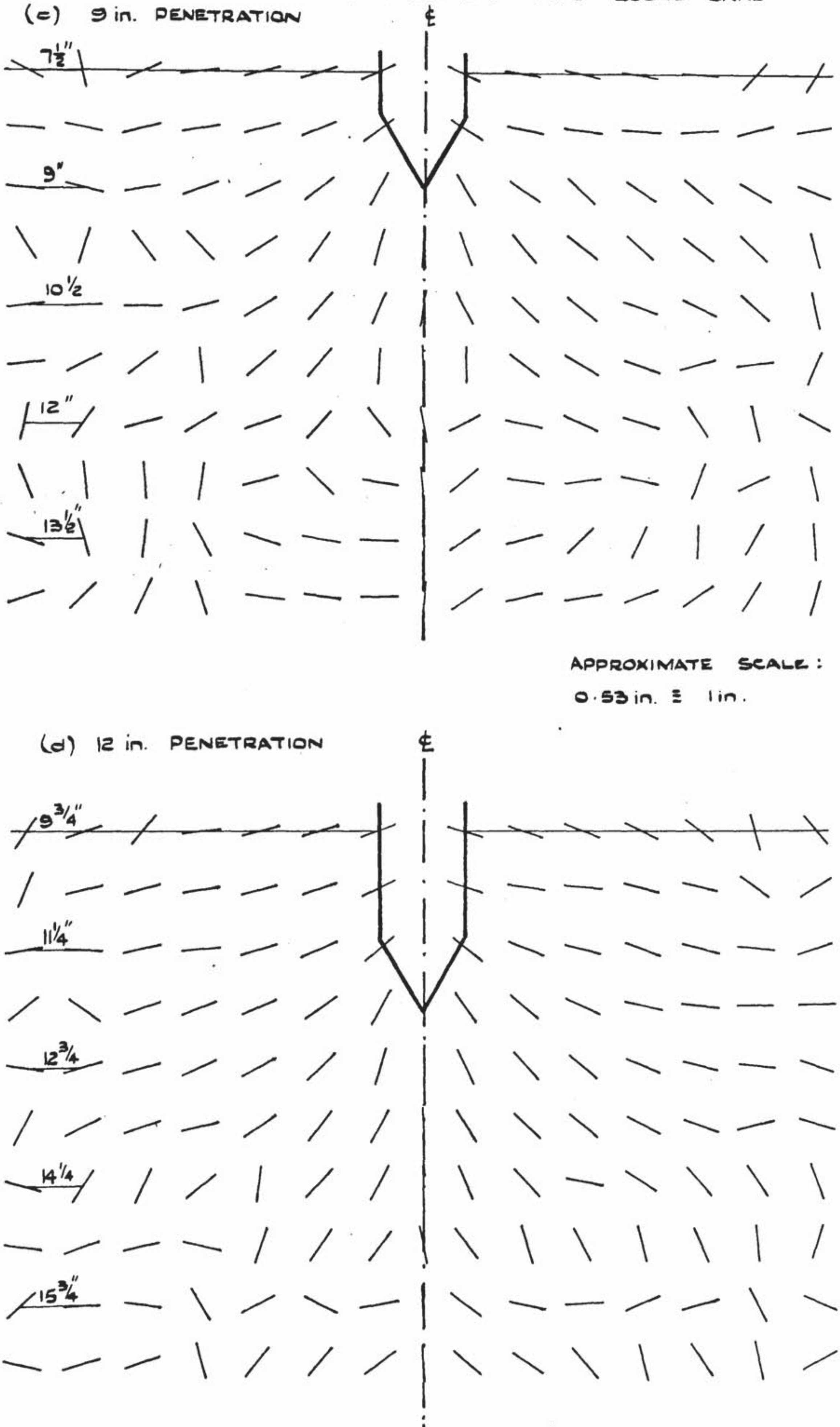

FIGURE 6.13. (a) & (b) PRINCIPAL STRAIN RATE DIRECTIONS DURING AXIALLY - SYMMETRIC PENETRATION INTO DENSE SAND

(a) 4 in. PENETRATION

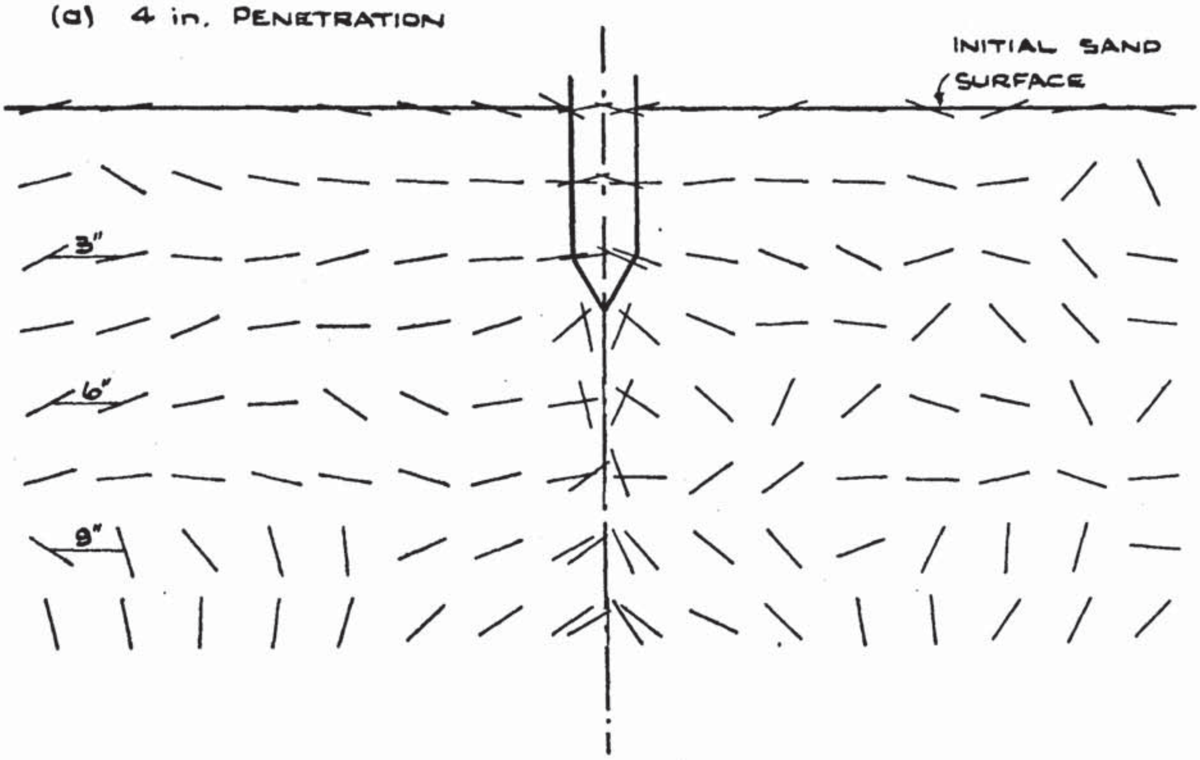

APPROXIMATE SCALE
0·26 in. ≡ 1 in.
(ie. 1 : 4)

(b) 9 in. PENETRATION

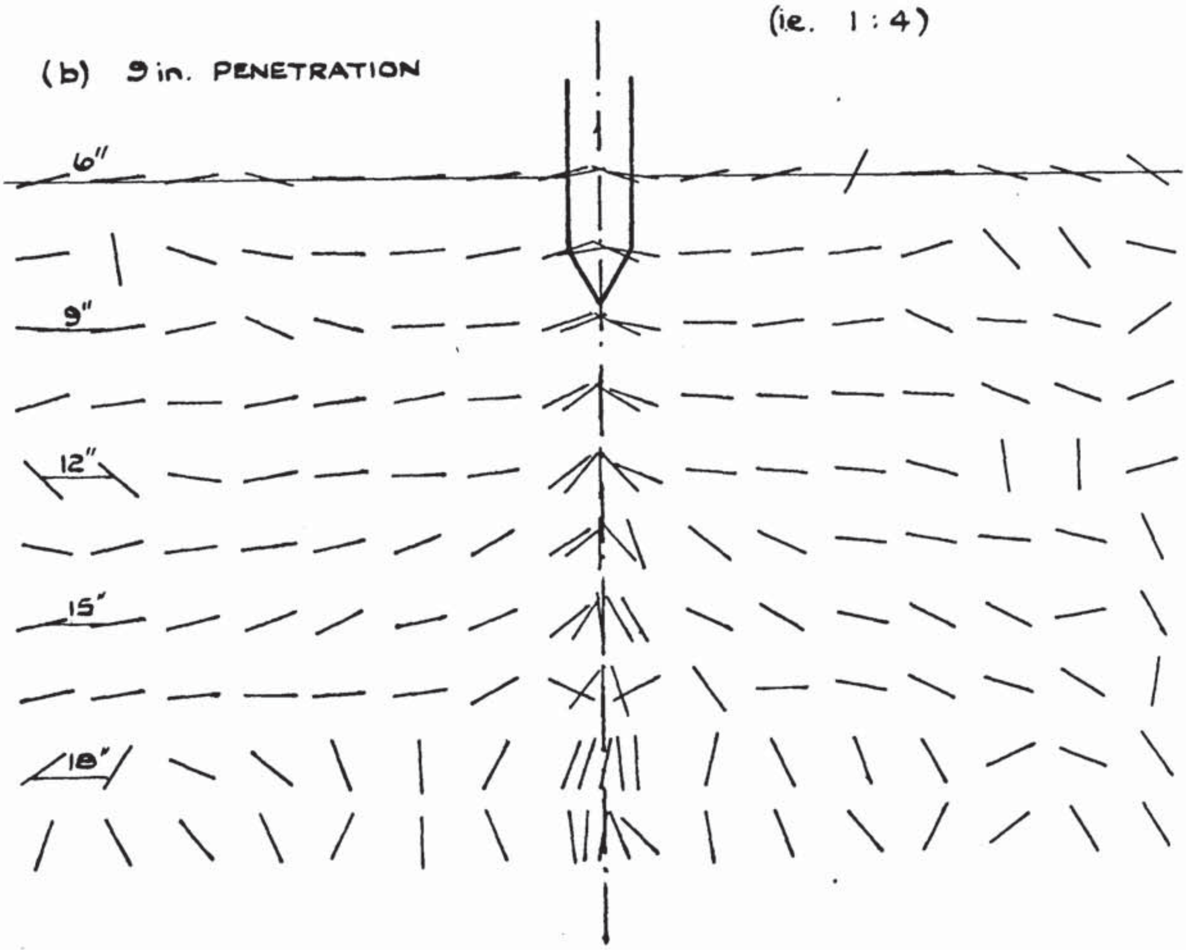

FIGURE 6.13 (c)& (d) PRINCIPAL STRAIN RATE DIRECTIONS DURING AXIALLY - SYMMETRIC PENETRATION INTO DENSE SAND

(c) 15 in. PENETRATION

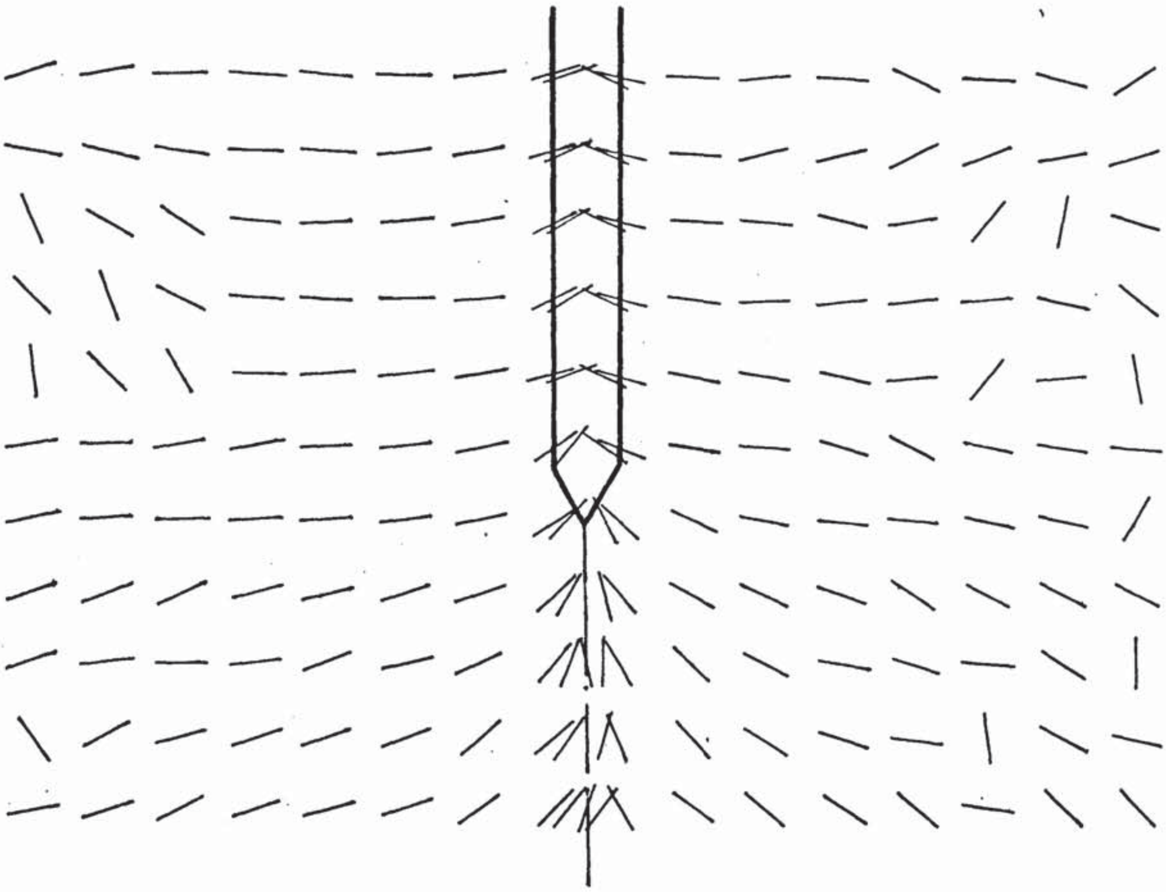

APPROXIMATE SCALE
0·26 in. ≡ 1 in. (i.e. 1:4)

(d) 24 in. PENETRATION

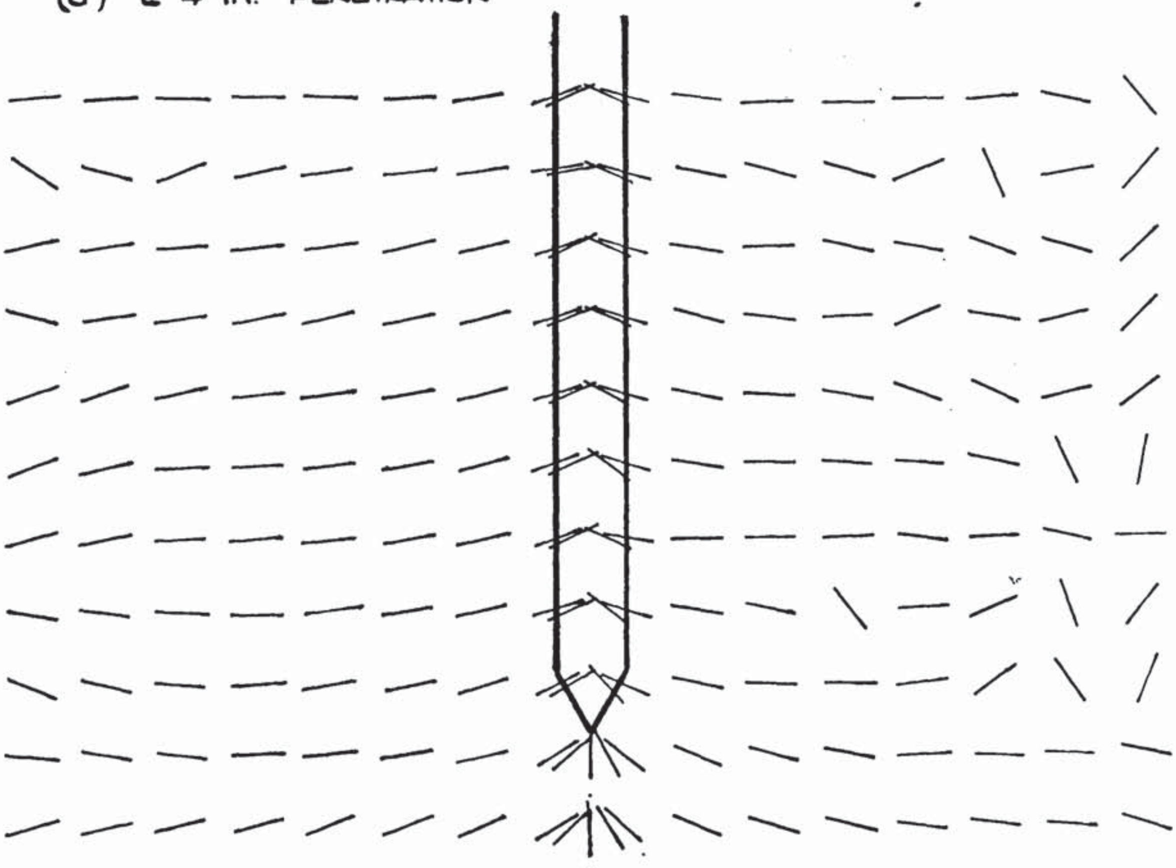

FIGURE 6.14 (a) MEASURED STRAIN RATE VERSUS PENETRATION FROM 'HALF - SECTION' EXPERIMENTS - LOOSE SAND.

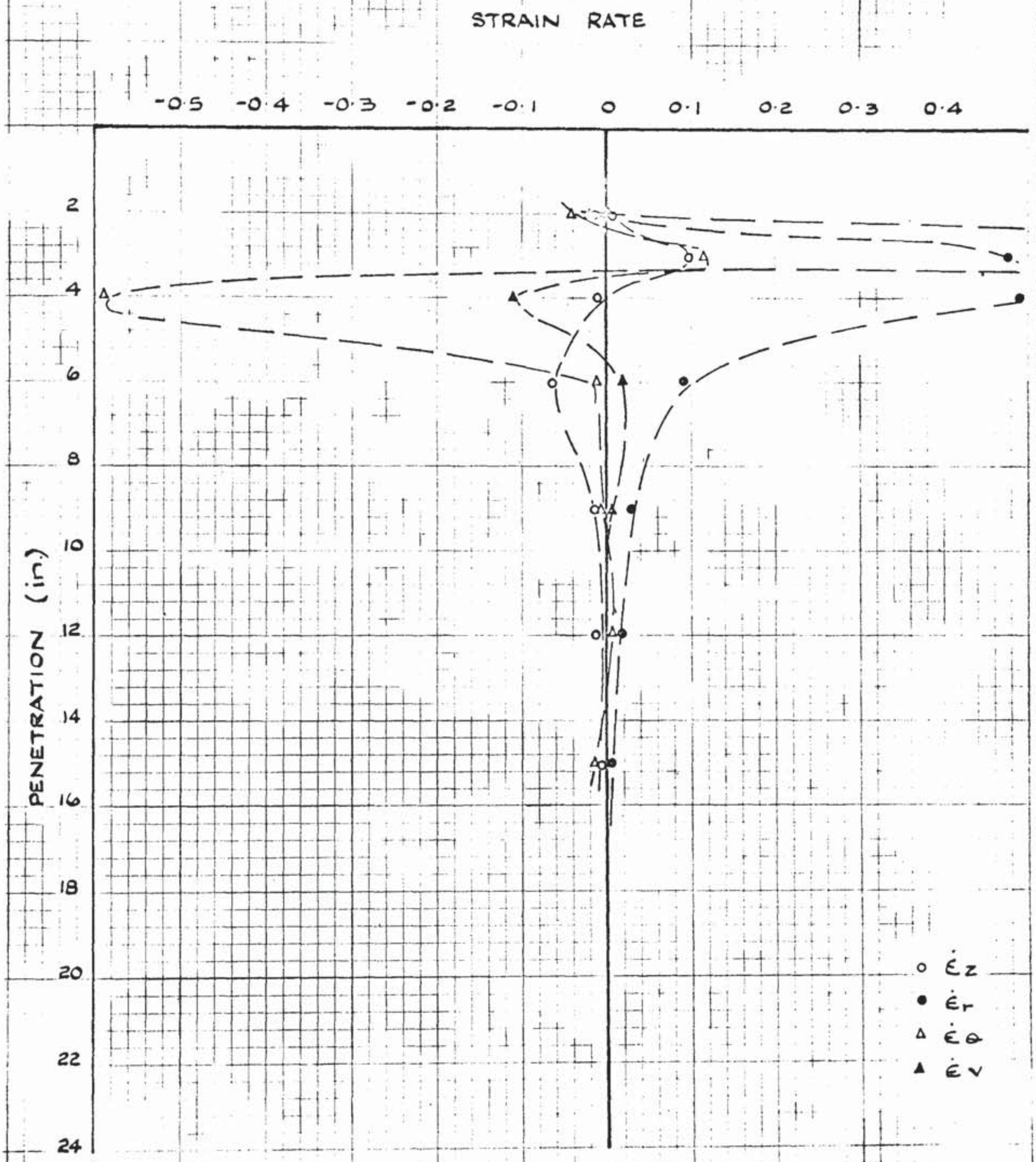

CO-ORDINATES OF POINT AT WHICH STRAIN RATES ARE PLOTTED :

r = 0·5 in.

z = 3·0 in.

FIGURE 6.14 (b) & (d) MEASURED STRAIN RATE VERSUS PENETRATION FROM 'HALF - SECTION' EXPERIMENTS - LOOSE SAND

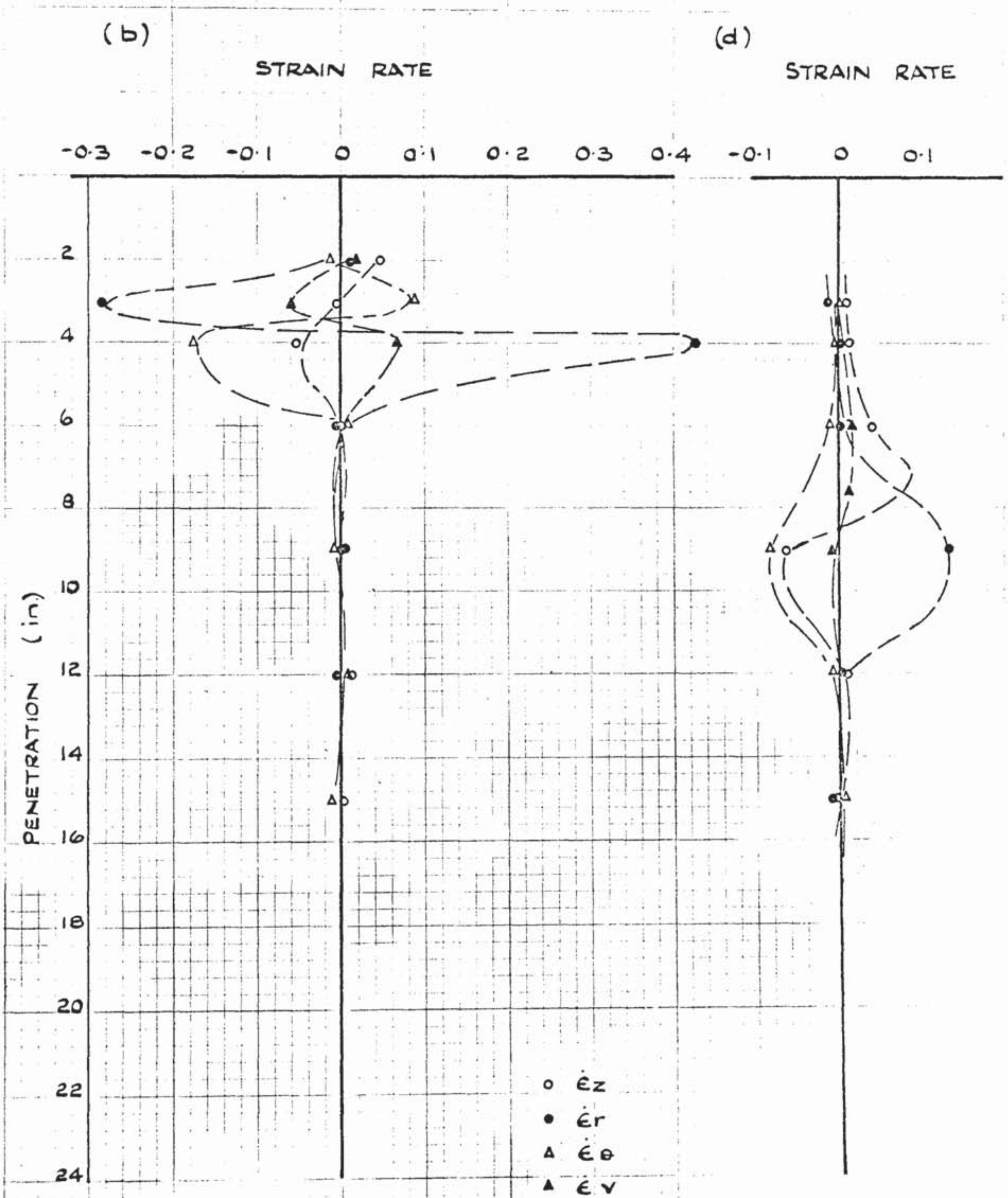

CO-ORDINATES OF POINT AT WHICH STRAIN RATES ARE PLOTTED:

r = 1·25 in.

z = 3·0 in.

CO-ORDINATES OF POINT AT WHICH STRAIN RATES ARE PLOTTED:

r = 1·25 in.

z = 6·0 in.

FIGURE 6.14.(c). MEASURED STRAIN RATE VERSUS PENETRATION FROM 'HALF - SECTION' EXPERIMENTS - LOOSE SAND.

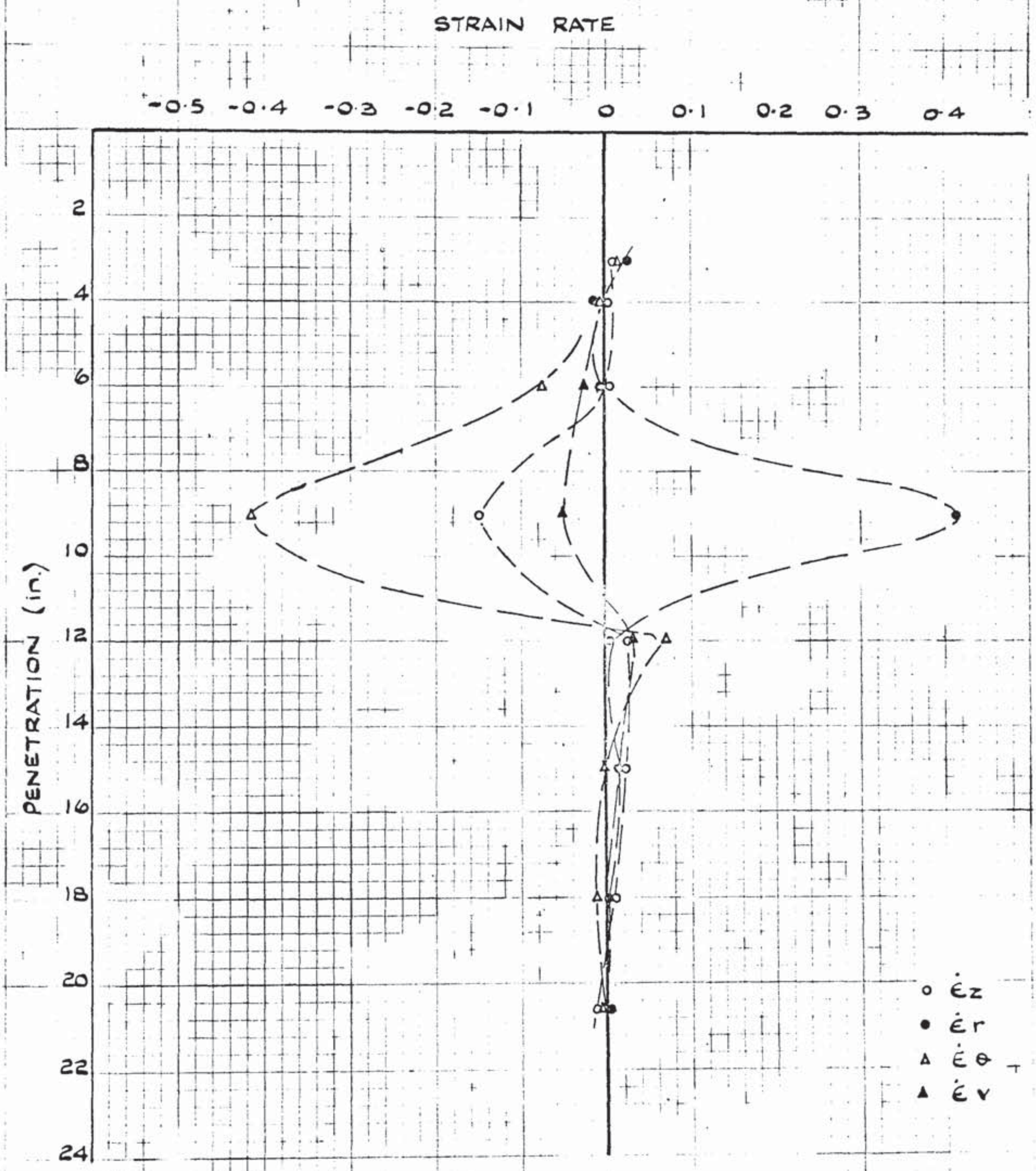

CO-ORDINATES OF POINT AT WHICH STRAIN RATES ARE PLOTTED :

r = 0.5 in.

z = 6.0 in.

FIGURE 6.14 (e) & (f) MEASURED STRAIN RATE VERSUS PENETRATION FROM 'HALF SECTION' EXPERIMENTS - LOOSE SAND

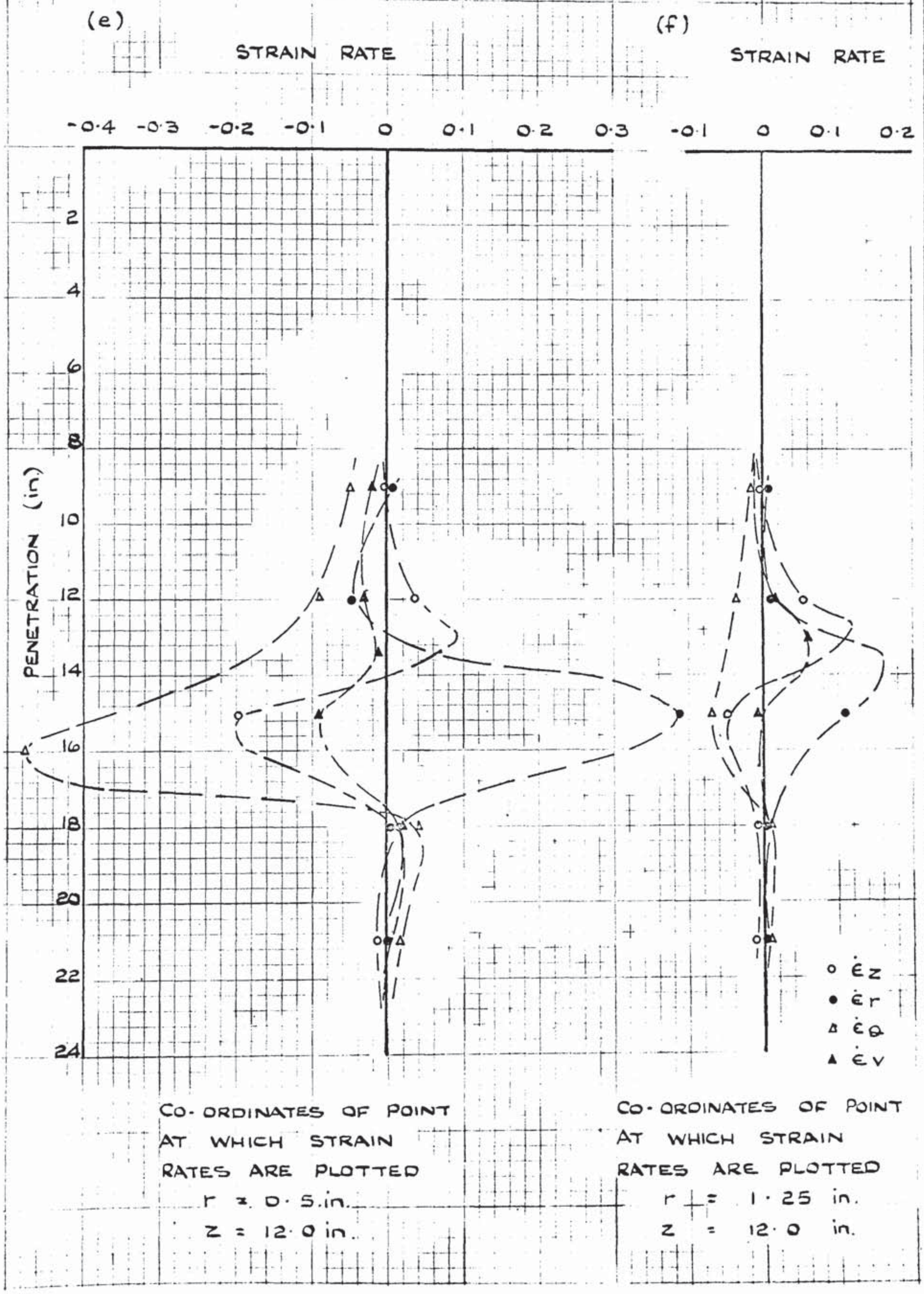

FIGURE 6.15. (a) & (b) MEASURED STRAIN RATE VERSUS PENETRATION FROM 'HALF-SECTION' EXPERIMENTS - DENSE SAND

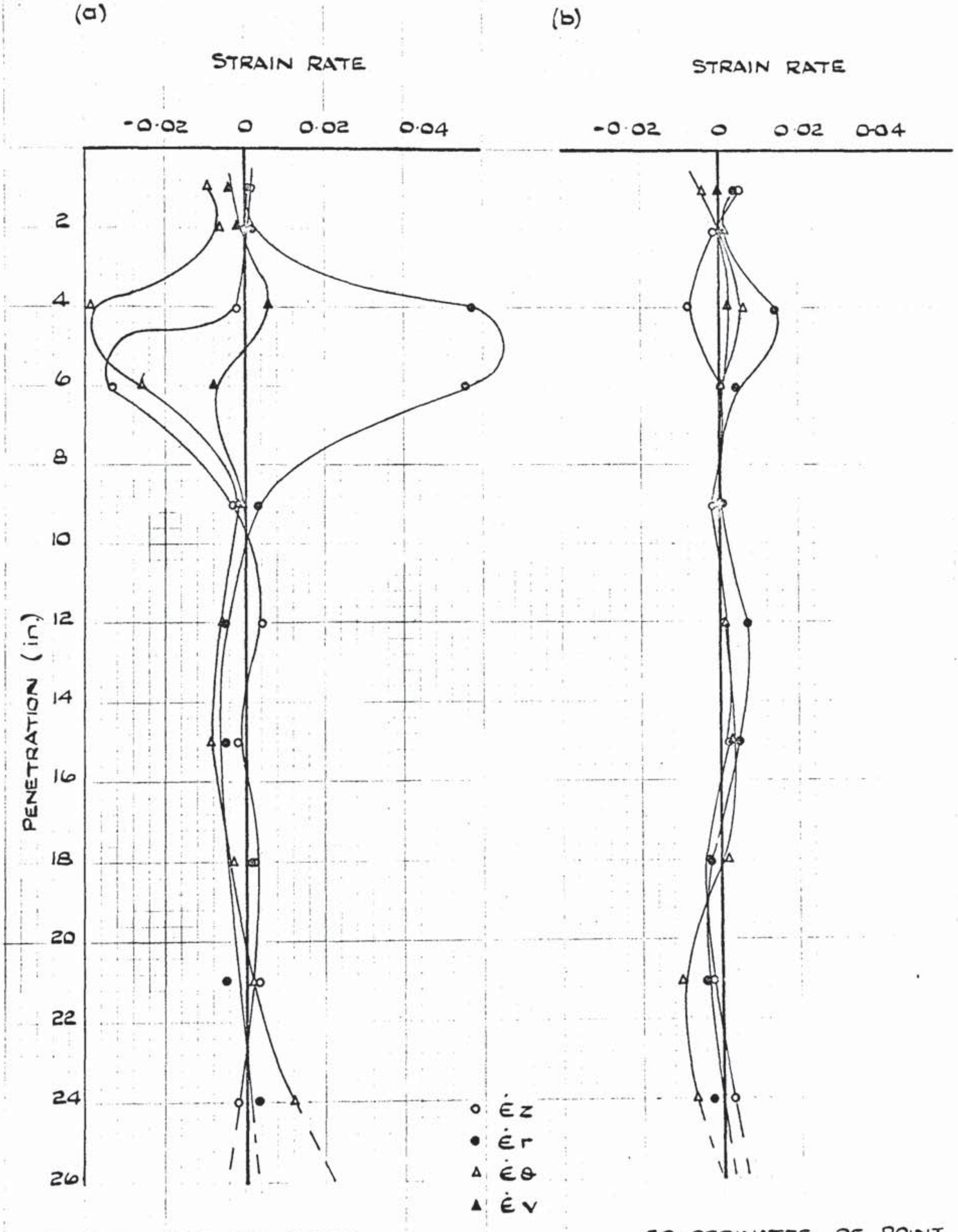

CO-ORDINATES OF POINT AT WHICH STRAIN RATES ARE PLOTTED :

r = 0·5 in.

z = 3·0 in.

CO-ORDINATES OF POINT AT WHICH STRAIN RATES ARE PLOTTED :

r = 2·0 in.

z = 3·0 in.

FIGURE 6.15 (c) & (d) MEASURED STRAIN RATE VERSUS PENETRATION FROM 'HALF-SECTION' EXPERIMENTS - DENSE SAND.

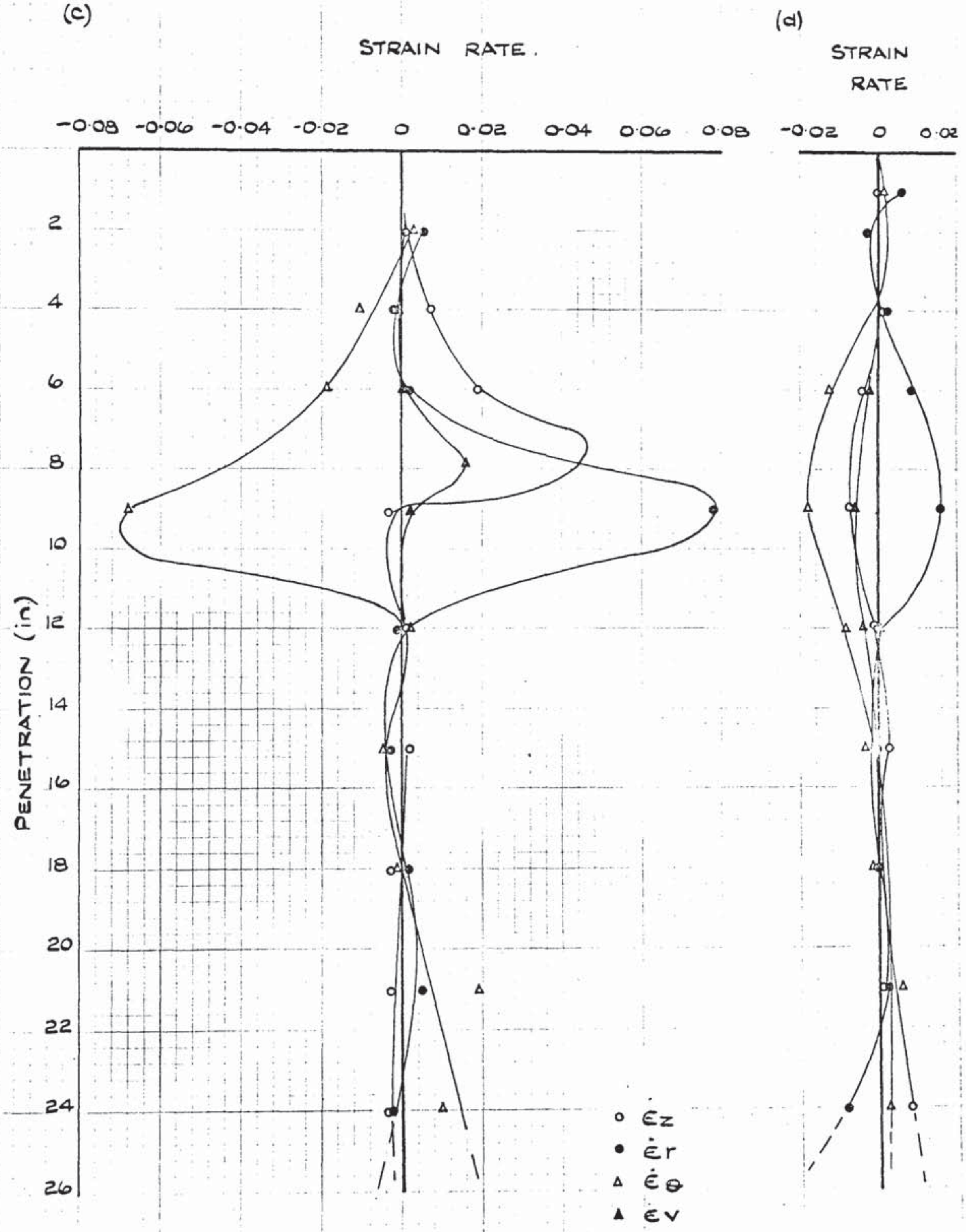

CO-ORDINATES OF POINT AT WHICH STRAIN RATES ARE PLOTTED

r = 0.5 in.

z = 6.0 in.

CO-ORDINATES OF POINT AT WHICH STRAIN RATES ARE PLOTTED

r = 2.0 in.

z : 6.0 in.

FIGURE 6.15 (e) & (f) MEASURED STRAIN RATE VERSUS PENETRATION FROM 'HALF - SECTION' EXPERIMENTS - DENSE SAND

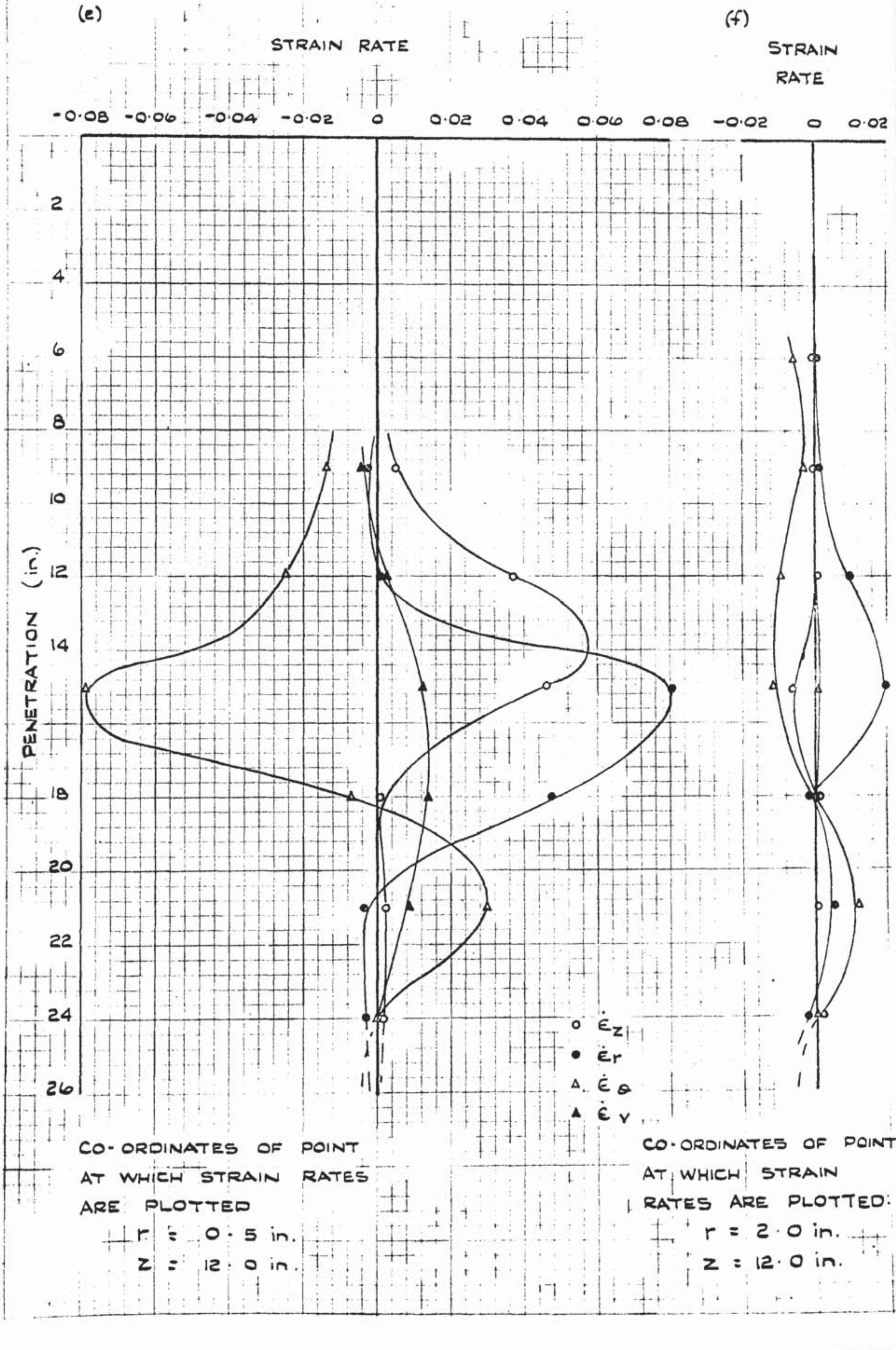

FIGURE 6.16 (a) & (b) STRESS DISTRIBUTION COMPUTED FROM THEORY OF LIMITING STRESS LOOSE SAND CONDITIONS

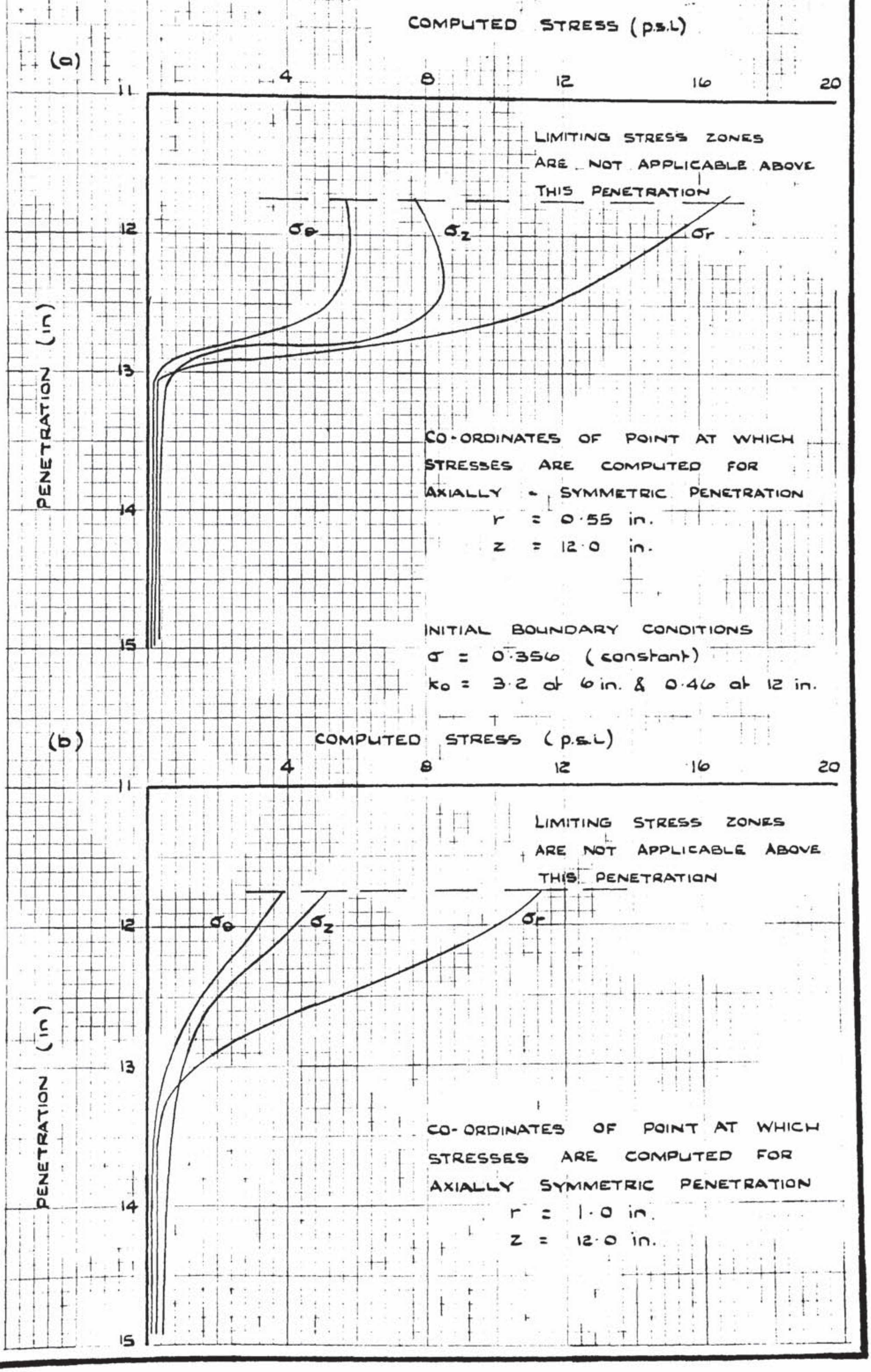

FIGURE 6.17. DIRECTIONS OF MAJOR PRINCIPAL STRESS DURING QUASI - STATIC AXIALLY - SYMMETRIC PENETRATION INTO LOOSE SAND

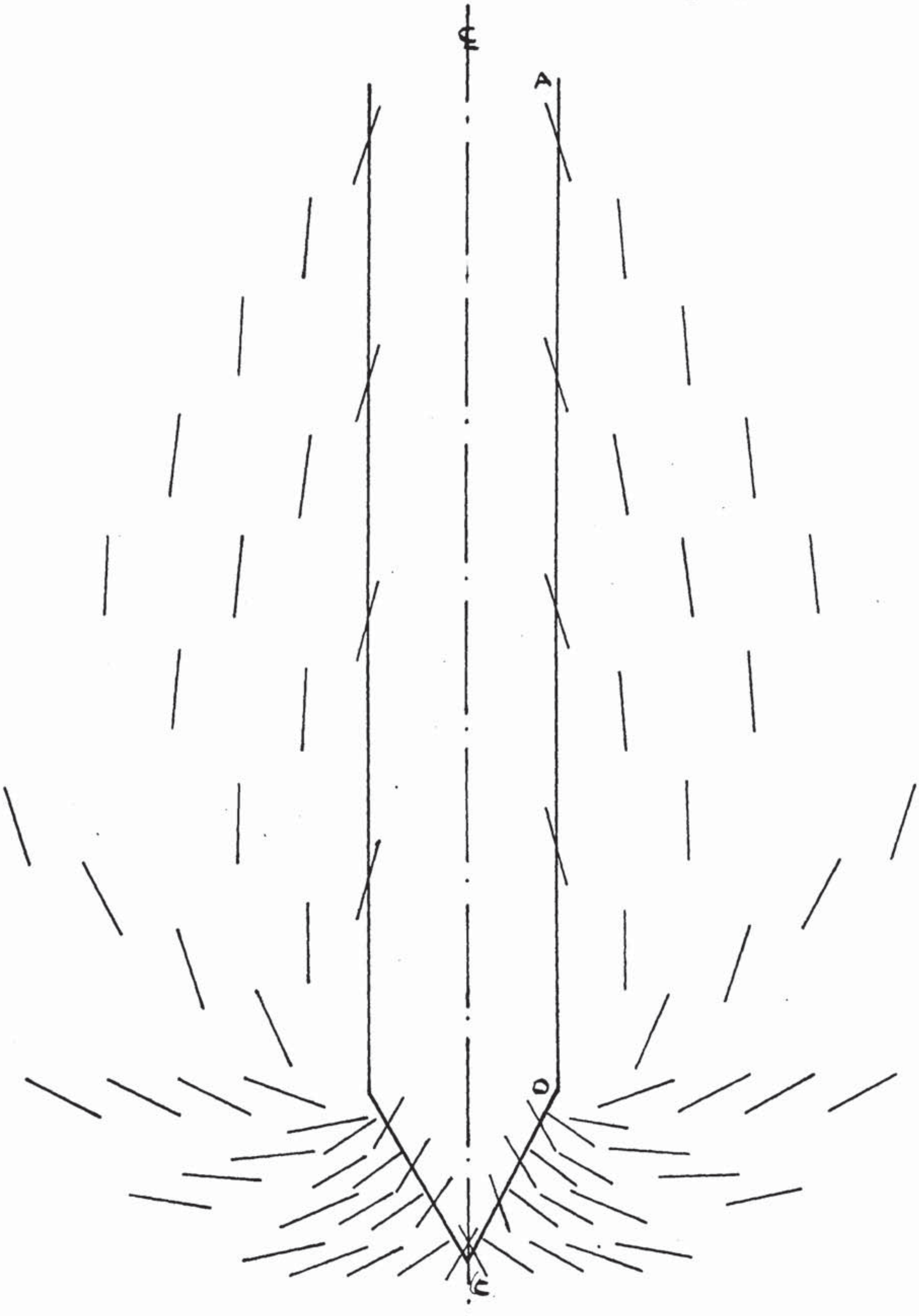

DEPTH OF PENETROMETER
= 12 · 866 in.

SCALE : 1·2 × FULL SIZE

COMPUTATIONS ARE BASED ON CONSTANT
σ ALONG THE VERTICAL FACE AO
(i.e. σ = 0·356 p.s.i.).

FIGURE 6.18 (a) & (b) STRESS DISTRIBUTIONS COMPUTED FROM THEORY OF LIMITING STRESS - DENSE SAND CONDITIONS

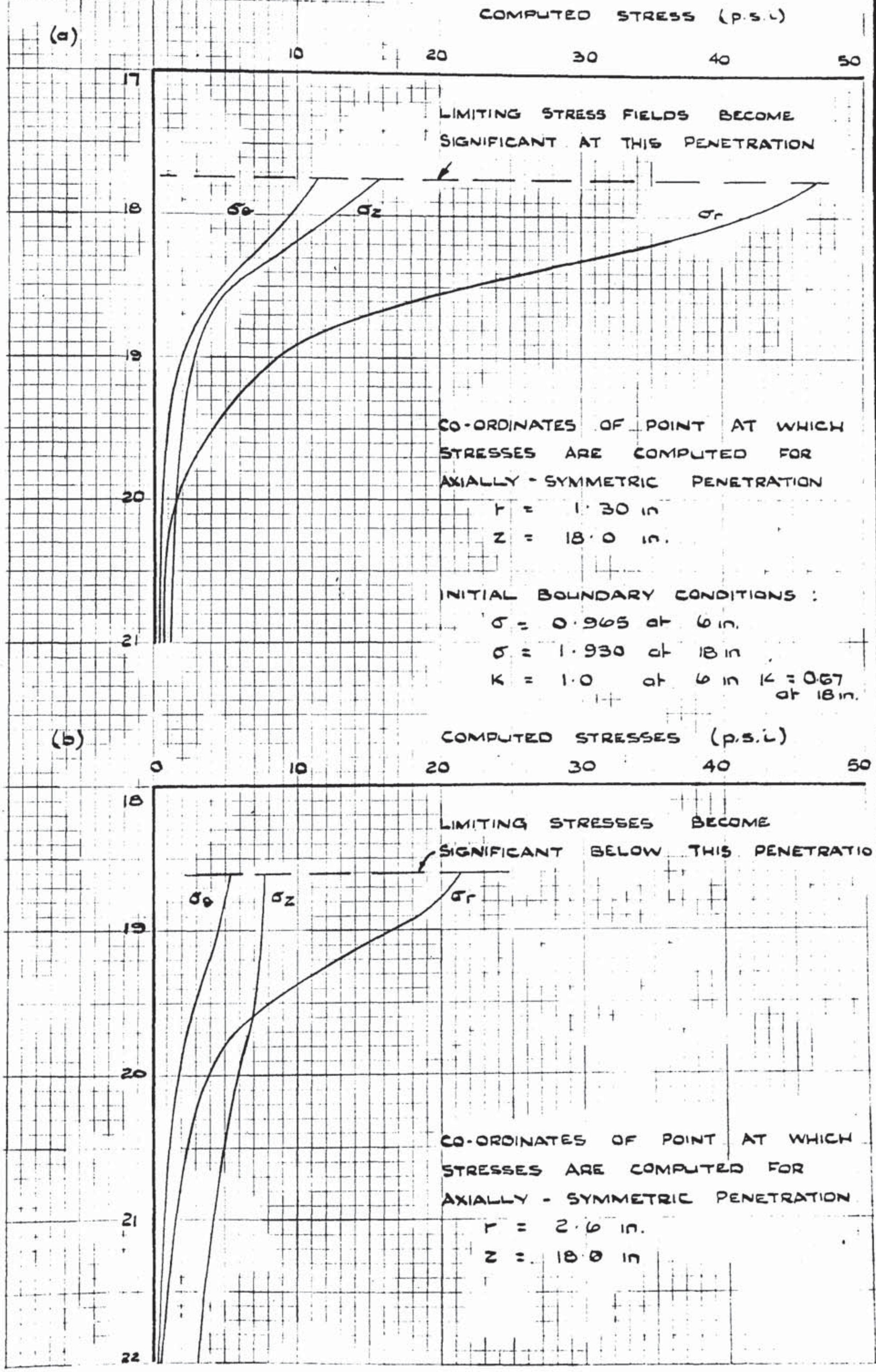

FIGURE 6.19. DIRECTIONS OF MAJOR PRINCIPAL STRESS DURING QUASI-STATIC AXIALLY-SYMMETRIC PENETRATION INTO DENSE SAND

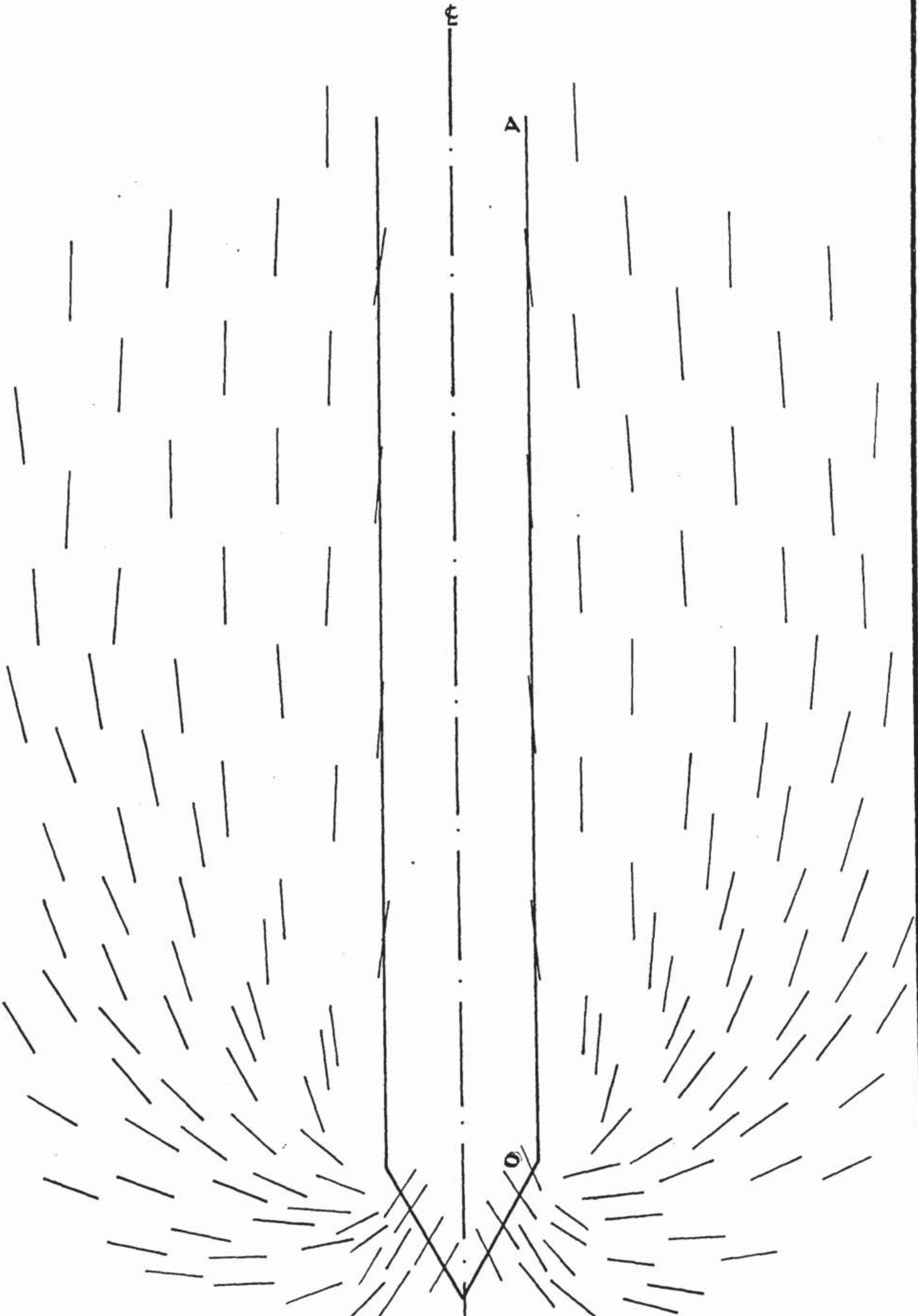

DEPTH OF PENETROMETER :
18.866 in.

SCALE : FULL SIZE

COMPUTATIONS ARE BASED ON CONSTANT σ ALONG THE VERTICAL FACE AO (i.e. σ = 0.356 p.s.i.).

FIGURE 6. 20 (a) TERZAGHI (1943) THEORETICAL FAILURE MECHANISM FOR FOUNDATION WITH SMOOTH BASE.

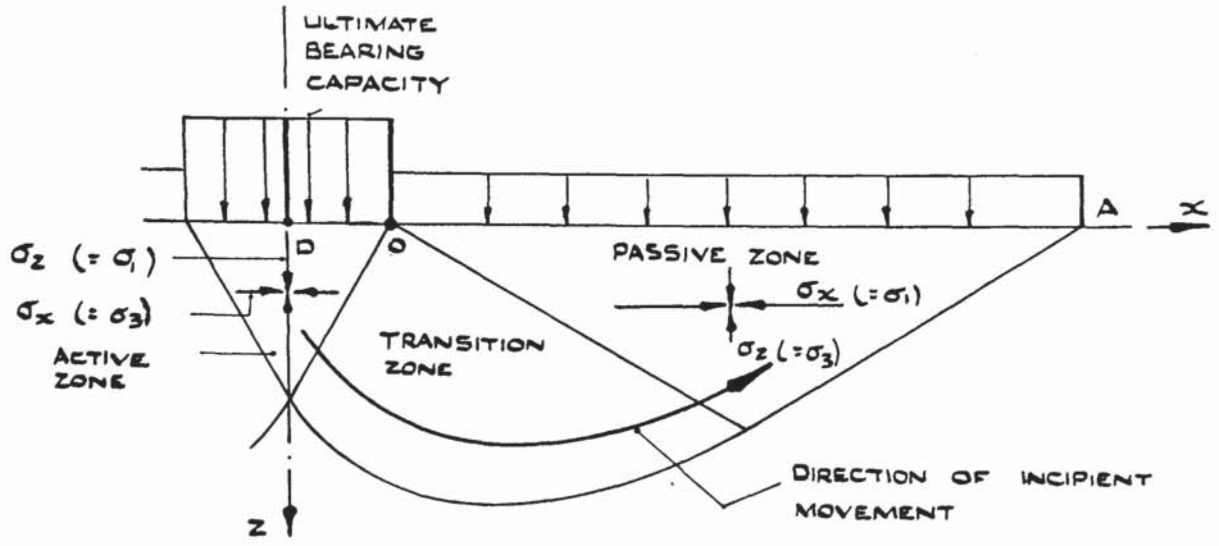

N.B. ACTIVE : $\sigma_x/\sigma_z < 1$

PASSIVE: $\sigma_x/\sigma_z > 1$

FIGURE 6. 20. (b) FIGURE 6. 20 (a) ROTATED ANTI- CLOCKWISE ABOUT O, THROUGH 90° - WITH SLIGHT GEOMETRIC MODIFICATIONS, AND ASSUMING SMOOTH BOUNDARIES

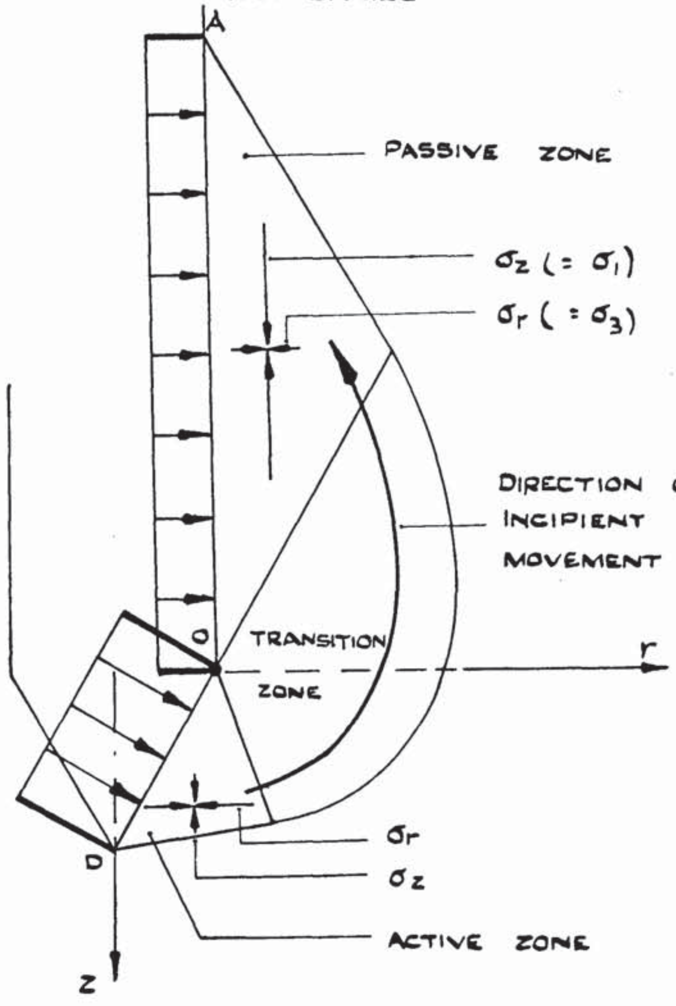

FIGURE 6.21. MEYERHOF (1951) THEORETICAL FAILURE MECHANISM FOR DEEP FOUNDATIONS.

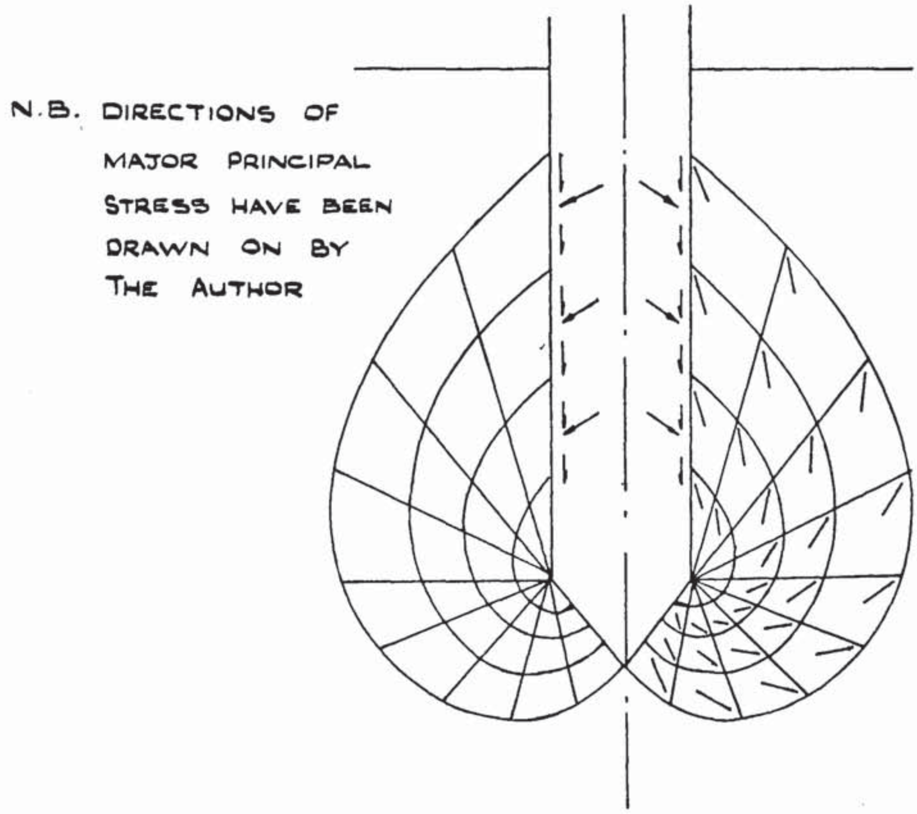

FIGURE 6.22 (a) & (b) ANGLES THROUGH WHICH THE MAJOR PRINCIPAL STRESS ROTATES IN COMPUTED SOLUTIONS

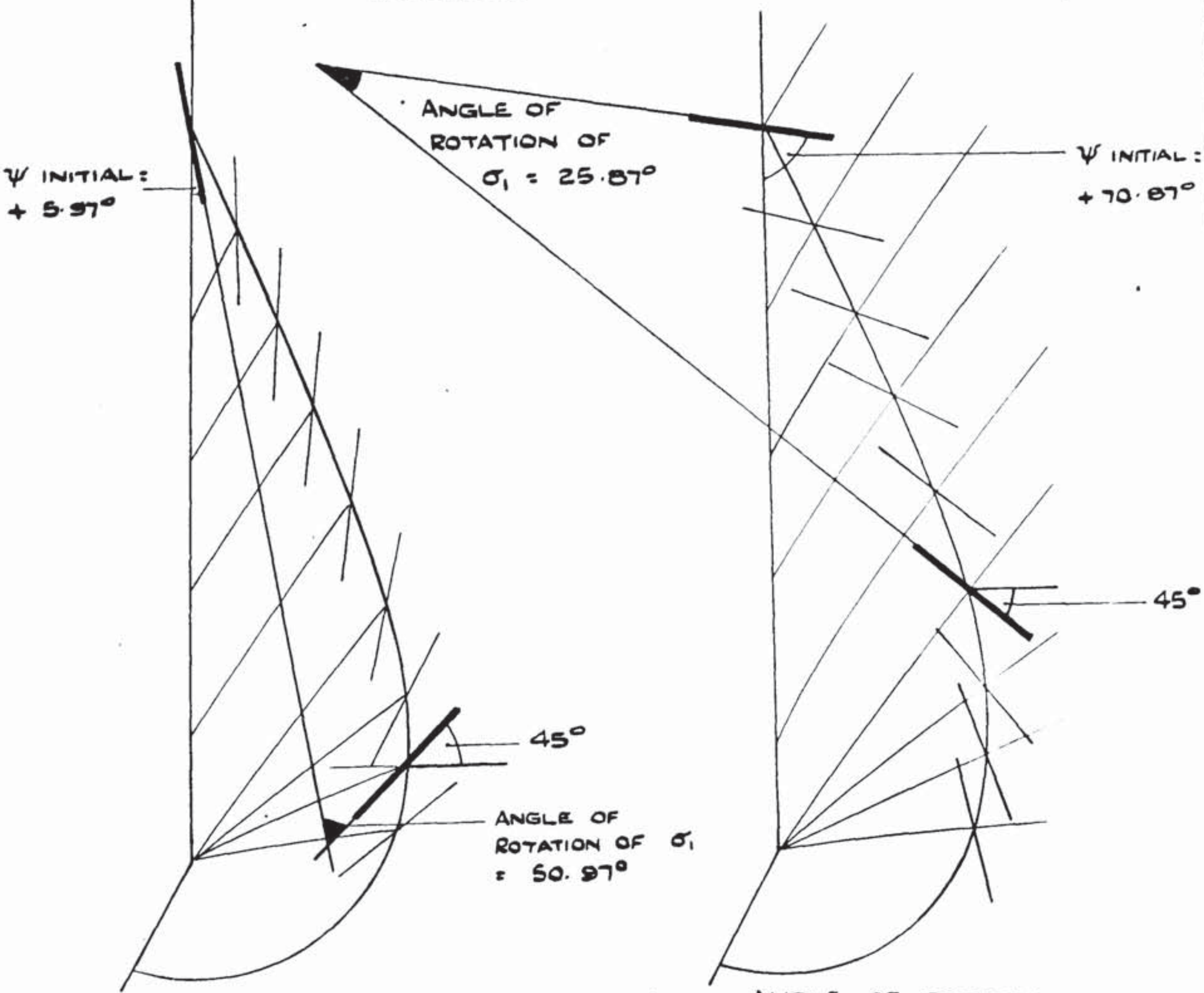

(a) ANGLE OF ROTATION FOR 'UNDISTURBED' SAND

(b) ANGLE OF ROTATION FOR SAND AFTER DRIVING PENETROMETER.

FIGURE 6.23 MOHR CIRCLE OF STRESS FROM PRESSURE CELL MEASUREMENTS IN DENSE SAND - ASSUMING $\sigma_3 = \sigma_\theta$ AND $\sigma = (\sigma_r + \sigma_z)\ ^1/_2$.
REPRODUCED FROM FIGURE 6.11 (d)

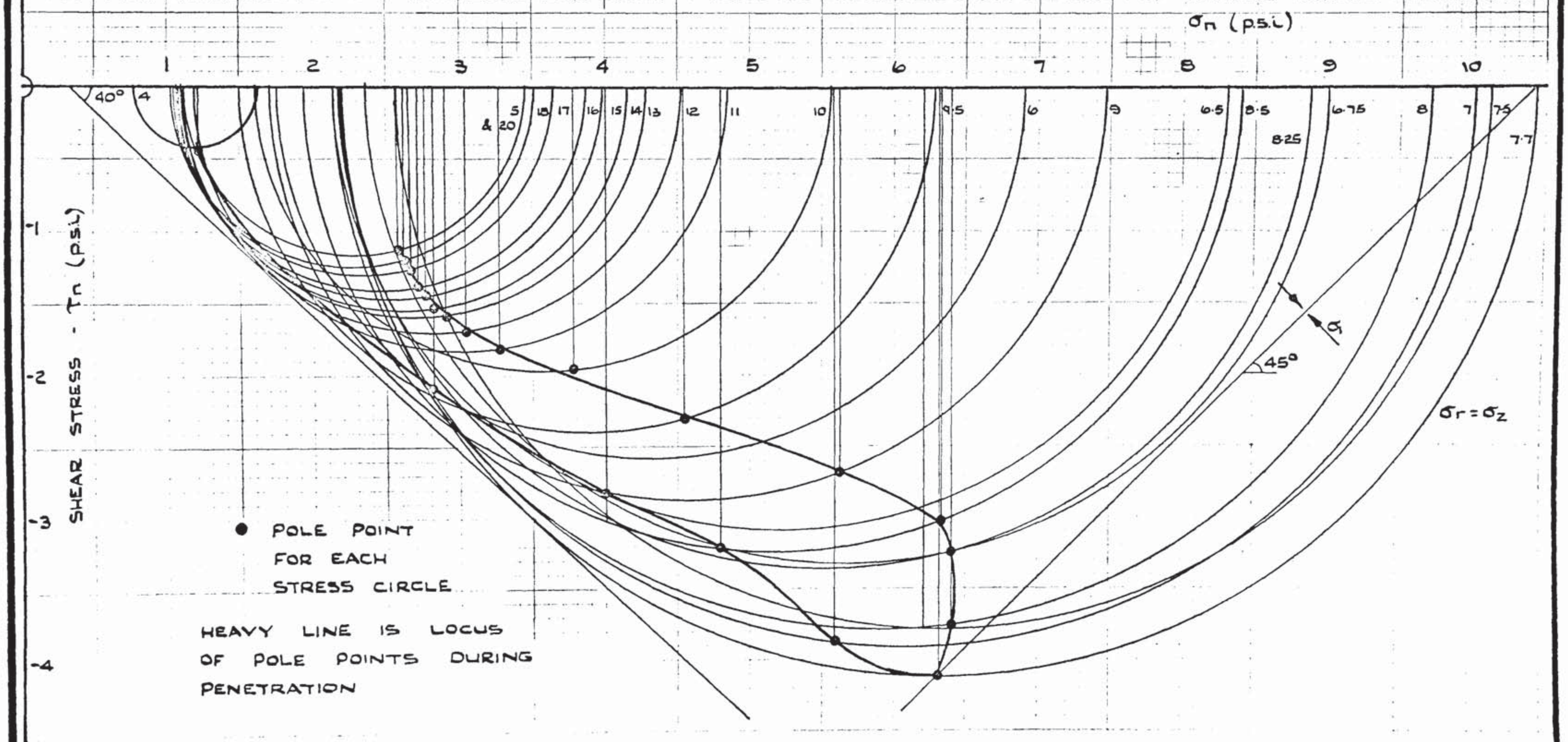

FIGURE 6.24. POSSIBLE POLE POINTS FOR MOHR STRESS CIRCLES CELL NO. 5. DENSE SAND

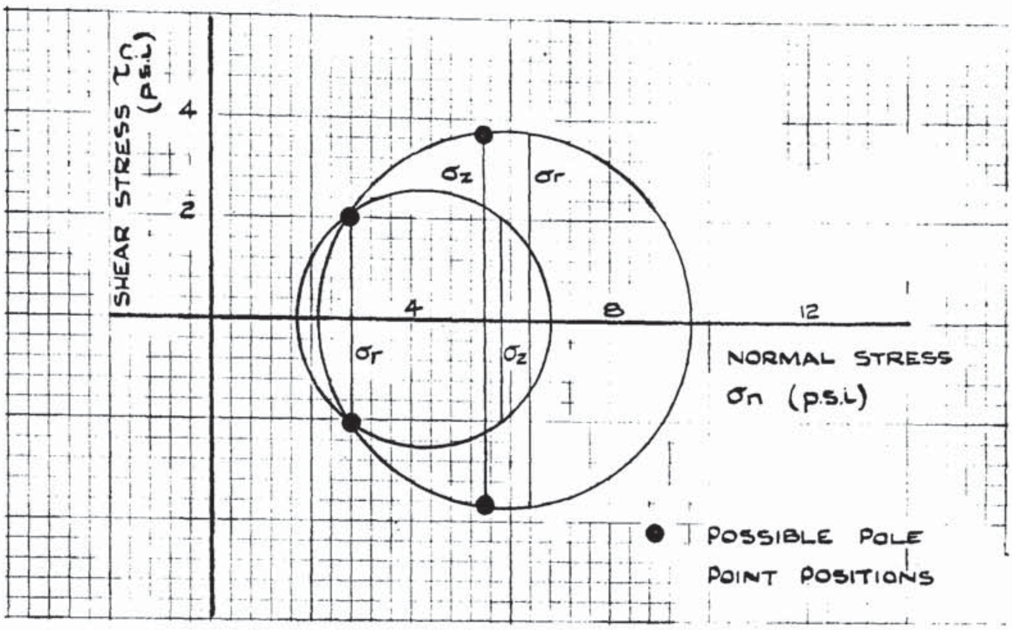

FIGURE 6.25 STRESS VECTORS DURING AXIALLY-SYMMETRIC PENETRATION INTO DENSE SAND

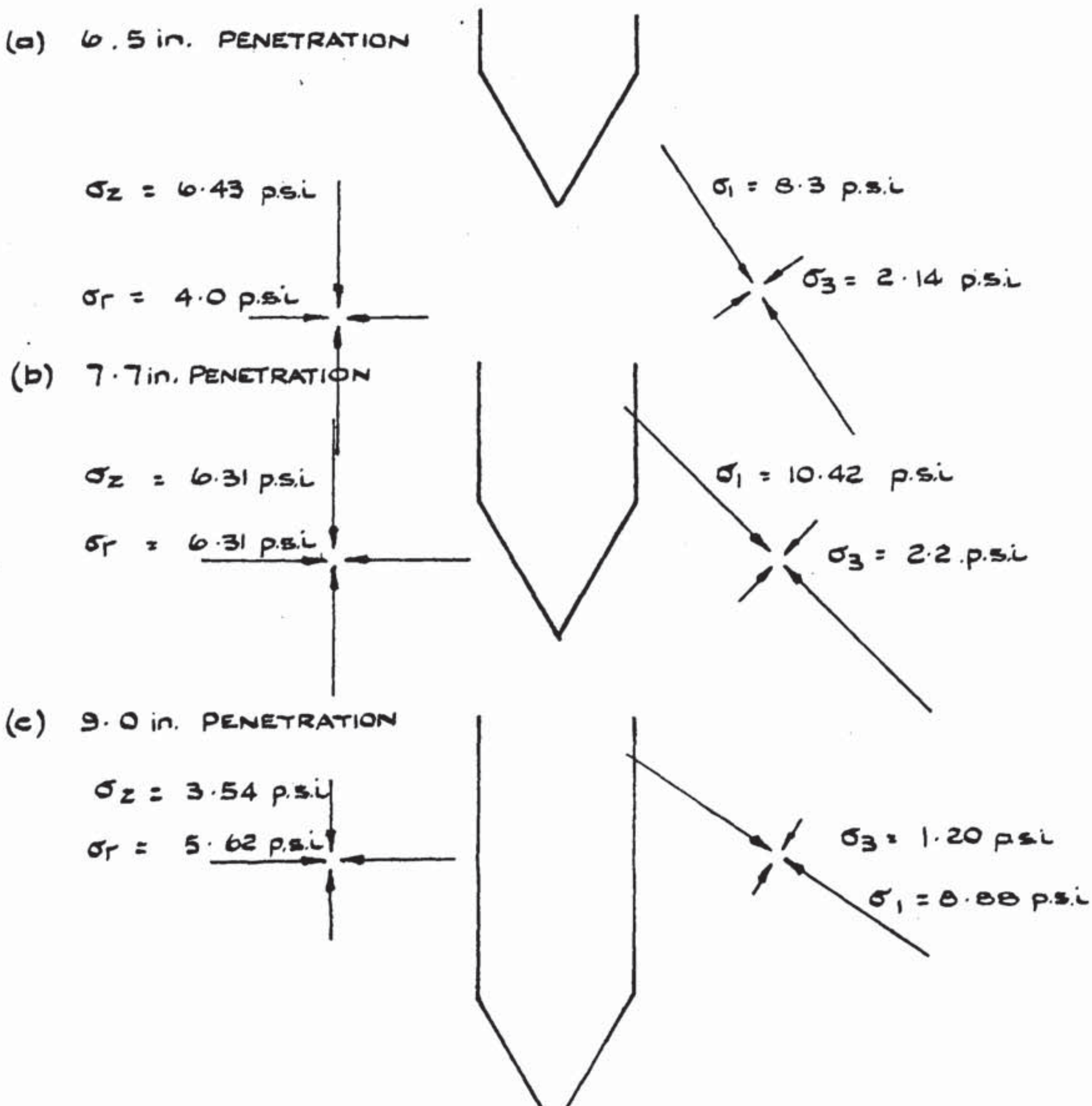

FIGURE 7.1. σ_r V σ_z PLOTS FROM PRESSURE CELLS IN LOOSE SAND.

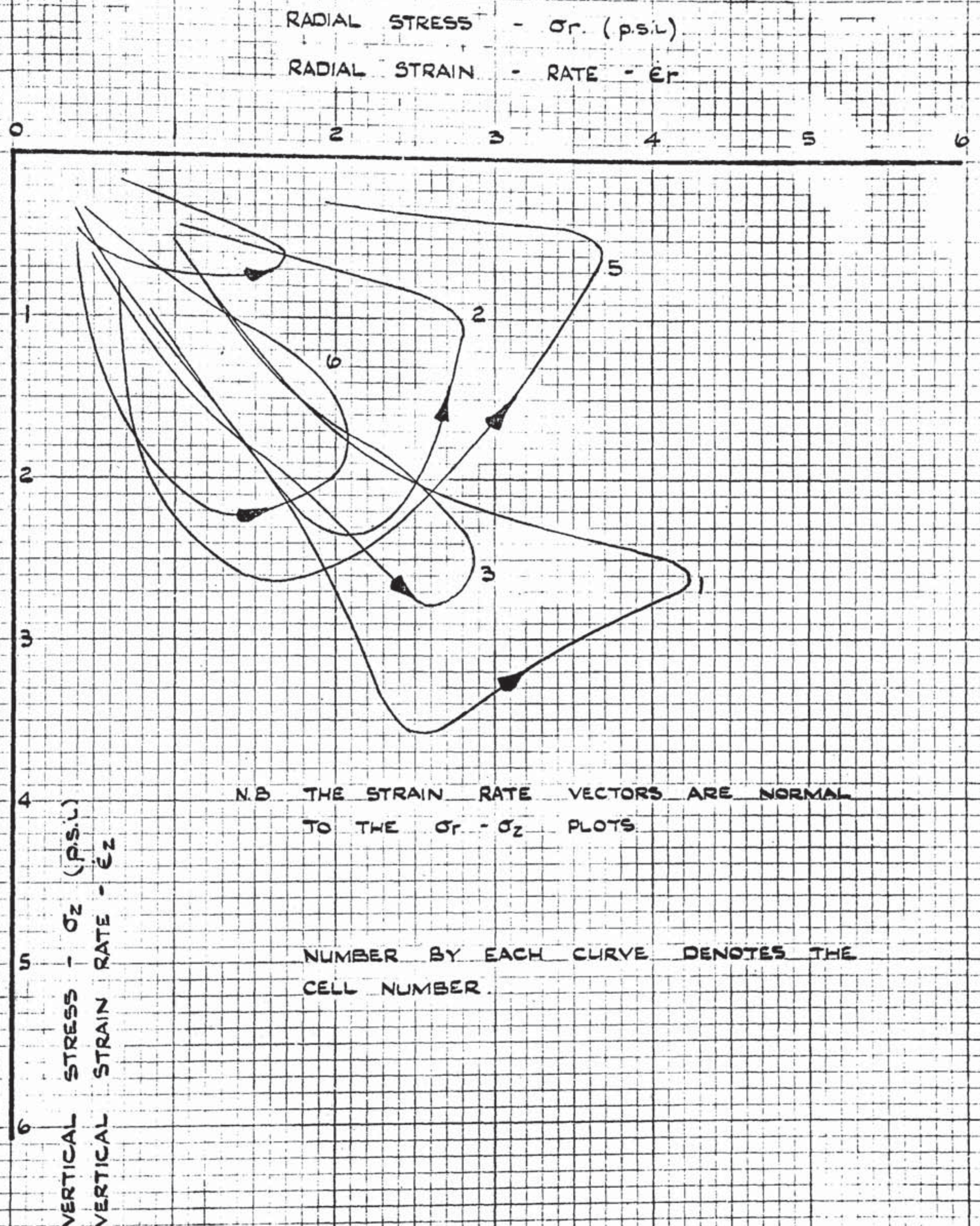

FIGURE 7.2. σ_r v σ_z PLOTS FROM PRESSURE CELLS IN LOOSE MEDIUM SAND

RADIAL STRESS - σ_r (p.s.i.)
RADIAL STRAIN - RATE - $\dot{\varepsilon}_r$

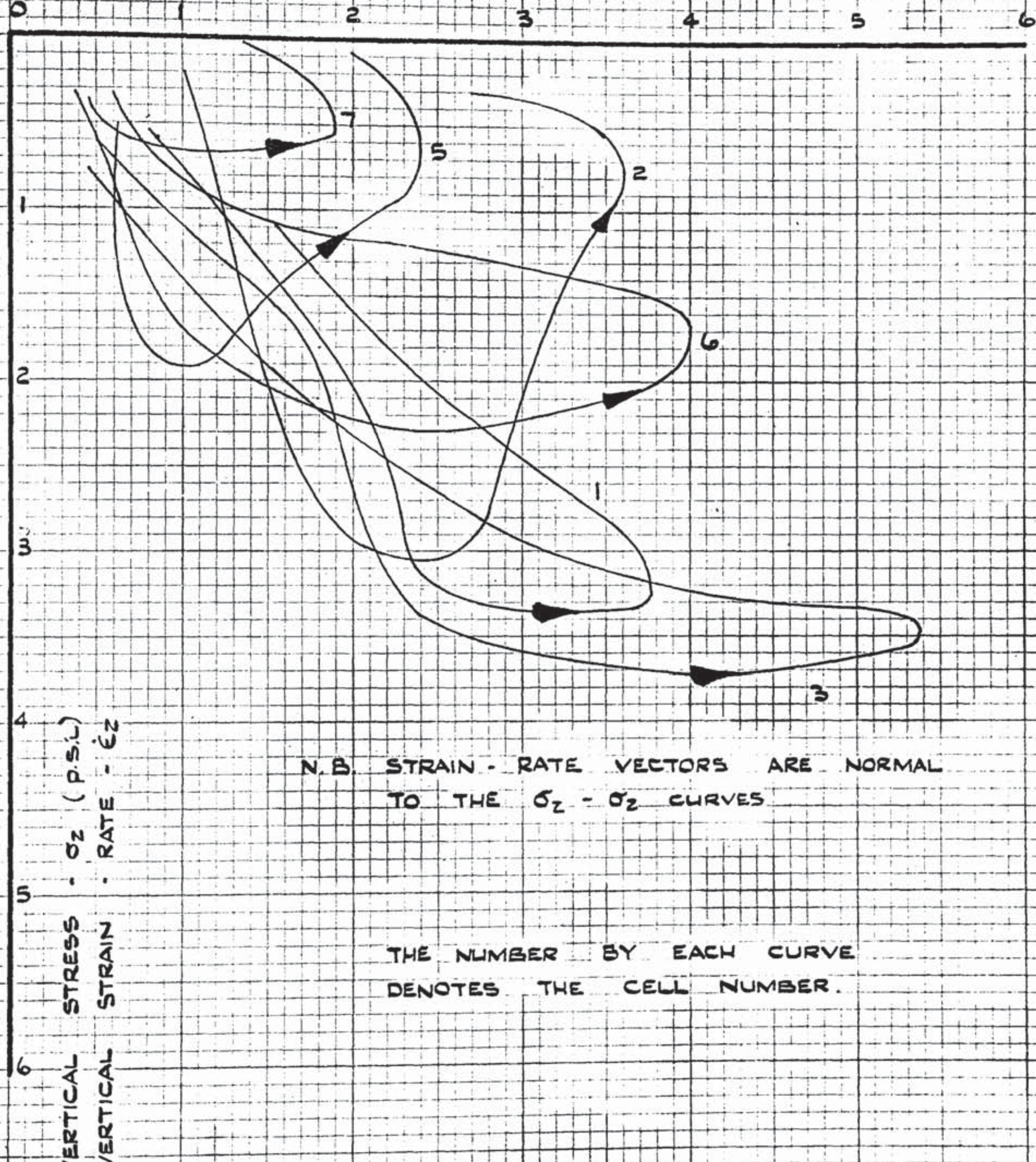

FIGURE 7.3. σ_r v σ_z PLOTS FROM PRESSURE CELLS IN DENSE SAND